

---

# Carbon Black Filler Reinforcement of Elastomers

Vineetkumar Jha

A thesis submitted to the University of London  
for the degree of Doctor of Philosophy

Department of Materials  
Queen Mary, University of London

October 2008

---

I hereby declare that the work carried out and presented in this thesis for the degree of Doctor of Philosophy is original and my own.

Vineetkumar Jha

---

## **Abstract**

Fillers enhance the properties of an elastomer by improving its mechanical properties such as the abrasion resistance or the fatigue life. In order to design a product and understand the properties of the filled elastomers used in industry; it is important to understand the effect of a filler on the composite elastomer. Strain amplification, a bound rubber layer, molecular slippage, hydrodynamic effects, occluded rubber and various other models have been previously used to describe filled rubber reinforcement and these various filler-rubber interactions. Different approaches such as finite element micro-structural modelling, molecular modelling, mathematical modelling, TEM and SEM imaging, tomography as well as measurements of the changes in electrical and mechanical properties with strain can be used to examine these various theories of filler reinforcement more closely.

Here, the finite element micro-structural analysis approach has been used to predict how the mechanical properties of elastomers changes with strain. The selection of appropriate boundary conditions and the correct stored energy function for the rubber phase are seen to be very important. To understand the filler network and the filler-rubber interactions more closely the electrical and mechanical behaviour of the filled elastomer under strain for various different conditions have also been measured. One particularly promising outcome is the discovery that for the filler, Printex-XE2, there is a fully reversible change in electrical resistivity with strain. This suggests that elastomer composites containing this filler may have practical applications as a strain sensor or a pressure sensor device.

---

## **Acknowledgement**

I would like to express my gratitude to my supervisor Dr. James Busfield for his continuous guidance, help and encouragement throughout the course of this programme. Also, I am thankful to Professor Alan Thomas, Martyn Bennett, Professor Yoshihide Fukahori and Professor Craig Davies for their guidance, supervision and suggestion.

I would like to thank the Avon Rubber (Artis UK) for the financial support and the Materials Department for the Scholarship throughout the course of the Ph.D. programme. I would like to thank Avon Rubber (Paul Marchant), and Columbian Chemicals, Cabot and OMG for supplying materials, their support and advice.

I would express my gratitude to my colleagues in the Rubber group namely Amir, Ioannis, Han, Rob, Mac, Philip and Praveen for their support and the staff and technicians in the Materials Department for their assistance.

Finally, I would like to express thanks to my parents Jatashankar Jha and Ratna Jha, my brother Manish Jha and my wife Kang Jing for their emotional support and encouragement throughout this study.

---

## Table of contents

<b>Abstract</b>	3
<b>Acknowledgements</b>	4
<b>List of contents</b>	5
<b>List of figures</b>	10
<b>List of tables</b>	21
<b>Abbreviation and symbols</b>	22
<b>Chapter 1: Introduction</b>	26
<b>Chapter 2: Literature review</b>	
2.1 Elastomer	
2.1.1 What is an elastomer	30
2.1.2 Types of elastomers	30
2.1.3 Elasticity due to structure of elastomer	31
2.2 Fillers	
2.2.1 Carbon black	33
2.2.2 Particles aggregate and agglomerate	35
2.2.3 Nomenclature	35
2.3 Filled elastomer	
2.3.1 Effect of carbon black on elastomer	37
2.3.2 Bound rubber	39
2.3.3 Occluded rubber	40

---

2.4	Theories on filled elastomer	
2.4.1	Stored energy function	43
2.4.2	Hydrodynamic theories	46
2.4.3	Strain amplification	47
2.4.4	Blanchard and Parkinson model of weak and strong linkage	47
2.4.5	The Bueche model	48
2.4.6	Dannenberg model of slippage at interface	49
2.5	Finite Element Analysis	
2.5.1	Introduction	50
2.5.2	Assembly processes	52
2.5.3	General theory of problem solving	52
2.5.4	Analysis in Abaqus	53
2.6	Modelling	
2.6.1	Numerical and molecular dynamics approaches to modelling	54
2.6.2	Finite element analysis of filled composite	56
2.6.3	Particle morphology, filler-polymer interface and mechanical properties	67
2.7	Conductivity of filled elastomers	
2.7.1	Effect of filler properties on conductivity	70
2.7.2	Conduction mechanism	73
2.7.3	Machalan effective media theory	77
2.7.4	Effect of carbon black morphology	78
2.7.5	Network visualization of carbon black aggregates	79

---

2.8	Investigation of filler reinforcement of elastomer	
2.8.1	Electrical properties of the carbon black loaded elastomers subjected to strain	81
2.8.2	Effect of swelling	87
2.8.3	Effect of temperature	90
2.8.4	Effect of polymer	91
2.8.5	Effect of mixing	91

### **Chapter 3: Experimental Methods**

3.1	Introduction	93
3.2	Resistivity behaviour under strain for filled elastomers	
3.2.1	Material	94
3.2.2	Resistivity measurements	96
3.2.3	Tensile strain testing	97
3.2.4	Tensile testing at elevated temperatures	99
3.2.5	Preparation of swollen samples	100
3.2.6	Silver filled bonding agent	102
3.2.7	Adhesion test	103
3.2.8	Samples preparation	103
3.2.9	Imaging technique: SEM and TEM	105
3.3	Finite element analysis	
3.3.1	Rubber material characterisation	106
3.3.2	Filler material characterisation	107
3.3.3	Boundary conditions	111
3.3.4	Types of smooth surface models: symmetry and distribution	111
3.3.5	Stepped surface model	113
3.3.6	Interfacial boundary conditions	114

---

**Chapter 4: Modelling of the effect of fillers on the stiffness of rubbers**

4.1	Introduction	115
4.2	Results and discussion	
4.2.1	Selection of stored energy function	117
4.2.2	Selection boundary conditions and discussion	121
4.3	Conclusions	135

**Chapter 5: Microstructural modelling of filler reinforcement: Effect of filler distribution and interface**

5.1	Introduction	136
5.2	Effect of distribution	138
5.3	Effect of slippage	149
5.4	Conclusions	157

**Chapter 6 Reversible electrical behaviour of carbon black filled natural rubber**

6.1	Introduction	159
6.2	Filled elastomers	160
6.3	Effect of strain	164
6.4	Filled rubber conductivity: Printex -XE2	174
6.5	Effect of temperature	177
6.6	Effect of swelling	184
6.7	Proposed model for filler aggregate structure	
6.7.1	Introduction	192
6.7.2	Printex-XE2 Filler aggregate structure model	196
6.7.3	HAF Filler aggregate structure model	198
6.7.4	MT Filler aggregate structure model	200



---

6.8 Evaluation of conductive bonding agent	
6.8.1 Introduction	201
6.8.2 Adhesion test results	202
6.9 Conclusions	
6.9.1 Effect of strain	204
6.9.2 Effect of temperature	205
6.9.3 Effect of swelling	206
<b>Chapter 7: Conclusions and Future Work</b>	<b>207</b>
<b>References</b>	<b>213</b>
<b>Appendix</b>	<b>225</b>

---

## List of figures

<b>Figure 2.1</b> Rubber structure: (a) before vulcanisation and (b) after vulcanisation.	31
<b>Figure 2.2</b> Tensile stress-strain curves for polymers in three different physical states, X denotes rupture, (Gent et al., 1999).	32
<b>Figure 2.3</b> Scheme of different zones of a carbon black reactor.	34
<b>Figure 2.4</b> Carbon black aggregate showing the primary particle: (small circle) and aggregate: (larger circle).	34
<b>Figure 2.5</b> Shape categories for carbon black aggregates, (Herd et al., 1991).	36
<b>Figure 2.6</b> Adhesion index for range of fillers, (adapted from Hess <i>et al.</i> , 1967).	37
<b>Figure 2.7</b> Glassy bound rubber (GH phase) and sticky layer (SH-phase) model proposed by Fukahor (2007).	41
<b>Figure 2.8</b> Variation in amount of bound rubber vs. surface area for different fillers, (Danennberg, 1986).	42
<b>Figure 2.9</b> Graph showing the bound rubber vs. CTAB surface area for SBR filled with carbon black, (Wolf <i>et al.</i> , 1991).	42
<b>Figure 2.10</b> Comparisons of prediction from a) Gent and Neo-Hookean stored function (Gent, 1996) b) Neo-Hookean, Mooney and Gent stored energy function.	45
<b>Figure 2.11</b> Proposed changes in the microstructure of a filled rubber system under strain, (Danenberg, 1966).	49

---

<b>Figure 2.12</b>	A range of models with different shape of fillers proposed by Bergström and Boyce (1999); a) A 2D Coarse Mesh, b) A 2D elliptical shaped filler and c) A 3D cubocahedral shaped particle.	57
<b>Figure 2.13</b>	Chord Young's modulus versus filler volume fraction at 2% strain for 3D octant and 2D circular filler models, Mullins and Tobin experimental results and the Guth Equation 2.32 shown as the solid blue line, (Hon <i>et al.</i> , 2003).	59
<b>Figure 2.14</b>	An idealised cylindrical matrix with spherical filler particle at the center, (Fukahori and Seki, 1993).	60
<b>Figure 2.15</b>	An idealised matrix with a spherical particle at the center of a cube, (Fukahori and Seki ,1993).	61
<b>Figure 2.16</b>	Two-dimensional random circular models at 2% tensile strain showing maximum principal stress contour plot, (Hon, 2005).	61
<b>Figure 2.17</b>	Stress contour plots around a rigid sphere, (Fukahori and Seki, 1993).	62
<b>Figure 2.18</b>	2D Simulation with Heterogeneous model of void in blended polymer for idealised cavitations or non adhering low modulus rubber particles. a) 2.5% void volume fraction b) 30% void volume fraction, (Smit <i>et al.</i> , 2000).	64
<b>Figure 2.19</b>	2D Finite element analysis representation of polycarbonate plate (2mm) with regular rubber inclusions, (Sluis <i>et al.</i> , 2001).	65
<b>Figure 2.20</b>	2D Finite element analysis representation of polycarbonate plate (1mm) with irregular rubber inclusions, (Sluis <i>et al.</i> , 2001).	65
<b>Figure 2.21</b>	Finite element representation adopted by Moshev and Kozhenikov (2002); a) the structural cell b) assumed packing c) Axisymmetric finite element representation.	66
<b>Figure 2.22</b>	DC resistivity of compsites of SBR with various carbon blacks 1. Ketjenblack EC 2. Carbolac 3.Vulcan XC-72 4. Acetylen Black 5) N330.	72

---

<b>Figure 2.23</b>	The variation of the electrical resistivity on addition of filler. DC conductivity of composites of NR with carbon black. A, insulating; B, percolation; C, limiting high conductivity, (Medalia, 1986).	72
<b>Figure 2.24</b>	Electrical resistivity versus volume fraction for a range of different carbon blacks in high density polyethylene, (Probst, 1984).	73
<b>Figure 2.25</b>	Reconstructed 3D-TEM images of carbon black loaded natural rubber in black and white (upper) and in multicoloured (lower) displays. (a) and (d) CB-10; (b) and (e) CB-40; (c) and (f) CB-80. In the black and white, the contrast was reversed, and the white parts represent carbon black. Coloured ones are for easy recognition of an aggregate, which is painted differently from the neighbouring ones. The white bar for each direction shows the distance of 100 nm (Kohjiya <i>et al.</i> , 2006).	80
<b>Figure 2.26</b>	The variation of the electrical resistivity of a 50phr and a 59phr HAF filled NR, (Deeprasertkul, 1999).	83
<b>Figure 2.27</b>	Variation of longitudinal and transverse electrical resistivity during various elongation cycles in tension as a function of strain, (Norman, 1970)	83
<b>Figure 2.28</b>	Reversible electrical (resistivity) response shown HAF N330 filled elastomer under cyclic loading, (Yamaguchi <i>et al.</i> , 2003).	84
<b>Figure 2.29</b>	Changes in resistivity as a function of strain for ethylene-octene elastomer at filler volume fraction of 20% for a high surface area black Conductex ultra 975, (Flandin <i>et al.</i> 1999).	84
<b>Figure 2.30</b>	Linear response to changes in the resistivity for a carbon nanotube filled polymer for first cycle, (Zhang <i>et al.</i> , 2007).	85
<b>Figure 2.31</b>	Variation in resistance as a function of elongation for Silicone-Ni type 287 composite, (Bloor <i>et al.</i> , 2005).	86
<b>Figure 2.32</b>	Changes in resistivity versus strain for a low structure carbon black such as MT carbon black in ethylene octane elastomer, (Flandin <i>et al.</i> , 1999).	86

---

<b>Figure 2.33</b> Changes in resistivity response versus extension ratio for filled NR with 70 phr carbon black swollen by solvent AC12, (Busfield <i>et al.</i> , 2004).	89
<b>Figure 2.34</b> Electrical behaviour of a filled composite; styrene butadiene with carbon black or graphite swollen in different solvent, (Carrillo <i>et al.</i> , 2005).	89
<b>Figure 2.35</b> Changes in resistivity of a filled composite as a function of temperature, (Lundberg and Sundqvist, 1986).	92
<b>Figure 2.36</b> Comparison of resistivity curve versus temperature for a) 5.4 wt % Multi-wall nanotube /HDPE b) 16 wt % carbon black / HDPE c) DSC for 5.4 % Multi-wall nanotube/HDPE sample, (He <i>et al.</i> , 2005).	92
<b>Figure 3.1:</b> Linear voltage versus current relationship (ohmic) behaviour for filled NR.	97
<b>Figure 3.2:</b> Schematic of the set up used to measure electrical resistivity of the test sample.	99
<b>Figure 3.3</b> The mass uptake of the Xylene solvent versus the square root of time for Carbon black filled rubbers	102
<b>Figure 3.4</b> The rubber specimen showing the bonded area, (All dimensions in cm).	104
<b>Figure 3.5</b> The fixture used for 90 degree peel test from ASTM D429-03,.(All dimensions in cm).	104
<b>Figure 3.6</b> Ideal lattice arrays of filler particles in rubber matrix with filler particles at centre of each cubic.	107
<b>Figure 3.7</b> Octant symmetry 1/8 Finite element analysis representation of MT carbon black carbon particle.	108
<b>Figure 3.8</b> 1/8 Symmetry model showing Plane surface boundary condition	109
<b>Figure 3.9</b> 1/8 Symmetry model showing the free surface boundary condition	110
<b>Figure 3.10</b> Four filler smooth surface model	111

---

<b>Figure 3.11</b> Eight filler smooth surface model with irregular distribution	112
<b>Figure 3.12</b> Steeped surface nine filler model having irregular distribution	113
<b>Figure 3.13</b> Critical shear stress friction model behaviour between two contacting bodies. (Abaqus 2001). Where $\gamma$ represents the extent of slippage.	114
<b>Figure 4.1</b> Comparisons of experimental behaviour of the unfilled rubber for Mullins and Tobin (1965) and Harwood <i>et al.</i> (1967) with the stiffness fitted using the Mooney and the Gent stored energy functions.	119
<b>Figure 4.2</b> MT carbon black filler particle.in a rubber matrix a) TEM image b) Spherical filler particle in the centre of a unit cube c) octant ( $1/8^{\text{th}}$ ) symmetry model	120
<b>Figure 4.3</b> Stress contour plots for ( $1/8^{\text{th}}$ ) octant symmetry model with a free surface boundary on two faces under a tensile strain of % at volume fraction of 13.8%.	124
<b>Figure 4.4</b> Stress contour plots for an ( $1/8^{\text{th}}$ ) octant symmetry model with plane surface boundary conditions under a tensile strain of % at volume fraction of 13.8%.	125
<b>Figure 4.5</b> A four filler smooth surface model	126
<b>Figure 4.6</b> Stress contour plots for the four filler model with plane surface boundary conditions under a tensile strains of % at volume fraction of 13.8%.	127
<b>Figure 4.7</b> Stress contour plots for the four filler model with free surface boundary under tensile strains of X% at volume fraction of 13.8%; (The two planes a and b acts symmetry making the model behave like a 16 filler model).	128

---

<b>Figure 4.8</b> Engineering stress versus extension ratio for MT carbon black filled rubber and models at 13.8% filler volume fraction. The limiting extension, $\lambda_c$ , of the planar surface single particle model is shown as the asymptote. (Mooney stored energy function).	129
<b>Figure 4.9</b> Engineering stress versus extension ratio for MT carbon black filled rubber and models at 20.9% filler volume fraction. The limiting extension, $\lambda_c$ , of the planar surface single particle model is shown as the asymptote. (Mooney stored energy function).	130
<b>Figure 4.10</b> Engineering stress versus extension ratio for MT carbon black filled rubber and models at 13.8 % filler volume	133
<b>Figure 4.11</b> Engineering stress versus extension ratio for MT carbon black filled rubber and models at 20.9 % filler volume fraction	134
<b>Figure 5.1</b> Eight filler smooth surface filler model when strained.	139
<b>Figure 5.2</b> Eight filler smooth filler surface model under uniaxial tension.	140
<b>Figure 5.3</b> Average engineering stress versus extension ratio for 4, 8, 16 and 32 filler models at 13.8% filler volume fraction for smooth filler surface models.	141
<b>Figure 5.4</b> Average engineering stress versus extension ratio for 8 filler smooth surface models at 13.8% filler volume fraction showing the extent of the isotropic behaviour in the three orthogonal loading directions and subjected to a shear stress.	142
<b>Figure 5.5</b> FEA filler model with stepped surface a) Nine filler stepped surface model with irregular distribution in the unstrained state b) Octant (1/8 <sup>th</sup> ) of the filler shown above.	144
<b>Figure 5.6</b> Mesh for the nine filler stepped surface model under strain and unstrained. Highlighting the occluded rubber on typical filler a) Single filler particle highlighting its bound rubber content in an octant model. highlights rubber elements adjacent to 2 filler surfaces, highlights rubber elements adjacent to 3 filler surfaces b) Nine filler model under a 100% tensile strain.	145

---

<b>Figure 5.7</b> Average engineering stress versus extension ratio for an 8 filler and 9 filler stepeed surface models at 13.8% filler.	146
<b>Figure 5.8</b> Average engineering stresses versus extension ratio for a 9 filler stepeed surface models at 13.8% filler volume fraction showing the extent of the isotropy in the three orthogonal loading direction directions and subjected to a shear stress.	148
<b>Figure 5.9</b> 2D quarter symmetry circular filler particle model at 5% filler volume fraction (left) undeformed shape (right) under deformation with the slippage of a node on the rubber surface highlighted as the black dot.	150
<b>Figure 5.10</b> Engineering stress versus extension ratio for various 2D models for a range filler volume fractions. Both the slippage models and the perfectly bonded models are shown at each volume fraction	151
<b>Figure 5.11.</b> Engineering stress versus extension ratio for 2D models with a $V_f$ of 40%. This figure shows the effects of various levels of critical shear stress on the onset of slippage at the rubber-filler interface	152
<b>Figure 5.12</b> Ratio of Young's Modulus versus filler volume fraction. A comparison between the stiffening effect of Einstein's and Taylor's theoretical relationships to the 3D octant (1/8 symmetry) FE models with perfect bonding and a frictionless interfacial slippage.	153
<b>Figure 5.13</b> 3D octant symmetry spherical particle with a filler volume fraction of 13% a) The undeformed shape. b) Under deformation with the slippage of a single node at 80% global tensile strain along the filler surface, highlighted as the black dot.	155
<b>Figure 5.14</b> Engineering stress, versus extension ratio. A comparison between 3D spherical finite element models and experimental MT carbon-black filled elastomer samples at large extensions and at high filler volume fractions.	156



---

<b>Figure 6.1</b> SEM image of filled rubber showing varying aggregate size. a) SEM of Printex XE-2 (5.2%). b) SEM of HAF (N330) (21%). c) SEM of MT N 990 (56%).	160
<b>Figure 6.2</b> TEM Image of Carbon black aggregate.a) Printex b) HAF N330 c) Printex –XE2 from Evonik Degussa GmbH	161
<b>Figure 6.3</b> Comparison of mechanical behaviours of different types of carbon black at a filler volume fraction of 5.2% / (10 phr).	162
<b>Figure 6.4</b> Resistivity versus extension ratio for Printex-XE2 filled NR at a filler volume fraction of 5.2% under cyclic tensile strains.	165
<b>Figure 6.5</b> Stress versus strain for Printex filled NR at a filler volume fraction of 5.2% under cyclic tensile strains.	166
<b>Figure 6.6</b> Initial resistivity versus nitrogen surface area at a filler volume fraction of 21% for three HAF blacks shown in Table 3.1 and figure 6.7.	168
<b>Figure 6.7</b> First cycle resistivity versus extension ratio at a filler volume fraction of 21% under cyclic tensile strains.	168
<b>Figure 6.8</b> First cycle stress versus strain for three different types of HAF black filled NR at a filler volume fraction of 21% under cyclic tensile strains.	169
<b>Figure 6.9</b> Twentieth cycle resistivity versus extension ratio at a filler volume fraction of 21% under cyclic tensile strains.	169
<b>Figure 6.10</b> Twentieth cycle stress versus strain for three different types of HAF black filled NR at a filler volume fraction of 21% under cyclic tensile strains. (20 <sup>th</sup> cycle	170
<b>Figure 6.11</b> First cycle resistivity versus extension ratio for MT N990 filled NR at a filler volume fraction of 56% under tension.	172
<b>Figure 6.12</b> First cycle stress versus strain MT N990 black filled NR at a filler volume fraction of 56% under tension.	172
<b>Figure 6.13</b> Resistivity versus extension ratio for MT N990 filled NR at a filler volume fraction of 56% under cyclic tensile strains.	173



---

<b>Figure 6.14</b> Stress versus strain for MT N990 black filled NR at a filler volume fraction of 56 % under cyclic tensile strains.	173
<b>Figure 6.15</b> Percolation behaviour of Printex-XE2 filled NR.	175
<b>Figure 6.16</b> Resistivity versus strain for different volume fraction of Printex-XE2.	175
<b>Figure 6.17</b> The scaling law (Percolation theory) used to determine the critical exponent, $t$ in equation 2.15.	176
<b>Figure 6.18</b> SEM charge contrast image obtained for NR rubber filled with a volume fraction of 5.2% of Printex.	176
<b>Figure 6.19</b> Resistivity versus extension ratio for Printex-XE2 filled NR at a filler volume fraction of 5.2% under cyclic tensile strains at 23°C and 80°C.	178
<b>Figure 6.20</b> Stress versus strain for Printex filled NR at a filler volume fraction of 5.2% under cyclic tensile strains at 23°C and 80°C.	179
<b>Figure 6.21</b> Resistivity versus extension ratio for MT N990 filled NR at a filler volume fraction of 56% under cyclic tensile strains at 23°C and 80°C.	180
<b>Figure 6.22</b> Stress versus strain MT N990 black filled NR at a filler volume fraction of 56 % under cyclic tensile strains at 23°C and 80°C.	181
<b>Figure 6.23</b> Resistivity versus extension ratio for CDX 7055 filled NR at a filler volume fraction of 21% under cyclic tensile strain (1st cycle only) at 23°C and 80°C	182
<b>Figure 6.24</b> Stress versus strain for CDX 7055 black filled NR at a filler volume fraction of 21% under cyclic tensile strains at 23°C and 80°C.	182
<b>Figure 6.25</b> Resistivity versus extension ratio for Raven p-5 filled NR at a filler volume fraction of 21% under cyclic tensile strain (1st cycle only) at 23°C and 80°C.	183
<b>Figure 6.26</b> Stress versus strain for Raven p-5 black filled NR at a filler volume fraction of 21% under cyclic tensile strains at 23°C and 80	183

---

<b>Figure 6.27</b> Effect of swelling with xylene on resistivity versus extension ratio for Printex-XE2 filled NR at a filler volume fraction of 5.2% under cyclic tensile strains	186
<b>Figure 6.28</b> Effect of swelling with xylene on stress versus strain for Printex filled NR at a filler volume fraction of 5.2% under cyclic tensile strains	186
<b>Figure 6.29</b> Effect of swelling with DBA on resistivity versus extension ratio for Printex-XE2 filled NR at a filler volume fraction of 5.2% under cyclic tensile strains.	187
<b>Figure 6.30</b> Effect of swelling with DBA on stress versus strain for Printex-XE2 filled NR at a filler volume fraction of 5.2% under cyclic tensile strains	187
<b>Figure 6.31</b> Effect of swelling with xylene on resistivity versus extension ratio for MT N990 filled NR at a filler volume fraction of 56% under cyclic tensile strains.	188
<b>Figure 6.32</b> Effect of swelling with xylene on stress versus strain MT N990 black filled NR at a filler volume fraction of 56 % under cyclic tensile strains.	188
<b>Figure 6.33</b> Effect of swelling with DBA on resistivity versus extension ratio for MT N990 filled NR at a filler volume fraction of 56% under cyclic tensile strains.	189
<b>Figure 6.34</b> Effect of swelling with DBA on stress versus strain MT N990 black filled NR at a filler volume fraction of 56 % under cyclic tensile strains	189
<b>Figure 6.35</b> Effect of swelling with xylene on resistivity versus extension ratio behaviour for CDX 7055 filled NR at a filler volume fraction of 21% under cyclic tensile strains. (1st cycle only).	190
<b>Figure 6.36</b> Effect of swelling with xylene on stress versus strain for CDX 7055 carbon black filled NR at a filler volume fraction of 21% under cyclic tensile strains.	190

---

<b>Figure 6.37</b> Effect of swelling with xylene on resistivity versus extension ratio for Raven p-5 filled NR at a filler volume fraction of 21% under cyclic tensile strains. (1st cycle only).	191
<b>Figure 6.38</b> Effect of swelling with xylene on the stress versus strain behaviour for Raven p-5 black filled NR at a filler volume fraction of 21% under cyclic tensile strains.	191
<b>Figure 6.39</b> Proposed filler aggregate structure re-arrangement. (  indicates when the aggregate breakdown is reversible).	194
<b>Figure 6.40</b> Proposed filler aggregate structure re-arrangement for Printex-XE2 filled elastomer and idealized behaviour of Printex –XE 2 under cyclic strain. (  indicates the aggregates are reversible in Type2),	196
<b>Figure 6.41</b> Proposed filler aggregate structure re-arrangement for HAF Raven p-5 and CDX 7055 filled elastomer and idealised behaviour for the same blacks under cyclic strain.	198
<b>Figure 6.42</b> Proposed filler aggregate structure re-arrangement for MT N990 filled elastomer and the idealised behaviour for the same carbon black filler under cyclic strain.	200
<b>Figure 6.43</b> 90 degree peel test measurement of force versus extension required to fracture the rubber bonded to steel plate using silver filled adhesive.	204
<b>Figure 6.44</b> Strain energy density for a rubber sample.	204
<b>Figure 7.1</b> STM (Scanning Tunnelling microscopy) analysis of carbon black a) N 234 b) Nanostructure blacks.	212

---

## List of Table

<b>Table 2.1</b> Effect of particle size on reinforcement (Donnet and Voet, 1976).	37
<b>Table 3.1</b> Morphology of the different carbon blacks used in this study	95
<b>Table 3.2</b> Compound formulations used in this study.	96
<b>Table 3.3</b> Properties of the liquids used in this study	101
<b>Table 3.4</b> Compositions for silver filled bonding agent	105
<b>Table 6.1</b> Chord moduli taken at 10% strain from stress-strain curve at filler volume fraction of 5.2% / 10phr (Figure 6.3).	163
<b>Table 6.2</b> Adhesion test Results at 25°C	203

---

## Abbreviations

COAN	Crushed oil absorption number
CTAB	Surface area measured with bromide using hexadecyltrimethyl ammonium
DBA	Dibutyl Adipate
DBPA	Dibutyl Phthalate Absorption
DCP	Dicumyl Peroxide
FE	Finite element
FEA	Finite element analysis
FEM	Finite element modelling
HAF	High abrasion furnace (carbon black)
MT	Medium thermal (carbon black)
NR	Natural rubber
NSA	Nitrogen surface area
NMR	Nuclear magnetic resonance
OAN	Oil absorption number
phr	parts by mass per hundred elastomer
RVE	Representative Volume element
SBR	Styrene-butadiene rubber
SEF	Stored energy function
SEM	Scanning electron microscope
STM	Scanning tunnelling microscopy
TEM	Transmission electron microscope

---

## Symbols

$\varepsilon$	Di-electrical constant,
$\varepsilon_0$	Di-electrical constant of unfilled rubber
$\eta'$	The viscosity of the first liquid
$\eta_0$	The intrinsic viscosity of the fluid
$\eta$	The viscosity of the system
$\lambda_1, \lambda_2$ and $\lambda_3$	Extension ratios in $\bar{x}$ , $\bar{y}$ and $\bar{z}$ co-ordinates respectively
$\mu$	Coefficient of friction
$\nu$	Poisons ratio
$\rho_{r.net}$	The densities of the rubber network
$\rho_s$	The densities the solvent respectively
$\rho_r$	Density of rubber
$\rho_c$	Density of carbon black
$\sigma$	Engineering stress
$\sigma_{con}$	Conductivity
$\sigma_{fric}$	Frictional stress
$\sigma_m$	Conductivity of the composite medium
$\sigma_l$	Conductivity of the low-conductivity phase
$\sigma_h$	Conductivity of the high- conductivity phase
$\rho$	Resistivity
$\rho_t$	Resistivity of filler
$\phi$	Filler volume fraction
$\phi_{eff}$	Effective filler volume fraction
$\phi_{crit}$	Critical volume fraction

---

$\bar{x}$ , $\bar{y}$ and $\bar{z}$	Axes of the strain co-ordinates
$A_0$	Initial cross-sectional area
$A_r$	Schottky Richardson constant
$C_1$ and $C_2$	Mooney SEF Material parameters that can be fitted from experiments
$T$	Temperature
$E$	The modulus of the carbon black filled rubber system
$E_0$	The modulus of the unfilled rubber
$E_s$	Applied electrical field strength.
$F$	Force (N)
$F_N$	Normal force (N)
$F_{\text{fric}}$	Frictional force
$G$	Shear modulus
$I_1$ , $I_2$ and $I_3$	Three strain invariants terms of the Green deformation tensor
$I_m$	Constant to introduce finite extensibility asymptote
$j_{\text{Tunneling}}$	Tunnelling current
$j_{\text{Hopping}}$	Hopping current
$k_b$	Boltzmann constant
$M_c$	The number average molar mass of the chain length between cross-links
$M_0$	The initial mass rubber before swelling
$M_f$	The final mass after swelling
$M_r$	The mass fraction of rubber
$N$	Number of chains per unit volume
$n$	The number of length $l_1$ in the chain
$P$	Peel energy
$R_c$	Constriction resistance
$R$	Gas constant per mole
$r$	Specified length such as radius
$S$	Entropy
$t_1$ , $t_2$ and $t_3$	True principal stresses
$t$ , $t'$	Critical exponent related percolation theory



---

$t_r$	Thickness of specimen
$w$	Width of sample
$V_f$	Volume fraction of the filler present in the rubber matrix
$V_m$	Maximum volume fraction = 0.635 for random packing of identical spheres
$V_r$	Volume fraction of rubber
$V_{r.net}$	Volume of the rubber network
$V_s$	Volume of the solvent in the swollen sample
$W$	Stored energy density

---

# 1

## Introduction

Filler reinforcement of rubbers has been an area of interest to the rubber industry for more than a century. Filled rubber is widely used for applications such as tyres and anti-vibration applications systems. As a result, it is often presumed that the phenomenon of filler reinforcement is widely understood. However, as this thesis shows the various models used to explain the filler reinforcement still do not permit a complete understanding and they are also not explained clearly or consistently in the literature. The detailed effects of filler properties such as surface area and shape on the filler reinforcement are not completely understood. A detailed understanding of the filler reinforcement should provide an insight into the increase in modulus and strength witnessed with as well as helping to understand the phenomena such as cyclic stress softening, abrasion or changes in the fatigue life resistance.

Finite element analysis has been widely used in engineering as a design tool for three decades; the technique has more recently been applied to the microstructural models of composite systems. The use of finite element analysis techniques to resolve these types of problem requires geometric simplification and a detailed validation. As a results MT N990 (Medium thermal) carbon black filled elastomers are often selected for investigation, as MT carbon black shows a low tendency to agglomerate and the filler shape can be approximated to a sphere. In order to develop a reliable model the choice of the boundary conditions is important. Also, an appropriate rubber material stored energy functions must be used. Selection of appropriate stored energy function and boundary conditions are investigated in this thesis. In order to study the significance of the polymer-filler interfaces two possible conditions of perfect adhesion at the polymer-filler interface and slippage of the polymer over the filler surface have been studied here. The predictions of the stiffness of these different

---

microstructural models are compared with the experimental behaviour. Conclusions about how to construct a model to predict the effect of size, shape and filler orientation are discussed.

One significant effect of adding electrically conductive fillers such as carbon black into an electrically insulating polymer is that the composite can also conduct once the volume fraction of the filler is greater than the percolation threshold. It was hoped that the experiments that measure the changes in the conductivity with strain might reveal insights into the changes in the microstructure with strain. The resulting investigation discovers there is a good potential for the development of strain or pressure sensors. In order to achieve this we need the filled elastomer to show a reversible and repeatable changes in the resistivity with strain.

The interaction between the polymer molecules, as well as between filler particles and also at the interface determines the electrical and mechanical behaviour of the elastomer. This interaction might be studied by direct observation of the changes in the filler network structure under strain by either using a scanning electron microscope (SEM) or a transmission electron microscope (TEM).

In order to study the effect of changes in filler properties on the resistivity behaviour several different fillers including MT, HAF and Printex were selected. The selection was made to ensure fillers with a range of particle sizes, surface areas and structure were studied. The changes in electrical conductivity behaviour under strain for a range of filled elastomers selected are related to filler properties such as particle size and structure. Also, the changes in the mechanical properties such as modulus and tensile strain can be related to the conductivity behaviour. This investigation leads to the construction of a polymer-filler and filler-filler models to explain the changes in modulus and electrical conductivity with strain. The thesis follows the following structure to examine this behaviour.

Chapter 2 contains a literature review which introduces the carbon filler as well as the models for the filler reinforcement discussed in the literature. This Chapter explains

---

how fillers modify the conductivity of the rubber. As finite element analysis has been extensively used in this work and a short introduction explaining the basic concepts also included.

Chapter 3 discusses the experimental procedures used throughout the present study. The various models used for the finite element analysis are also introduced. The various friction models used to describe slippage are also explained. The materials preparations and testing methods used to measure the stiffness and the resistivity of sample under strain are also discussed. Finally the analysis used to calculate the behaviour from the measured results is also given.

Chapter 4 describes the finite element model used to predict the stiffness of MT carbon black filled elastomer. The micromechanical models was used to derive an appropriate boundary condition and to select a suitable stored energy function to model the behaviour of an MT carbon black filled rubber under tensile strain.

In Chapter 5 the effect of the number of filler particles and their position and shape on the stiffness prediction of MT carbon black filled elastomer under strain is described. Several different models with number of fillers particles ranging from 4-64, of different shape and size distribution are described. This Chapter also address the effect of the interfacial boundary condition on the contribution of the filler to the stiffening of the rubber. An appropriate friction law is derived to describe the effect of slippage between the rubber matrix and the filler on stiffness prediction with strain of a filled elastomer.

Chapter 6 discusses the effect of filler properties on the conductivity behaviour of the filled rubbers under strain, with changes in temperature and after swelling with a solvent. A range of fillers with different filler properties such as surface area and structure are used. This work also discusses the appropriateness of the various models used to explain the conductivity behaviour of the composite under strain.

Finally, Chapter 7 presents the general conclusion as well as plans that could be

---

examined as part of any ongoing investigation.

## Literature review

### 2.1 Elastomer

#### 2.1.1 What is an elastomer?

Elastomers are generally defined as polymers which exhibit rubber like behaviour. In their raw form elastomers flow under strain. In order to make elastomers more useful a process called either curing or vulcanisation is often carried out. Figure 2.1 shows the polymer structure before and after vulcanisation. During the process of curing crosslinks are formed between polymers chains. The crosslinked polymer is called “moulded rubber”. This material exhibits elastic reversible behaviour under strain. The general class of polymers which are “plastic” under strain undergo an initial elastic deformation, yield, plastic flow, necking, strain hardening and fracture. However, elastomers are highly elastic and fail often at very large strains as shown in Figure 2.2 (Gent *et al.*, 1992). There two most common types of curing systems are sulphur based and peroxide based systems.

#### 2.1.2 Types of elastomers

Elastomers can be classified as either thermoset or thermoplastics. Thermosets consist of polymer chains with chemical crosslinks as shown in Figure 2.1. Hence, in a solvent thermosets may swell, but do not dissolve. Thermoplastic elastomers chains are joined only by linkages such as physical entanglements and they may dissolve in some suitable solvents. Another classification of elastomer is by polymer types such as natural rubber or styrene butadiene rubber, both of which are widely used in the industry. In addition, specialty elastomers have been developed for use in extreme

---

conditions where increased resistance to swelling, an improved aging or a better chemical resistance are required. For such conditions speciality polymers such as poly-chloroprene, silicone rubber and chlorinated polyethylene have been developed.

### 2.1.3 Elasticity due to structure of elastomer

Chemically elastomers have a backbone of either carbon or silicon atoms to which other elements such as hydrogen or chemical groups such as a methyl unit are attached. In order to exhibit rubbery behaviour the following characteristics are required for the structure of the elastomer.

1. The polymer chain must be flexible
2. There should be sites on the backbone where the polymer can be crosslinked
3. The polymer chain must not be highly crystalline.

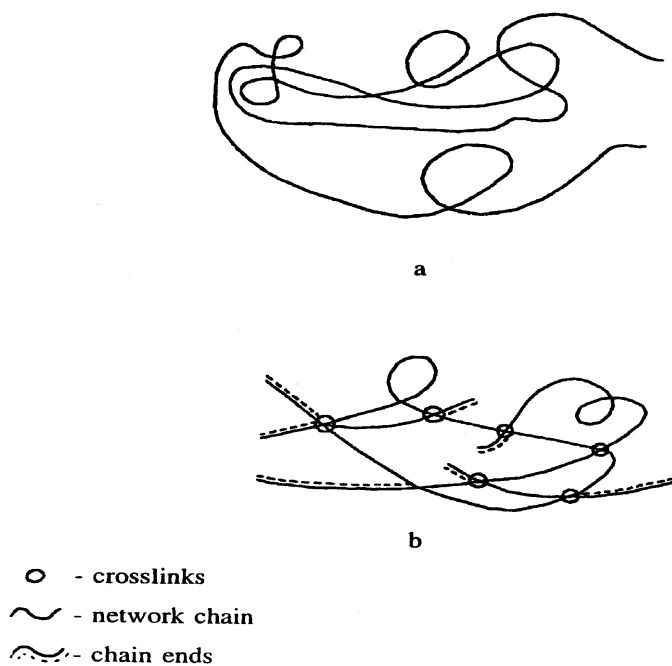


**Figure 2.1** Rubber structure: (a) before vulcanisation and (b) after vulcanisation

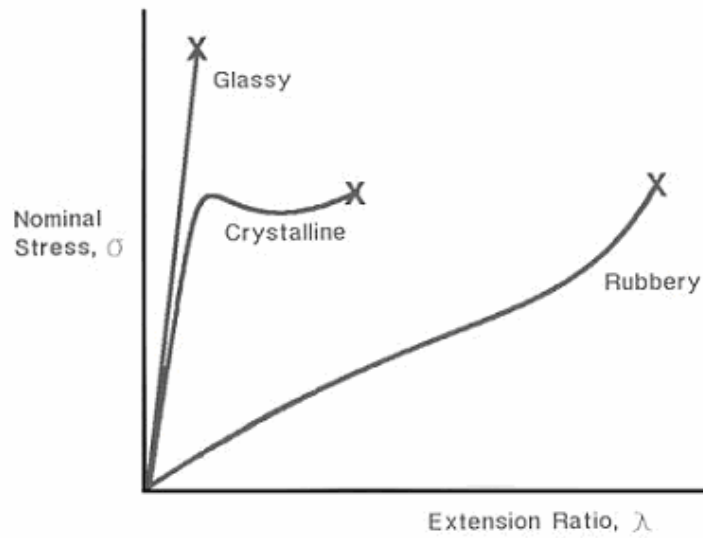


**Figure 2.2** Tensile stress-strain curves for polymers in three different physical states, X denotes rupture, (Gent *et al.*, 1992).

## 2.2 Fillers

Most commercial elastomer compounds include fillers that are used either to reduce cost or to improve the properties; the two most commonly encountered fillers are carbon black and silica.



---

### 2.2.1 Carbon black

Carbon black is a colloidal form of elemental carbon. It is produced by partial combustion of oil or natural gases. The production process involves following steps.

1. Introduction of feedstock (oils, air and other additives) in a combustion chamber
2. Complete or partial oxidation
3. Water quenching

The different zones of the reactor that are used for carbon black production are shown in Figure 2.3. The first step involves production of a high temperature zone using a fuel such as natural gas. The hydrocarbon is cracked in the high temperature zone after which the reaction is stopped using water quenching. The variables such as the reaction time, temperature, water quenching or no quenching control the final properties of carbon black particles (such as surface area and structure). Small reaction time and a high temperature results in a high structure and a smaller particle size for carbon black particle produced. High surface area and structure carbon black such as Printex-XE2 are produced using a shell gasification process. A controlled partial oxidation of heavy oil results into a gas and a carbon black product (Printex-XE2). The smallest individual building block formed is called as a particle as shown in the small circle in Figure 2.4. Clusters of these particles fuse together to form aggregates. These primary aggregates flocculate together to form larger secondary agglomerates. These agglomerates are held together by Van der Waals forces of attraction. The detailed morphology of carbon black is defined as the structure of the filler aggregate. To be completely defined, it is necessary to know the range of the sizes and shapes of the filler. ASTM D-2414, explains how the Dibutyl-Phthalate (DBP) oil absorption test measures the amount of DBP absorbed on 100g of carbon black. The resulting oil absorption number (OAN) or Dibutyl-Phthalate absorption number is used as a measure of filler structure. These tests involve measuring the absorption of oil by the carbon black and they indicate the internal void volume present in both the primary and secondary aggregate structure.

---

When carbon black is mixed with rubber in a mill, the aggregate is damaged by shear forces and is reduced in size and structure. To estimate this breakdown, a test called the crushed oil absorption test is done. Here the carbon black is first crushed in a press and its structure is again measured using Dibutyl-Phthalate oil absorption. This test produces a crushed oil absorption number (COAN).

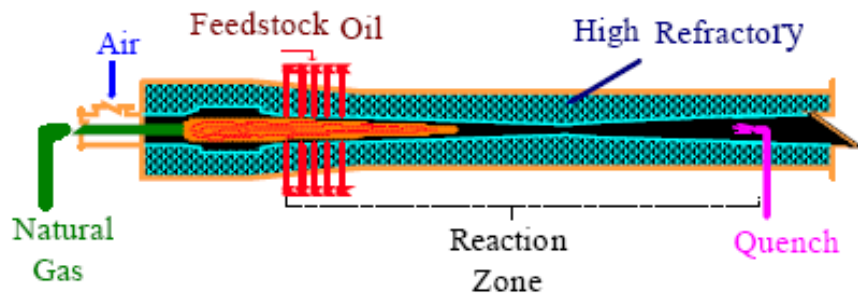


**Figure 2.3** Scheme of different zones of a carbon black reactor.

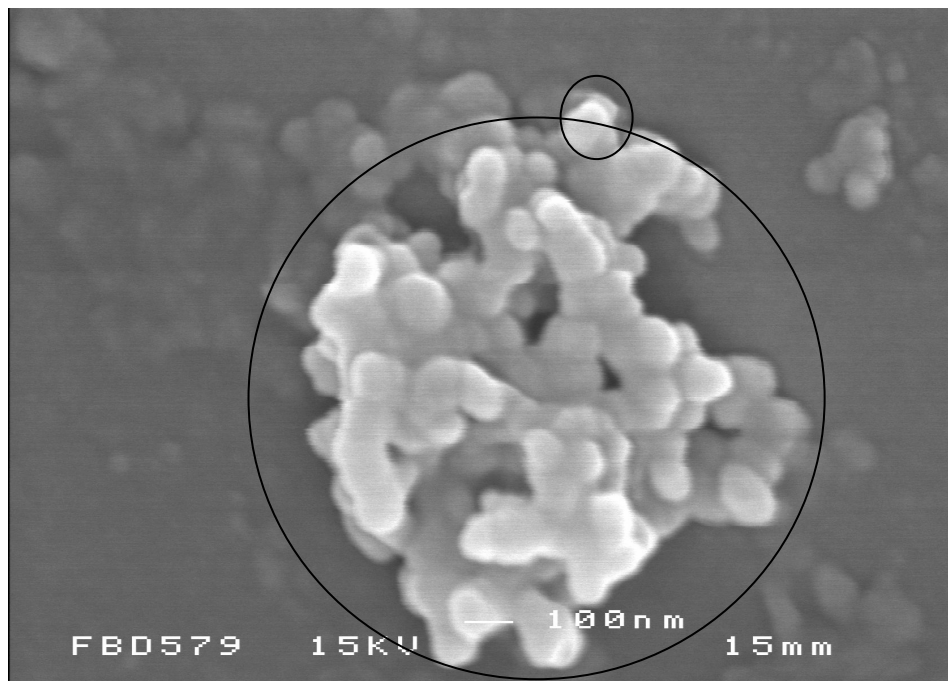


**Figure 2.4** Carbon black aggregate showing the primary particle: (small circle) and aggregate: (larger circle).

---

Another carbon black characterisation technique is the nitrogen surface area (NSA) test. The surface area of the solid is determined by measuring the volume of nitrogen adsorbed on the filler surface. The Brunauer, Emmett and Teller (1938) model for multilayer adsorption is used to calculate the nitrogen surface area, which is the total external surface of the filler.

A further test used to characterise the carbon black is the statistical thickness surface area (STSA) test: This technique measures the surface area of carbon black particle excluding micropores. This is also an absorption test, but using a higher viscosity materials such as hexadecyltrimethyl ammonium bromide. This is too viscous to penetrate the smallest micropores. The resulting measured surface area is called CTAB. It provides a good measure of the area available to the rubber material.

### **2.2.2 Particles aggregate and agglomerate**

The average particle sizes of carbon blacks commonly available for industrial use; range from 10nm to 500nm. In the rubber industry the distribution of particle sizes is considered to be important as it affects the mechanical properties and performance. Aggregate size also varies with particle size. Aggregates can have any shape or morphology. The generally encountered shapes are incomplete spheres having very long dimensions. Herd *et al.* (1991) have classified carbon blacks in four different categories as shown in Figure 2.5. The aggregates that have a high structure have a higher degree of branching and chain like structures as shown in Figure 2.5. Figure 2.4 shows the particle aggregate and agglomerate. The aggregates tend coalesce to form agglomerates. The degree of agglomeration affects the final properties of the filled elastomer. Carbon black fillers such as MT N990 and HAF N330 with low surface area and shape factor show a low tendency to agglomerate. Where as, carbon black filler such as Printex-XE2 with high surface area and shape factor shows a high tendency of agglomeration.

---

### 2.2.3 Nomenclature

The D 24 ASTM standard defines the nomenclature of different carbon blacks. It consists of a prefix letter followed by a three digit number. The prefix indicates the type of cure with N designated for normal and S for slow. The first digit indicates the mean particle diameter. For example N330 means normal curing material black has a primary particle size of 26-30 nanometre. The last two digits have been assigned as new products are developed.

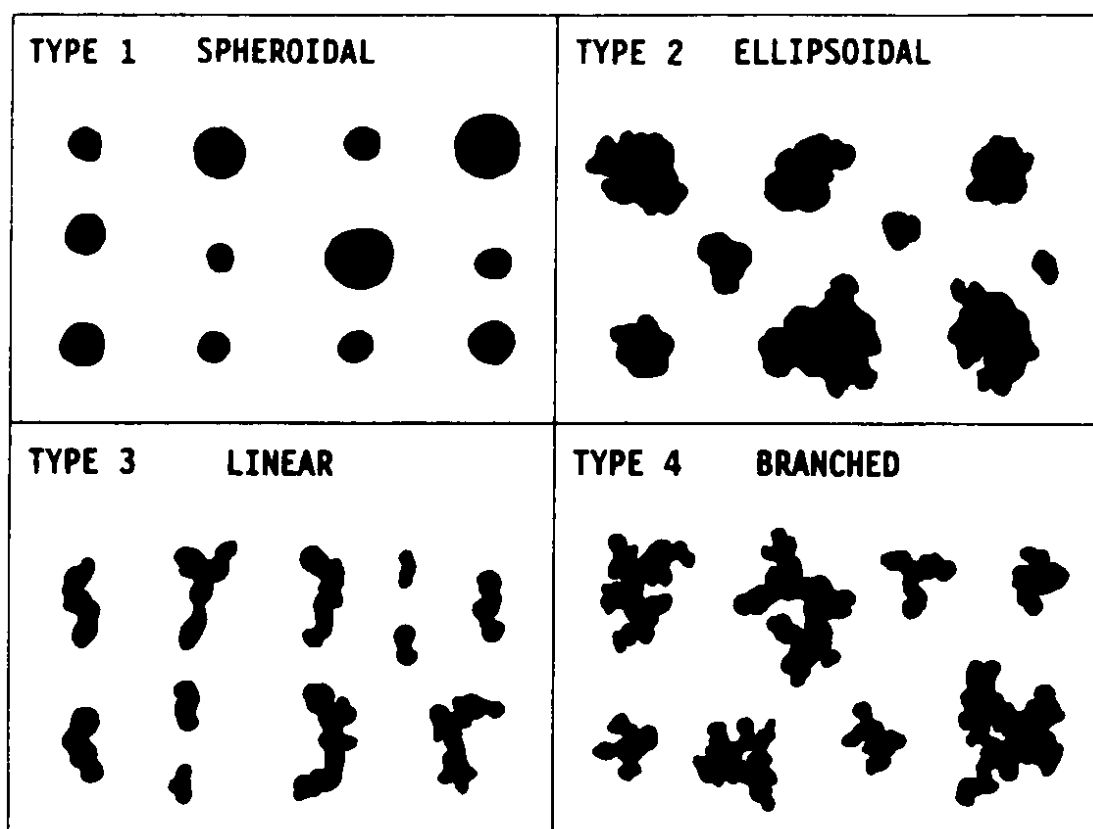


**Figure 2.5** Shape categories for carbon black aggregates, (Herd *et al.*, 1991).

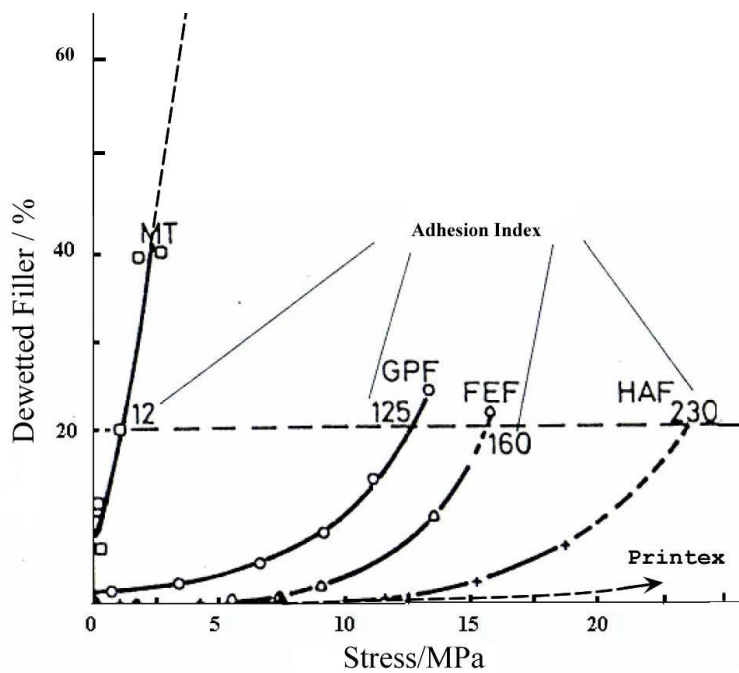


**Figure 2.6** Adhesion index for range of fillers, (adapted from Hess *et al.*, 1967).

## 2.3 Filled elastomer

### 2.3.1 Effect of carbon black on elastomer.

The fundamental property of the filler used in a filled elastomer is the particle size. This affects the reinforcement of elastomer most strongly. The particle size of carbon black particles varies from 10-500nm.

**Table 2.1** Effect of particle size on reinforcement (Donnet & Voet, 1976).

Size / nm	Strength
1000-5000	Small reinforcement
<1000	Medium reinforcement
<100	Strongest reinforcement

---

One of the sources of reinforcement between the carbon black surface and the rubber matrix is the Van Der Waals force attraction. Also, rubber chains are grafted onto the carbon black surface by covalent bonds. The interaction is caused by a reaction between the functional group at the carbon black particle surface and free radicals on polymer chains. Hence, filler-rubber interface is made up of complex physical-chemical interaction. The adhesion at the rubber-filler interface also affects the reinforcement of rubber. Hess *et al.* (1967) worked with SBR (Styrene Butadiene Rubber) filled with different grades of carbon black. They found that small reinforcing particles had a greater adhesion between the filler and the rubber. The degree of adhesion was measured using an adhesion index. Thin cross-sections of filled rubber were observed using transmission electron microscopy. The thin layer of sample was stressed and changes at the filler rubber interface were observed. The adhesion index was calculated by measuring the percentage of the filler interface that dewets from the rubber matrix under strain. The stress required to dewet an arbitrary 20% of carbon black from the rubber matrix was defined as the adhesion index. They found out that the small reinforcing particles had a greater adhesion between the filler and the rubber as shown in Figure 2.6. Conversely, larger particle sized fillers have a lower adhesion index. So MT (N990) carbon black has a low adhesion index and HAF carbon black has a high adhesion index. As the larger particle sized MT carbon black fillers do not adhere as well to rubber matrix they are considered as non reinforcing carbon black. Smaller sized HAF carbon black adhere well to the rubber and hence are know as reinforcing carbon black.

There are many reviews of filler reinforcement by authors such as Kraus (1976) and Leblanc (2002). The principal factors that determine the reinforcement capability are,

1. The Van der Waal forces between the carbon black and the polymer
2. The chemical crosslinks or chemisorptions of the polymer on to the filler surface due to free radical reaction between carbon atoms in the filler and in the rubber

---

### 3. The mechanical interlocking of the polymer on to the filler surface.

These result in a general model of fillers and rubber consisting of the rubber matrix, the interface and the fillers. The bulk of fillers in polymers will have three zones as shown in Figure 2.7. One common theme is that there is an immobilised 'bound' polymer layer around the filler. There has been lot of focus in determining the amount of bound rubber and how this affects the reinforcement capability. The assumption is that the interface zone is stronger in the bound rubber layer than the bulk of elastomer. Hence, a measurement of the size of the bound rubber layer will indicate the reinforcement capability. The morphology of carbon black will have some effect on the bound rubber layer. One possibility being that some portion of the rubber is completely interlocked onto the filler indicating an increase in the effective filler volume fraction of rubber. Regardless of the nature of the interaction between the filler surface and polymer, the bound rubber layer should be a measure of the surface activity. At fixed and practical volume fractions of carbon black the bound rubber content increases with an increase in the surface area of the carbon black. This is related to the difference in interfacial area in the compound between different grades of carbon black. With regard to the surface activity of carbon blacks, meaningful information can only be obtained by a comparison of the bound rubber per unit surface. By normalizing the bound rubber content with the interfacial area in the compound, Dannenberg (1986) showed a decrease in bound rubber per unit surface with decreasing particle size of the carbon blacks for SBR compounds filled with 50 phr of carbon black. Wolff *et al.* (1991) reached the same conclusion with different volume fraction of carbon black as shown in Figure 2.9

#### **2.3.2 Bound rubber**

When an uncured but well dispersed filled elastomer is subjected to solvent extraction, not all of the elastomer is recovered. The portion of elastomer which is not extracted is called the bound rubber. The bound rubber layer results from a complex combination of physical adsorption, chemi-adsorption and mechanical interlocking. The surface activity of carbon black is related to the bound rubber. Dessewefy (1962),

---

Kaufman *et al.* (1971), Brien *et al.* (1976), Dannenberg (1986), Wolff *et al.* (1991) and Wolff (1996) have investigated the existence of the bound rubber layer and studied its characteristics. Dessewefy (1962), Dannenberg (1986) and Wolff (1996) measured the bound rubber content using NMR and the thickness of the bound rubber layer was found to be 0.5-5nm. Heinrich and Vilgis (1995) and Zhang *et al.* (2001) suggested a mechanical coupling between polymer matrix and filler is due to adsorption of polymer chains on to the filler surface.

Kaufman *et al.* (1971) studied the bound rubber layer in a filled cis-polybutadiene and an ethylene propylene diene terpolymer (EPDM). They demonstrated the existence of two distinct layers of different mobility around the filler. The inner immobilized layer immediately surrounding the filler. The outer layer of bound rubber displays the mobility intermediate to the inner immobilized layer and pure gum rubber. Brien *et al.* (1976) used NMR to study the interaction of carbon black filler and cis-polybutadiene. They supported the investigations of Kaufman *et al.* (1971) regarding the inner immobilized layer and outer more mobile layer around the filler. Further, they suggested that the inner layer accounts for only a fifth of the total bound rubber layer.

Wolff *et al.* (1991) and Danneburg (1986) measured the bound rubber layer for SBR filled with carbon black shown in Figure 2.8 and Figure 2.9. They found at a constant carbon black volume fraction the bound rubber increases as the surface area of carbon black increases. Kraus (1976) suggested that the bound rubber layer can only be used as criteria to compare fillers of similar morphologies. The general idea being that the degree of reinforcement depends on a specific surface area and degree of structure.

### **2.3.3 Occluded rubber**

Some of the polymer in a filled rubber is totally shielded by the primary aggregate structure. This would increase the effective filler volume fraction of a filled elastomer. In case of the bound rubber layer, the elastomer chains in the vicinity of filler are restricted from molecular motion. However, in the case of occluded rubber



---

there no reduction in the chain mobility of the rubber. The occluded rubber increases the contribution arising due to filler. Kraus (1971) and Medalia (1970) have discussed the contribution due to occluded rubber. They suggested that fillers with high surface area would have a greater amount of occluded rubber. Conversely, fillers with low surface would have lower amount of occluded rubber.

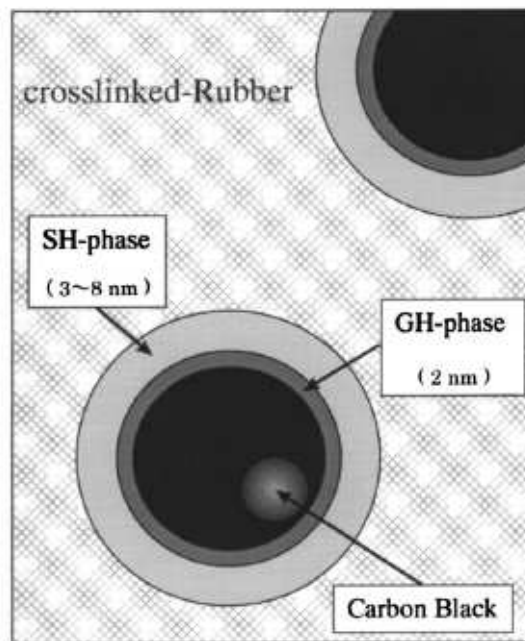


**Figure 2.7** Glassy bound rubber (GH phase) and sticky layer (SH-phase) model proposed by Fukahori (2007).

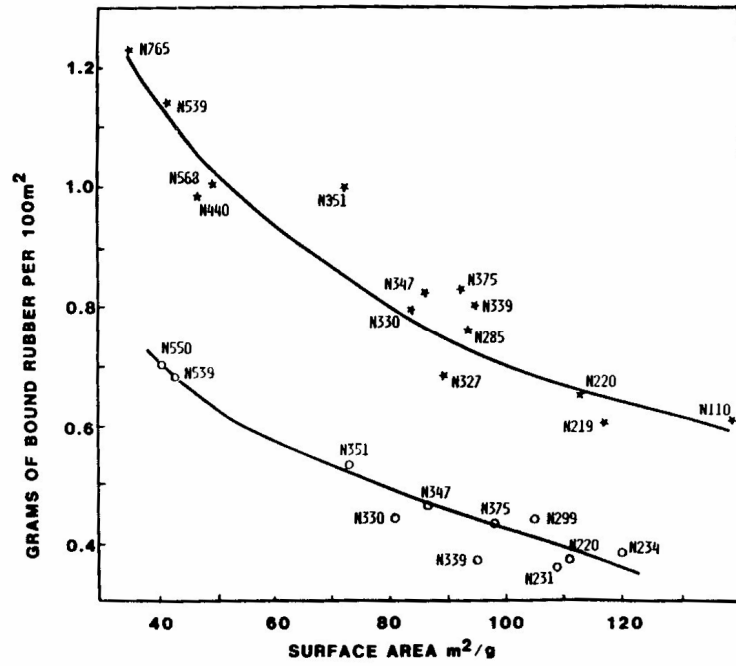


**Figure 2.8** Variation in amount of bound rubber vs. surface area for different fillers, (Dannenberg, 1986).

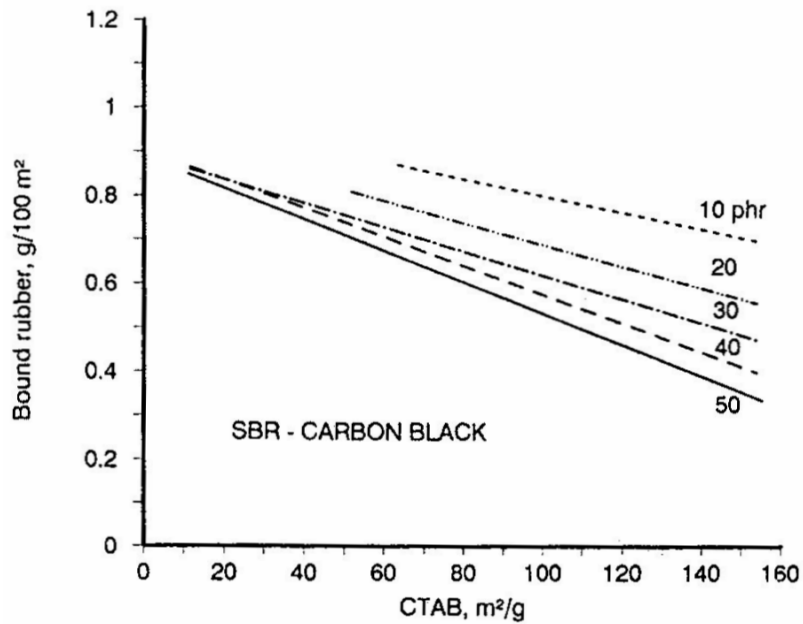


**Figure 2.9** Graph showing the bound rubber vs. CTAB surface area for SBR filled with carbon black, (Wolff *et al.*, 1991).

---

## 2.4 Theories on filled elastomer

### 2.4.1 Stored energy function:

The statistical theory of rubber elasticity utilises thermodynamic concepts to derive the relationship between stress and strain. The stress rises as the entropy of the system changes the order of system. In this case the order or disorder of system is related to the extension of the molecular chains. In an un-stretched elastomer, the disordered single chain is like a random coil. As the elastomer is stretched it starts aligning with other chains and the structure becomes more ordered as a result the entropy of the system decreases (Treloar, 1943). Using this assumption the following Neo-Hookean (sometime also know as the Gaussian or statically theory) stored energy function was derived,

$$W = \frac{1}{2} G (\lambda_1^2 + \lambda_2^2 + \lambda_3^2 - 3) \quad \text{Equation 2.1}$$

$$W = \frac{G}{2} (I_1 - 3) \quad \text{Equation 2.2}$$

Where  $I_1$  is the strain invariant;  $\lambda_1$ ,  $\lambda_2$  and  $\lambda_3$  are the extension ratios in  $\bar{x}$ ,  $\bar{y}$  and  $\bar{z}$  co-ordinates respectively. The term  $G$ , the elastic constant, in above expressing can be calculated as,

$$G = N \mathbf{k}_b T = \frac{\rho_r R T}{M_c} \quad \text{Equation 2.3}$$

Where  $N$  is number of chains per unit volume,  $\mathbf{k}_b$  is the Boltzmann constant,  $T$  is Temperature,  $M_c$  is average molar mass of the chain length between crosslinks,  $\rho_r$  is the density of the rubber, and  $R$  is the gas constant per mole. The Neo Hookean stored energy function is applicable at low strains for unfilled materials in tension up to 100% (Gent, 1992).

---

Mooney (1940) proposed the following stored energy function,

$$W = C_1(I_1-3) + C_2(I_2-3). \quad \text{Equation 2.4}$$

Where,  $I_1 = \lambda_1^2 + \lambda_2^2 + \lambda_3^2$  and  $I_2 = \lambda_1^2\lambda_2^2 + \lambda_2^2\lambda_3^2 + \lambda_3^2\lambda_1^2$  are strains invariants defined on assumption that rubber is isotropic and volume remains same. Using Rivlin's (1956) approach the derivatives of the stored energy function can be used to deduce the stress as,

$$\sigma = \left(2C_1 + \frac{2C_2}{\lambda}\right) \left(\lambda - \frac{1}{\lambda^2}\right) \quad \text{Equation 2.5}$$

If the  $C_2$  term is assumed to be zero then Equation 2.5 reduces to the statistical theory. So  $C_2$  can provide the deviation from the ideal Gaussian behaviour. If the filler is dispersed in a rubber matrix, then the filler the strain is greater than global applied strain. Mooney stored energy function does not predict the upsweep observed in the actual rubbers at larger strains.

Gent (1996) derived a SEF from empirical considerations,

$$W = -\frac{E}{6} I_m \ln \left[ 1 - \left( \frac{I_1}{I_m} \right) \right] \quad \text{Equation 2.6}$$

In the above expression  $E$  represents the low strain tensile modulus and  $I_m$  introduces a finite extensibility asymptote for the larger strain behaviour. Gent's SEF is applicable to larger strains, giving a good fit at higher extension ratios and can be used in any deformation mode. This allows flexibility in terms of representing the behaviour of an elastomer over a range of strains as shown in Figure 2.10.

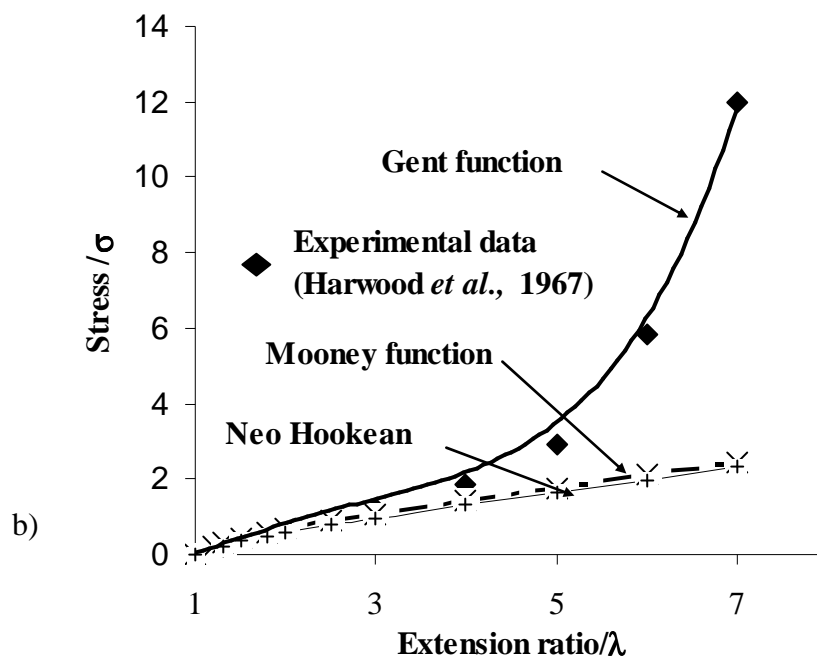
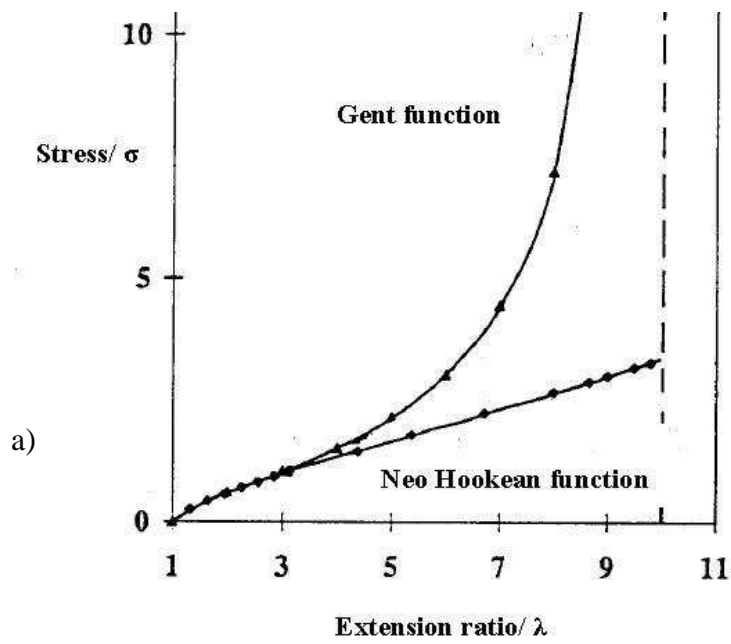


**Figure 2.10** Comparisons of prediction from a) Gent and Neo Hookean stored function (Gent, 1996) b) Neo- Hookean, Mooney and Gent stored energy function.

---

## 2.4.2 Hydrodynamic Theory

Rigid fillers typically increase the stiffness of an elastomeric material. A theory for the stiffening of elastomers by a rigid fillers is based on the Einstein's theory (Einstein, 1906, 1911) for the increase in viscosity of a suspension due to the presence of spherical colloidal particles.

$$\eta = \eta_0(1 + 2.5\phi) \quad \text{Equation 2.7}$$

where,  $\eta$  is the viscosity of suspension,  $\eta_0$  is the viscosity of the incompressible fluid and  $\phi$  is the volume fraction of the spherical particles.

Guth and Gold (1938) adapted the viscosity law to predict the small strain modulus of an elastomer filled with a rigid spherical particles and they included an additional term to account for the interaction of fillers at larger filler volume fractions. They proposed that the increase in the modulus due to the incorporation of spherical fillers was given by,

$$E = E_0(1 + 2.5\phi + 14.1\phi^2) \quad \text{Equation 2.8}$$

Where,  $E$  is the modulus of the filled rubber,  $E_0$  is the modulus of the unfilled rubber and  $\phi$  is the filler volume fraction. This relation assumes that the filler particles are spherical, well dispersed throughout the matrix, and that each is fully coated in rubber. These assumptions do not represent a realistic rubber-filler composite, as the fillers are not typically just spherical in shape and they tend to agglomerate. As a result, Guth (1945) derived another Equation where the filler particles are considered to have a representative average aspect ratio  $f$  defined as the ratio of its longest length to its perpendicular breadth.

$$E = E_0(1 + 0.67f\phi + 1.62f^2\phi^2) \quad \text{Equation 2.9}$$

---

Filled rubbers show a decrease in the modulus with strain. At strains less than 10% this modulus reduction is attributed to the breakdown of the filler aggregate structure (Payne, 1962). At medium to large strains (100-600%) the changes in the structure with strain are not clear. It is agreed, that the presence of rigid fillers, results in the local strains which is greater than globally applied strains. This effect is referred to as strain amplification. The strain amplification effect increases with increased volume fraction and structure of the carbon black.

### 2.4.3 Strain Amplification

The Guth and Gold relation is inappropriate at higher strains. As the polymer chains no longer behave in a Gaussian manner. Mullins and Tobin (1965), Blanchard and Parkinson (1948) and Bueche (1960) have suggested modifications to hydrodynamic model. Mullins and Tobin's derived the following relationship for the average strain in the matrix rubber based on Guth and Gold's Equation 2.8,

$$\lambda = \lambda(1 + 2.5\phi + 14.1\phi^2) \quad \text{Equation 2.10}$$

Where  $\lambda$  is the global extension ratio and  $\phi$  is the filler volume fraction. This Equation is only valid up to a moderate strains of 20-50% and only for MT carbon black. In case of other carbon blacks having higher structure the amount of occluded rubber shielded by the filler is greater, thus increasing the effective filler volume fraction.

### 2.4.4 Blanchard and Parkinson model of weak and strong linkage

Blanchard and Parkinson (1948) proposed a different view that the filled rubber could be considered to be made of strong and weak linkages as shown in the Figure 2.11. The weak linkage would fail before the strong linkage under stress. This progressive failure of the weak linkages can be used to explain cyclic stress softening or the Mullins effect. Under cyclic loading the softening depends upon the maximum stress applied. Blanchard and Parkinson suggested that different stresses, causes different weak linkages to break and contribute to softening. The Blanchard and Parkinson

---

model presumes that the increase in modulus is only due to increased linkages.

Blanchard and Parkinson (1952) also explained the increasing tear strength in rubber using their model of weak and strong linkage. They suggested that when a rubber is strained the short linkages are tightened and the polymer chains align along the direction in which stress is applied. Molecular chains can slip around the filler and align in the direction of the applied stress. These factors would increase tear strength in a filled rubber as slippage of molecular chains would distribute stress.

#### **2.4.5 The Bueche model**

Bueche (1961, 1965) suggested that for a filled rubber, the fillers are connected with the molecular network chains. These molecular chains connecting different fillers are the source of the filler reinforcement. Therefore, filled rubber is stiffer than unfilled rubber. These molecular chains also break under a load and thus results in cyclic stress softening. During cyclic loading the chains broken during the first cycle no longer contribute to the stiffness of elastomer during successive cycles. Bueche suggested that some of molecular chains can reform to create new links between neighbouring fillers.,But the net result is that the filled rubber is stiffer than the unfilled rubber. According to the Bueche model, the increase in strength is attributed to the filler particles acting effectively as a means of distributing the load more equitably. The breakage of a single chain between particles does not cause stress to be transferred to relatively few adjacent chains. (This is usually the case for unfilled rubbers where it results in failure). The stress is distributed to much larger number of chains attached to filler particles. Except for the emphasis on chain breakage and omission of chain alignment Bueche reinforcement process are similar to molecular-slippage model.



## 2.4.6 Dannenberg model of slippage at interface

Dannenberg (1966) proposed a model of filler reinforcement which includes slippage at the interface between the molecular chains and the filler. Slippage of the molecular chains under strain also redistributes the stress. The redistribution of stress again inhibits a molecular rupture. The model suggested that the hysteresis observed can be attributed to the loss of the strain energy as frictional heat occurring during the relative motion between molecular chains and the filler.

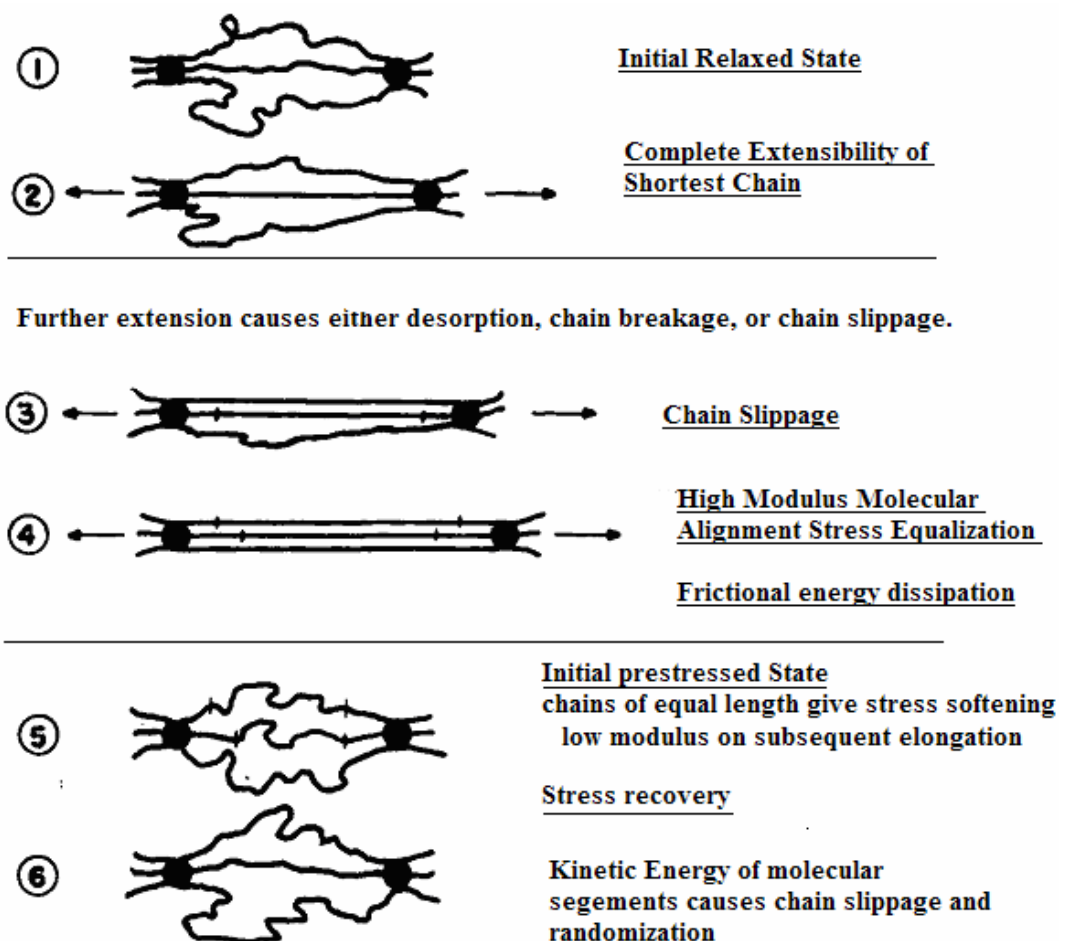


**Figure 2.11** Proposed changes in the microstructure of a filled rubber system under strain, (Dannenberg, 1966).

---

## **2.5 Finite Element Analysis**

### **2.5.1 Introduction**

Finite element analysis (FEA) is the numerical simulation of the behaviour of components acquired by discretising them into a finite number of building blocks, so called elements and analysing their behaviour whilst verifying their acceptability and reliability.

FEM (finite element modelling) or FEA (finite element analysis) were started with the intention of prototyping, design validation, design optimisation, identifying failure and estimating fatigue life. FEA finds its application in all the fields of engineering such as automotive, aerospace and marine engineering, as well as fluid mechanics, electrical appliances and for product design. Over the last few decades improvements in the computing including increases in processor speed, data storage capacity coupled with a reduction in the cost of the computer hardware and easy access to the various software has lead to the use FEA in many fields of research and the field of elastomer reinforcement is no exception. FEA uses the process of subdividing all systems into their individual components or ‘elements’ whose behaviour is readily understood. These individual subsystems are then used in rebuilding the original system to study its behaviour. This process of disintegrating the original system into finite number of well defined subsystems is know as discretisation.

FEA is a mathematical means of solving a complex problem with the help of a generalised theory developed for a material, which can be utilised in the FEA model for simulating the actual material behaviour. The actual loading conditions are simulated by applying appropriate boundary conditions. FEA involves developing the actual component as a simulation. This is achieved by representing the simulated model by a set of elements. Nodes are the points where two or more elements meet. A mesh is defined by the grid of the nodes and the elements. The way the FEA solver produces results is by solving a number simultaneous equation to represent the

---

material behaviour, based on a generalised theory. As the complexity of the structure increases the number of conditions or simultaneous equation also increases. This approach works well for small structures, but real life components are more complex. With an increase in the processing speed this so called “matrix method” can now also be used to solve complex structural problems.

It is possible in many problems to make approximations that facilitate the use of finite element modelling and reduce solution time. If the geometry and loads of a problem can be completely described in one plane, then the problem can be modelled as two-dimensional. Bodies which are long and whose geometry and loading do not vary significantly in the longitudinal direction can be modelled by using a plane strain representation. Similarly, bodies that have negligible dimensions in one direction, and are loaded in the plane of the body, can be assumed to be in a plane stress condition. In the FEA problems where geometrical approximation is not possible a full three-dimensional model of the structure is needed. However, in many analyses it is still possible to limit the size of the model by taking advantage of any symmetry that exists. There are four types of symmetry commonly encountered in engineering problems axial, planar, cyclic and repetitive.

Problems solved using FEA techniques are based on the concept of the discrete system where there are a finite numbers of subsystem (or equation) are to be handled. As discussed, a system of elements and nodes is used to represent a physical problem depending on the material and its behaviour under loading. There is a relationship relating the force acting at each node and the other variables such as displacement.

$$f_n = k_c * d_n + f_d + f \quad \text{Equation 2.11}$$

Where  $f_n$  is the component force in the three principal direction at any given node and  $d_n$  is corresponding displacement,  $k_c$  is stiffness of the material (representing the characteristic material),  $f_d$  is the distributed load acting at a node and  $f$  any other constraint acting at a node.

---

The FEA solver assumes the forces acting on a system to be a matrix and the corresponding displacement as another matrix. For example, in Equation 2.12 shown  $[F_m]$  and  $[D_n]$  represent the matrix of forces and displacements acting on a system.

$$[F_m] = [K_c] * [D_n] + [F_d] + [F_{an}] \quad \text{Equation 2.12}$$

Where,  $[K_c]$  is called the stiffness matrix. Further,  $[F_d]$  is the total distributed load at all the nodes and  $[F_{an}]$  can represent other constraints such as temperature.

### **2.5.2 Assembly Processes:**

In order to solve an FEA problem we need to assemble the stiffness matrix and assume that compatibility of the displacements exists at all nodes and that equilibrium exists throughout the model. The building of a model begins with the elements. For an FEA solver, the equations initially assume the displacements at the nodes as unknown. The structural problem is submitted to a solver such as ABAQUS. The final internal forces calculated in an element depending upon the material behaviour as defined by the user. This approach is common to all FEA problems.

### **2.5.3 General theory of problem solving**

The solver receives the problem as system of matrices which must be solved for example, for force if all the displacements are entered as the boundary conditions. These equations are solved by the processor following the following process

*Step1.* The material parameters describing the material behaviours must be determined. In case of ABAQUS solver and elastomeric materials this can be entered as coefficients of the stored energy function used for describing the material behaviour. The FEA solver then determines the stiffness matrix based upon the spatial distribution and the material behaviour and the corresponding nodal loads at each element (Equation 2.12).

---

*Step2.* Then processor determines the assembly equation.

*Step3.* The prescribed boundary conditions are built into the assembled matrix.

*Step4.* The processor then solves these sets of simultaneous equations to give a unique solution.

*Step5.* Then output obtained is converted to a useful form like engineering stress depending on the requirement using standard relationships.

#### **2.5.4 Analysis in ABAQUS**

In this thesis Abaqus is used to solve the microstructural models. In Abaqus the input deck is made up of five sections:

*Header.* This part is made up of personal statements which indicate the problem definition, type of analysis and the format of output.

*Geometry.* This section gives information about the spatial arrangement of the nodes and elements in 3D space; this can be a result of a model made using any CAE software.

*Material Definition.* Hyper-elastic material definition is used to describe the mechanical behaviour of an elastomer using a suitable stored energy function. The fillers can be either elastic or rigid.

*Boundary Conditions.* The boundary conditions describe the loading and symmetry. Care must be taken to ensure these boundary conditions are correct, especially in cases where representative geometry or symmetry constraints are used.

*Step Definition.* Defines the type of analysis and the actual loading conditions.

---

## 2.6 Modelling

### 2.6.1 Numerical and molecular dynamics approaches to modelling.

Mathematical models, molecular dynamics simulations and finite elements analysis have been extensively used to model and study the behaviour of filled rubber composites. Sen *et al.* (2005), Kloczkowski *et al.* (1994), Sharaf *et al.* (2000) and Bicerano *et al.* (1997) all used Monte Carlo computer simulation to study and predict the properties of a filled composite. Sen *et al.* (2005) investigated the elastic properties of the polymer filled with spherical shaped fillers. They were able to verify the conformational and deformational properties of the polymer chains as a function of chain length, temperature and filler size. The effect of the occluded volume present with spherical filler particles and non-Gaussian characteristics of the molecular chains on the elastic properties of the filled networks was studied using a single chain Monte Carlo computer simulation by Kloczkowski *et al.* (1994). Sharaf *et al.* (2000) extended the work of Kloczkowski *et al.* (1994) to elliptical shaped particles placed in a cubic lattice. Bicerano *et al.* (1997) used numerical modelling and implemented a slippage model in a 2D model to calculate the stress-strain behaviour for an amorphous rubbery polymer. Slippage was controlled by the kinetic properties such as the activation energy and the activation volume. However, the simulation using a Monte Carlo algorithm for EPDM was unable to predict the observed behaviour. The deviations were attributed to limited computing time and a difficulty in the determination of an appropriate value for the activation energy. However, Sen *et al.* (2005), Kloczkowski *et al.* (1994), Sharaf *et al.* (2000) and Bicerano *et al.* (1997) all suggest that the simplifying assumptions made during the simulation needed further modification in order to improve the accuracy of prediction.

Simoes *et al.* (2005) used molecular dynamics simulations to study the mechanical and visco-elastic property of an amorphous polymeric material. They noted that at a molecular level the local stresses are often higher than the global stress. These localised points of high stress act as a source of flaw and failure initiation. Hence, the true stress in a localised area is a better predictor of failure than the globally applied

---

engineering stress. However, Simoes *et al.* (2005) concluded that their present work was insufficient to make the connection between the microscope, the meso-scale and the macro-scale behaviour of filled polymers.

Coveney *et al.* (1995) modelled a carbon black filled natural rubber composite using a standard tribo-elastic solid (STS). The standard tribo-elastic solid (STS) consisted of a leading spring, a parallel spring and a tribo-elastic assemblage (columbic frictional sliders). This STS model gave good correlation with behaviour of filled elastomer at low strains, higher damping behaviour of filled elastomer and non elliptical force deformation loops for different deformation histories. Coveney and Johnson (1999) used STS to model behaviour of NR filled with variety of carbon blacks at different loading fillers. They showed STS shows a good agreement with the experimental data for dynamic stiffness for shear strain amplitudes down to 0.01. Coveney and Johnson (2000) presented two variants of the STS model, a four parameter rate dependent tribo-elastic (RT) model and five parameter viscous modified standard tribo-elastic solid (TVS) model. The RT model included a rate dependent frictional slider in series with a tribo-elastic assemblage. A TVS model had a combination of a STS and a parallel (dashpot) Maxwell body. The RT model showed a good correlation with the dynamic stiffness and a reasonable correlation with loss angle and stress relaxation. The behaviour of TVS model was similar to the RT model. However, TVS model did not show good correlation with stress relaxation behaviour.

Kashani and Padovan (2006) used a hybrid numerical-experimental model to calculate the approximate modulus, effective filler volume fraction and local stress and strain. They showed that the mechanical properties of filled rubbers follow a spring in series model. They suggested that the rubber matrix and the fillers are in state of uniform stress rather than state of uniform strain.

Most researchers have assumed that the rubber matrix can be represented as either single or multiple polymer chains with fillers that are spherical or have a simple shape factor that models the rubber elasticity. A generalised tube model for the

---

polymer network and rigid filler clusters was proposed by Kluppel and Schramm (1999). They used this approach to model the hyperelasticity and stress softening. Breakdown of the aggregates by the applied stress causes stress softening under cyclic loading or pre-strain. Their model shows fair agreement for a filled SBR polymer and an unfilled NR in uniaxial tensile loading. The application of this model to different filler materials along with varying load condition was verified by Kluppel and Meier (2001). This model showed a reasonable correlation in uniaxial loading for SBR filled with either silica or carbon black. However, there were significant deviations for filled rubber simulation of stress softening under equi-biaxial loading.

### **2.6.2 Finite element analysis of filled composite**

Finite element analysis has been used to model the microstructural behaviour of filled rubbers by workers such as Fukahori and Seki (1993), Bergström and Boyce (1999), Van der Sluis *et al.* (2001) Hon *et al.* (2003). Bergstrom and Boyce (1999) used a range of filled rubber models to investigate the mechanical behaviour at small deformations under compressive loading conditions. They considered a range of filler shapes and mesh representation as shown in Figure 2.12a, 2.12b and 2.12c. They showed that the Young's modulus of the material can be predicted by using a FEA model having representative volume element of many filler particles. Their study compared the effect on modulus of using one (unit) filler particle model and a multiple filler particle of a same shape. They also studied effect of the area to volume ratio of the filler particle on the mechanical behaviour. The models used do not accurately represent the filler shapes used in their experiments. Axial symmetry and planar surfaces (shown in figure 2.19 and 2.20) were the boundary conditions used in their investigation as shown in Figure 2.12b and Figure 2.12c respectively. Hon *et al.* (2003) discussed the disadvantages of the plane surface boundary conditions as the stiffness prediction of the filled elastomers. They adopted a spherical shaped filler in a cubic matrix to demonstrate that plane surface boundary conditions which shows an artificial increase in the predicted stiffness due to geometrical constraints of the model. This is explored further in detail in Chapter 4. Bergström and Boyce (1999) used axi-symmetric boundary conditions with an elliptical shaped filler in a



cylindrical matrix. This model can not readily represent a repeat geometry that is packed to fill space. Use of an axi-symmetric boundary conditions in the simulated models underestimates the modulus observed under experimental conditions.

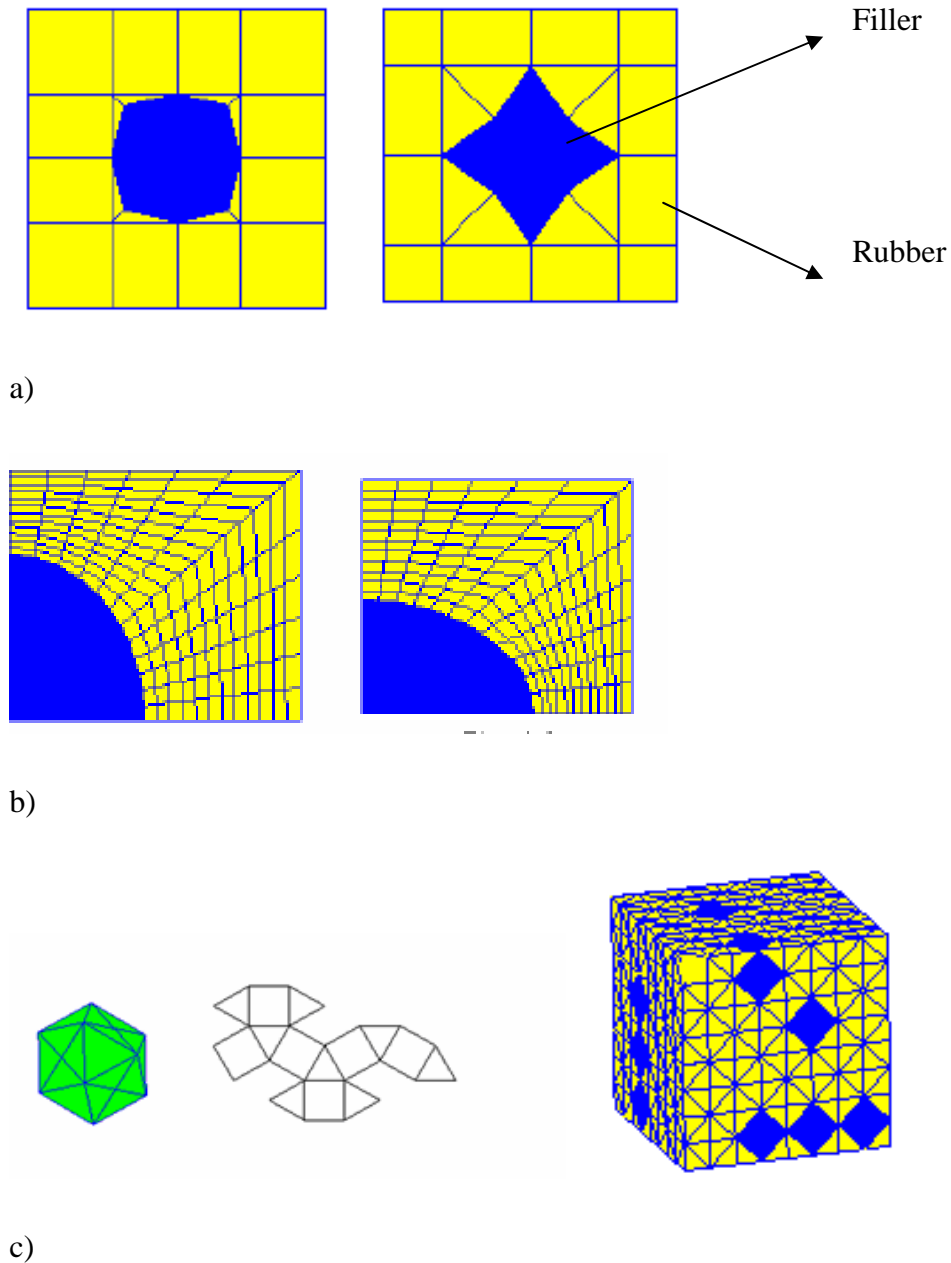


**Figure 2.12** A range of models with different shape of fillers proposed by Bergström & Boyce (1999); a) A 2D Coarse Mesh, b) A 2D elliptical shaped filler and c) A 3D cubocahedral shaped particle.

---

Hon *et al.* (2003) used a micromechanical model to predict the stiffness of a filled elastomer. They evaluated a range of 2D and 3D models to predict the stiffness of both MT and HAF filled elastomers. A simple Mooney stored energy function was used to characterise the rubber elasticity. For MT carbon black filled elastomer the models were able to predict the stiffness of the filled elastomers at low to moderate strains for filler volume fraction up to 10%. A 3D simulation of the elastomers filled with MT carbon black showed a good correlation with the Guth and Gold equation given as 2.8 (shown in section 2.4.2) and as shown in Figure 2.13. HAF carbon black (filled elastomers) was modelled as simple rod like particles in a cubic matrix. Simulation of the HAF black filled elastomers did not correlate well with the experimental data. However, they were able to study the effect of the orientation of the rod like particles in a cubic matrix. The simulations carried out in the present work are contrasted to the work carried out by Hon *et al.* (2003). Fukahori and Seki (1993) analysed the stress around a filled particle using different geometrical models. Their first model is shown in Figure 2.14; it assumed a filler particle at the centre of a cylinder. A second model shown in Figure 2.15 assumed filler particle at the centre of a cube. The first model used axial symmetric elements for the simulation of the behaviour. This model again showed a poor correlation with the experimental data. The second model shown in Figure 2.15 is similar to the model used by Hon *et al.* 2003. However, Fukahori and Seki (1993) assumed an extra layer of rubber around the filler which they referred to as a glassy layer as shown in Figure 2.7. The layer was assumed to be 1000 times stiffer than the matrix rubber. This approach can be considered to model the bound rubber layer around filler. This approach results in the modelling of the bound rubber layer as discussed in Chapter 5.

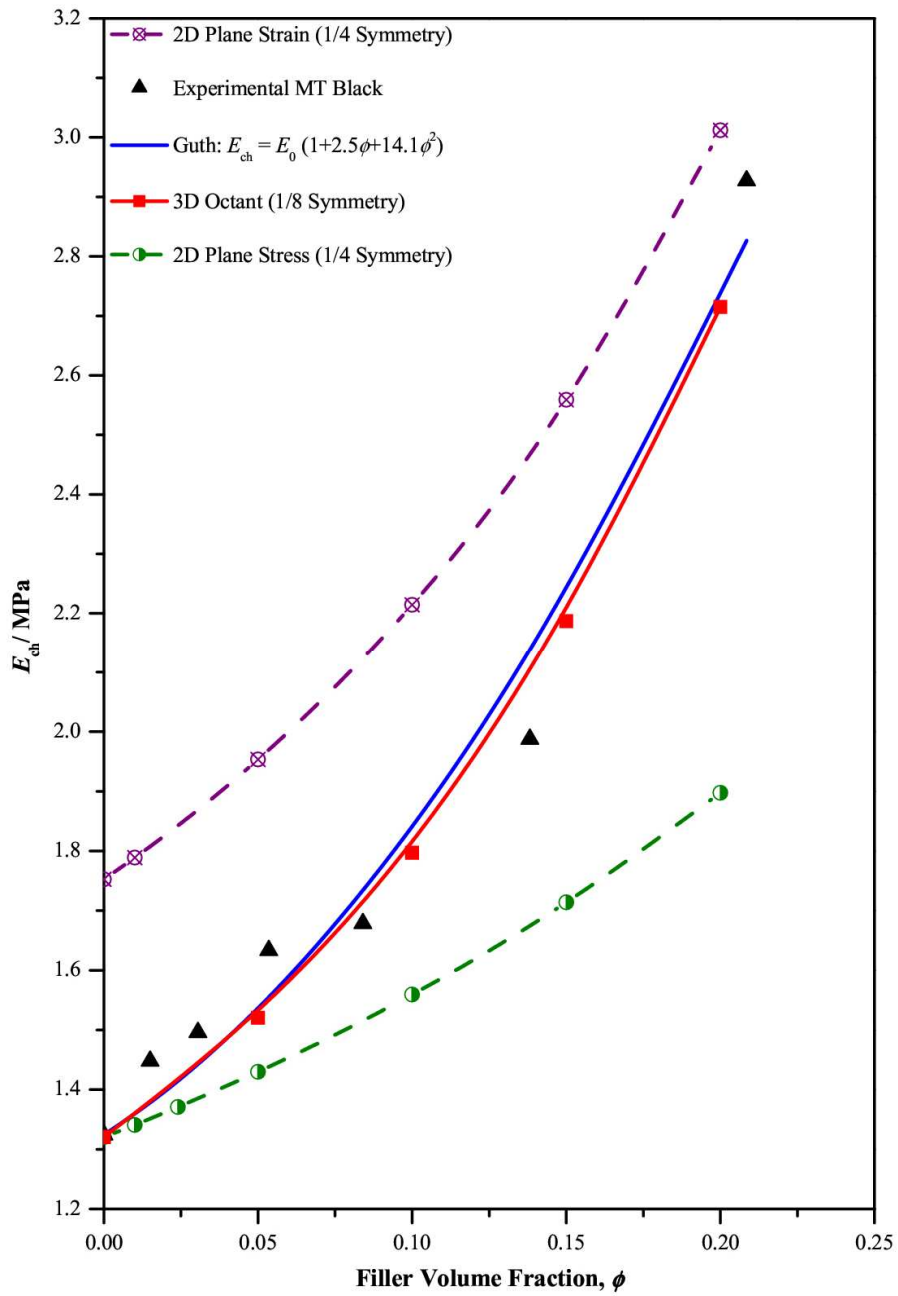


**Figure 2.13** Chord Young's modulus (Force required to strain a model is used to calculate stress and then, divided by strain to calculate the modulus) versus filler volume fraction at 2% strain for 3D octant and 2D circular filler models, Mullins & Tobin experimental results and Equation 2.8 shown as the solid blue line, (Hon *et al.*, 2003).

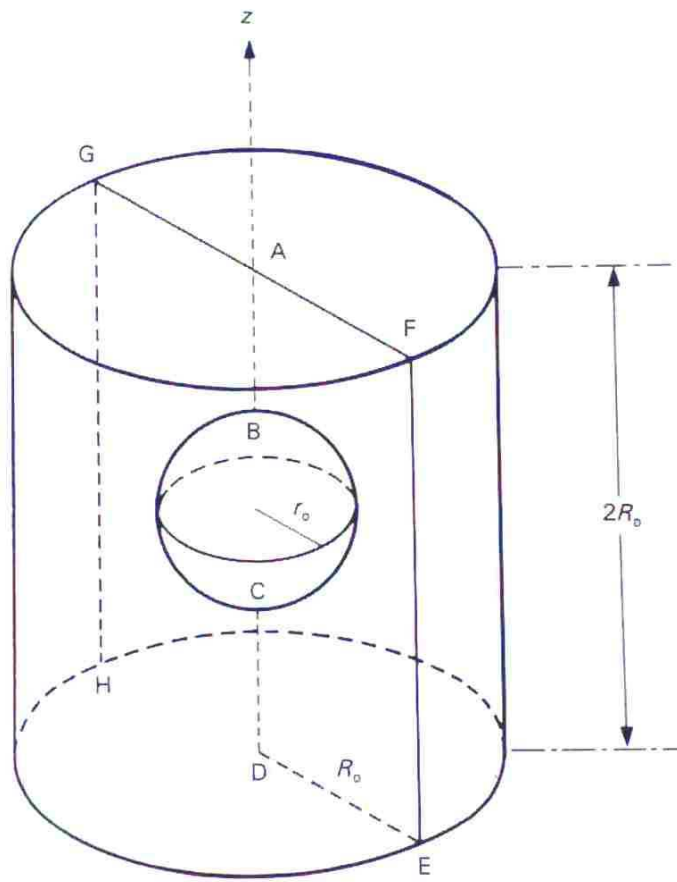


**Figure 2.14** An idealised cylindrical matrix with spherical filler particle at the center (Fukahori & Seki, 1993).

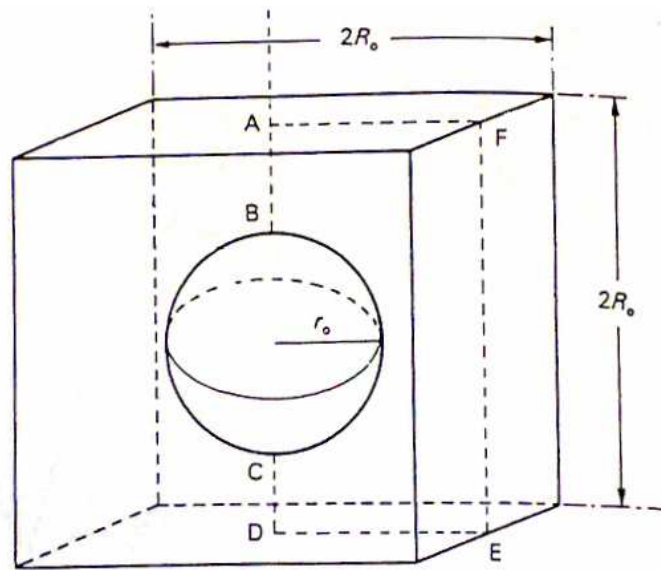


**Figure 2.15** An idealised matrix with a spherical particle at the center of a cube (Fukahori & Seki ,1993).

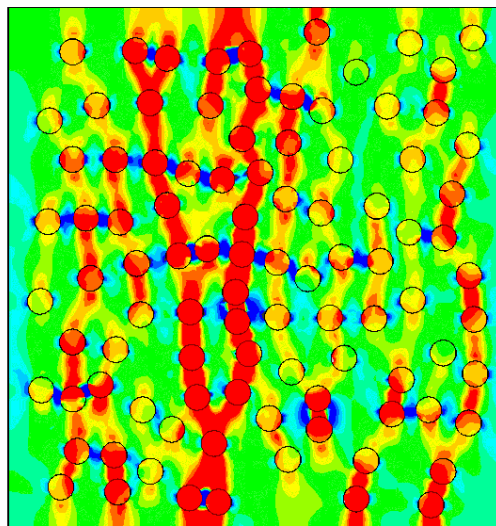


**Figure 2.16** Two-dimensional random circular models at 2% tensile strain showing maximum principal stress contour plot, (Hon, 2005).

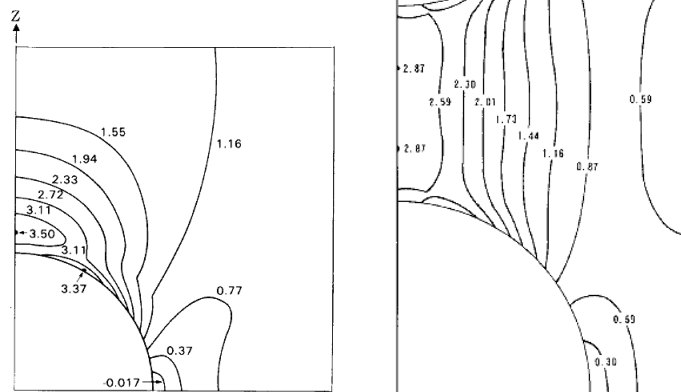


**Figure 2.17** Stress contour plots around a rigid sphere, (Fukahori & Seki, 1993).

---

Hon (2005), Smit *et al.* (2000) and Sluis *et al.* (2001) tried a range of 2D models to study the effect of the heterogeneous distribution (random distribution) of filler particle in the matrix polymer as shown in Figure 2.16, 2.18 and 2.20 respectively. As expected Hon (2005) found the 2D plane stress and plane strain models with a random distribution of the filler particles shows a significant deviation from the experimental stress versus strain behaviour and the prediction at small strains of the Guth and Gold equation shown in Equation 2.8. A model with random circular filler particles at strain 2 % is shown in Figure 2.16. Smit *et al.* (2000) used a similar 2D model to study the effect of random distribution of voids on the mechanical response. The finite element representation used for the simulation is shown in the Figure 2.18. However, the materials used as the matrix were polystyrene and polycarbonate. They found that their voids easily cavitated under hydrostatic pressure and the irregular distribution of voids promoted the spread out of plastic strains over the whole microstructure. Van der Sluis *et al.* (2001) developed a numerical homogenisation method to model mechanical behaviour of elasto-viscoplastic solids at finite strains. The materials used were a polycarbonate with rubber elastic inclusions. The typical models used are shown Figure 2.19 and 2.20. In Chapter 4 of the present work, the influence of an appropriate stored function is discussed. Sluis *et al.* (2001) also suggested a localised stress introduced by the microstructure presented problem for their proposed models. Hence, further work is needed to get a better representation of the observed microstructure. A spherical filler particle in the centre of cylindrical matrix, similar to Fukahori and Seki (1993) is shown in Figure 2.14 and Figure 2.21 shows the models used by Moshev and Kozhenikov (2002) to model a rubber composite. They tried to study the mechanism of debonding of the rubber matrix from the filler surface. They concluded natural sub microscopic imperfections were the main failure mechanism.

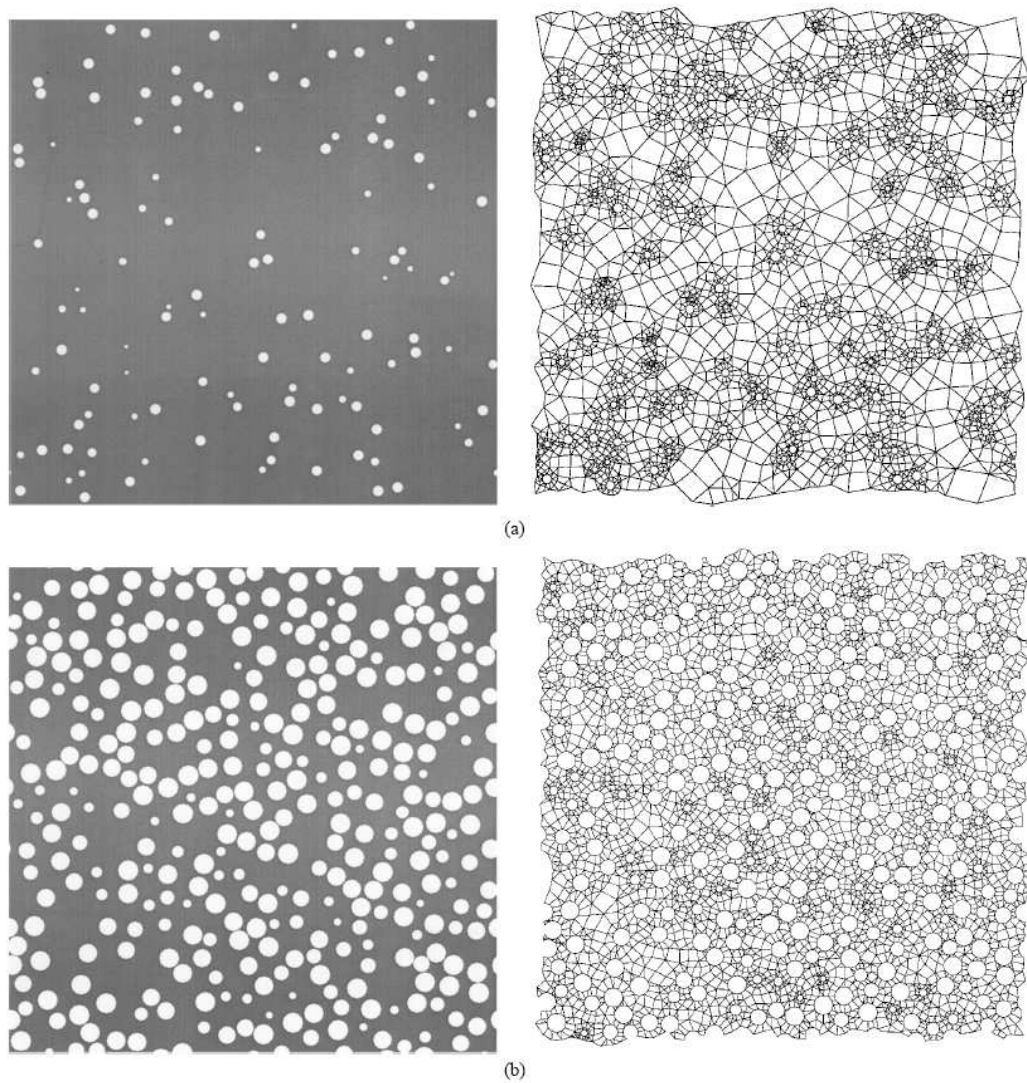


**Figure 2.18** 2D Simulation of a heterogeneous model of voids in a blended polymer for idealised cavitations or non adhering low modulus rubber particles. a) 2.5% void volume fraction b) 30% void volume fraction, (Smit *et al.*, 2000).



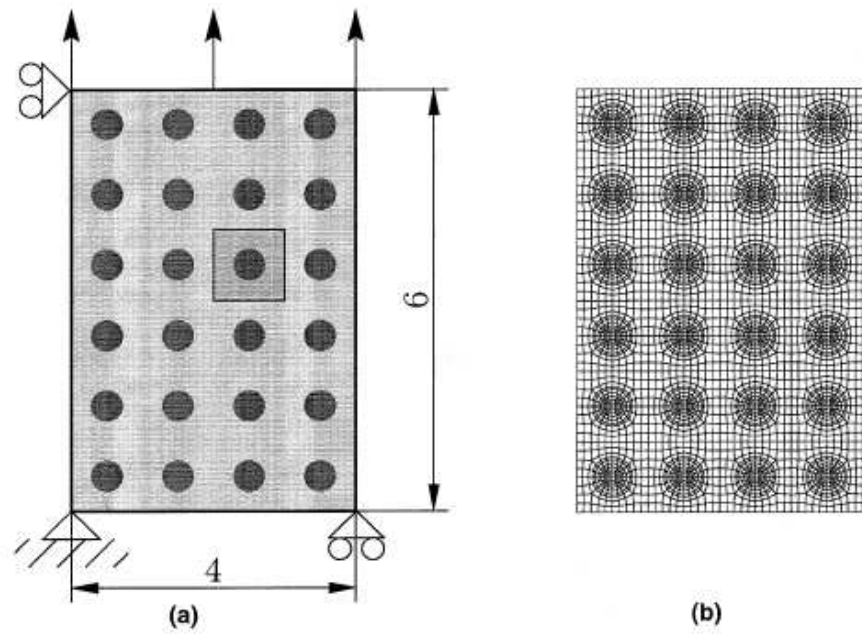


**Figure 2.19** 2D Finite element analysis representation of polycarbonate plate (2mm) with regular rubber inclusions, (Sluis *et al.*, 2001).

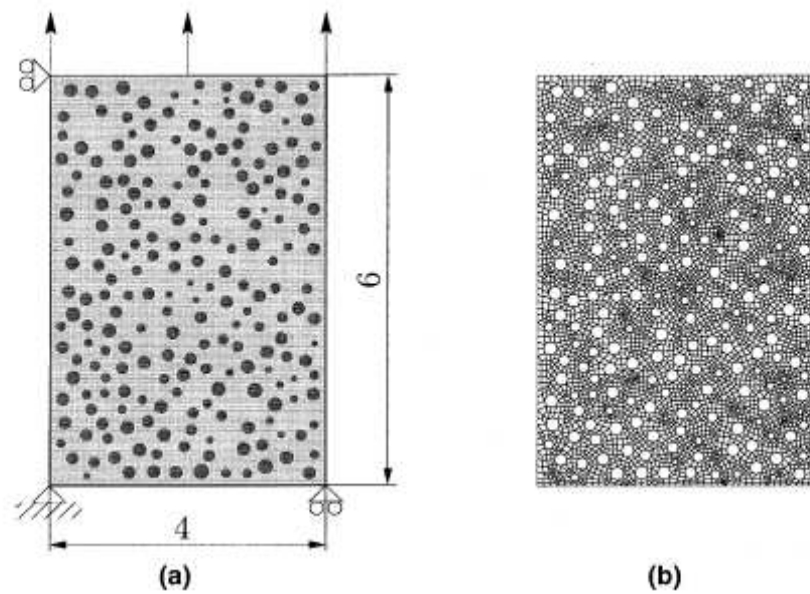


**Figure 2.20** 2D Finite element analysis representation of polycarbonate plate (1mm) with irregular rubber inclusions, (Sluis *et al.*, 2001).

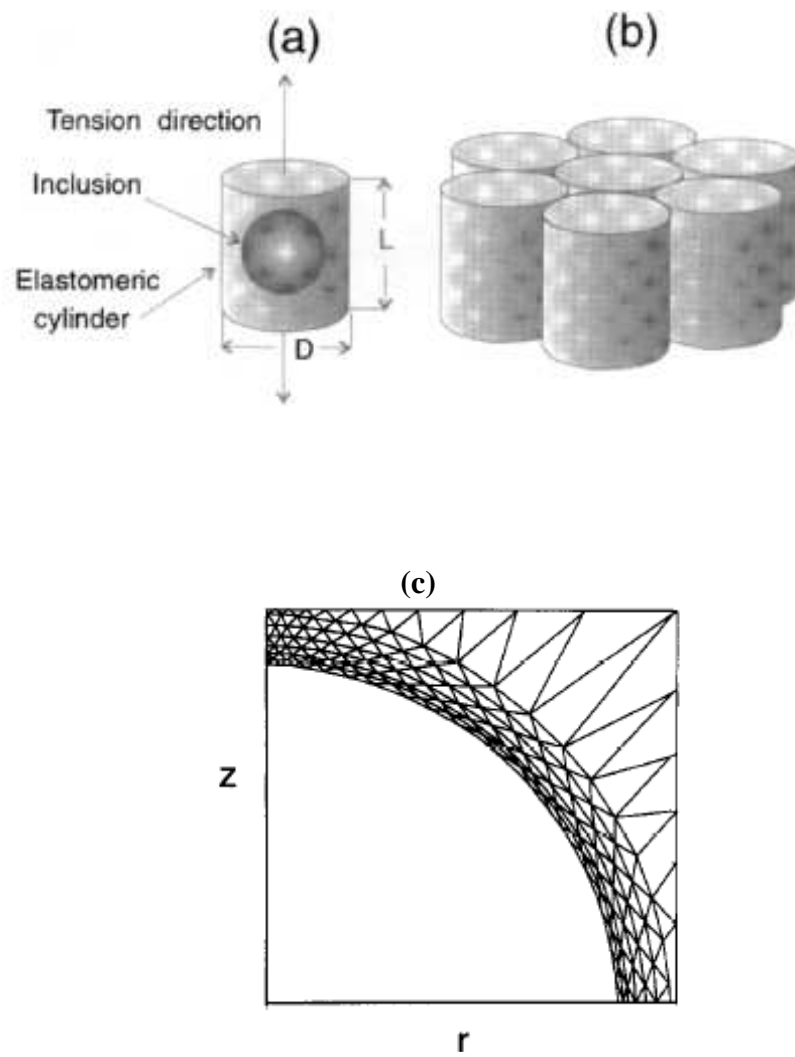


**Figure 2.21** Finite element representation adopted by Moshev & Kozhenikov (2002); a) the structural cell b) assumed packing c) Axi-symmetric finite element representation.

---

### 2.6.3 Particle morphology, filler –polymer interface and mechanical properties

Authors such as Fukahori (2007), Zhu and Sternstein (2003), Heinrich & Kluppel (2002), Wolff *et al.* (1991), Paipetis (1984), Kaufman (1971), Dannenberg (1966) and Boonstra (1967) have discussed filler-polymer interface models to explain both changes in the mechanical properties due to the stiffening on the addition of filler and the increase in cyclic stress softening. Paipetis (1984) studied the interfacial phenomena and reinforcement mechanisms in a rubber-carbon black composite. He concluded that the mechanical behaviour of a filled rubber cannot be predicted using the theories of composite mechanics. He suggested this is due to the physical and chemical interaction between the filler and the rubber resulting in very high mechanical modulus for filled rubber composite. Hence, mechanical reinforcement and dynamic effects such as cyclic stress softening observed in the case of filled rubber cannot be explained using available theories of composite mechanics. Therefore, during finite element modelling the interfacial boundary conditions should be carefully modelled. As discussed in section 2.3.2 Kaufman *et al.* (1971) demonstrated the existence of two distinct layer of different mobility around the filler. The inner immobilized layer immediately surrounding the filler. The outer layer of bound rubber displays the mobility intermediate to inner immobilized layer and pure gum rubber. Fukahori (2007) proposed a filler rubber interface model shown in Figure 2.7 in section 2.3.2. The interface consisted of two layers namely the glassy layer (GH, that extends couple of nanometres) and the sticky layer (SH, around 3-8 nanometre). Glassy layers have restricted chain mobility and increase the stresses at small strains. The sticky layer extends from the glassy layer into the polymer and contributes an increase to the stress at larger extensions. However, experiments have not yet identified any distinction between these two layers. Polymer filler interface and its interaction is a combination of the physical and chemical interaction. Dannenberg (1966) and Boonstra (1967) suggested that the rubber matrix can slide over the filler surface. If the rubber can slide over the filler than it would acts as stress distributor. Polymer chains under applied stress would distribute stress by slipping and this could avoid chain breakage. This would result in energy dissipation and increase the strength of the filled elastomer. This model was used by

---

Dannenberg to explain the hysteresis and the cyclic stress softening observed in the case of a filled elastomer. Fukahori (2007) suggested that when the sticky layer shown in Figure 2.7 is strained extensively it gets caught between the rigid particles that are in tri-axial loading conditions. As a result, this layer slides creating vacuoles in the spaces they leave behind.

Taylor (1932) derived an alternative relation to the Einstein equation for rigid fillers to calculate the viscosity of a fluid containing another immiscible liquid in suspension (similar to Equation 2.8), the combined viscosity law being given as

$$\eta = \eta_0 \left[ 1 + 2.5\phi \left( \frac{\eta' + \eta_0 / 2.5}{\eta' + \eta_0} \right) \right] \quad \text{Equation 2.13}$$

where,  $\eta_0$  and  $\eta'$  are the viscosity of the first and the second liquid, and  $\phi$  is the volume fraction of the second liquid. Therefore, a new relationship for the modulus assuming no friction at the interface was derived by Busfield *et al.* (2005a).

$$E = E_0(1 + \phi) \quad \text{Equation 2.14}$$

This can be achieved by assuming  $\eta'$  as zero in Taylor equation. An effort has been made in Chapter 5 to model the interfacial slippage and compare the results to the other described theories.

Busfield *et al.* (2004) and Deeprasertkul (1999) studied the effect of the changes in the filled rubber properties under strain and swollen in an oily solvent. They suggested that the filler aggregate orientation under strain could explain the changes in conductivity under strain. This phenomenon is discussed in section 2.8.1 and again in Chapter 6 of the present work. For such filler aggregate orientation to take place the filler should allow the polymer to slide around it. Deeprasertkul (1999) studied the effect of swelling the elastomer on dynamic properties of filled elastomers. He found as the viscosity solvent changes the dynamic loss modulus changes. Therefore a solvent can change the extent to which fillers can slip over the rubber matrix. They

---

also studied effect of the temperature on the dynamic loss modulus. As the temperature increases the slippage of the rubber over the filler increases which raises the loss modulus.

The filler has a higher modulus than the matrix polymer. When two bodies are in contact there is a chance of slippage under strain. It is clear from the models discussed so far that the interfacial properties of the filled elastomers would affect the mechanical properties differently at both small and large strains. In the present work an attempt has been made to simulate the interfacial slippage in the case of a filled elastomer using an appropriate interfacial model. The interfacial friction depends on factors such as applied pressure and temperature. Coulombic friction is described by Amonton's law such that,

$$\mu = \frac{F_{\text{fric}}}{F_{\text{N}}} \quad \text{Equation 2.15}$$

Where  $F_{\text{fric}}$ , is the frictional force,  $F_{\text{N}}$ , is the normal force and  $\mu$ , is coefficient of friction. This model assumes that with an increase in the normal load that the contact area between the two contacting bodies increases. However, in this case it can be presumed that there is virtually intimate contact even without a normal load between the filler and the rubber. Hence, Coulomb's law is inappropriate. In the present case the frictional force is influenced by the extent of deformation as well as the interfacial shear strength between rubber and the filler (Roberts, 1992). Therefore in the present work the interface surface has been modelled using a critical shear stress law. The extent of slippage of the rubber can be modelled by setting a limit on the allowable shear stress prior to the onset of slipping. As described in Chapter 3 slippage only occurs when the stress in a local area exceeds this critical shear stress.

---

## 2.7 Conductivity in filled elastomer

### 2.7.1 Effect of filler properties on conductivity:

Fillers are usually added to an elastomer to improve the mechanical properties. Conductive carbon black fillers can also increase the conductivity of elastomers. However, there is a minimum concentration of fillers required to make the elastomer conductive. This minimum concentration is known as the percolation threshold. Below this threshold, the polymer is non-conductive and considered to be an insulator. Above the percolation threshold, the polymer becomes conductive and is called a conductor as shown in Figures 2.22, 2.23 and 2.24.

Percolation theory (Medalia, 1972) uses the probability of forming contact paths between fillers to explain the changes in the electrical conductivity of a polymer with the volume fraction of carbon black. Above percolation, the conductivity of the filled elastomer can be described by a scaling law based on the percolation theory,

$$\sigma_{\text{con}} = \sigma_{\text{con0}} (\phi - \phi_c)^t \quad \text{Equation 2.16}$$

Where,  $\phi$  is the volume fraction of filler,  $\phi_c$  is the percolation volume fraction,  $t$  is the conductivity exponent,  $\sigma_{\text{con}}$  is the conductivity of the composite and  $\sigma_{\text{con0}}$  is the compound conductivity at percolation. Figure 2.24 shows the conductivity of various fillers in a high density polyethylene (Probst, 1984). It can be seen that filler properties have significant effect on the percolation threshold. As the filler surface area and structure increase, the percolation threshold shifts towards the left (lower filler volume fraction). The precise aggregate size, surface area, volume fraction, structure and porosity of the filler all affect the mechanical and the electrical properties of the filler-rubber composite. For example, rubber may enter the filler aggregate and therefore may be unable to deform under load. This occluded rubber has the effect of increasing the effective filler volume fraction. Therefore, an effective measure of the filler volume fraction should also reflect this occluded rubber volume.

---

A relation between effective volume fraction and DBP was given as follows by Medalia, (1972),

$$\phi' = \phi \left( \frac{1 + 0.02139 DBP}{1.46} \right). \quad \text{Equation 2.17}$$

Where  $\phi$  is the effective filler volume fraction including the occluded rubber and  $\phi$  is actual volume fraction of filler. *DBP* is Dibutyl-Phthalate absorption number which is measure of structure of filler (discussed in section 2.2.1). An alternate way of altering the electrical conductivity can be achieved by using fillers with smaller primary particles or by using fillers with an increased structure. The effect of carbon black structure on conductivity of filled elastomer was studied by Janzen (1975). Janzen suggested that the number of contact points between filler aggregates determines the electrical conductivity. A higher DBPA absorption number reflects a higher filler structure and more points of contact. Janzen's equation is as follows,

$$\phi_{\text{crit}} = 1 / (1 + 4\rho_c DBPA) \quad \text{Equation 2.18}$$

Where,  $\phi_{\text{crit}}$  is critical volume fraction at threshold and  $\rho_c$  is the density. The percolation threshold or the critical weight fraction is inversely related to DBPA.

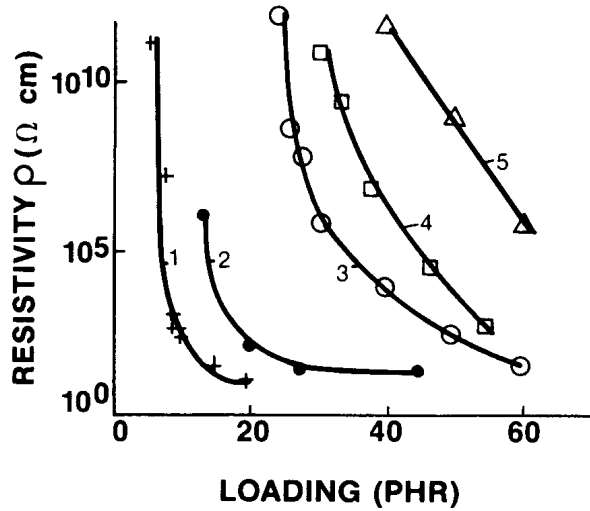


**Figure 2.22** DC resistivity of composites of SBR with various carbon blacks 1- Ketjenblack EC 2- Carbolac 3- Vulcan XC-72 4- Acetylen Black 5- N330, (Verhelst *et al.*, 1977)

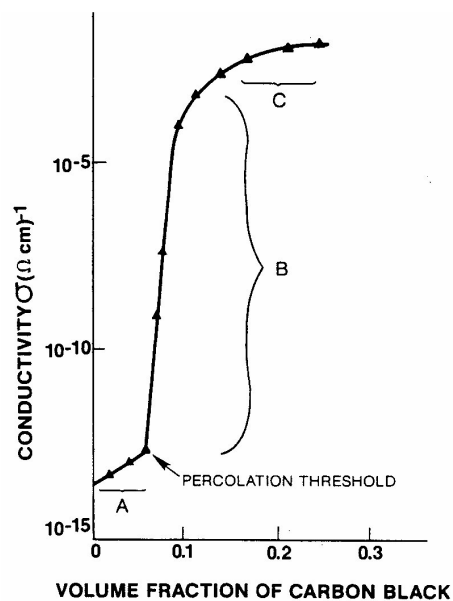


**Figure 2.23** The variation of the electrical resistivity on addition of filler. DC conductivity of composites of NR with carbon black. A, insulating; B, percolation; C, conductivity zone, (Medalia, 1986).



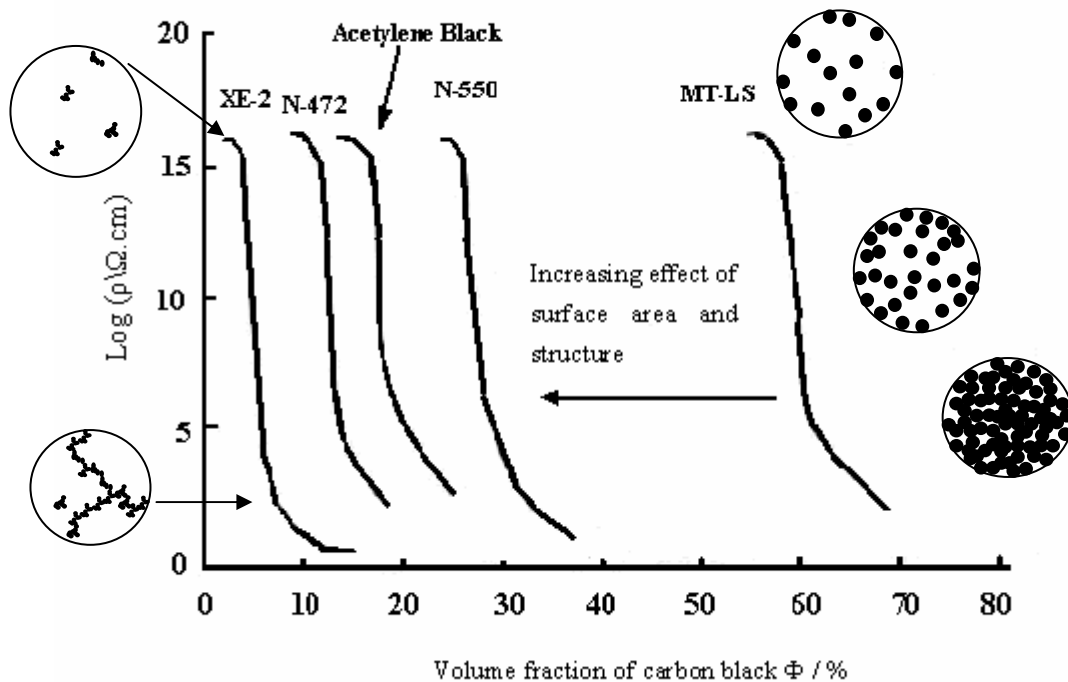


**Figure 2.24** Electrical resistivity versus volume fraction for a range of different carbon blacks in high density polyethylene, (Probst, 1984).

### 2.7.2 Conduction mechanisms

Medalia (1986) and Strumpler and Glatz-Reichenback (1999) have reviewed the various possible conduction mechanisms which include electron tunnelling and electron hopping in a filled composite. According to Strumpler and Glatz-Reichenback (1999) there are three different cases,

1. Filled polymer below the percolation threshold.
2. Filled polymer in which the mean distance between fillers is below 2-5nm.
3. Polymers containing particles in direct contact.

---

### 2.7.2.1 Below percolation threshold

In filled polymers, which are below the percolation threshold the particle to particle contact is ruled out as the primary conduction mechanism. Hence, the limited conduction mechanism can only result from electron tunnelling, Rubin *et al.* (1999). The electron tunnelling occurring between filler particle is related to the mean separation distance. Electron tunnelling occurs if the mean particle to particle separation is around 2nm-5nm. [(Balberg, 1987), Rubin *et al.* (1999) Toker *et al.* (2003) and Balberg *et al.* (2004)] . In the case of polymer below the percolation threshold and in the insulating zone, the conductivity may be mainly due to intrinsic conductivity of polymer. The conductivity in this polymer material could also be due to the impurities which tend to enhance the conductivity.

### 2.7.2.2 When the mean distance is less than 2nm-5nm

In polymer composites when the mean distance is less than 2nm-5nm but not touching two possible mechanism of conduction have been suggested.

Beek (1962) suggested that when the average particle distance is less than 2nm-5nm then electrical field assisted tunnelling takes place.

$$j_{\text{Tunneling}} = A.E_s^n \exp\left(-\frac{B}{E_s}\right) \quad \text{Equation 2.19}$$

Where  $A$ ,  $B$  and  $n$  are the constants whose values vary from 1 to 3,  $j_{\text{Tunneling}}$  is tunnelling current and  $E_s$  is the applied electrical field strength.

The probability that charges carriers can move between the filler and the polymer is indicated by ratio  $B/E_s$ . The term  $B$  represents the measurement of energy barrier between polymer and filler

Another model of conduction model was suggested by Frenkel (1930),

---


$$j_{\text{Hopping}} = A_r \cdot T^2 e^{\left(\frac{K \cdot E_s^{0.5} \phi}{k_b \cdot T}\right)}$$

Equation 2.20

Where,  $A_r$  is the Schottky Richardson constant, a work function of the filler material.  $k_b$  is the Boltzmann constant  $j_{\text{Hopping}}$  is the Hopping current and  $T$  is the temperature. Accordingly, the conduction takes place due to electron hole separation; know as hopping transfer assisted by the electrical field. The mechanism of hopping transport of electrical conduction has been usefully applied in printing. Factors such as the properties of the filler, the polymer and the interfacial contact area are all very important.

### 2.7.2.3 Particle to particle contact

When the filler volume fraction is greater than the critical percolation threshold then filler to filler contact takes place. In this case the primary conduction mechanism is conduction through the filler aggregate network. A network visualisation of this would be important and is discussed later in section 2.7.8.

### 2.7.2.4 Electrical contact between filler

When there is a contact between two conducting fillers there is a contact resistance which contributes to overall resistivity. This contact resistance can be described as the constriction resistance and tunnelling resistance between the particles. Contact resistance acts as a spot where maximum energy loss takes place. This energy loss is mostly in the form of heat.

Assume two spherical particles which are in contact. If the Young's modulus is assumed to be to infinite then contact between the spheres is only at a single point. If these assumptions are used to calculate the constriction resistance then it results in a singularity. Holm (1967) considered that a more realistic macroscopic contact be used with a finite radius  $a$ .

---

Accordingly the constriction resistance is as follows,

$$R_c = \frac{\rho_t}{2a} \quad \text{Equation 2.21}$$

Here  $\rho_t$  is the bulk resistivity of the filler. If the radius of the filler is larger than the radius of contact than a constriction resistance will be of greater effect than the filler resistance. This equation can be applied only to the fillers which are homogenous, having no surface contamination and which do not show any dependence on a large temperature gradient. Contact resistance estimation depends on an accurate estimation of the contact area. In calculating the contact area the mechanical properties of filler are very important.

If we assume that a sharp protrusion of a filler is in contact with a flat surface of the filler, then the elastic force between them for a small deformation is given by Bush (1982),

$$F = \frac{2}{3} \frac{E}{1-\nu^2} \frac{a^3}{r} \quad \text{Equation 2.22}$$

Where  $E$  is Young's modulus and  $\nu$  is Poissons ratio. From Equation 2.21 and 2.22 we get.

$$R_c = \frac{\rho_t}{2} \left( \frac{2}{3} \frac{E}{1-\nu^2} \right)^{\frac{1}{3}} F^{-\frac{1}{3}} r^{-\frac{1}{3}} \quad \text{Equation 2.23}$$

The contact resistance between filler particle decreases as the force applied increases. The contact resistance will also decrease if the protrusion radius increases. According to the above equation softer materials tend to have a higher constriction resistance.

---

### 2.7.3 McLachlan effective media theory

In effective media theory a composite consisting of filler (spherical or elliptical) and a polymer can be represented by the effective conductivity of the medium. There are two different cases in which effective media theory is applied. The first case is when the particle is perfectly spherical and dispersed in a matrix. In this case there is a smooth transition from conductor to polymer. This scenario is also referred to as a symmetric case. The second case is asymmetric; when the one component is covered with the other component (Filler covered by polymer matrix and vice versa). McLachlan (1987,1988) proposed a generalised effective media equation for composite conductivity. This equation referred as the effective media equation is an interpolation between the two cases mentioned above. Also, within the appropriate limits the above equation reduces to the percolation theory shown in Equation 2.16.

The following is the McLachlan (1987, 1988) effective media theory.

$$(1-\phi)\left(\frac{\Sigma_1-\Sigma_m}{\Sigma_1+[(1-\phi_c)/\phi_c]\Sigma_m}\right)+\phi\left(\frac{\Sigma_h-\Sigma_m}{\Sigma_h+[(1-\phi_c)/\phi_c]\Sigma_m}\right)=0 \quad \text{Equation 2.24}$$

Where,  $\Sigma_m = \sigma_m^{t'}$  ;  $\sigma_m$  = conductivity of the composite medium

$\Sigma_1 = \sigma_1^{t'}$  ;  $\sigma_1$  = conductivity of the low-conductivity phase

$\Sigma_h = \sigma_h^{t'}$  ;  $\sigma_h$  = conductivity of the high- conductivity phase

Where, t' the exponent relates both to the critical volume fraction  $\phi_c$  at which the high conductivity phase first percolates and to the shape of the grains.

---

#### **2.7.4 Effect of carbon black morphology**

There are various factors affecting the conductivity of carbon black filled elastomers Medalia (1986),

1. Particle size
2. Porosity
3. Number of particle per aggregate
4. Openness / clustering
5. Anisometry
6. Dispersion of particle

The effect of particle size or particle diameter and structure is discussed in section 2.3. Particle size clearly has a significant effect on the conductivity of rubbers. The (amount of) pores present in the carbon black is referred as porosity. Generally these pores are 2nm in size including the slits formed from burning away the individual layers of planes Voet (1968). Medalia (1986) suggested that as porosity increases there will be a greater probability of aggregate to aggregate contact. However, studies by Boonstra and Dannenberg (1955) on the effect of porosity on conductivity contradict this. They found that carbon black made in the furnace with higher porosity gave higher conductivity. However, these blacks tend to oxidise in a lab environment resulting in reduced conductivity. Medalia suggested that greater anisometry in carbon black shape should lead greater conductivity.

---

### **2.7.5 Network visualisation of carbon black aggregates using (SEM/TEM) Scanning electron microscopy/Transmission electron microscopy.**

Sandler *et al.* (2003) and Loos *et al.* (2003) have shown that the conventional SEM can be used to provide information about the morphology of single wall nano-tubes. They also stated that this technique relies on the charge contrast imaging mode to provide the morphological information. Furthermore, it can be used for a range of fillers ranging from nanometre to micrometre-sized particles. One major disadvantage of the SEM and the conventional TEM is that it does not provide any information about the depth. To understand the changes of electrical response under strain for a filled rubber, it is very important to understand the changes in the structure occurring in the rubber matrix. As is the case in most filled rubbers the changes in the aggregates structure take place in 3 dimensions. Kohjiya *et al.* (2006) have used a TEM and computerised tomography to obtain a 3D image of filler aggregate structure. They demonstrated that in case of NR filled rubber (N330 carbon black), the percolation threshold is 40. N330 filled NR having 40 phr black is shown in Figure 2.25. It can be seen that 3D TEM combined with tomography shows a continuous filler aggregate structure for filled rubbers. Kohjiya *et al.* (2006) have also used TEM/electron tomography with an AFM to study silica filled rubber. It is proposed that atomic force microscopy (AFM) could provide enough information in combination with TEM/ electron tomography to understand the relationship between structure and properties of these filled rubbers.

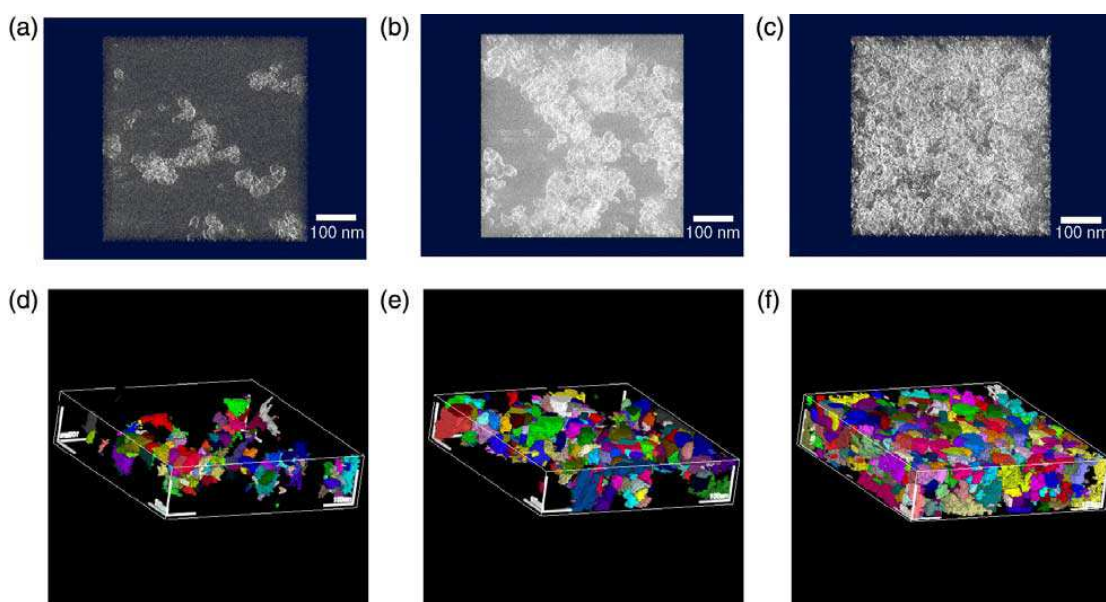
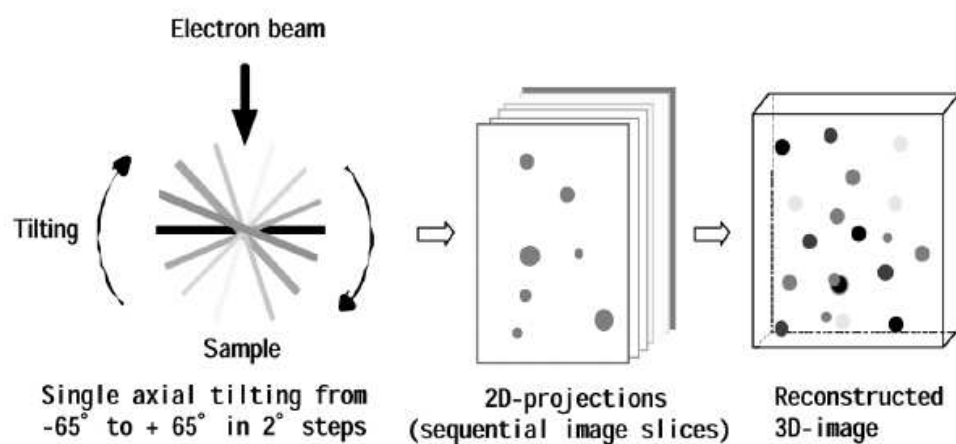


**Figure 2.25** Reconstructed 3D-TEM images of carbon black loaded natural rubber in black and white (upper) and in multicoloured (lower) displays. (a) and (d) CB-10; (b) and (e) CB-40; (c) and (f) CB-80. In the black and white, the contrast was reversed, and the white parts represent carbon black. Coloured ones are for easy recognition of an aggregate, which is painted differently from the neighbouring ones. The white bar for each direction shows a distance of 100 nm (Kohjiya *et al.*, 2006). Key: CB-10 = 100 grams of rubber with 10 part per hundred grams of carbon black.



---

## 2.8 Investigation of filler reinforcement of elastomer

### 2.8.1 Electrical properties of the carbon black loaded elastomers subjected to strain.

As discussed in section 2.5, finite element analysis and other modelling techniques have been used to model the filled rubber reinforcement by making suitable assumptions about the filler structure and polymer. However, finite element analysis has its limitation and hence there is a need to understand the behaviour of the filled elastomer and the microstructural changes using alternative approaches. One possible approach is to measurement of electrical response under strain. Many researchers have investigated changes in the carbon black arrangement and electrical conductivity under strain of the filled composite to study the filler rubber reinforcement and interaction. These include Wang *et al.* (2008), Zhang *et al.* (2007), Yamaguchi *et al.* (2003), Sichel *et al.* (1982), Aneli *et al.* (1999), Deeprasertkul (1999), Carmona *et al.* (1986), Flandin *et al.* (2000, 2001), Lundberg and Sundqvist *et al.*, (1986) and Norman *et al.* (1970). These filled materials also show responses to external stimuli such as the temperature, pressure and gases [Abraham *et al.* (2004), Jiang *et al.* (1986), Zhang *et al.* (2005), Kang *et al.* (2006), Wei *et al.* (2006)]. As previously mentioned in section 2.7.2.4, contact resistance is very important when measuring the electrical response in a filled elastomer. Norman (1970) has discussed various methods to measure the electrical response. It has been demonstrated that brass forms the best contact with the rubber during curing. Burton *et al.* (1989) has shown that silver paint or silver loaded epoxy forms a good contact with rubber. Norman showed that a four point (measurement) was the best way of measuring resistivity changes under strain.

Yamaguchi *et al.* (2003, 2005) and Flandin *et al.* (2000, 2001) have measured the changes in resistivity for a typical black such as HAF N330 in a natural rubber and HAF-Conductex 975 in an ethylene-octane filled polymer respectively, shown in Figure 2.28 and Figure 2.29. Yamaguchi *et al.* (2003) reported a reversible change in the resistivity under cyclic loading (after 1<sup>st</sup> cycle) between 100% and 300% strain,

---

whereas Flandin *et al.* (2000) reported a different irreversible behaviour at strains between 100% and 300%. Further, they have proposed an alternative microstructural model to explain the observed behaviour for the respective filled polymer composite. Also, different irreversible and reversible change in the resistivity under strain for a filled composite have been reported by other workers such as Zhang *et al.* (2007) and Bloor *et al.* (2005) shown in Figure 2.30 and 2.31 (have been discussed in following paragraphs). So, we can conclude that the filler- polymer interaction and the microstructural (models) the aggregate structure changes under strain must be different for specific polymer-filler composite systems. In the present work, changes in the resistivity have been measured for a range of low structure blacks such as MT and high structure black such as Conductex-7055 and Printex-XE2 mixed in natural rubber. Their behaviour has been analysed in detail and corresponding microstructural models are proposed.

Yamaguchi *et al.* (2003) measured the changes in the electrical resistivity under strain for an HAF-N330 filled natural rubber. They showed that HAF carbon black aggregate structure breaks down under strain. A typical measurement of changes in the electrical resistivity under strain is shown in Figure 2.28. During the loading cycle there is an initial increase in resistivity. This is attributed to breakdown of filler aggregate structure. If the strain is increased the resistivity does not increase but rather decreases and reaches a plateau. This was attributed to arrangement of filler aggregate structure in the direction perpendicular to strain. When the load is removed the resistance does not go back to the initial value but reaches a higher value. This indicates that the changes taking place in filler aggregate structure are irreversible. During subsequent cyclic loading the behaviour is more reversible. Hence, the changes in filler aggregate structure that take place are due to changes in “filler orientation” under cyclic loading.

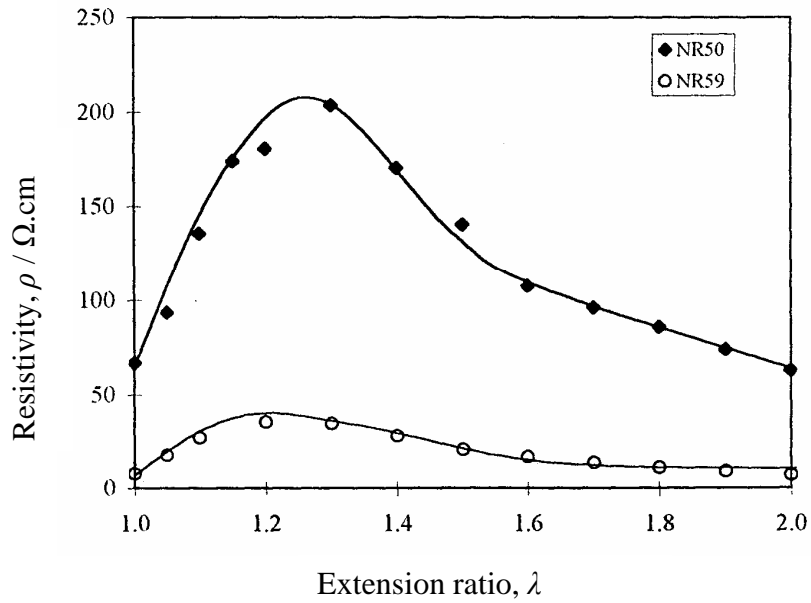


**Figure 2.26** The variation with strain of the electrical resistivity of a 50phr and a 59phr HAF filled NR, (Deeprasertkul, 1999)

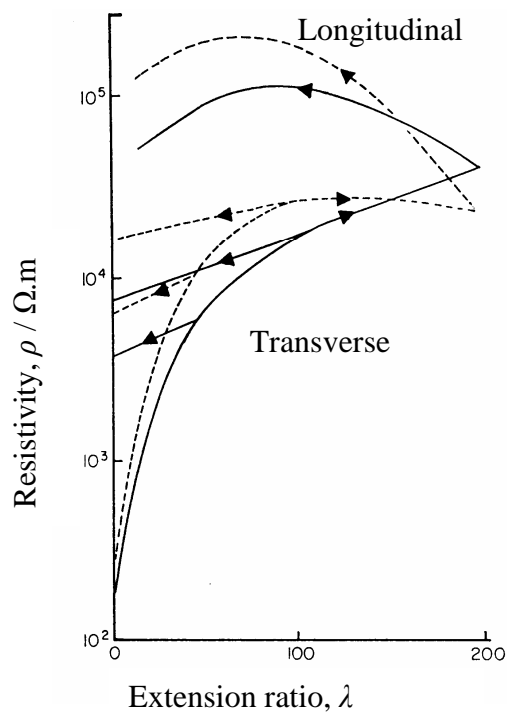


**Figure 2.27** Variation of longitudinal and transverse electrical resistivity during various elongation cycles in tension as a function of strain, (Norman, 1970)

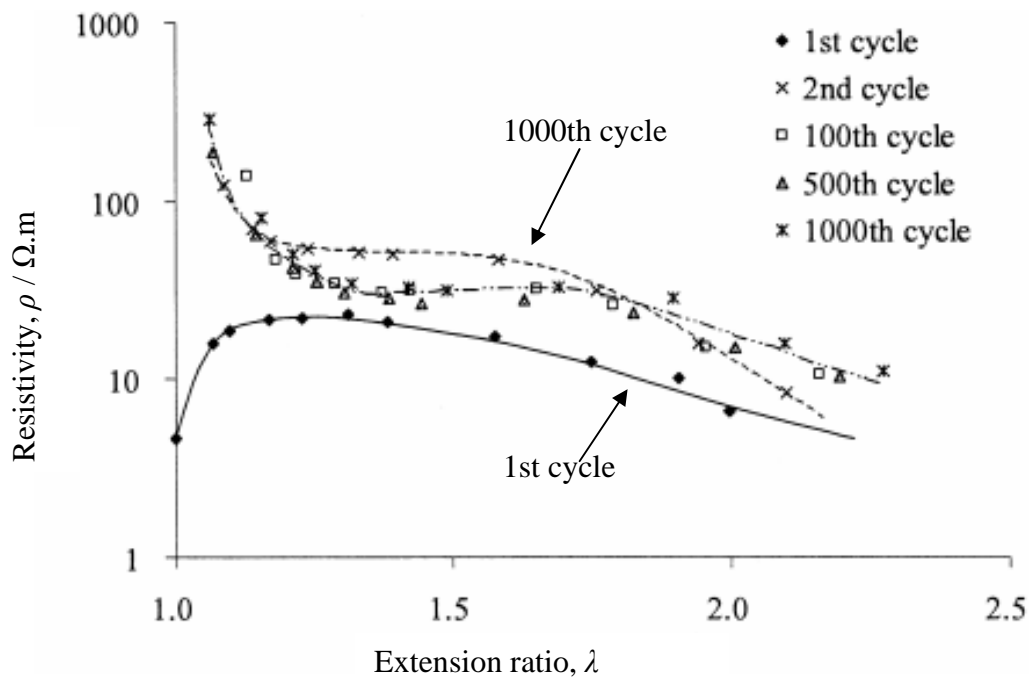


**Figure 2.28** Electrical resistivity response shown by HAF N330 filled elastomer under cyclic tensile loading, (Yamaguchi *et al.*, 2003).

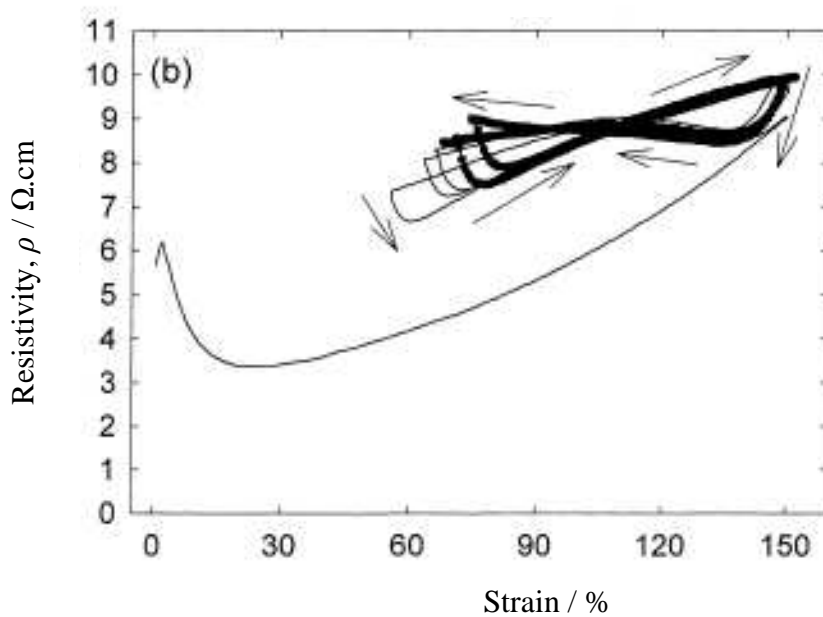


**Figure 2.29** Changes in resistivity as a function of strain for ethylene-octene elastomer at filler volume fraction of 20% for a high surface area black Conductex ultra 975, (Flandin *et al.* 2000).

Bloor *et al.* (2005) measured the change in resistivity for a composite of nanoscale nickel powder in the elastomer matrix. Nickel particles are coated by the polymer during mixing and curing. Hence, the initial resistivity of filled polymer was very high as shown in Figure 2.31. Bloor *et al.* (2005) suggested that the particle morphology of nickel particle coated with polymer affects the behaviour under strain. Under tensile strain the filled composite shows a 12 orders of magnitude change up to 30% strain.

Zhang *et al.* (2007) studied the changes in resistivity of a thermoplastic elastomer filled with carbon nanotubes. The changes in the resistivity for the first cycle for a range of filler volume fraction are shown in Figure 2.30. They were able to determine the conduction mechanism as fluctuation-induced tunnelling. This was achieved by studying the temperature dependence of the resistivity of a carbon nanotube filled polymer for filler volume concentration greater than 0.3 % and fitting the data to a fluctuation induced tunneling model. Wang *et al.* (2008) studied the effect of compression and pre-compression pressure on the piezo-resistivity of carbon black filled silicone rubber composite. They found, if the applied load pressure is less than the maximum pressure in the pre-compression cycle, the repeatability of the piezo-resistivity is improved. They were able to explain the phenomena using a micro structural model of filler aggregate and slippage of polymer molecule chains over the filler surface.

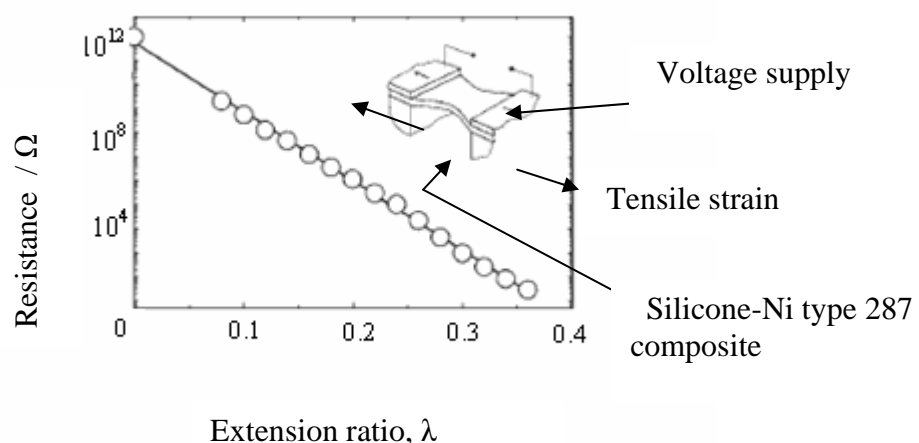


**Figure 2.31** Variation in resistance as a function of extension ratio for Silicone-Ni type 287 composite, (Bloor *et al.*, 2005).

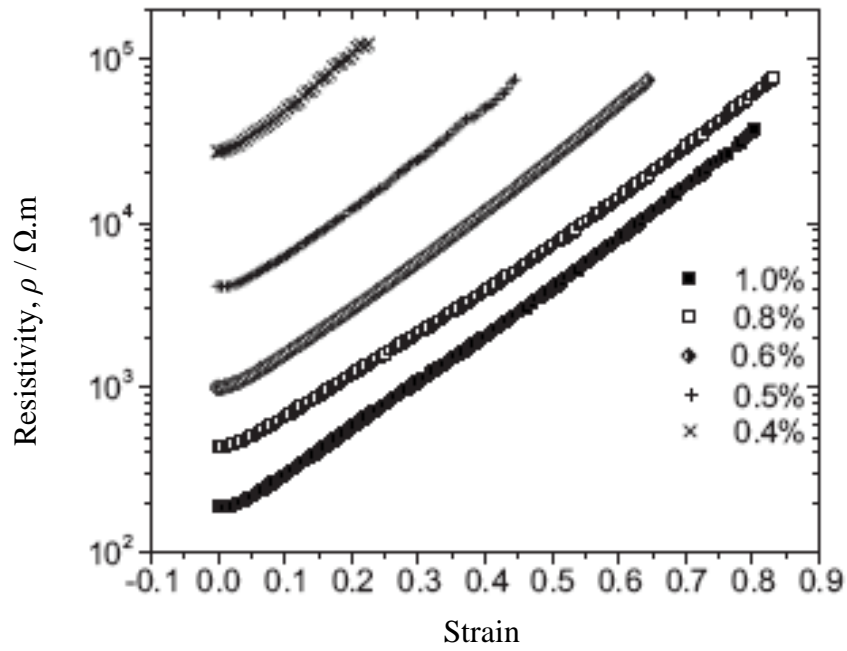


**Figure 2.30** Changes in electrical resistivity for a carbon nanotube filled polymer for first cycle, (Zhang *et al.*, 2007).

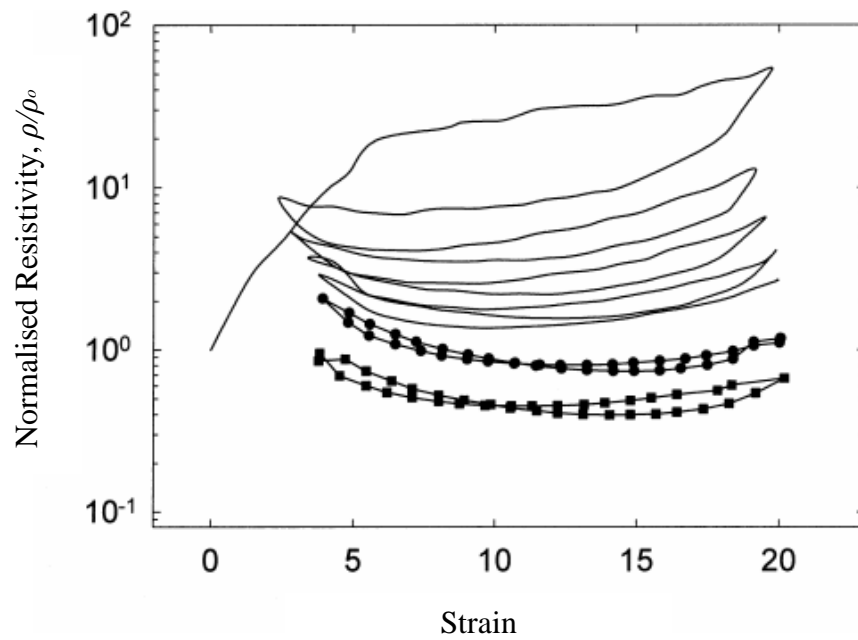


**Figure 2.32** Changes in resistivity versus strain for a low structure carbon black such as MT carbon black in ethylene octane elastomer, (Flandin *et al.*, 2000).

---

### 2.8.2 Effect of swelling

When a polymer absorbs solvent and swells this results in the application of a tri-axial stress to the polymer network. Deeprasertkul (1999), Abdel-Ghani *et al.* (2000), Busfield *et al.* (2004) and Carrillo *et al.* (2005) have studied the effect of swelling on the properties of filled rubber composites. Carrillo *et al.* (2005) studied the effect of swelling on the resistivity of butadiene based elastomer filled with carbon black particles shown in Figure 2.34. They used different solvents to swell carbon black and graphite filled PB and SBR. The results for carbon black filled SBR are shown in Figure 2.34. This shows that the conductivity of these samples decreases after swelling with solvents. Previous studies indicate that this reduction of conductivity is due to the migration of solvent into the matrix, which leads to a net separation of the conductive fillers and therefore a breakdown of the conductive paths (Busfield *et al.*, 2004). Carrillo *et al.* (2005) proposed that their experimental results cannot be explained by this percolation model alone. They suggested that there may be the influence of the heterogeneous solvent distribution and the effect of the location of the solvent deposition in different regions of the composite. Carrillo *et al.* (2005) used the concept of the wetting coefficient to explain the observed behaviour. They employed the generalised effective media model suggested by Blaszkiewicz *et al.* (1992) to calculate the apparent percolation threshold for swollen samples. Based on this theory, they observed that a larger wetting coefficient corresponds to a larger apparent percolation threshold. They proposed that it is enough to absorb a small amount of solvent to disconnect the conductive fillers from each other if the wetting coefficient is large. In contrast, it is necessary to absorb more solvent to disconnect fillers if the wetting coefficient is small.

Abdel-Ghani *et al.* (2000) studied the electrical properties and swelling mechanism in compressed HAF carbon black filled butyl rubber. They observed that the HAF filled butyl rubber demonstrates different dielectric properties in different carbon black concentrations. Butyl rubber filled with HAF with a low concentration (0-25 phr) shows load-independent (force) dielectric constant value. From 35-45 phr, the dielectric constant is affected by load. However, when the carbon black

---

concentration rises to 65-85 phr, it seems that the load only slightly affects the dielectrical constant. At 105 phr, the dielectrical constant is completely load-dependent. They proposed that this irregular behaviour is due to the dispersion of carbon black. They described the relationship between volume fraction and dielectric constants in load independent region (0-25phr) as

$$\varepsilon = \varepsilon_0 (1 + \alpha_1 \phi + \alpha_2 \phi^2 + \dots) \quad \text{Equation 2.25}$$

Where,  $\varepsilon$  is dielectrical constant,  $\varepsilon_0$  = dielectrical constant of unfilled butyl rubber,  $\alpha_1$ ,  $\alpha_2$  are constants, depending on the load used in measuring,  $\phi$  = volume fraction of carbon black.

Busfield *et al.* (2004) studied the effect of swelling on the changes electrical behaviour with strain of HAF carbon black filled NR elastomer shown in Figure 2.33. In their work, as the extent of swelling increases, the electrical resistivity increases, with a relatively modest swelling of 8% producing a 2-decade increase in the initial resistivity. At a volume swelling of about 8%, which equals to a linear swelling of 2.60%, a decreasing resistivity versus strain behaviour without a peak value is found. They suggested swelling is a much more efficient way of breaking down the carbon black network than a simple tensile strain of an equivalent magnitude. This is due to preferential migration of solvent at filler-rubber interface disrupting the conductive filler network. They proposed that a very small strain can only create a tiny influence of two rigid surfaces, whereas a thin layer of insulator (organic solvent) between surfaces could affect the resistivity substantially (Busfield *et al.*, 2004).



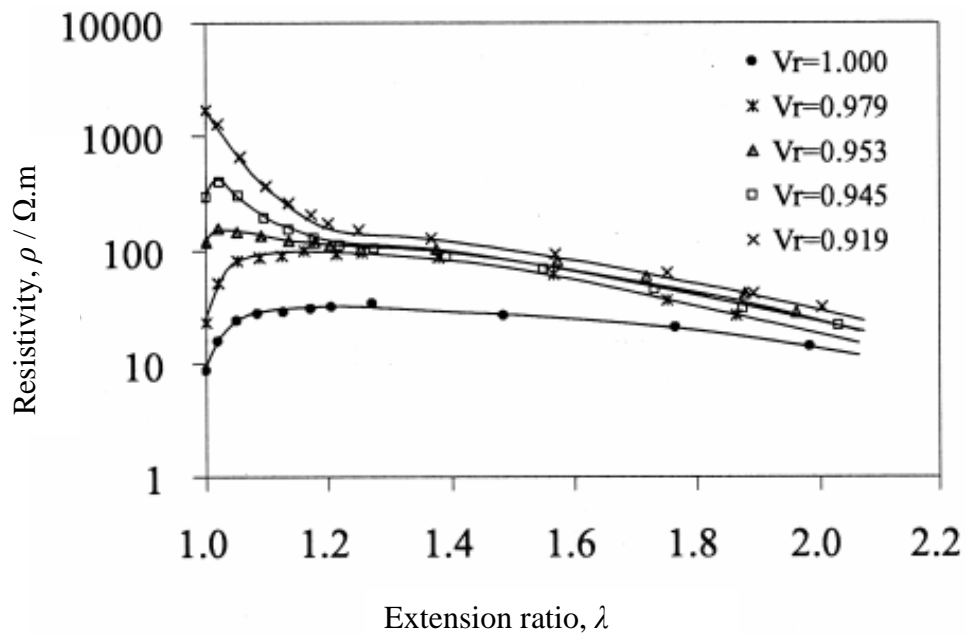


**Figure 2.33** Changes in resistivity response versus extension ratio for filled NR with 70 phr carbon black swollen by solvent AC12, (Busfield *et al.*, 2004).

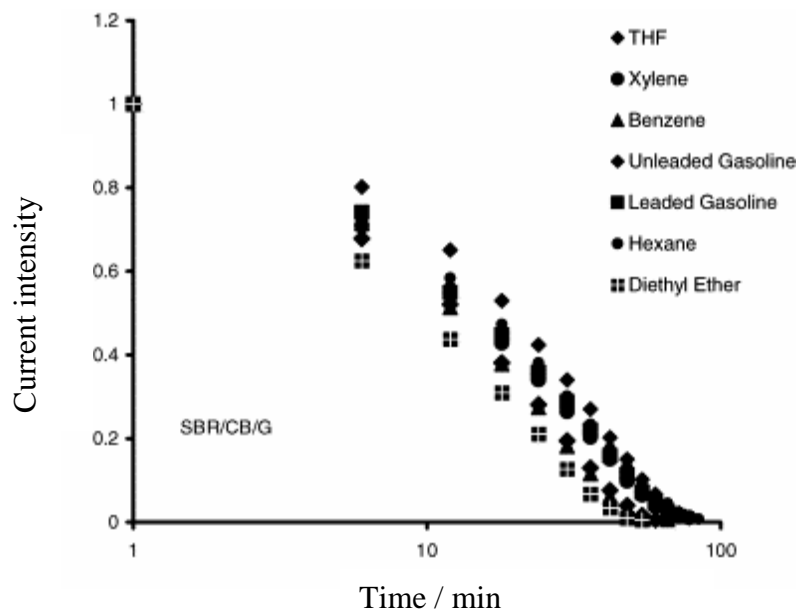


**Figure 2.34** Electrical behaviour of a filled composite; styrene butadiene with carbon black or graphite swollen in different solvent, (Carrillo *et al.*, 2005).

---

### 2.8.3 The effect of temperature.

Due to thermal expansion an increase in temperature would result in a volumetric expansion of the filled elastomeric matrix and result in a change in the resistivity response of the filled composite. Several authors Xu *et al.* (2008), Zhang *et al.* (2007) Jiang *et al.* (2006), He *et al.* (2005), Busfield *et al.* (2004), Aminabahvi and Cassidy (1990), Lundberg and Sundqvist (1986) and Voet *et al.* (1981) have investigated the behaviour of filled elastomers resistivity at higher temperatures. Responses of the filled elastomers to temperatures can be classified into, negative temperature coefficient (NTC), a low positive temperature coefficient (L-PTC) and a high positive temperature coefficient (H-PTC). Generally, filled elastomers have a negative temperature coefficient or low positive temperature coefficient behaviour.

Sau *et al.* (1998) studied the effect of a heating-cooling cycle and a pre-strain cycle on filled elastomers. The resistivity decreases when the sample was heated. Then a plateau is observed during the cooling cycle. They proposed that the decrease in resistivity was due to the contributions of electron emission at high temperature, flocculation and polar group. Sau *et al.* (1998) concluded that the change in resistivity due to temperature effect was more significant than that due to the pre-strain. Wack *et al.* (1947) investigated the effect of temperature on the electrical resistivity. They suggested that the positive temperature coefficients are due the kinetics of breaking and reformation of the carbon black aggregated structure.

He *et al.* (2005) compared the behaviour of multiwall nanotube filled HDPE (high density polyethylene) and carbon black filled HDPE shown in Figure 2.36, around the melting temperature of the polymer. He *et al.* (2005) found for a multiwall nanotube filled HDPE exhibited PTC and a carbon black filled HDPE had NTC above the melting temperature of polymer. They concluded that NTC is due to filler particle agglomeration for carbon black particles in the filled polymer at higher temperature. PTC of multiwall nanotube material was due to high aspect ratio of carbon nanotube filler preventing the agglomeration at a higher temperature.

---

#### **2.8.4 Effect of polymer**

The electrical responses of a filled rubber composite depend on the type of carbon black and polymer (Medalia, 1986). Miyasaka *et al.* (1982) have shown that the viscosity and surface tension of polymer affects the percolation threshold of filled elastomer. Kraus and Svetlik (1956) showed that NR (natural rubber) has a higher resistivity than SBR and BR. However, filled SBR has a higher resistivity than a filled NR. Geuskens *et al.* (1987) have shown that blends of two polymers show a minima in the conductivity. This was also observed for polyethylene and a natural rubber blend. However the mechanism of carbon black aggregation on blending the polymer is not clearly understood. It was observed that, at low concentration of polyethylene the resistivity of the blend was higher. This is most likely due to the homogeneous distribution of the carbon filler in natural rubber.

#### **2.8.5. Effect of mixing**

Process incorporation of the carbon black filler in a polymer has an effect on the electrical properties in filled elastomer. If the inter-particle or inter-aggregate distance is greater then the resistivity would be greater. Dannenberg (1981), Boonstra and Medalia (1963) and Medalia (1982) have shown that improved dispersion reduces the conductivity of filled elastomer (Donnet *et al.*, 1976). As mixing time increases the dispersion improves. An improved dispersion would cause decrease in the resistivity, as it increase the inter-aggregate distance and reduces the conduction paths. This is because more conductivity network path can be formed in the polymer above percolation threshold. During mixing the mechanical work can cause shear force to act on the carbon blacks aggregates. This causes the breakdown of filler aggregate structure and increases the resistivity.

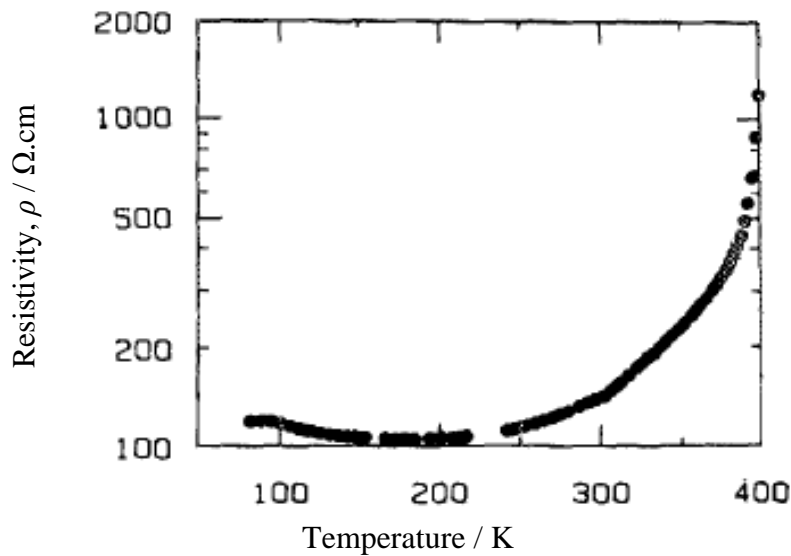
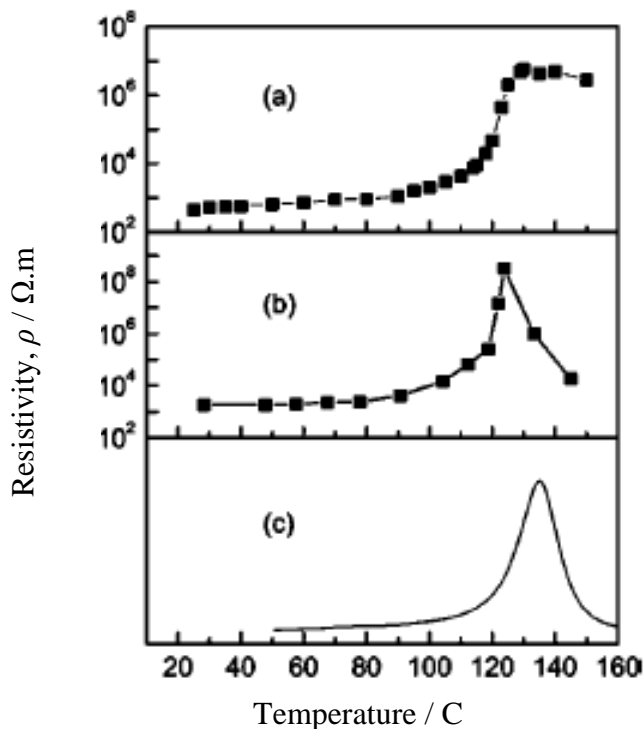


**Figure 2.35** Changes in resistivity of a filled composite as a function of temperature, (Lundberg and Sundqvist, 1986).

a) 5.4 wt % Multi-wall nanotube/HDPE



Above the melting temperature (between 120 and 130 °C) the electrical resistivity of the composite increases with the increase of temperature, showing a PTC effect

b) 16 wt % carbon black / HDPE Shows the PTC effect at temperature below 120. Moreover, when temperature is above the melting temperature of HDPE, the CB/HDPE composite exhibits a negative temperature coefficients NTC effect, the resistivity of the composite decreases rapidly with the increasing of temperature.

c) DSC for 5.4 wt % Multi-wall nanotube / HDPE

**Figure 2.36** Comparison of resistivity curve versus temperature for a) 5.4 wt % Multi-wall nanotube/HDPE b) 16 wt % carbon black / HDPE c) DSC for 5.4 % Multi-wall nanotube/HDPE sample, (He *et al.*, 2005).

---

## Experimental Method

### 3.1 Introduction

The aim of the present work is to understand filler reinforcement and filler-polymer interaction using a combination of finite element analysis as well as parallel mechanical and electrical behaviour measurements. A range of models have been used such as strain amplification, bound rubber model, occluded rubber and slippage models to describe the phenomena of filler reinforcement (which have been discussed in Chapter 2 section 2.4.). In this thesis a range of micromechanical finite element analysis models have been used to simulate filler reinforcement and filler-rubber interaction. During the simulation of filled elastomeric materials the choice of the boundary conditions for the unit cell and the stored energy function are both very important. Hence, the procedure used for the construction of model, the material properties, the boundary conditions are each discussed section 3.3. A range of models incorporating different numbers of fillers in the unit cell ranging from 1-32 were constructed. Two different approaches for the creation of a random filler distribution in the unit cell have been developed. The first uses a smooth surface model and the second uses stepped surface model. The effect of slippage of rubber matrix over filler using an appropriate slippage model has also been included. The results from this micromechanical modelling are discussed in Chapters 4 and 5.

It was hoped that parallel measurements of the changes in resistivity of a filled elastomer under strain might unravel the filler-filler, filler-polymer and polymer-polymer interactions. In the present work changes in resistivity under a tensile strain have been measured under normal conditions, as well as at higher temperatures and after swelling (tri-axial loading) in a suitable solvent. The experimental procedure

---

used for the measurement of resistivity under different conditions is described in the section 3.2 of this Chapter. The results of this investigation are discussed in detail in Chapter 6.

In order to create a practical strain sensor device it is necessary to bond an electrical connector to the rubber. Any bonding agent used must be electrically conductive. Therefore a brief investigation of silver particle filled bonding agent was also carried out. The effect of the volume fraction of silver particles on resistivity and bond strength was studied and the experimental procedure used is described in section 3.2.

## **3.2 Resistivity behaviour under strain for filled elastomers**

### **3.2.1 Materials**

Natural rubber, NR, used in present work has a chemical structure of cis-1.4 polyisoprene. It has a glass transition temperature of approximately  $-70^{\circ}\text{C}$  and is known to be a strain-crystallising rubber. Hence, at large strains NR exhibit extremely high strength and fatigue resistance.

In present study a range of fillers were selected to study the behaviour of filled elastomer. The properties of filler used in present case are shown Table 3.1. The fillers chosen were MT N990 (Medium thermal), HAF (High Abrasion furnace: N330, CDX 7055 and Raven p-5) and Printex-XE2. Table 3.1 shows MT carbon black has the lowest surface area per unit mass and the highest particle size and Printex-XE2 has highest surface area. Table 3.2 shows the detailed compositions and volume fraction of filler in natural rubber. A sulphur based curing system was used throughout. The volume fractions of filler used in the compound were all above the percolation threshold so that the filled rubber compound conducts. Hence, the carbon black filled samples were mixed and cured in different ways to depending on the volume fraction of carbon black needed to achieve percolation. HAF carbon blacks (N330, CDX 7055 and Raven p-5) filled system were mixed using two roll mill. Printex-XE2 has a very high surface area results in a greater energy being required to mix the compound. MT carbon black filled posed a great challenge in mixing as

the volume fraction of filler required for electrical conduction was 56%. Hence, Printex-XE2 and MT carbon black were mixed with NR in an internal mixer. During mixing first the polymer, the carbon black and some of the other non-reactive additives were thoroughly mixed to produce a master batch. Later, the curing ingredients were added on a two roll mill. The filled rubber samples were all cured at a temperature of 160°C. All samples were cut to be rectangular in shape with approximated dimension of 24mm for the width, 100mm for the length of and a thickness of 2.2mm. The error in the measurements of the length and area of the cross section of the sample was minimized by using a thickness gauge. In order to measure the changes in resistivity with changes in strain in different conditions filled rubber samples were tested in uni-axial tension on a Hounsfield tensile testing machine.

**Table 3.1** Morphology of the different carbon blacks used in this study.

	N990	CDX 7055	Raven p-5	N330	Printex-XE2
Mean aggregate size (nm)	483	181	78	105	100
Mean primary particle size (nm)	285	42	24	32	30
Surface area (CTAB) /m <sup>2</sup> gm <sup>-1</sup>	8	55	105	76	600
Oil absorption number (DBPA )/ (cc/100gm)	43	170	114	102	380

CTAB: (ASTM D 3765): Cetyltrimethyl ammonium bromide absorption

DBPA: (ASTM 2414): Dibutyl phtalate absorption

**Table 3.2** Compound formulations used in this study.

Ingredient /g	N990	CDX 7055	RAVEN P-5	N330	Printex- XE2	Unfilled rubber
NR	100	100	100	100	100	100
Carbon black	231	50	50	50	10	
Zinc oxide	5	5	5	5	5	5
Stearic Acid	2	3	3	3	2	2
MBTS		0.6	0.6	0.6		
Anti-ozone wax	1.5				1.5	1.5
6PPD	1.5				1.5	1.5
TBBS	1.5				1.5	1.5
Sulphur	1.5	2.5	2.5	2.5	1.5	1.5
Volume fraction of carbon black $\Phi$	56%	21%	21%	21%	5.2%	

MBTS: 2,2\_-dibenzothiazyl disulphide;

6-PPD N-(1,3-Dimethylbutyl)-N'-phenyl-p-phenylenediamine,

TBBS N-tert-Butyl-2-benzothiazolesulfenamide

### 3.2.2 Resistivity measurements

The resistivity was measured by using specially made clamps with four connections, to achieve four point contact method in order to eliminate (reduce) the contact resistance effect. The specially made clamps had four electrode parallel contact points that were long enough to go across the width of the sample. Schematics of the measuring equipment are shown in the Figure 3.2. The two outer connections measured current (in amps) and were connected in series with the applied voltage (source) and the ammeter. The two inner connections were connected in parallel to the voltmeter. The applied voltage for each of the samples was set between 30-40V. The current flow through the specimen was measured using a Hewlett Packard 34401A ammeter. The voltage was measured using an ALTAI HC-779 Voltmeter. At steady state the filled elastomer behaved like a Ohmic resistor as shown in Figure



---

### 3.1

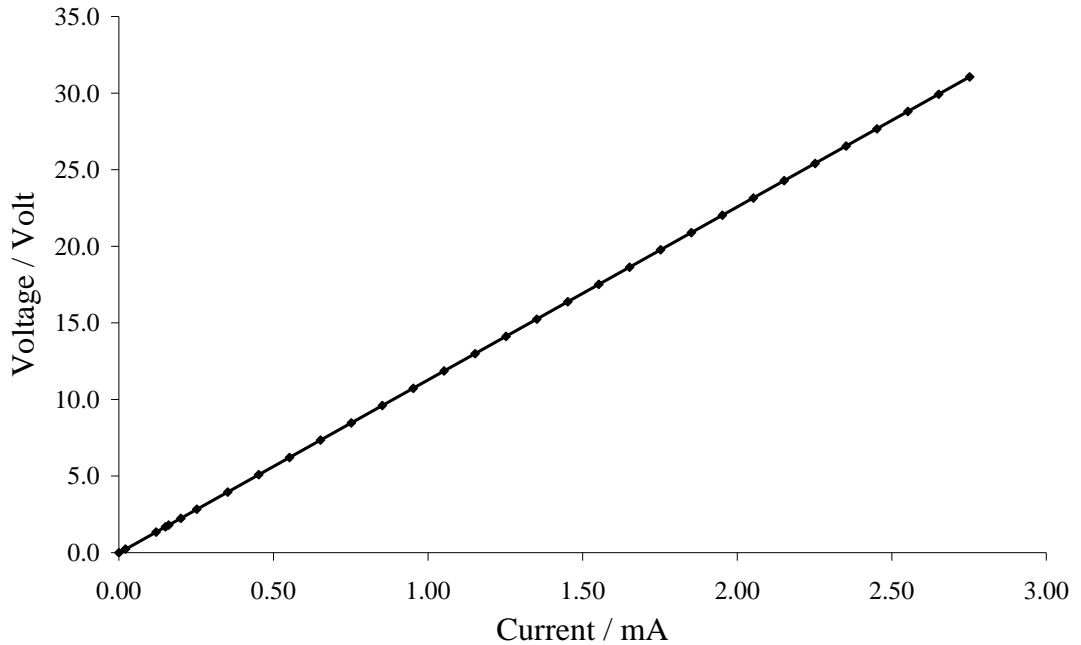


**Figure 3.1:** Linear voltage versus current relationship (Ohmic) behaviour for filled NR.

#### 3.2.3 Tensile strain testing

Samples were generally extended in a screw driven tensile test machine in discrete steps, initially of 1mm at an average strain rate of 0.02/min (up to a strain of 0.1), 2mm at an average strain rate of 0.04/min (for strains from 0.1 to 0.25) and 10mm at an average strain rate of 0.2/min (for strains above 0.25). All readings were made within 10 seconds of each elongation step to standardise the effect of stress relaxation. The tensile testing machines were operated manually, to allow the machine to be stopped at any time to measure the resistivity. The samples were loaded up to 100% to 300% strain and then unloaded, with both the force and the displacement recorded. Also, for each reading, the resistivity measuring clamps were placed on the sample in order to measure voltage and current accurately. In order to study the effect of cyclic loading on changes in resistivity. Changes in resistivity

---

under cycle loading were generally measured for the 2<sup>nd</sup>, 10<sup>th</sup>, 20<sup>th</sup> and 1000<sup>th</sup> cycles. The stress ( $\sigma$ ) was calculated as follows:

$$\sigma = \frac{F}{A_0} \quad \text{Equation 3.1}$$

Where  $F$  is the force measured in Newtons and  $A_0$  the cross sectional area.

The strain is converted to extension ratio,  $\lambda$ . Where the ratio is calculated is of the extended length  $l$  and the initial length  $l_0$ .

$$\lambda = \frac{l}{l_0} \quad \text{Equation 3.2}$$

The main results are presented in the form of log resistivity,  $\log(\rho / \Omega.m)$ , and the calculations were carried out as shown below.  $R_e$  is resistance,  $V$  is voltage and  $I$  is the current,

$$R_e = \frac{V}{I} \quad \text{Equation 3.3}$$

$$\rho = \frac{R_e A_0}{l_e} = \frac{R_e A_0}{l_e \lambda} \quad \text{Equation 3.4}$$

Resistivity under strain was calculated as shown above.

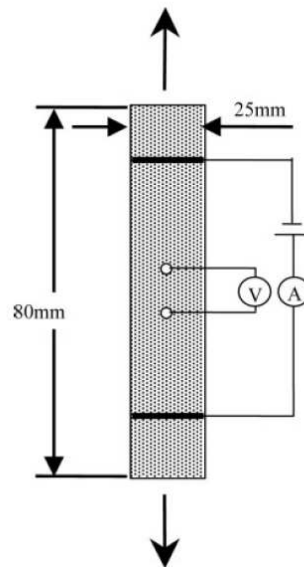


**Figure 3.2:** Schematic of the set up used to measure electrical resistivity of the test sample.

### 3.2.4 Tensile testing at elevated temperatures

The tensile tests at 80°C was done using an Instron tensile testing machine with an environmental chamber. The sample was placed inside the chamber at a temperature of 80°C and closed. Once the temperature is stabilised at 80°C, the chamber was then opened and the clamps were inserted and the door was closed quickly. Although these set of experiments were done carefully as to ensure temperature was maintained and measurements were always done at the specified temperature, there was always a drop of about 1-3°C, that quickly recovered, when the door was opened to attach the resistance measuring clamps.

---

### 3.2.5 Preparation of swollen samples

The swelling of the samples was carried out using two different solvents, DBA (Dibutyladipate) and xylene. Properties of the solvent are listed in Table 3.3. DBA is a more viscous and oily solvent while xylene is less viscous and more volatile. The amount of solvent absorbed (the change in mass) at specific times was recorded and a mass uptake curve was calculated. A typical mass uptake is shown in Figure 3.3. The mass uptake curve was calculated in order to determine the time it took to reach an equilibrium swelling. This gives us an idea of the time required for partially swollen sample to reach an even swelling after removal from solvent.

The samples were first weighed accurately on an electronic scale in the unswollen state, then submerged inside a solvent and swollen. Once swollen they were weighed again and kept inside individual medium sized sealable plastic container to maintain the solvent content and to allow time to reach equilibrium. The samples are refereed to, depending on amount of rubber network  $V_r$  in sample of rubber and solvent (swollen sample).

The volume fraction of rubber ( $V_r$ ) for each sample was calculated from the initial mass in grams before swelling and the final mass, after swollen. The formula to calculate the  $V_r$  is the following:

$$V_r = \frac{V_{r.net}}{V_{r.net} + V_s} \quad \text{Equation 3.5}$$

In order to calculate  $V_{r.net}$ , the volume of the rubber network and  $V_s$  the volume of the solvent in the swollen sample, the following calculations were carried out.

$$V_{r.net} = \frac{M_0 \times M_r}{\rho_{r.net}} \quad \text{Equation 3.6}$$

$$V_s = \frac{M_f - M_0}{\rho_s}$$

Equation 3.7

Where  $M_0$  is the initial mass and  $M_f$  is the final mass after swelling, calculating the difference gives the mass uptake.  $M_r$  is the mass fraction of rubber which can be calculated by taking the ratio of the mass of the polymer and the sulphur divided by the total mass of the mix, for natural rubber the mass fraction is 0.94.  $\rho_{r.net}$  and  $\rho_s$  are the densities of the rubber network and the solvent respectively.

**Table 3.3** Properties of the liquids used in this study

Index	Liquids	$M_w$	Density /g.cm <sup>-3</sup>	Viscosity /Pa.s at 20°C
DBA	Dibutyl adiapte	258.4	0.962	0.037
xylene	p-xylene	107.2	0.864	0.000603

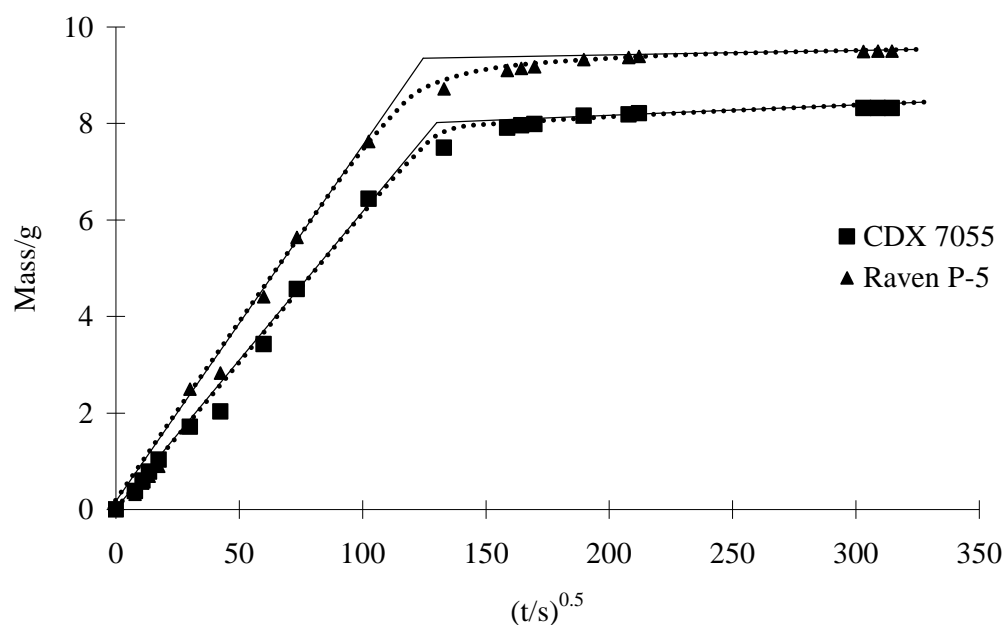


**Figure 3.3** Typical mass uptake of the xylene solvent versus the square root of time for carbon black filled rubbers (Initial sample size: 5gms).

### 3.2.6. Silver filled bonding agent

The bonding agent used in this study was Chemosil NL 411 which is an organic solvent system filled with polymers. It contains 22-26% by mass of solids. Chemosil NL 411 is a lead-free version of Chemosil 411. The silver filler particles, which were supplied by OMG, had a primary particle size of 50nm and surface area about 20m<sup>2</sup>/g. Chemsoil NL 411 adhesive was added into organic solvent xylene under magnetic stirring. The adhesive to xylene volume ratio used was 80:20. The mixture was stirred for 5 min. Then, silver filler particle was added to the solution. The composition of the samples used is shown in Table 3.5. Approximately ten percent by volume of the dispersion agent EFKA-4400 was added into the solution. The solution was then ultrasonicated (cell disruptor XL 200) for 5 min. It was crucial to maintain the water temperature at room temperature; otherwise the xylene would evaporate. The silver filler particle filled adhesive solution was stable and no

---

aggregation was observed for at least two weeks.

### 3.2.7 Adhesion test

The peel test (ASTM D429-03) describes the peel strength of the rubber-to-metal bond. The rubber-to-metal strips were peeled at an angle of 90°. The peel energy used to compare the bond strength of silver filled adhesive bonded to metal plate is calculated as follows

$$P = \frac{2F\lambda}{w} - t_t W \quad \text{Equation 3.8}$$

Where  $P$  is the peel energy ( $\text{J/m}^2$ ),  $F$  is the average peel force (N),  $\lambda$  is the average extension ratio in the specimen,  $w$  is the width of sample (m),  $W$  is the average strain energy ( $10^6\text{J/m}^3$ ) and  $t_t$  is the thickness of specimen (m).

The experiment measures the force necessary to separate a rubber from a metal surface. A standard test specimen is shown in Figure 3.4. The bonded area refers to part of rubber matrix bonded to the metal substrate. The metal substrate and fixture used for testing the adhesive bonded strength are shown in Figures 3.4 and 3.5.

### 3.2.8 Sample preparation

The metal substrate used must clean and free of dirt. This achieved by first cleaning the metal surface with ethanol. Then, the metal surface is blasted with iron grit. A thin layer of adhesive was applied on metal surface in the area labelled as bonded area in Figure 3.4 and left overnight to dry. The adhesive coated metal strip and MT carbon filled rubber were cured at temperature 160°C. During the curing of sample the adhesive forms bond with rubber. The sample is tested 24 hr after curing the sample.

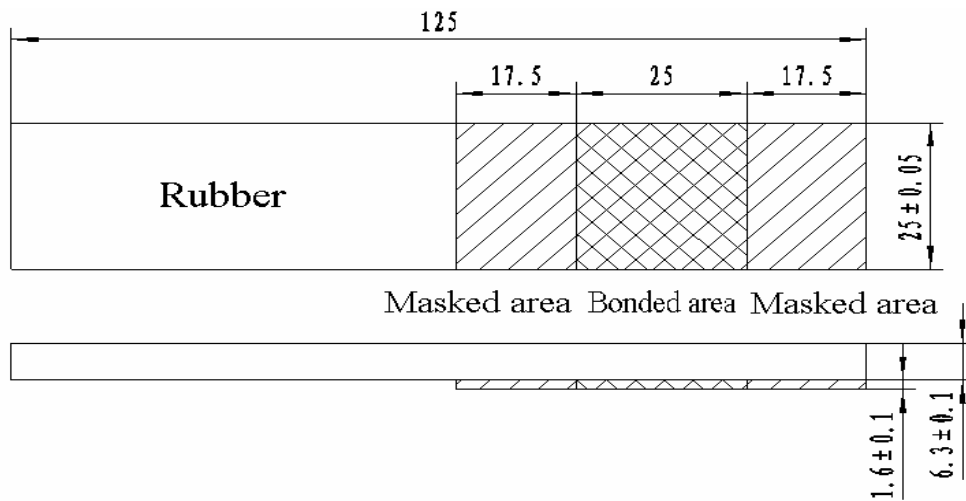


**Figure 3.4** The rubber specimen showing the bonded area, (All dimensions in cm).

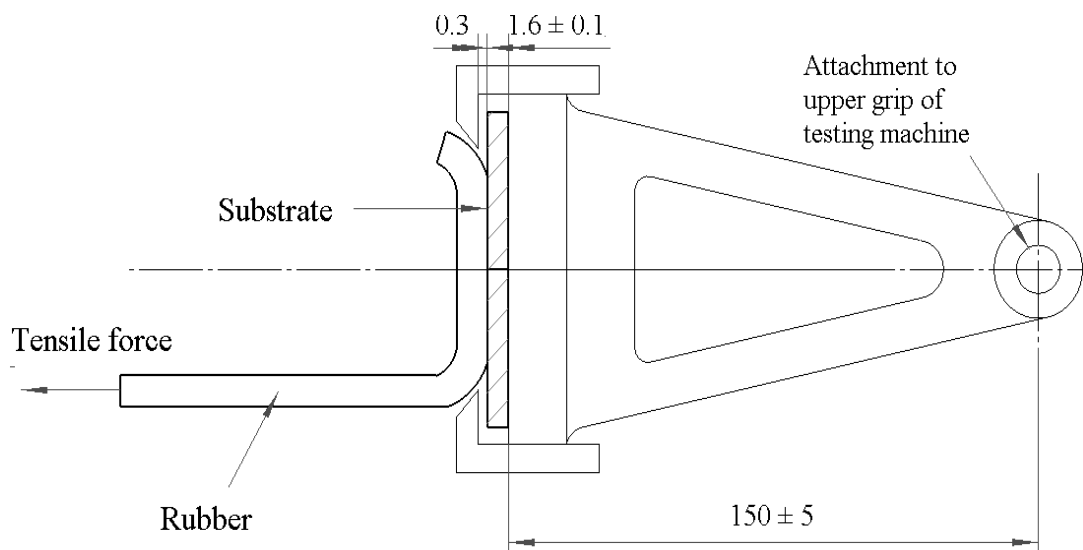


**Figure 3.5** The fixture used for 90° peel test from ASTM D429-03, (All dimensions in cm).



---

**Table 3.4** Compositions for silver filled bonding agent

Volume fraction of silver filler in adhesive / %	Silver/g	Adhesive/g	Dispersant agent (EFKA-4400)/g
7.5	0.1	4.5	0.23
31	0.5	4	0.23

### 3.2.9 Imaging techniques: SEM and TEM

The SEM images were taken by a PHENOM (FEI), using 20 to 30kV at magnifications ranging from 25,000x to 100,000x in order to see the carbon particles and aggregates in each of the samples. The samples were prepared by creating a fracture surface by freezing them in liquid nitrogen until they became hard and brittle enough to fracture them using a pair of tweezers. Carefully, as to not compromise the fracture surface, the tip was cut using a sharp blade across, and placed, for the fracture surface to be facing upwards, on a sample holder suitable for the SEM. The sample was pasted on to the surface with silver cement. Due to the conductive nature of the sample no coating was needed and the image was able to be taken in vacuum.

In order to prepare samples for the fillers to be viewed in a TEM the carbon particle was mixed with ethanol. The solution was ultra-sonicated for 10 minutes in order ensure the carbon particle was completely dispersed. A TEM grid was dipped at angle in the solution. The Grid was dried in closed container to avoid contamination. The grid was then observed using the TEM microscope.

---

### 3.3 Finite element analysis

#### 3.3.1 Rubber material characterisation

In order to simulate the rubber-filler interaction using FEA, the matrix elastomer behaviour has to be characterised first. Elastomeric materials are commonly characterised using stored energy functions,  $W$ , which can be expressed as functions of strain invariants thus,

$$W = f(I_1, I_2) \quad \text{Equation 3.9}$$

$I_1$  and  $I_2$  are the first and second strain invariants respectively. Rubber for the purpose of this work is assumed to be isotropic and incompressible in bulk.

Both the Mooney stored energy function and the Gent stored energy function have been used in this thesis. The Mooney stored energy function is a two term function which is applicable for low to moderate strains. The two constant terms are derived from experimental behaviour of an unfilled elastomer.

$$W = C_1(I_1 - 3) + C_2(I_2 - 3) \quad \text{Equation 3.10}$$

Where  $C_1$  and  $C_2$  are material constants.  $C_1$  is related to cross link density and  $C_2$  is related to the contribution due to free chain ends and network entanglements.

The Gent stored energy function also has two material constants and is applicable at moderate to high strains. Gent (1996) derived a SEF from empirical considerations which has the form

$$W = -\frac{E}{6} I_m \ln \left[ 1 - \left( \frac{I_1}{I_m} \right) \right]. \quad \text{Equation 3.11}$$

---

In the above expression  $E$  represents the low strain tensile modulus and  $I_m$  introduces an asymptote for the finite extensibility effect. The coefficient used for both stored energy functions and the type of stored energy functions used have a significant effect on the stiffness prediction for an elastomeric material. This is discussed in detail in Chapter 4

### 3.3.2 Filler material characterisation

In the microstructural models the filler particles, being much stiffer than the rubber, were modelled as rigid spheres. Typical models used in this work are shown in Figures 3.6 and 3.7. Figure 3.6 shows ideal lattice array of spherical filler particles in rubber matrix. In these models the fillers are assumed to be at centre of the cube in Figure 3.7 and each at the quarter points in Figure 3.7

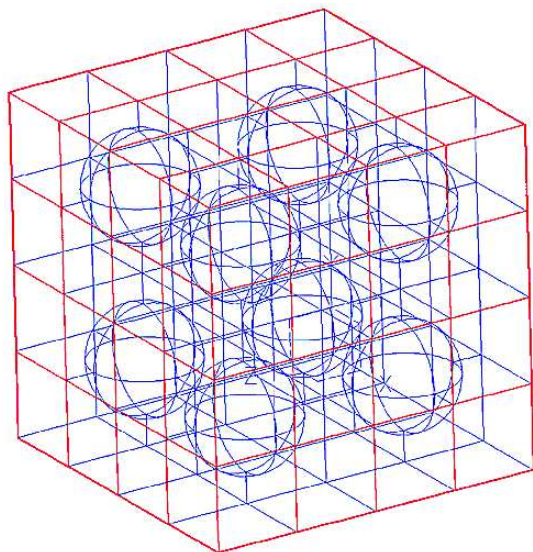


**Figure 3.6** Ideal lattice arrays of filler particles in rubber matrix with filler particles at centre of each quarter point.

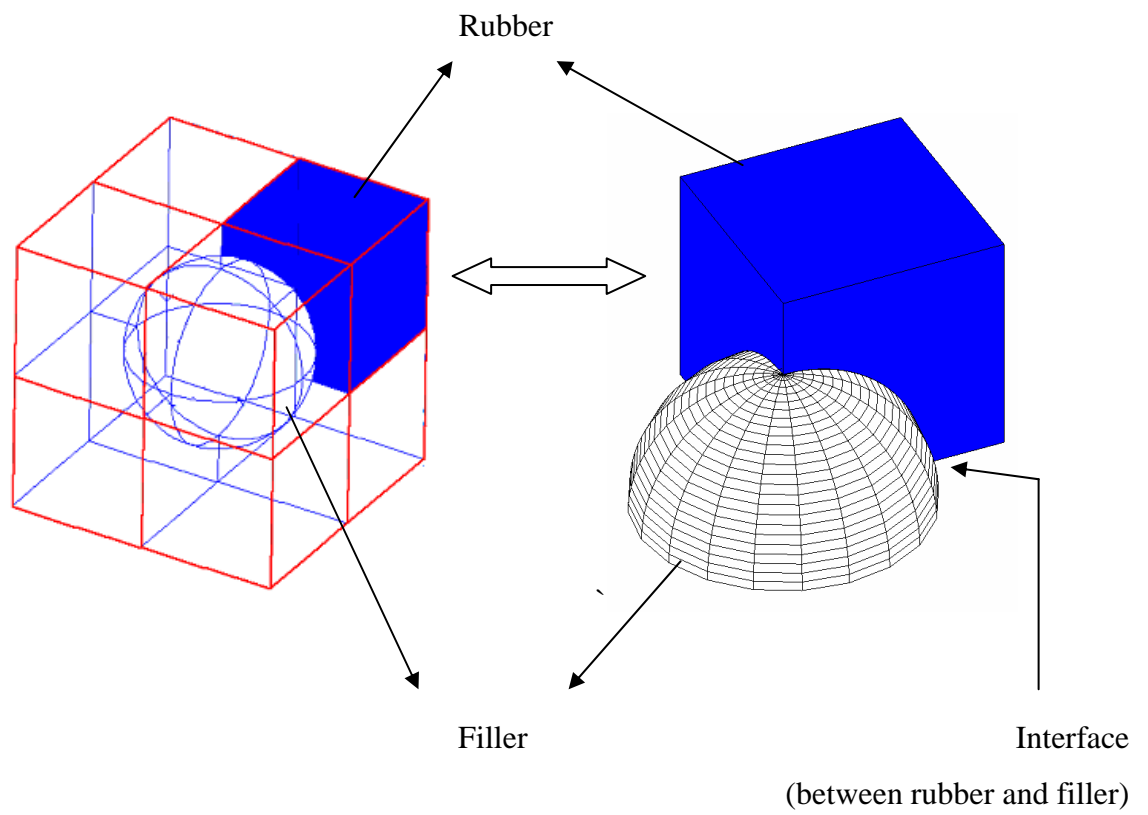


**Figure 3.7** Octant symmetry 1/8 finite element analysis representation of MT carbon black carbon particle.

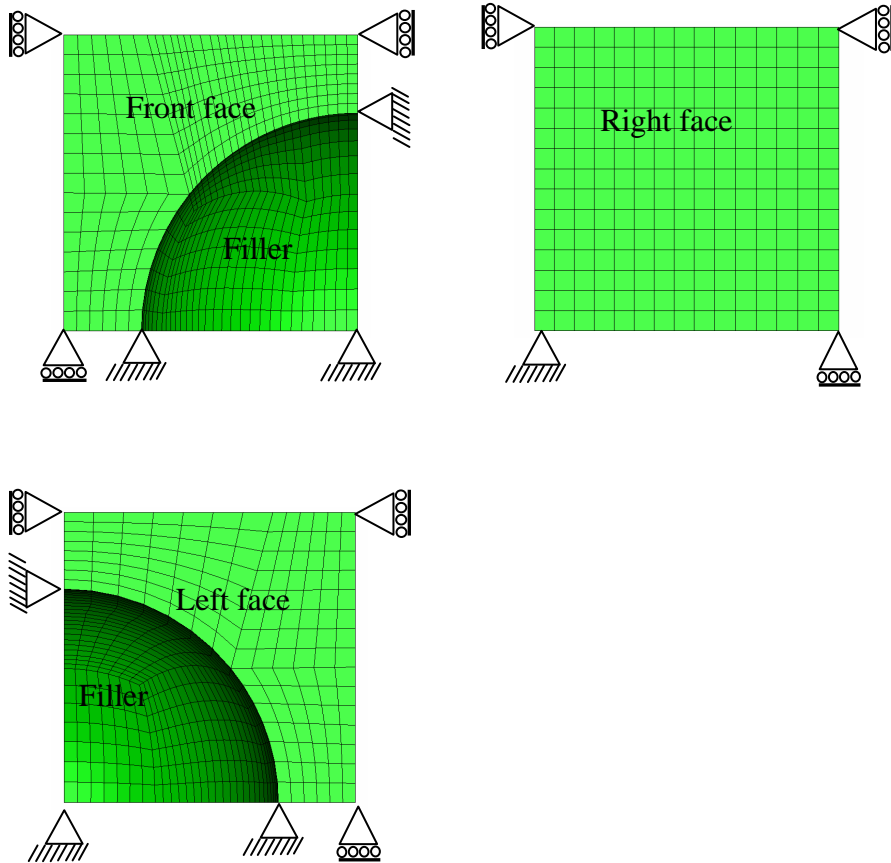
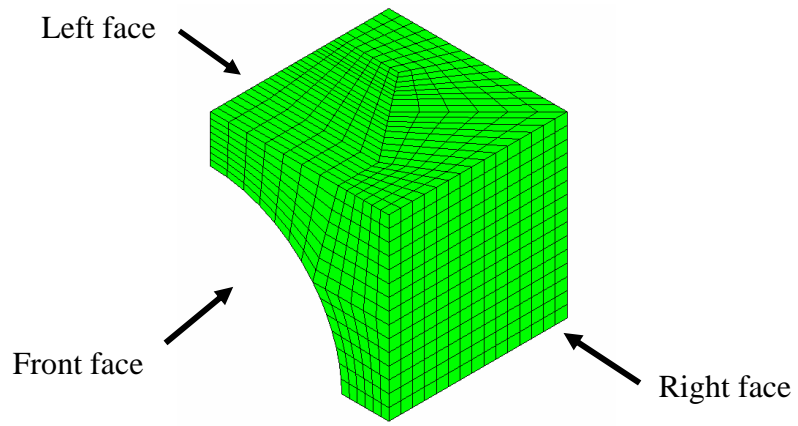


**Figure3.8** 1/8 Symmetry (octant) model showing plane surface boundary conditions.

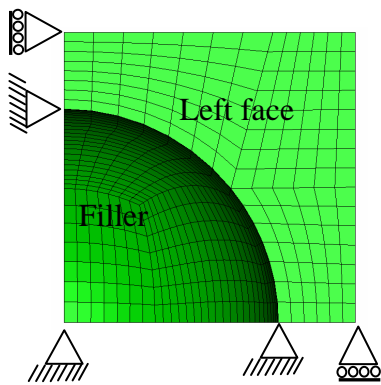
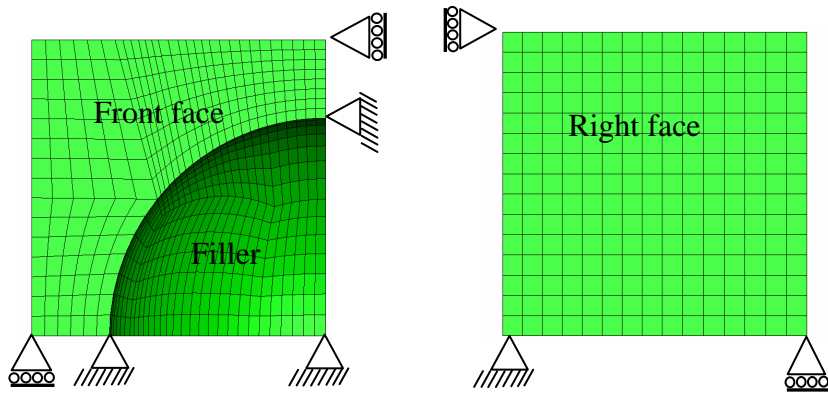
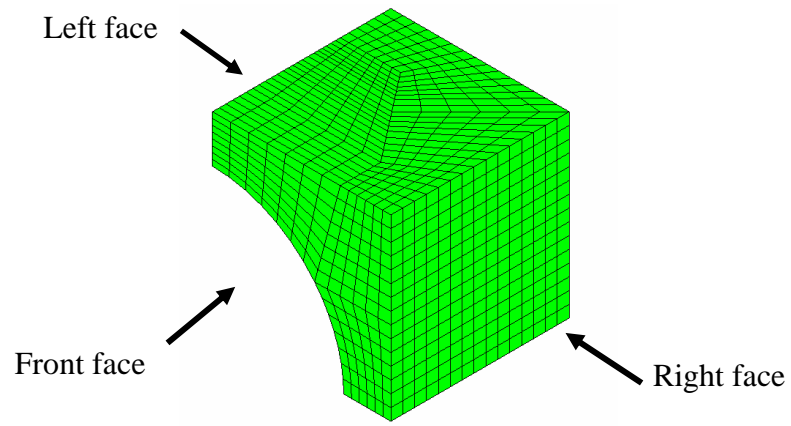


**Figure 3.9** 1/8 Symmetry (octant) model showing the free surface boundary conditions.

---

### 3.3.3 Boundary conditions

Two different types of boundary condition were used for the sides of the unit cells. The first boundary condition assumed that all the surfaces are plane and remain plane shown in Figure 3.8. The second model assumed that some of the outer surfaces not in contact directly with the filler particle were free to deform shown in Figure 3.9. The plane boundary conditions represent the interactions present in the bulk of the elastomers assuming that the fillers are evenly distributed with perfect packing and the free surface conditions represent the behaviour that is more typical close to the free surfaces of a filled rubber model.

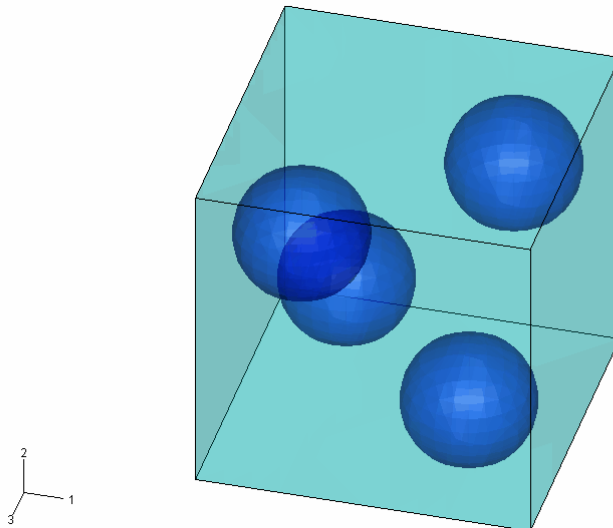


**Figure 3.10** Four filler smooth surface model

### 3.3.4 Types of smooth filler surface models: Symmetry and distribution

In the smooth filler surface models it is assumed that the near curvature matches approximately that of a sphere. The single particle model, with an assumed idealised packing array (Figure 3.7), exploits symmetry, so that only  $1/8^{\text{th}}$  of the rubber around a single filler particle was modelled. The single filler octant symmetry models are shown in Figures 3.7, 3.8 and 3.9.

---

The other models differed by either using an increased number of particles in the model (Figure 3.10 and 3.11) or by altering the surface boundary conditions.

Figure 3.10 shows a four filler particle model with an irregular distribution of particles. The rubber was assumed to be perfectly bonded to the filler. Two symmetry planes are adopted in the model; the front and right hand face as shown in Figure 3.10, make the four filler particle model behave as if it was a 16 filler particle model. The models were created using I-DEAS 9 pre-processor software and were analysed using ABAQUS v6.4 software.

Figures 3.10 and 3.11 show unstrained typical four and eight filler particle models respectively with an irregular distribution of particles. As mentioned, by exploiting symmetry it was possible to model the effect of increasing the number of particles in the model. If two of the four previously free surfaces, say the front and the right face were acting as symmetry planes then the 8 filler model now behaves as if it were a 32 filler model.

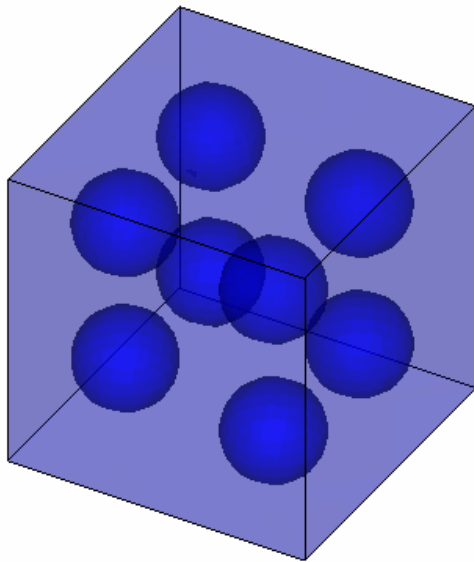


**Figure 3.11** Eight filler smooth surface model with an irregular distribution of filler particles.



---

### 3.3.5 Stepped surface model

The creation of a smooth spherical surface was difficult to achieve within the constraints of using a mesh with only solid regular brick elements. Therefore, an alternative approach was used whereby a number (in this case 9) of filler particles are incorporated into the FEA model by making a regular mesh of identical cubic elements. By selecting some elements that approximated to spherical shapes in the model it was possible to create random filler configurations. A typical mesh for this type of problem is shown in Figure 3.12.

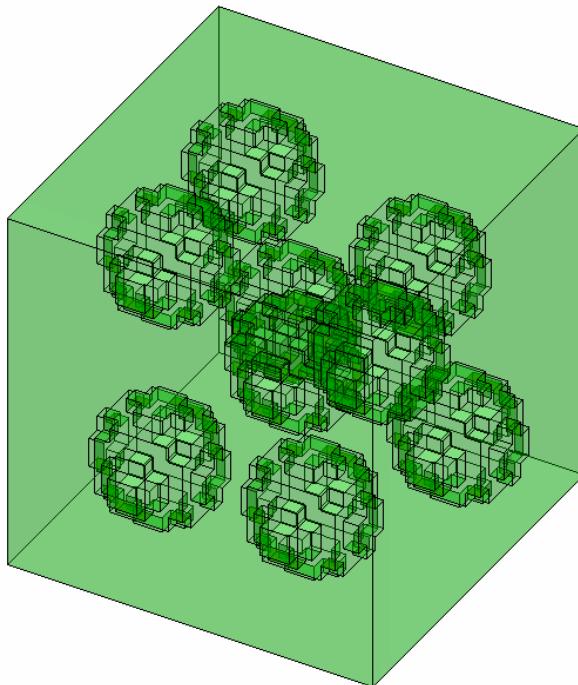


**Figure 3.12** Stepped surface nine filler model having an irregular distribution.

---

### 3.3.6 Interfacial boundary Conditions

The models discussed in section 3.3.3-3.3.5 assumed perfect boundary at the interface between filler and rubber. However, Dannenberg suggested the rubber matrix can slip over rigid filler resulting viscous-elastic energy dissipation. In present case, the interface was also modelled using the critical shear stress friction model shown in Figure 3.13, where the rubber was allowed to slide over the filler surface when the interfacial shear stress,  $\tau$ , was above a critical value,  $\tau_{crit}$ , until the rubber had slipped far enough to reduce the shear stress to below this critical value. In slippage models, the rubber was constrained to neither penetrate the filler nor to pull away from the filler surface. (Abaqus, 2001).

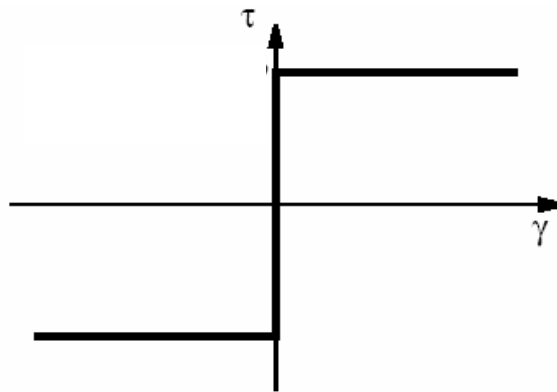


**Figure 3.13** Critical shear stress friction model behaviour between two contacting bodies. Where  $\gamma$  represents the extent of slippage.

---

## Modelling of the effect of fillers on the stiffness of rubbers

### 4.1 Introduction

Finite element analysis (FEA) is a useful technique to predict the mechanical properties such as Young's modulus, tear resistance, stiffness of the elastomeric material (such as natural and styrene butadiene filled rubber) [Bergström and Boyce (1999), Gent and Hwang (1990), and Hon *et al.* (2003)], fatigue life (Busfield *et al.*, 2005c), and abrasion resistance (Fukahori *et al.* 2007). Busfield *et al.* (2005c) used a fracture mechanics approach coupled with a combination of the experimental characterisation of rubber and FEA to predict the fatigue life of an elastomeric component. In present case a continuum mechanics approach is used to model the filled composite using finite element analysis. Being able to predict the mechanical properties of a filled composite will improve the design of rubber compounds and perhaps give a unique insight into polymer-filler interaction. Fukahori and Seki (1993) used FEA to study the stress distribution around a circular filler particle in a cubical and a cylindrical rubber matrix at small strains and large strains. Hon *et al.* (2003, 2004) used finite element analysis to understand and predict the mechanical properties for a range filled composite. Bergström and Boyce (1999) used FEA simulation for a range filler shapes in 2D and 3D to predict the behaviour of filled elastomers under compressive loading shown in Figure 2.12. Moshev and Kozhenikov (2002) studied the mechanism of debonding of the rubber matrix from the filler surface using finite element analysis. They concluded the natural sub microscopic imperfections due tiny gas inclusion are root source or micro-damage in polymers. Alternative approaches used by the researchers to study and understand the filled rubber composite behaviour have been discussed in Chapter 2. These included Sen *et al.* (2005), Kloczkowski *et al.* (1994), Sharaf *et al.* (2000), Bicerano *et al.*

---

(1997), Kluppel and Schramm (1999), Kluppel and Meier (2001) and Coveney and Johnson (1999).

The prediction of the stiffness of filled rubber is described well at small strains below about 10% by the relationship derived by Guth and Gold (1938) and Smallwood (1945). Hon *et al.* (2003) have shown that these stiffness predictions at small strains were well represented using finite element microstructural models. For moderate strains of less than 100%, Kashani and Padovan (2006) showed that the mechanical properties of filled rubbers follows a spring in series model. Further, the rubber matrix and fillers are in a state of uniform stress rather than state of uniform strain. At larger strains these existing theories cannot predict the stiffness accurately and the microstructural finite element approach has not been tried. Hence, the present work uses micromechanical modelling to predict large strain behaviour including a consideration of the finite extensibility effects for filled elastomers. A range of single filler and four filler particle models in an elastomer matrix have been investigated as shown in Figure 4.2 and 4.5. The precise boundary conditions applied to the model are important. Two extreme boundary conditions termed ‘plane surface’ and ‘free surface’ were investigated. The behaviour of unfilled elastomers is frequently modelled using a Mooney (1940) stored energy function. However, it is clear that the Mooney equation can not represent the finite extensibility stiffening behaviour at large strains. Therefore, in this work a more appropriate stored energy function proposed by Gent (1996) is used to predict the large strain behaviour and the finite extensibility effects.

Modelling of the filler reinforcement using a finite element analysis approach is a challenging problem. As discussed in Chapter 2 understanding the filler structure and the interface behaviour presents a difficulty in understanding the reinforcement mechanism. Hence, in the present case, a 3D Finite element simulation has been used to study and predict the mechanical properties. The problems associated with the complex shape, distribution and interface are discussed further in the next Chapter. The work presented is based on the publication whose abstract is listed in the

---

appendix.

Medium Thermal (MT) N990 carbon-black filled rubber composite was used due to the availability of the experimental and theoretical data. The shape of MT carbon-black can be approximated to a simple spherical shape as shown in the torn surface of a MT carbon black filled rubber in Figure 4.2. Figure 4.2 also shows that MT carbon black has a random distribution resulting from its low tendency for agglomeration. Hence, the MT carbon blacks were easier to model than the more complex structures branching and aggregation that are encountered in other types carbon blacks. The 3D finite element representations used in the present work are shown in Figure 4.2 and Figure 4.5.

## 4.2 Results and discussion

### 4.2.1 Selection of stored energy function

In order to simulate the rubber-filler interactions using FEA, the matrix elastomer behaviour has to be characterised. Elastomeric materials are characterised using stored energy functions. Stored energy functions are related to the strain invariants,

$$W = f(I_1, I_2)$$

Mooney (1940) derived a two term stored energy which has the following form,

$$W = C_1(I_1 - 3) + C_2(I_2 - 3) \quad \text{Equation 4.1}$$

Where,  $C_1$  and  $C_2$  are the material constants. The constants  $C_1$  and  $C_2$  used in this work were derived from the unfilled rubber stress versus strain measurements of Mullins and Tobin (1965). This was achieved by plotting the curve of reduced stress versus the inverse of extension ratio. The curve fitting was done so that the Mooney stored energy function represented the behaviour of the unfilled elastomer accurately up to 50% strain as shown in Figure 4.1. The constants derived for the Mooney SEF were  $C_1=0.1658\text{MPa}$  and  $C_2=0.0598\text{MPa}$ . Typically the Mooney SEF represents

---

reasonably the behaviour of an unfilled elastomer up to 100% strain in simple extension, although the fit for a more general strain is less good.

Gent (1996) derived a SEF from empirical considerations which has the form,

$$W = -\frac{E}{6} I_m \ln \left[ 1 - \left( \frac{I_1}{I_m} \right) \right] \quad \text{Equation 4.2}$$

In the above expression  $E$  represents the low strain tensile modulus and  $I_m$  introduces a finite extensibility asymptote. Gent's SEF is applicable over large strains, gives a better fit at a higher extension ratio and can be used in any deformation mode. This allows flexibility in terms of representing the behaviour of an elastomer over a range of strains. In the present case,  $E$  was fitted to represent the small strain behaviour accurately up to 50% strain as shown in Figure 4.1. The finite extensibility term was fitted to represent the behaviour accurately at 600% strain. The constants used here were  $E = 1.29\text{MPa}$  and  $I_m = 63$ .

As Mullins and Tobin's data (1965) for unfilled rubber were not available at a higher extension ratio; the fitting at higher extension ratio was carried out using data acquired on a nominally identical unfilled rubber examined by Harwood *et al.* (1967). Figure 4.1 shows that Gent's SEF shows a significant and realistic upsweep at the higher extension ratios to represent the finite extensibility of the elastomeric network.

The Mooney SEF function is widely used in industry especially for tensile loading conditions. Its use here allows a comparison to be made between the geometric stiffening behaviour and the material non linearity which the Gent equation would also be able to model at higher strains.

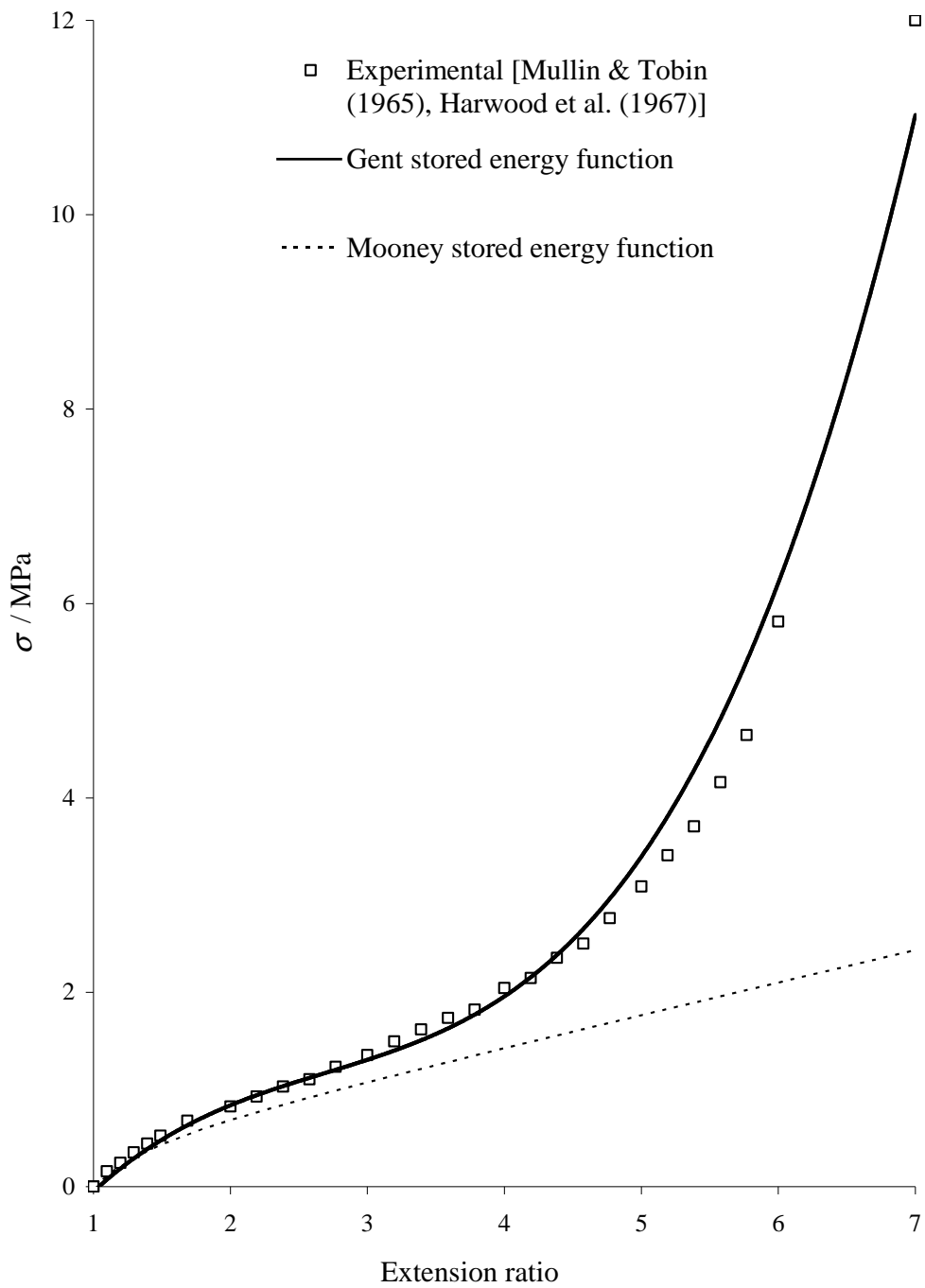


**Figure 4.1** Comparisons of experimental behaviour of the unfilled rubber from Mullins and Tobin (1965) and Harwood *et al.* (1967) with the stiffness fitted using the Mooney and the Gent stored energy functions.

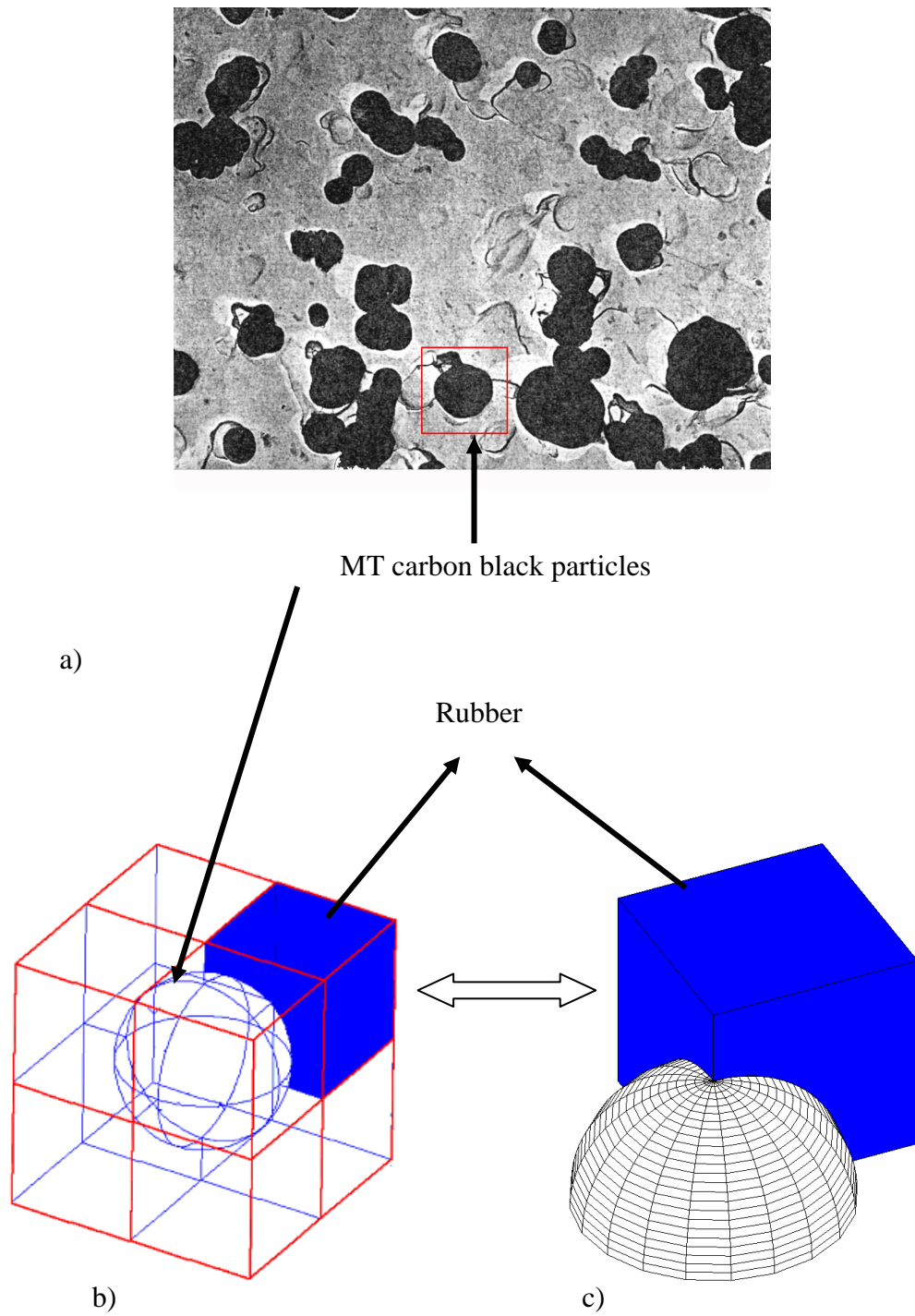


**Figure 4.2** MT carbon black filler particle in a rubber matrix a) TEM image b) Spherical filler particle in the centre of a unit cube c) octant ( $1/8^{\text{th}}$ ) symmetry model.



---

## 4.2.2 Selection boundary conditions and discussion

Earlier work by Hon *et al.* (2003, 2004) showed that the stiffness at large strains and at higher filler volume fractions was unrealistic for the plane surface models. This is because the constraints applied in these models, that all the surfaces remain plane, presents a difficulty when the deformed width of the unit cube approaches the radius of the filler. By examining such a cube in a simple extension it is possible to deduce the limiting extension,  $\lambda_c$ , at which the filler particles would touch for a given volume fraction of filler as,

$$\lambda_c = \frac{1}{4} \left( \frac{4\pi}{3\phi} \right)^{\frac{2}{3}} \quad \text{Equation 4.3}$$

The plane surface asymptotes are shown in Figures 4.8 and 4.9 as solid vertical lines for volume fractions of 13.8% and 20.9%. These asymptotes are an artefact of these particular models and will not occur with a more realistic, random arrangement of the filler particles. An initial modification to the cell boundary conditions was introduced in order to remove the limiting extension effects at large extensions and to help improve the correlation with the experimental data. To affect this change the two non symmetrical outer surfaces not in contact with the filler particle, that is the right and back surfaces as shown in Figure 4.3 were allowed to move freely. This boundary condition is termed the free surface condition. In previous work by Hon *et al.* (2003) and in the initial work discussed against here. The Mooney SEF was used. Mooney SEF can represent filler rubber behaviour accurately up to extension ratio of 1.5 and is widely used in industry for engineering applications.

Figure 4.8 shows the experimental data obtained by Mullins and Tobin (1965), as well as the FE predictions for both the single filler and four filler particle models with the plane surface as well as the free surface boundary conditions using Mooney SEF. The limiting extension effects are clearly removed in the free surface model. However, in comparison to the plane surface model, it underestimated the stress-strain behaviour quite considerably even at lower extensions. There two reasons

---

for this underestimation. First, it is apparent that the free surface boundary condition does represent the behaviour of fillers near to the edges of rubber with a softer stiffness response. In practise at larger filler volume fractions the behaviour lies somewhere in between these two extremes. Secondly, the Mooney SEF does not predict the large strain stiffening that is observed in an unfilled rubber as shown in Figure 4.1. Figure 4.3, 4.4, 4.6 and 4.7 all show the single filler ( $1/8^{\text{th}}$  symmetry) models and four filler particle models all at a 13.8% filler volume fraction with contours of maximum principal stress. Clearly the introduction of the free surface boundary condition reduces the stress when compared with the plane surface model and the model can be deformed to a greater displacement before it locks up.

Figure 4.8 shows the experimental data for the 13.8% volume fraction filled rubber and Figure 4.9 shows the experimental data for the 21% filled rubber. Firstly, a comparison of single filler and the four particle model plane surface models with the experimental data, shows that for both the stiffening effect was overestimated and unrealistic. This was largely due to the limiting extensibility effect as discussed previously. With the 13.8% filler content, the free surface four particle model shows a reasonable correlation with the experimental data over a wide range of extension ratios. Unfortunately, so far all the free surface models have underestimated the larger strain stiffening of the materials. This is as expected though as only the Mooney SEF was used. Clearly at larger strain the stresses will be underestimated as shown in Figure 4.1.

To predict the behaviour of an MT carbon-black filled rubber at larger strains and at filler volume fractions greater than 10% can not be achieved by simply altering the boundary conditions of the unit cell. At higher filler volume fractions there is greater filler-filler interaction. Gent concluded that one of the reasons the filler reinforces the rubber is due to strain amplification. This means that the local strain in rubber would be much higher than the globally applied strain. To model this Gent SEF was used in the present case. Gent SEF was fitted to represent the behaviour well up to an extension ratio of 7 as shown in Figure 4.1. As the filler volume fraction increased, larger models which incorporate more than one filler particles into the FE models

---

such as that shown in Figure 4.5 were tried. The question that needs to be addressed is how many particles would be deemed as adequate to determine the behaviour of an MT carbon-black filled rubber at large strains. In this Chapter a maximum of four particles with irregular arrangement were included in the rubber matrix model as shown in Figure 4.5. Plane and free-surface are two extreme boundary conditions, at larger filler volume fractions the behaviour lies somewhere in between these two extremes. Hence, to predict the behaviour at a higher filler volume fraction (13-20%) and especially at extension ratios above 2 the following simplifying assumptions were made,

1. Though the actual behaviour lies between the free surface and plane surface boundary conditions, free surface boundary conditions were used to avoid the geometry complexity faced during the modelling of the plane surface boundary conditions.
2. To model the filler-filler interaction multiple filler models were used in addition to a single filler model
3. To represent the asymptote (the upsweep) observed with real unfilled rubber materials, a Gent SEF was used

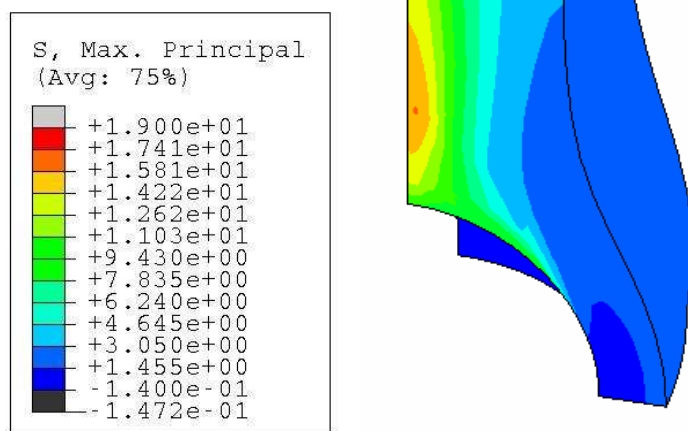


**Figure 4.3** Stress contour plots for (1/8<sup>th</sup>) octant symmetry model with a free surface boundary on two faces under a tensile strain of 150% at volume fraction of 13.8%.

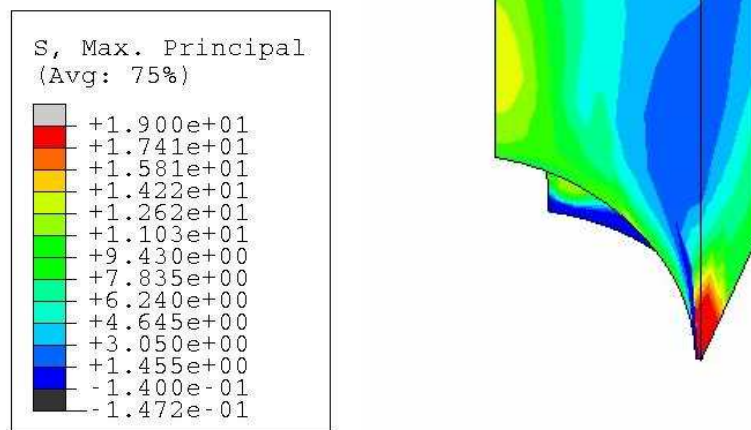


**Figure 4.4** Stress contour plots for an ( $1/8^{\text{th}}$ ) octant symmetry model with plane surface boundary conditions under a tensile strain of 100% at volume fraction of 13.8%.

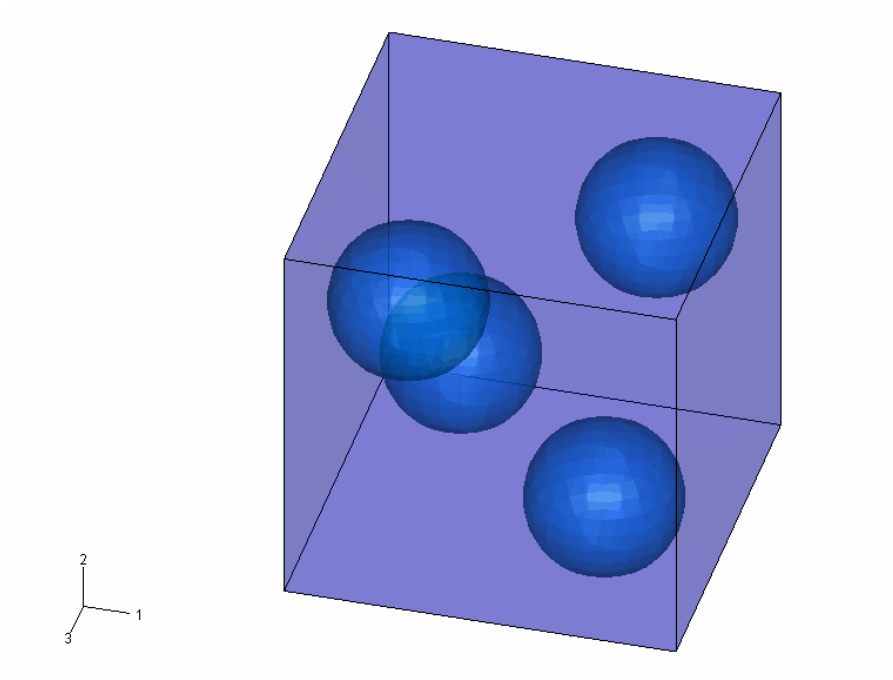


**Figure 4.5** A four filler smooth surface particle model

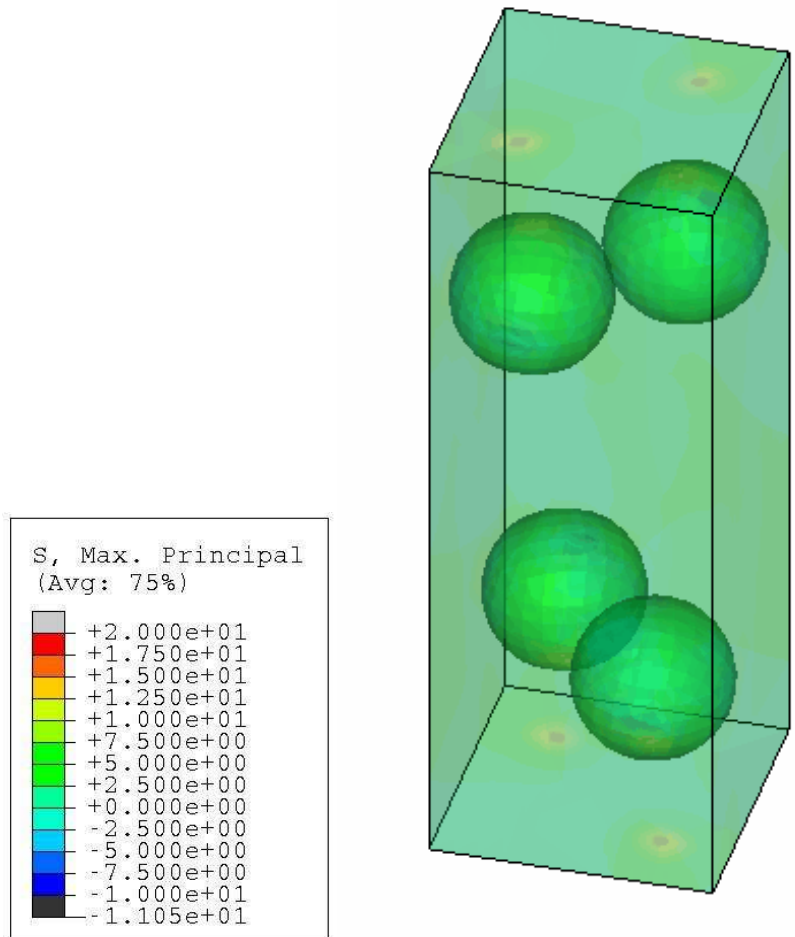


**Figure 4.6** Stress contour plots for the four filler particle model with plane surface boundary conditions under a tensile strain of 100% at volume fraction of 13.8%.

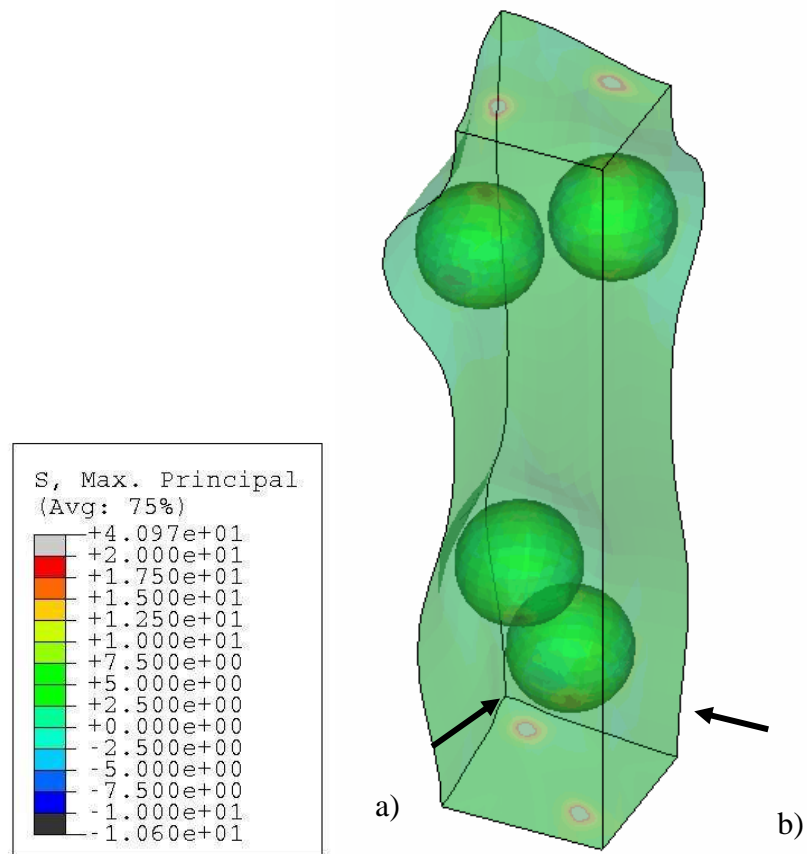


**Figure 4.7** Stress contour plots for the four filler particle model with free surface boundary under tensile strains of 100% at volume fraction of 13.8%; (The two planes a and b acts symmetry making the model behave like a 16 filler particle model).



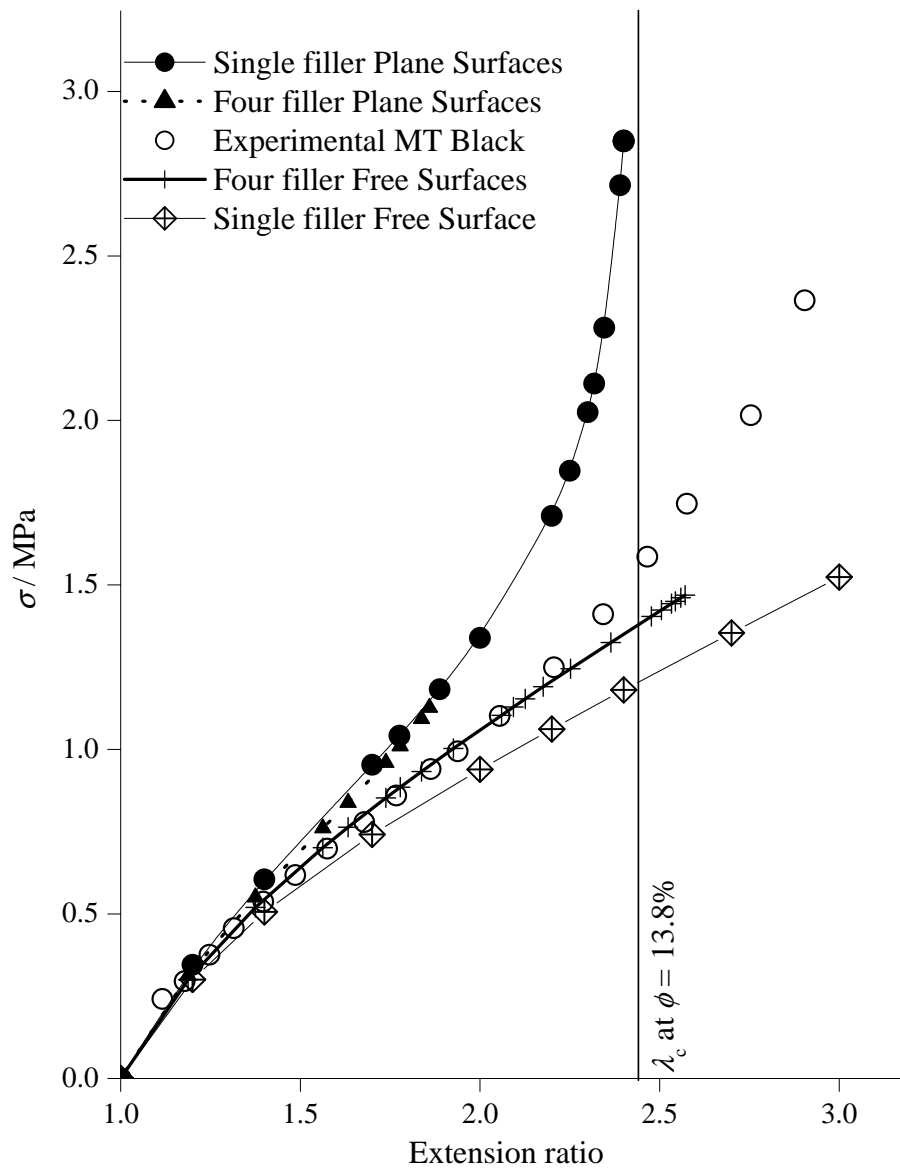


**Figure 4.8** Engineering stress versus extension ratio for MT carbon black filled rubber and models at 13.8% filler volume fraction. The limiting extension,  $\lambda_c$ , of the planar surface single particle model is shown as the asymptote. All models use a Mooney stored energy function.

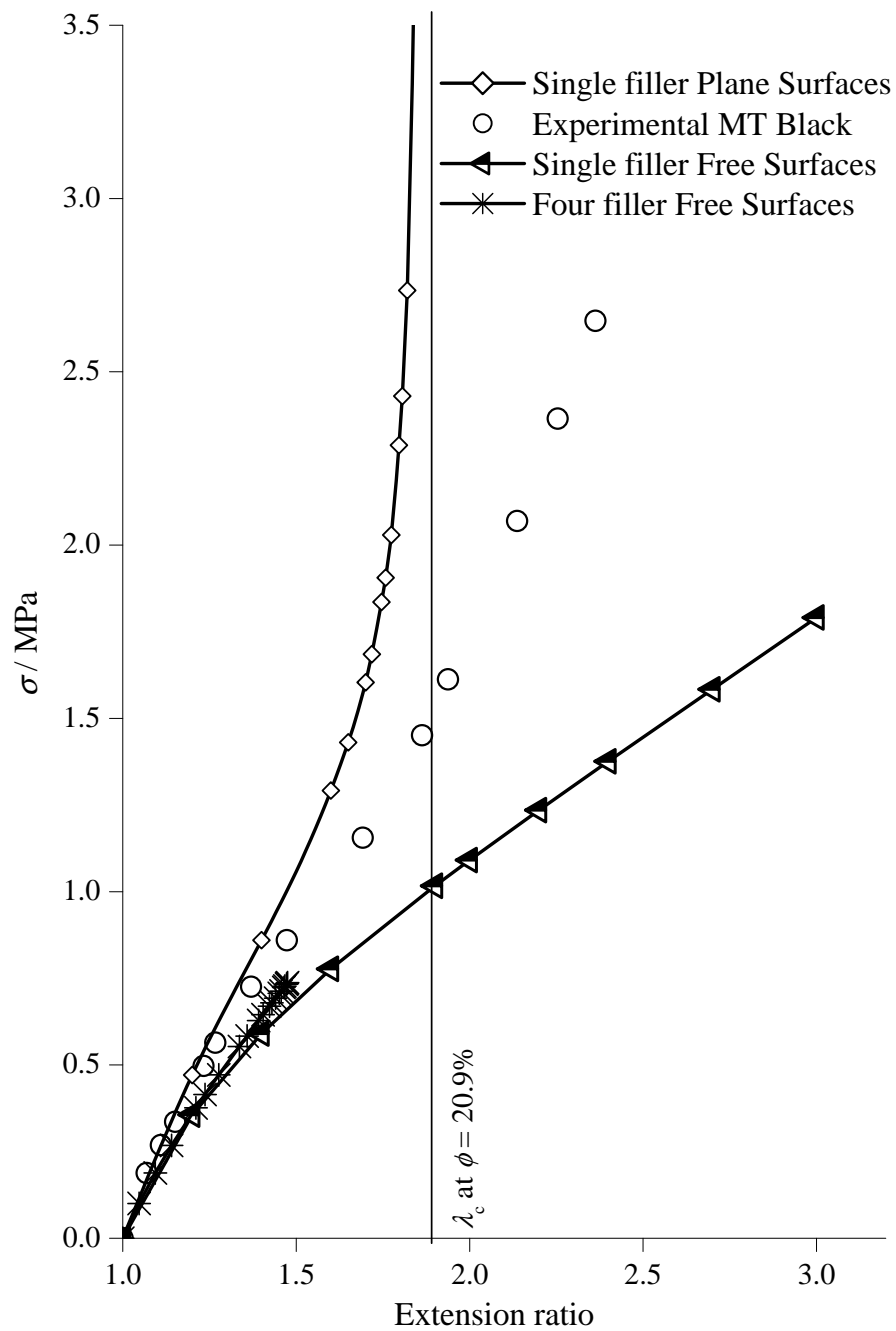


**Figure 4.9** Engineering stress versus extension ratio for MT carbon black filled rubber and models at 20.9% filler volume fraction. The limiting extension,  $\lambda_c$ , of the planar surface single particle model is shown as the asymptote. All models use a Mooney stored energy function.

---

Figures 4.10 and 4.11 show the calculated stress versus extension results at 13.8% and 20.9% filler volume fractions respectively based on these assumptions.

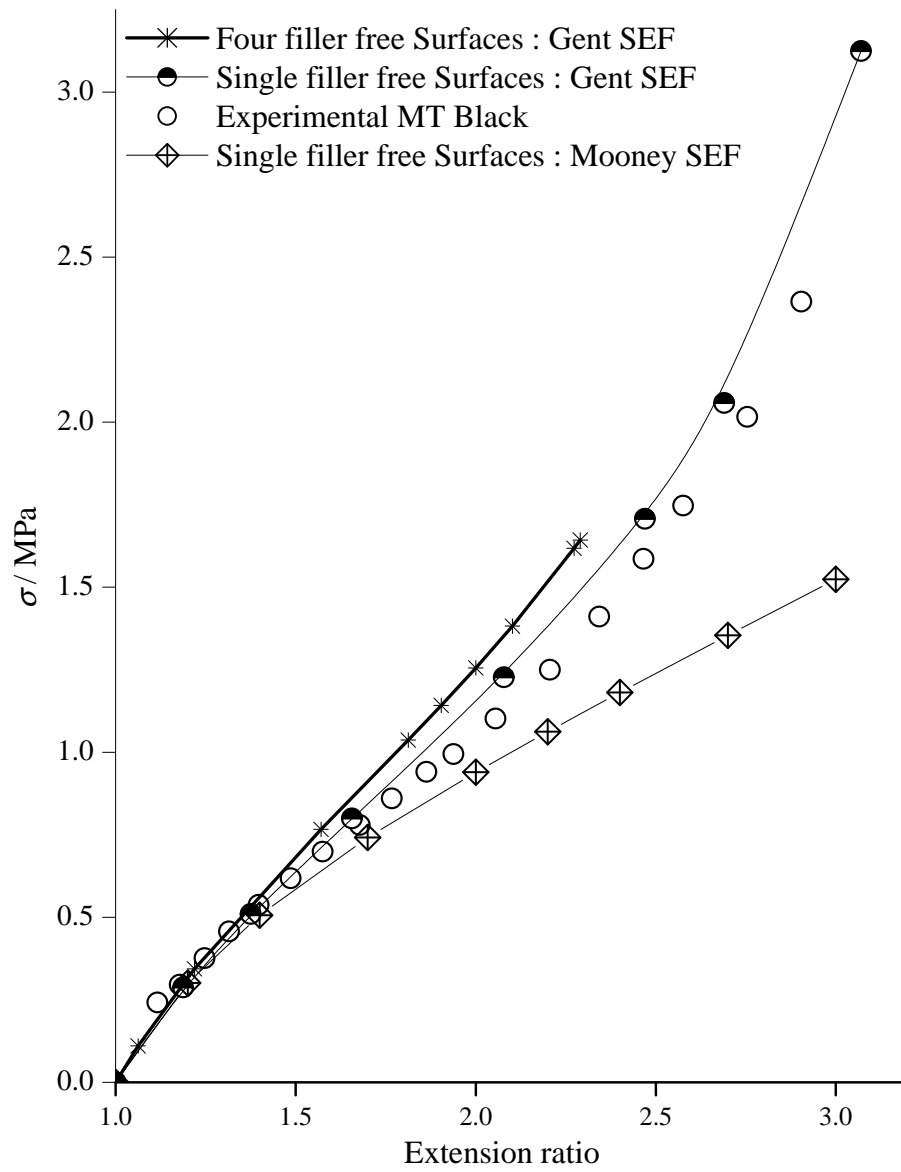
Figure 4.10 shows that a single filler particle model using Gent SEF follows the experimental observed behaviour more closely than single filler particle model based on Mooney SEF. This is because Mooney SEF is unable to predict the finite extensibility behaviour. The four filler particle model using the Gent SEF over predicts the stiffness when compared to the experimental observed behaviour at 13.8% volume fraction. This could be attributed to an over simplification of the filler-rubber interface as being perfectly bonded.

Figure 4.11 shows the results at a filler volume fraction of 20.9%. The single filler particle model using the Gent SEF shows an upswing in stiffness when compared to model based on the Mooney SEF which at extension ratio above 2 under predicts the experimental observed behaviour. The single filler free surface models using either the Mooney or Gent stored energy functions at 20.9% filler volume fraction show a much softer response than the experimentally observed behaviour when compared to the model at a 13.8% filler volume fraction as shown in Figures 4.8, 4.9, 4.10 and 4.11. This indicates that at a higher filler volume fraction there are greater filler rubber and filler-filler interactions. So the single filler particle is no longer appropriate for modelling this higher filler volume fraction.

The four filler particle models (random free surface) using Gents stored function at 13.8% volume fraction (shown in Figure 4.10 and 4.11) over predicts the experimentally observed behaviour as the applied strains increase. This indicated there is a greater filler interaction at higher strains in these multiple filler particle models. It appears that as the filler volume fraction rises then an increased number of particles are required to model the behaviour. For all the cases discussed the filler was perfectly bonded at the interface, this is the most likely reason for the over prediction of stiffness by the multiple filler particle model based on the Gent stored energy function. Dannenberg (1966) suggested that at larger strains there is some slippage of the rubber over the filler surface. In the next Chapter 5, different boundary conditions

---

at the filler rubber interface are investigated to model this behaviour. This can be done by considering slippage at filler rubber interface. Slippage at filler rubber interface will allow filler particle to slide at an appropriate shear stress, causing a decrease in the stiffness and an increase in the internal viscosity. This model will overcome the limitation of perfectly bonded model presented here. The four filler particle model in Figure 4.5 shows how the spatial arrangement of particles in elastomeric matrix model can affect the stiffness predictions. Hence, future models should consider the effects of particle distribution. The ideal filled rubber model should be made with fillers randomly distributed in elastomeric matrix.



**Figure 4.10** Engineering stress versus extension ratio for MT carbon black filled rubber and models at 13.8 % filler volume

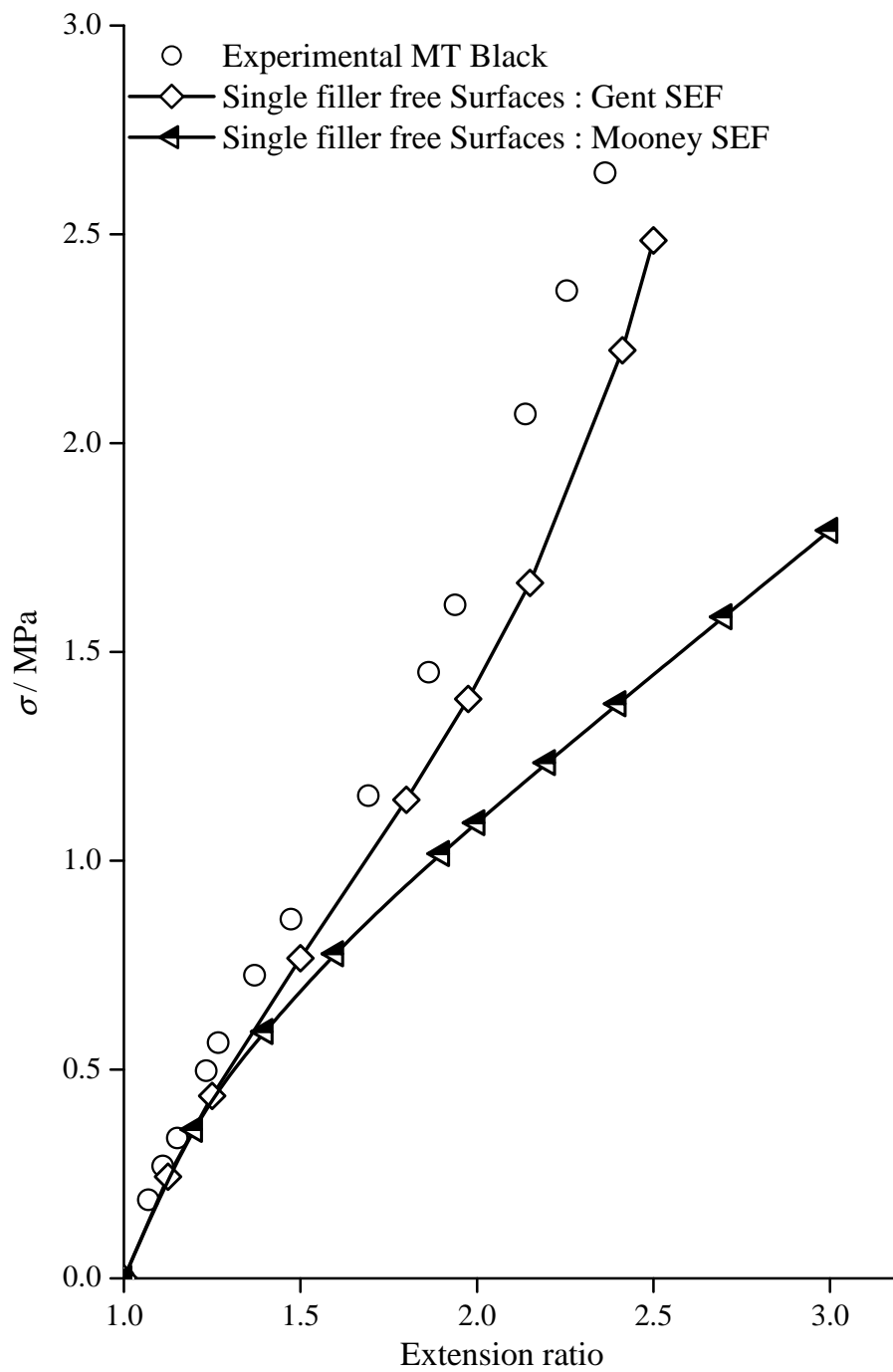


**Figure 4.11** Engineering stress versus extension ratio for MT carbon black filled rubber and models at 20.9 % filler volume fraction.

---

### 4.3 Conclusions

1. A single filler model ( $1/8^{\text{th}}$  symmetry with perfect bonding) using plane surface boundary conditions was able to predict the behaviour of carbon black filled rubber well at small strains. Although the single filler model was able to model large strain behaviour at low filler volume fractions, complexities arise when trying to use the same model to predict large strain behaviour.
2. The model either overestimated or underestimated depending on the type of boundary condition used. This led to the development of a four filler model in an irregular arrangement which improved the predictions of the stiffness behaviour, but still resulted in either an overestimation or an underestimation depending upon the exact boundary conditions adopted and stored energy function used.
3. The Mooney stored function can be used at to describe the rubber behaviour at lower extension ratios of less than 1.5.
4. Strain amplification due to the presence of the filler results in local strains being significantly higher than the globally applied strain, therefore a stored energy functions such as the one proposed by Gent that can introduce finite extensibility effects is more appropriate.
5. Future work carried out in Chapter 5 considers expanding the four filler particle model to investigate the effect of different spatial arrangements and the effect of modifying the interfacial boundary between the filler and the rubber.

---

## Microstructural modelling of filler reinforcement: Effect of Filler distribution and Interface

### 5.1 Introduction

Individual carbon black particles have sizes that range from 10nm to 500nm in diameter. Donnet and Voet (1976), Kraus (1978) and Hepburn (1984) have all shown that the basic size of the carbon black particle plays an active part in the reinforcing effects when included in the rubber. An increased carbon black particle size having a reduced reinforcing effect. The critical effect appears to be the ratio of surface area to volume, carbon black with large values having increased reinforcement behaviour. The phenomena of filler reinforcement is explained in the literature review using a combination of hydrodynamic, strain amplification, bound rubber and occluded rubber models. However, these models are not able to describe all the observed phenomena such as stress softening or the hysteresis behaviour completely. Hence, there is a need to understand the effect of size, shape, particle distribution and the interfacial boundary conditions on filler reinforcement.

Smit *et al.* (2000) and Sluis *et al.* (2001) tried a range of 2D models to study the effect of the heterogeneous distribution (random distribution) of voids and filler particles in the matrix polymer as shown in Figures 2.16, 2.18 and 2.20 respectively. Smit *et al.* (2000) proposed that the irregular distribution of voids promotes the spread out of plastic strains over the whole microstructure. Fukahori (2007) proposed the filler rubber interface model shown in Figure 2.7. The interface consisted of two layers namely glassy layer (GH, extending couple of nanometres) and sticky layer (SH, around 3-8 nanometers). Polymer filler interface and interaction is a combination of the physical and chemical interaction. Dannenberg (1966) and



---

Boonstra (1967) suggested that the rubber matrix can slip over the filler. If rubber can slip over the filler surface then it can also act as a stress distributor. Polymer chains under the applied stress would be able to distribute stress by slipping and hence avoid the chain breakage. Bicerano *et al.* (1997) used a numerical modelling and implemented slippage in a 2D model to calculate the stress for amorphous rubbery polymers. Slippage was controlled by the kinetic properties such as the activation energy and activation volume.

Jha *et al.* (2007), Busfield *et al.* (2005a) and Hon *et al.* (2003) used a range of micro structural finite element models to predict the stiffness behaviour in filled elastomers. Some aspects of this work are described in chapter 4. Strain amplification in a filled elastomer creates local strains in the rubber that are significantly higher than the global strains and the effects of finite extensibility of the polymer network are therefore important at relatively modest strains. To predict the up-sweep observed in experimental behaviour a stored energy function that exhibits finite extensibility, such as that proposed by Gent (1996) is required to predict the stiffness of the filled elastomer at higher strains.

In deriving Einstein's viscosity law it is presumed that there is no slippage at the rigid particle / liquid interface. This assumption is carried forward into the work of Guth and Gold (1938) and their predictions for the increase in the modulus are given by Equation 2.8. However, many workers such as Fletcher and Gent (1950) have proposed that at larger strain there is some slippage at the surface. By adopting a similar approach to that of Guth and Gold (1938), it is proposed here that from the Taylor (1932) viscosity law equation, a modulus relationship for a rigid spherical filler around which the rubber can easily slide can be derived by assuming that the viscosity of one of the liquids in Equation 2.13 is zero. Therefore, a new relationship for the modulus assuming zero friction at the interface is derived as.

$$E = E_0(1 + \phi) \quad \text{Equation 5.1}$$

This chapter discusses how the number and the spatial location of the filler particles modifies the stiffness calculations under strain using a finite element analysis

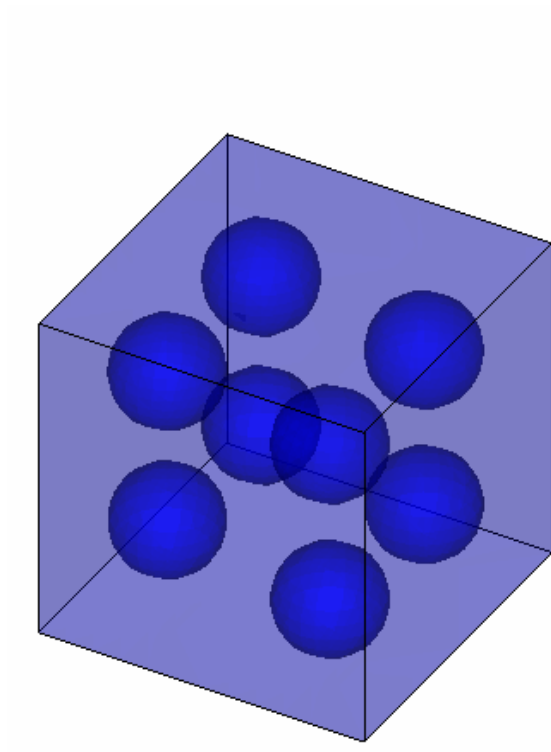
---

micro-mechanical modelling approach. Different modelling approaches are discussed. This work also aims to model the larger strain behaviour for a range of filler volume fractions by using an appropriate interfacial slippage model using an FEA technique. The results of the model have been compared with theoretical relationships derived from either Einstein's or Taylor's equations for perfect bonding or zero bonding respectively. The work presented is based on the publication whose abstract is listed in the appendix.

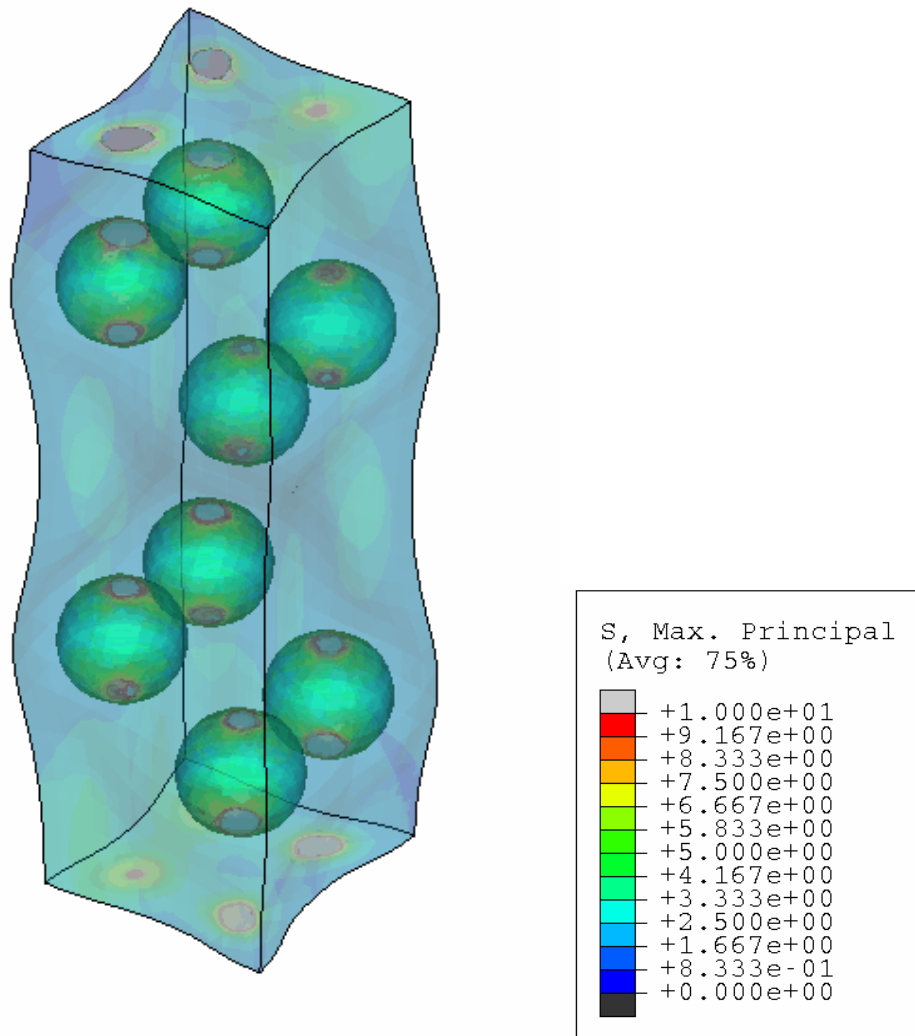
## 5.2 Effect of distribution

Figure 5.3 compares the stiffness of the 4, 8, 16 and 32 sphere models all with the fillers in an irregular arrangement compared with the experimentally observed behaviour and the single filler model taken from Figure 4.10 (Jha *et al.* 2007). At a filler volume fraction of 13.8% these models are all stiffer than the experimentally observed behaviour. As the number of fillers is increased then the model becomes progressively stiffer. This is the result of increasing the number of filler particles which increases the filler-filler interaction and this reduces the significance of the free edges to the model that are present in the single filler model.

For the model to be an appropriate one for a rubber material it is important that the model should exhibit isotropy. This is easily confirmed by imposing a uniaxial tensile stress in each of the three principal orthogonal directions independently, in addition the shear stress behaviour can be modelled as well. The results are shown in Figure 5.4. It can be seen that the tensile stiffness for the 8 filler model was the same in all three directions. At small strains for an incompressible material such as rubber, the tensile modulus is three times the shear modulus. To compare isotropy the average shear stress x3 (three times the shear stress) was compared with the average tensile stress. Between 0-50% strains the two curves showed reasonable correlation confirming atleast at modest strains the isotropic nature of this model.



**Figure 5.1** 8 filler smooth surface filler particle model when unstrained.



**Figure 5.2** Eight filler particle model smooth filler surface model under uniaxial tensile strain of 100%.

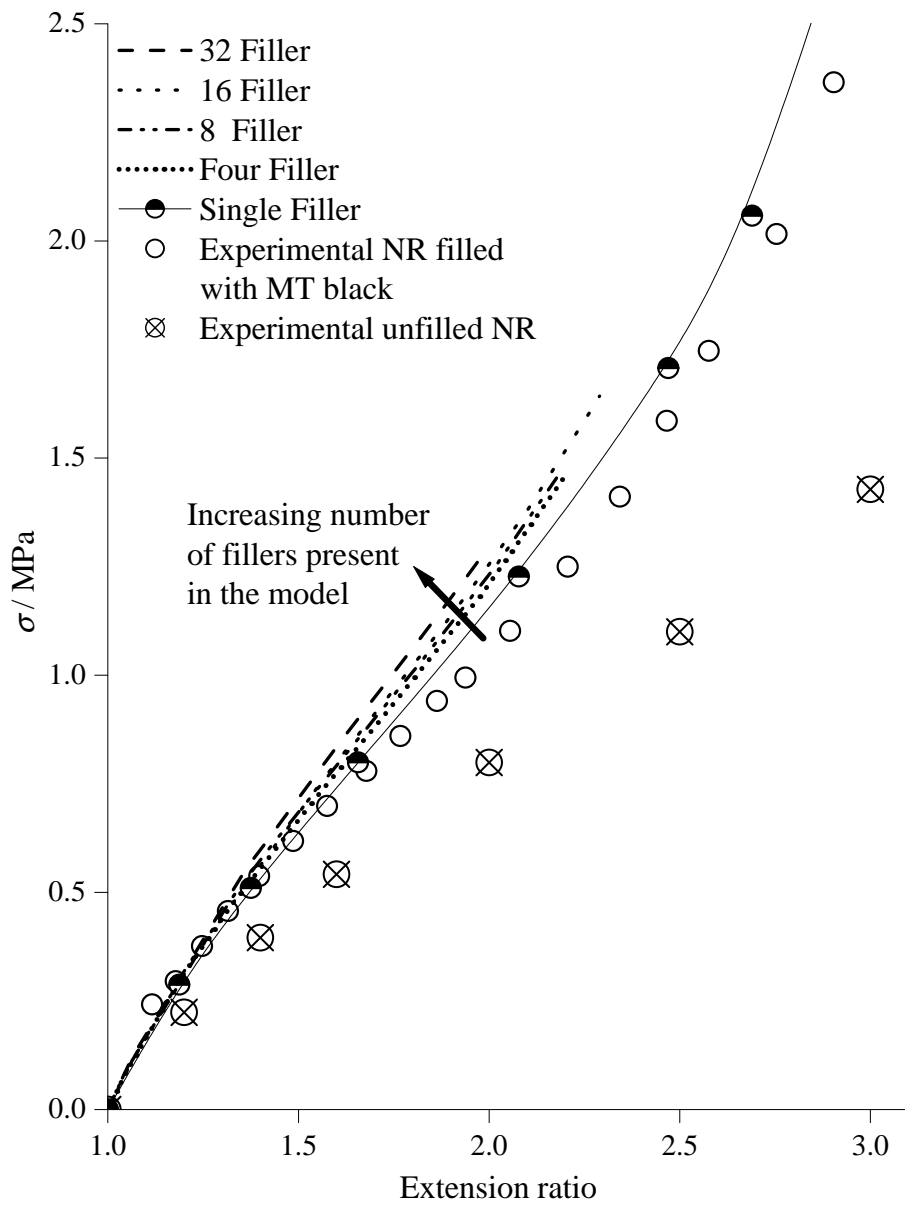


**Figure 5.3** Average engineering stress versus extension ratio for 4, 8, 16 and 32 filler particle models at 13.8% filler volume fraction for smooth filler surface models.

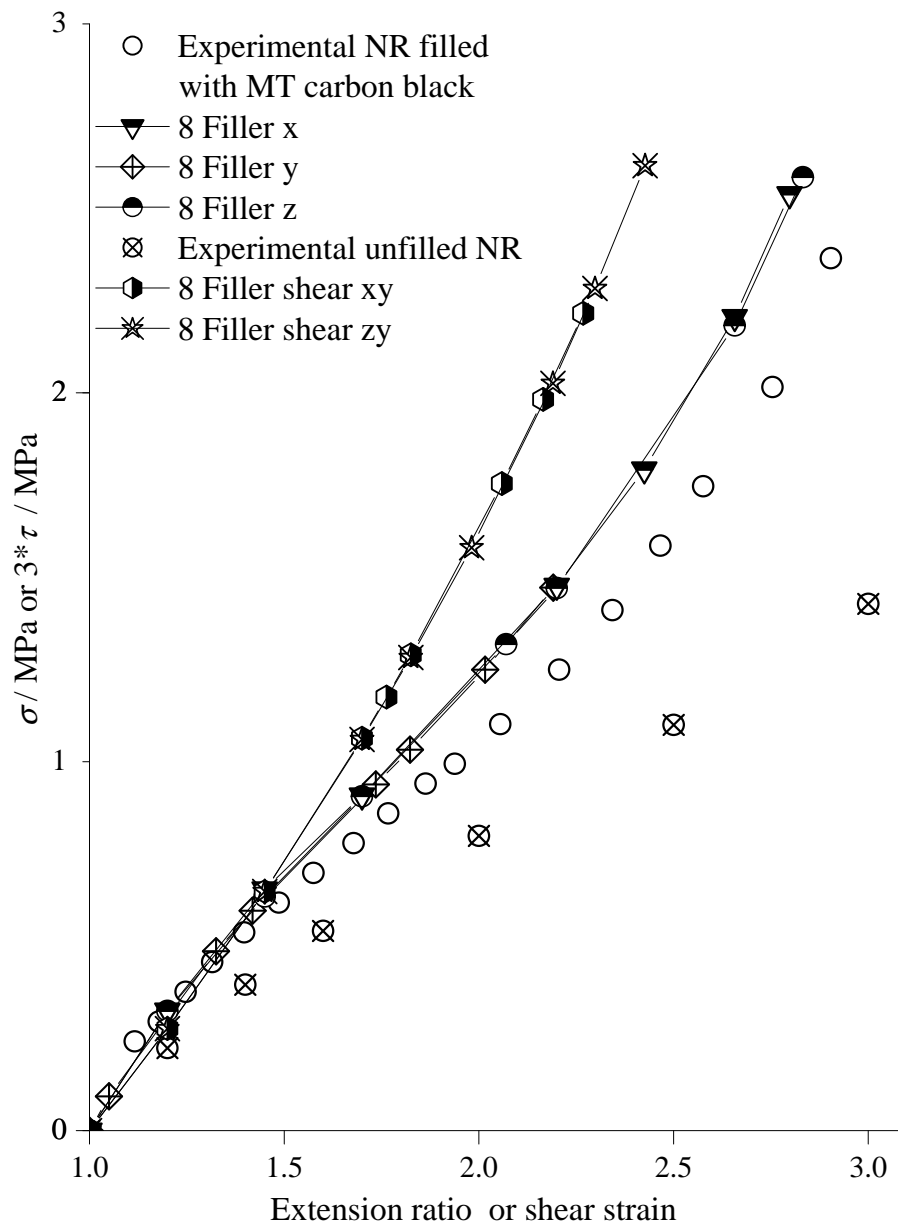
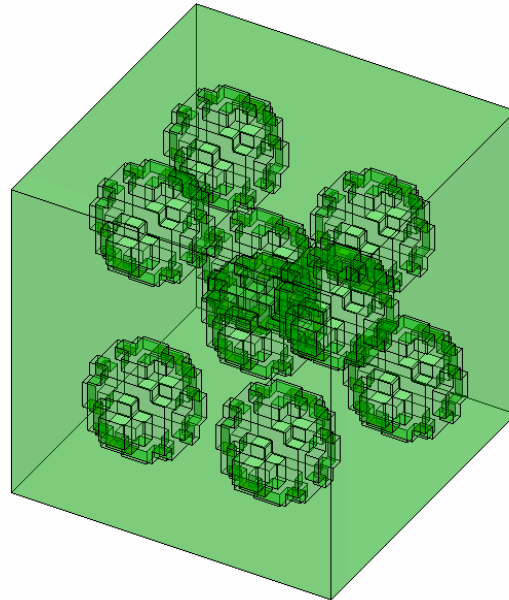


**Figure 5.4** Average engineering stress versus extension ratio for 8 filler particle smooth surface models at 13.8% filler volume fraction showing the extent of the isotropic behaviour in the three orthogonal loading directions and subjected to a shear stress.

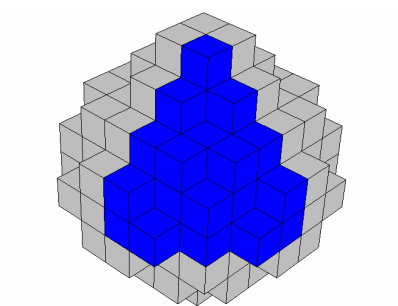
---

There were considerable meshing and modelling difficulties associated with the creation of models with a totally random arrangement of smooth surface spherical fillers. A new approach is suggested here. First a cube is tightly meshed with some of the elements in defined areas that approximate to the correct shape and volume fraction for the filler being given the material properties for a rigid filler. This gives rise to a stepped surface on the filler as shown in Figure 5.5.

This type of modelling approach gives total freedom in terms of the location, number and shape of the filler particles present in model. A nine filler particle model was created at a filler volume fraction of 13.8%, as shown in Figure 5.5. Figure 5.7 shows that this nine filler particle model at a specific filler volume fraction was significantly stiffer than the experimentally observed behaviour. This was because the effective filler volume fraction modelled was greater than that of the filler alone. As a result of the stepped filler surface there were a significant number of rubber elements adjacent to the filler having a reduced mobility. A condition similar to that of occluded rubber whereby some of the rubber chains are trapped within the confines of the filler. This increases the effective filler volume fraction. In the present case, the amount of the occluded rubber was calculated from the volume which was restricted to move due to filler surface. Figure 5.5b and 5.6a shows a single filler and a filler octant. Figure 5.6a shows there are three types of rubber element adjacent to the fillers. The first are the elements adjacent to just a single surface, these are effectively totally free rubber. The second are rubber elements adjacent to 2 filler surfaces which are shown in Figure 5.6a as the empty ovals. The third types are adjacent to 3 surfaces which are shown as the full ovals. It appears that the elements adjacent to 2 surfaces are not tightly constrained but the ones that are adjacent to 3 surfaces are highly constrained. If it is assumed that  $\frac{3}{4}$  of the volume of the elements adjacent to the 3 filler surfaces are fixed then the additional volume of bound rubber in the 13.8% model was 1.8% and the effective filler volume fraction was 15.6%. At small strains (2%) the effective filler volume fraction and the initial stiffness calculated by the Guth and Gold (1938) relation (Equation 2.8) were in good agreement.



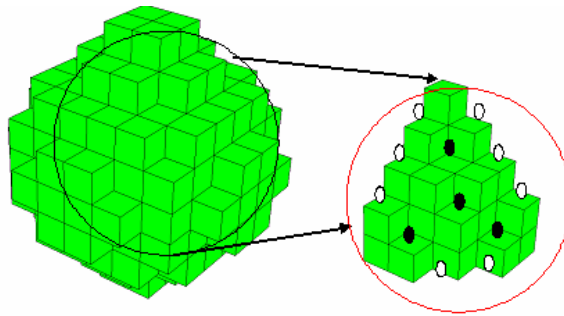
a)



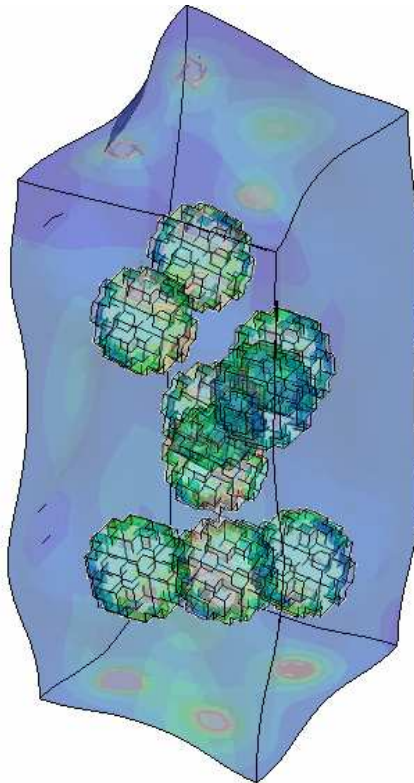
b)

**Figure 5.5** FEA filler model with stepped surface a) Nine filler stepped surface particle model with irregular distribution in the unstrained state b) Octant ( $1/8^{\text{th}}$ ) of the filler highlighted.





a)



b)

**Figure 5.6** Mesh for the nine filler stepped surface particle model under strain and unstrained. Highlighting the occluded rubber on a typical filler surface a) Single filler particle highlighting its bound rubber content in an octant model. ○ highlights rubber elements adjacent to 2 filler surfaces, ● highlights rubber elements adjacent to 3 filler surfaces b) Nine filler particle model under a 50% tensile strain.

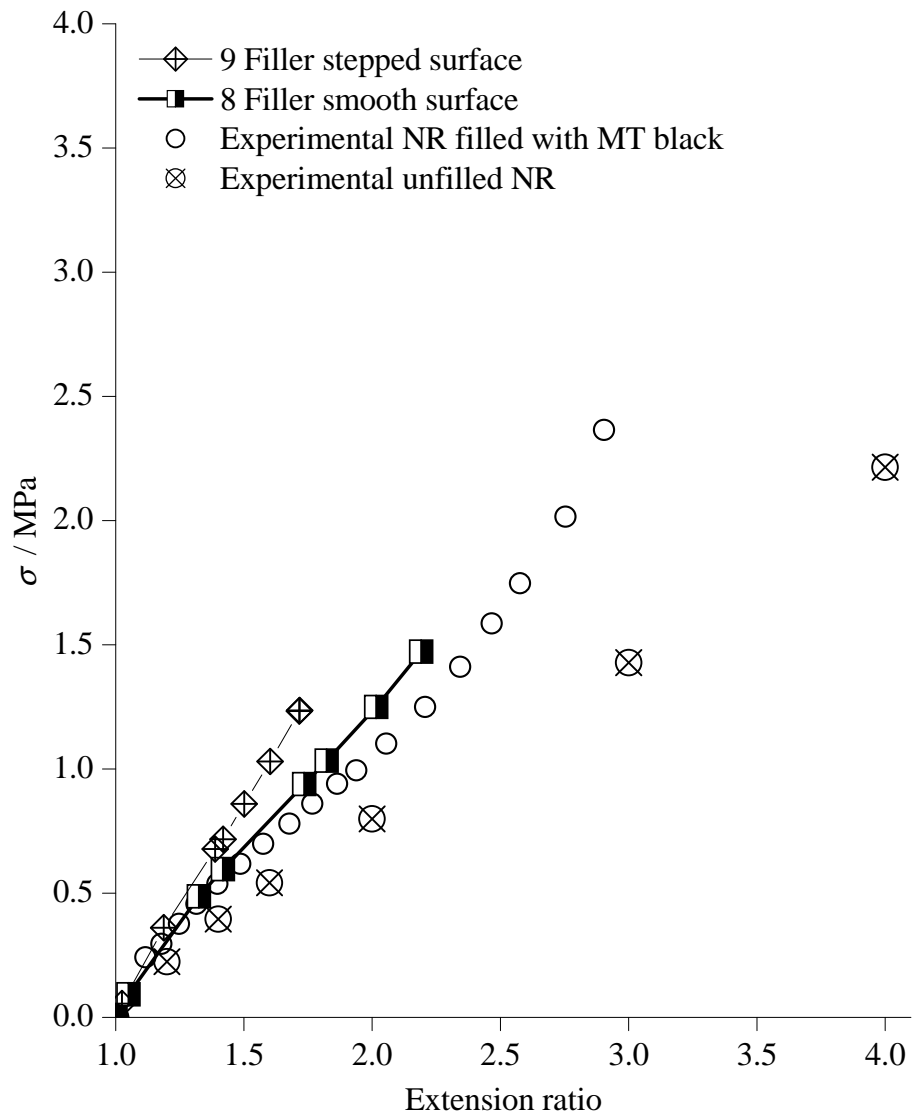


**Figure 5.7** Average engineering stresses versus extension ratio for an 8 filler and 9 filler stepped surface particle models at 13.8% filler.

---

In order to check the isotropy of this 9 filler particle model, it was also strained in the three orthogonal directions and in shear. Figure 5.8 shows that the model when strained in the z direction was stiffer than in the x and y directions. However, the difference was small. The 3 times average shear stress value for the nine filler particle model also showed a reasonable correlation with the average tensile stress at small strains.

Further work is required to use these approaches to model an even greater number of filler particles to see if effects such as the bound rubber and the occluded rubber can be effectively modelled. One underlying assumption so far has been that the filler rubber interface can be considered perfectly bonded. An alternative approach might be to introduce an appropriate amount of slippage at the interface; this might help explain the complete behaviour for the filled elastomer models.

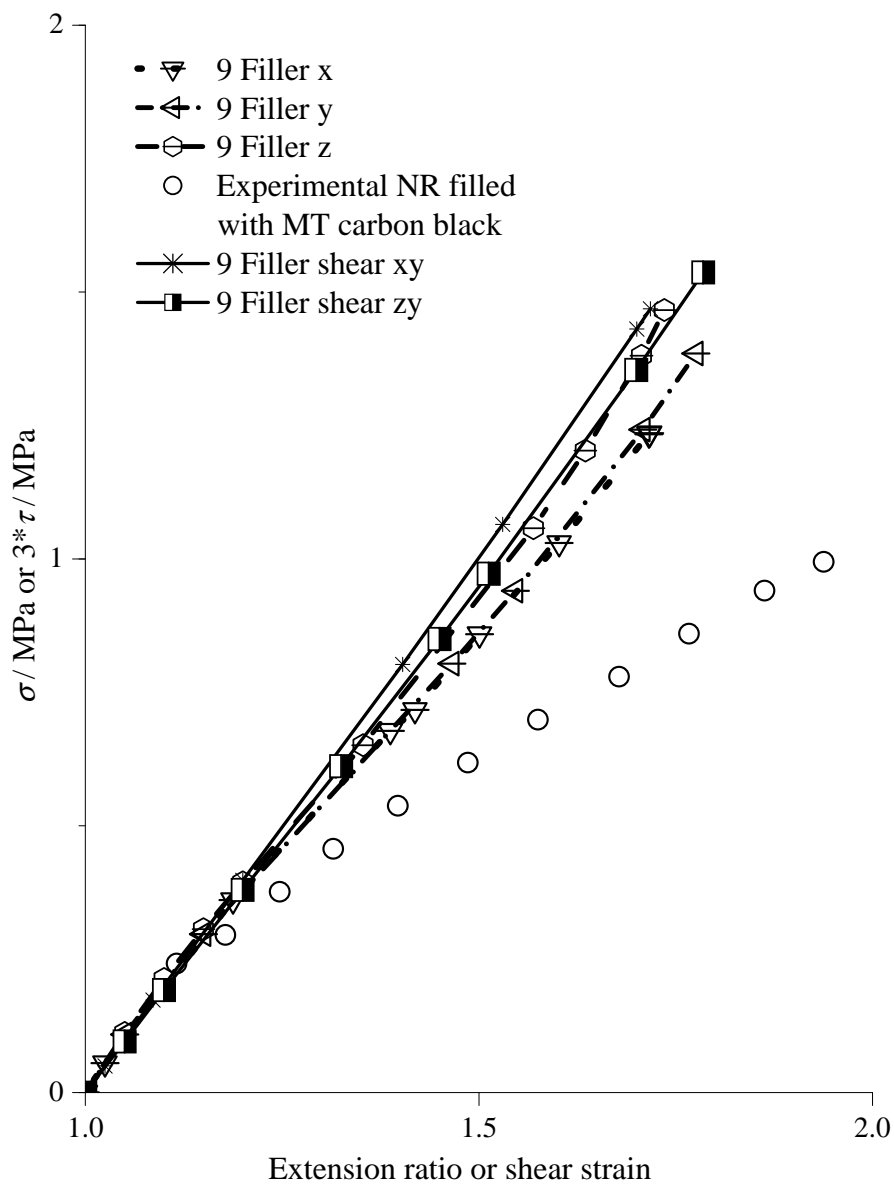


**Figure 5.8** Average engineering stresses versus extension ratio for a 9 filler stepped surface particle models at 13.8% filler volume fraction showing the extent of the isotropy in the three orthogonal loading direction directions and subjected to a shear stress.

---

### 5.3 Interfacial slippage

Figure 5.10 shows a comparison between the predicted stiffness of a series of 2D models in an idealised packing array with both perfect interfacial bonding and also with interfacial slippage at a critical shear stress value ( $\tau_{\text{crit}}$ ) of 0.5 MPa. The modulus increases with the filler volume fraction, as does the apparent change in behaviour at larger extensions resulting from the introduction of some slippage at the rubber-filler interface. The local shear stresses at the interface clearly increase as the filler volume fractions increases. At the highest filler volume fraction of 40% there is a clear differentiation in the behaviour seen even at the relatively modest extension ratio of about 1.5. Figure 5.11 shows a stress-versus extension ratio plot for various 2D models at the largest 40% filler volume fraction. It compares the perfectly bonded model with a frictionless model as well as models with  $\tau_{\text{crit}}$  values of 5, 0.5 and 0.0001 MPa. As expected the perfectly bonded model has the highest stiffness response and the frictionless model has the lowest stiffness response which is almost identical to the model with a critical shear stress value of 0.0001 MPa. The  $\tau_{\text{crit}} = 0.5$  MPa model showed a decrease in stiffness response starting just below an extension ratio of 1.5. This is the starting point where rubber at the filler interface started to slip across the filler surface, resulting in a decrease in the stiffness. By further increasing the critical shear stress to 5 MPa, the model gave a stiffness response that was virtually identical to the behaviour of the perfectly bonded sample.

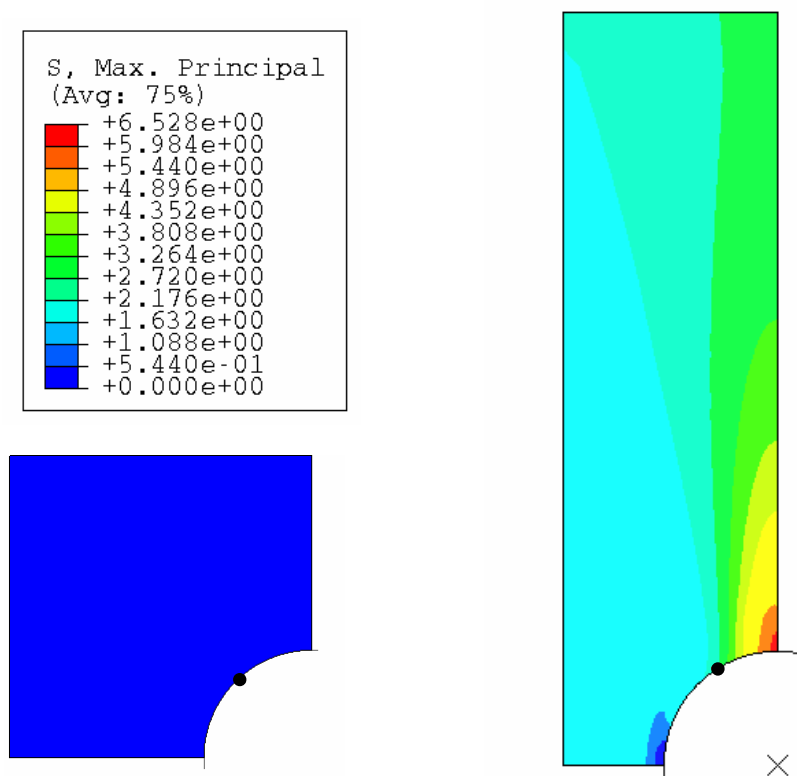


**Figure 5.9** 2D quarter symmetry circular filler particle model at 5% filler volume fraction (left) undeformed shape (right) under deformation with the slippage of a node on the rubber surface highlighted as the black dot.

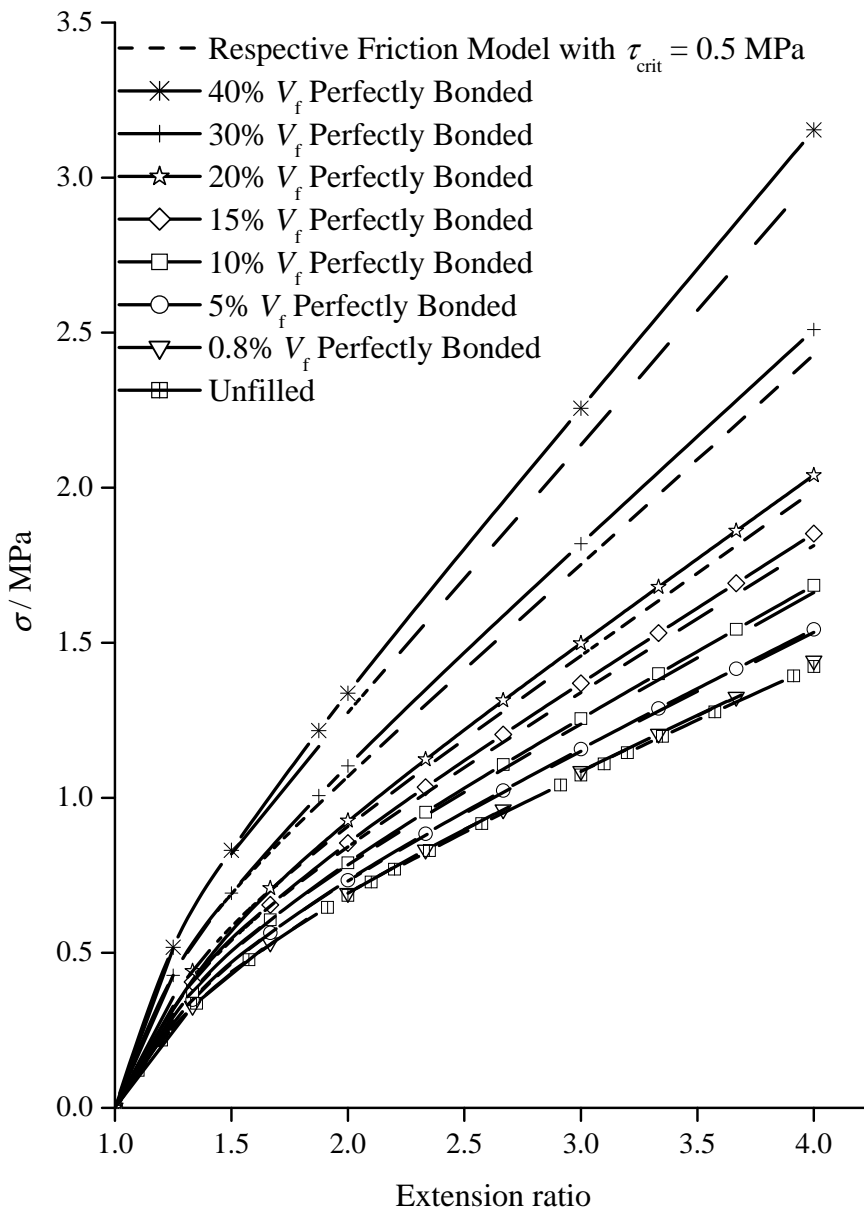


**Figure 5.10** Engineering stress versus extension ratio for various 2D plane stress models for a range filler volume fractions. Both the slippage models and the perfectly bonded models are shown at each volume fraction.

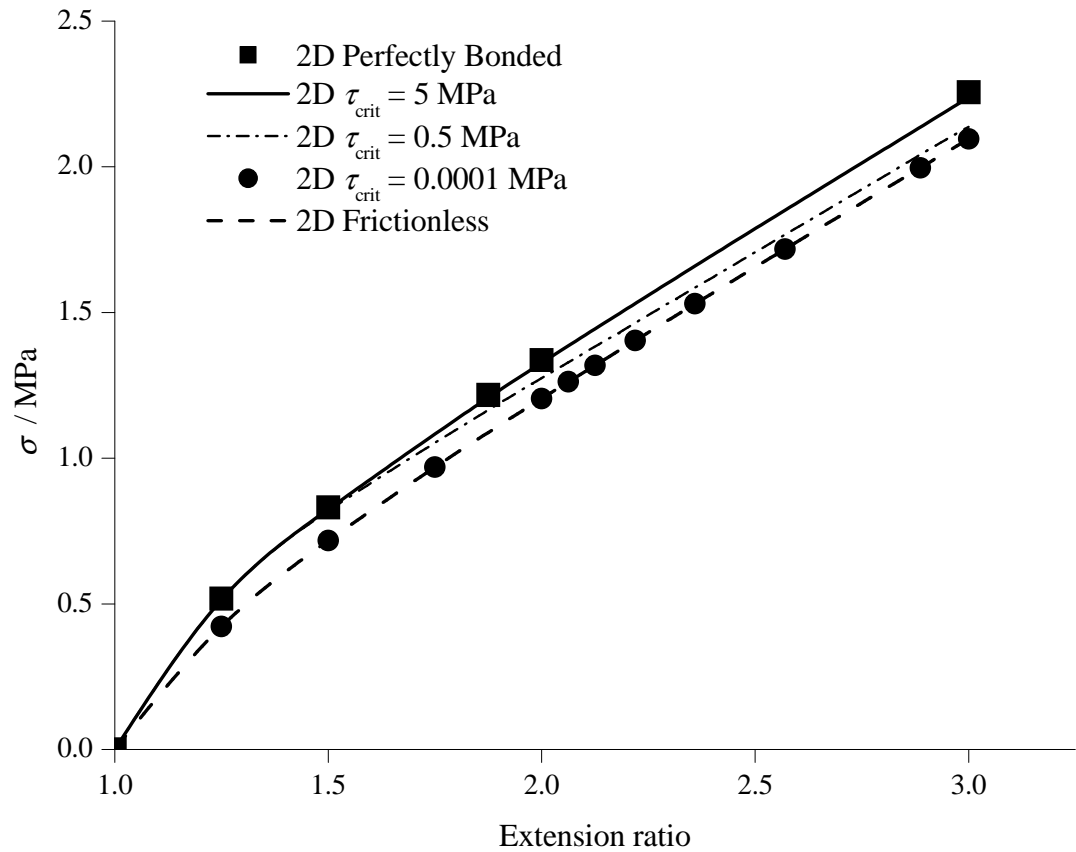


**Figure 5.11** Engineering stress versus extension ratio for 2D models with a  $V_f$  of 40%. This Figure shows the effects of various levels of critical shear stress on the onset of slippage at the rubber-filler interface.

Figure 5.12 shows that the modified Taylor equation (Equation 5.1) gives a good agreement with the three dimensional octant frictionless model for filler volume fractions below 10%. As the filler volume fraction is increased it is possible to derive from the model a relationship similar to Equation 5.2 for the limiting case of a frictionless interface which includes an additional term due to the interaction from adjacent particles thus,



$$E_{ch} = E_0 (1 + \phi + 2.3\phi^2)$$

Equation 5.2

Figure 5.12 also shows the other extremes of a perfectly bonded filler surface interface. Thus the actual modulus for a material filled with spherical fillers would lie somewhere between these two limiting cases, the precise modulus depending upon the onset and extent of slippage at the interface.

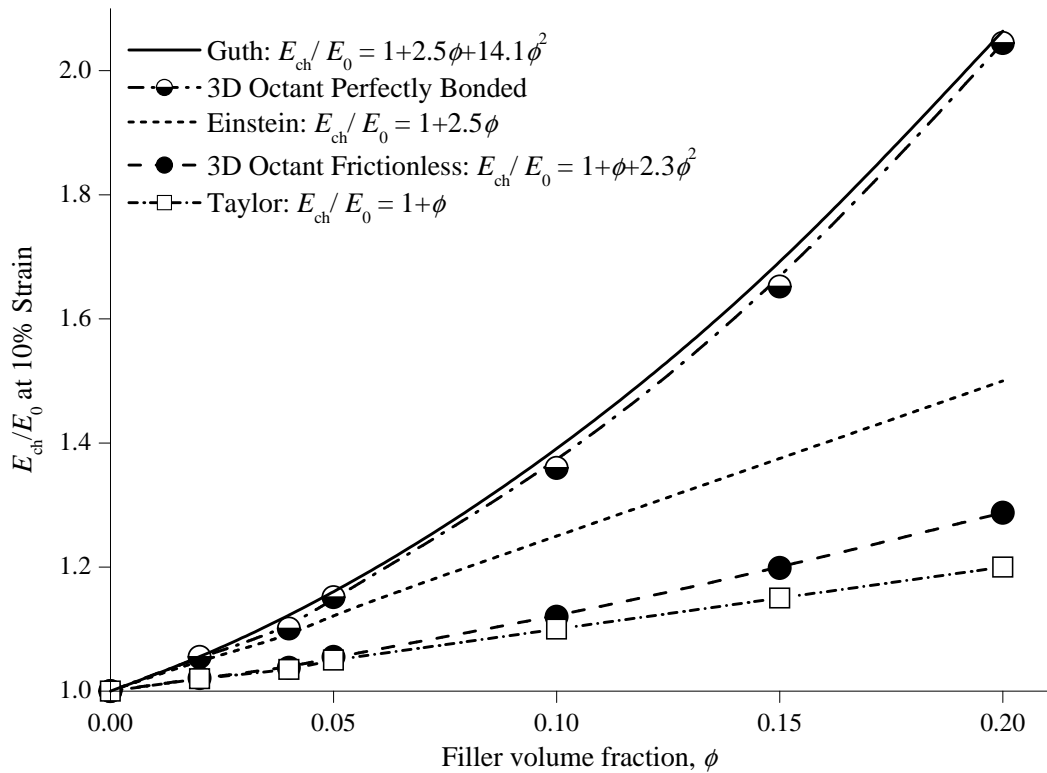
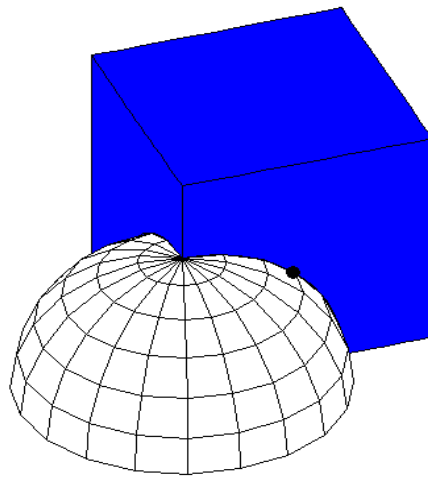


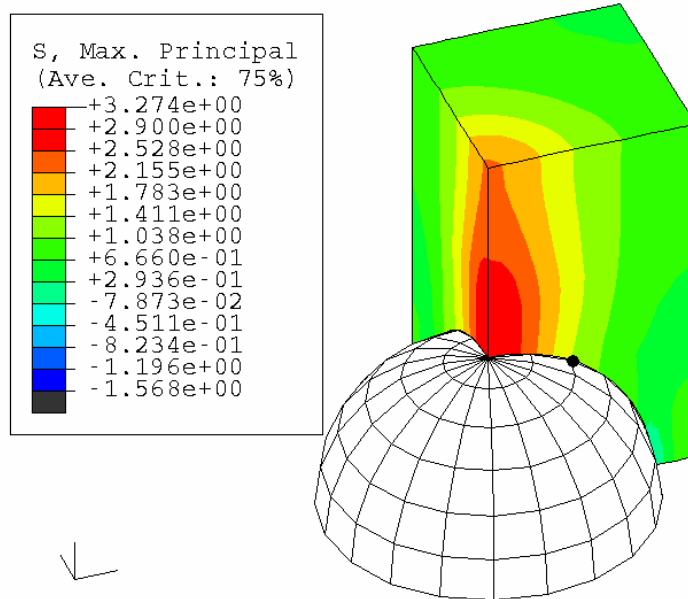
**Figure 5.12** Ratio of Young's Modulus versus filler volume fraction. A comparison between the stiffening effect of Einstein's and Taylor's theoretical relationships to the 3D octant (1/8 symmetry) FE models with perfect bonding and a frictionless interfacial slippage.

---

In Figure 5.14 a 3D octant model with interfacial slippage ( $\tau_{\text{crit}} = 0.7\text{MPa}$ ) has been compared to the perfectly bonded models and Mullins and Tobin's (1965) experimental data for MT carbon black over a wide range of strains up to 300%. Hon *et al.* (2003) showed that at low filler volume fractions below 10% the 3D octant model assuming perfect bonding at the interface compared well with Mullins and Tobin's (1965) experimental data. It appears that at lower volume fractions the rubber-filler interfaces does not generate stresses large enough to cause a significant amount of slippage and that conditions are close to perfect bonding. Figure 5.8 shows the larger filler volume fraction models of 13.8% and 20.9%. Here the perfect bonding at the interface no longer correlates well with the Mullins and Tobin's (1965) experimental data with the FEA model showing a stiffer response. At these higher volumes fractions of 13.8% and 20.9%, it can be seen that the 3D octant model with an interfacial slippage  $\tau_{\text{crit}} = 0.7\text{ MPa}$  fits well with the experimental data at low to moderate strains (2%-80%). This gives an insight into the actual rubber-filler interaction under tensile loading conditions. It is clear that a realistic rubber-filler model requires for the rubber to slide over the filler surface.



a)



b)

**Figure 5.13** 3D octant symmetry spherical particle with a filler volume fraction of 13% a) The undeformed shape. b) Under deformation with the slippage of a single node at 80% global tensile strain along the filler surface, highlighted as the black dot.

- FEA 20.9% 3D Octant Perfectly Bonded (Hon *et al.* 2003)
- FEA 20.9% 3D Octant interfacial slippage with  $\tau_{crit} = 0.7$  MPa
- EXP 20.9% Mullins and Tobins (1966)
- ▼— FEA 13.8% 3D Octant Perfectly Bonded (Hon *et al.* 2003)
- ▽— FEA 13.8% 3D Octant interfacial slippage with  $\tau_{crit} = 0.7$  MPa
- ▼ EXP 13.8% Mullins and Tobins (1966)

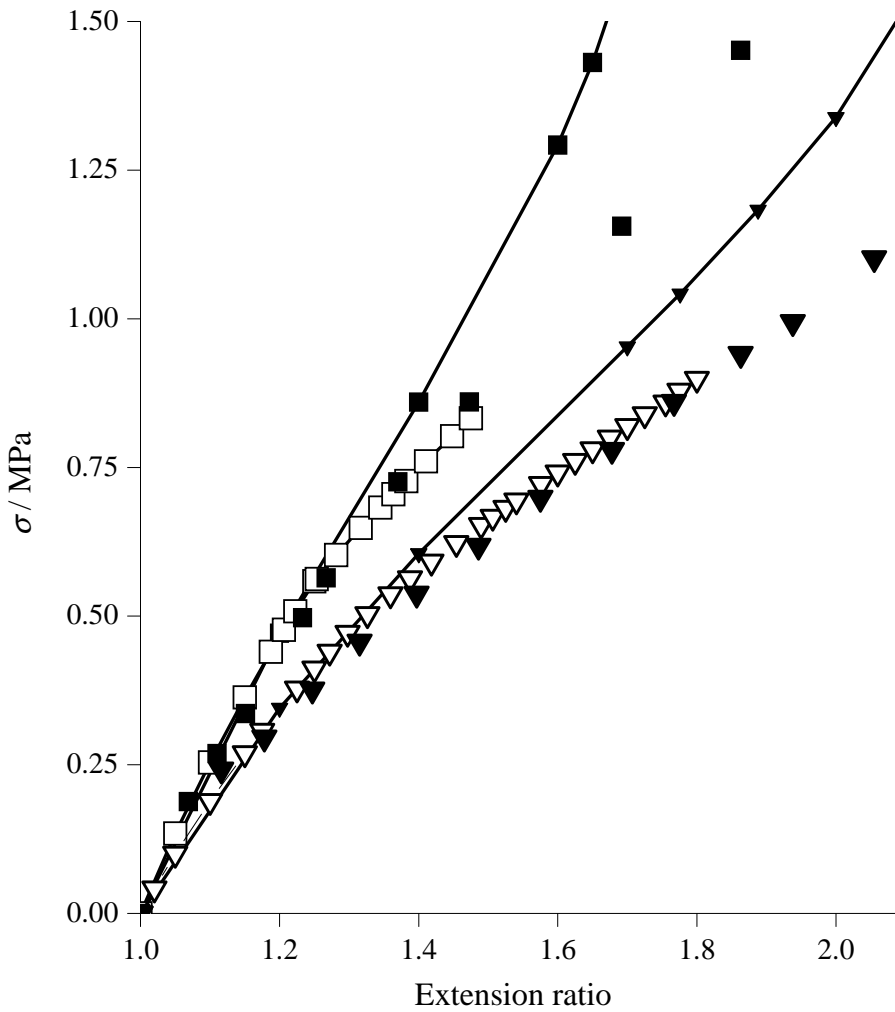


**Figure 5.14** Engineering stress, versus extension ratio. A comparison between 3D spherical finite element models and experimental MT carbon black filled elastomer samples at large extensions and at high filler volume fractions.

---

## 5.4 Conclusions

1. In the present work, the effect of increasing the number of filler units and their spatial arrangement on the calculated stiffness has been studied using different modelling approaches. It was shown that for a fixed filler volume fraction as the number of filler particles in a unit cell increased from 1 to 32 there was always an increased filler-filler interaction and a resulting increase in stiffness of the filled rubber. A simple test showed that the 8 filler particle model was isotropic in nature under different loading conditions. It seemed likely that to predict the correct stiffness over a wide range of strains that some additional slippage at the filler interface would have to be introduced.

2. An alternative approach allowed a significant increase in the number of filler particles as well as a range of size, shape and location to be developed. This modelling approach was based upon a cubic mesh and within the constraints of the meshing it introduced an occluded volume of rubber into the model. However, if this additional volume is taken into consideration then a good prediction of at least the initial stiffness was possible.

3. The 2D interfacial slippage models showed that when slippage occurred at the rubber filler interface the elastomeric response becomes softer. At higher filler volume fractions the onset of the deviation between the perfectly bonded and the slippage models to occur at lower global strains. The critical shear the point above which the rubber slips over the filler surface.

4. The Guth-Gold equation based upon the Einstein viscosity law represents an upper limit in the stiffness behaviour and the new equation based up on the Taylor viscosity law represents a lower limit for the stiffness behaviour for a range of filler volume fractions. At lower volume fractions the 3D perfectly bonded models follow the experimentally observed behaviour for a wide range of strains. At higher filler volume fraction of 13.8 % and 20.9% the 3D perfectly bonded model is stiffer than experimentally observed behaviour. Here the interfacial slippage (critical shear stress

---

value of 0.7MPa) gave the best correlation with experimental data. This shows that a realistic rubber-filler model should include a component to demonstrate how the rubber can slip over the filler surface.

---

## Reversible electrical behaviour of carbon black filled natural rubber

### 6.1 Introduction

Most unfilled elastomers exhibit a high electrical resistivity. The fillers most commonly used in the rubber industry are carbon blacks. These fillers are usually added to elastomers to enhance their mechanical properties such as strength (Tsunoda *et al.*, 2000) and abrasion resistance or to increase the modulus or visco-elastic properties. In a filled elastomer the local strain in the rubber is greater than the applied strain. This effect is known as strain amplification (Nakajima, 1988). Under cyclic loading the modulus of an elastomer progressively decreases. The modulus in the second cycle being smaller when compared to the first cycle (Harwood and Payne 1970). For unfilled elastomers the reduction in the modulus under cycle loading is due to the breaking and reformation of labile links (Derham and Thomas, 1977).

Fillers such as carbon black, carbon nanotubes, metal flakes and fibres have also been used to modify the functional properties of matrix materials (polymer) such as electrical conductivity and thermal conductivity [Sichel *et al.* (1982), Aneli *et al.* (1999), Carmona *et al.* (1986), Flandin *et al.* (2000, 2001), Lundberg and Sundqvist (1986) and Norman 1970)]. Properties of these materials also change with their external stimuli such as temperature and pressure [Abraham *et al.* (2004), Jiang *et al.* (1986), Zhang *et al.* (2005), Kang *et al.* (2006), Wei *et al.* (2006)]. Earlier work by Yamaguchi *et al.* (2003) has shown, for elastomers containing HAF carbon black fillers at a volume fraction above the percolation threshold that the resistivity behaviour also changes with strain. They showed that the precise resistivity versus strain behaviour was non linear and irreversible during the initial loading and

---

subsequent unloading. To develop a strain measuring device, which monitors the strain directly from a measure of the resistivity requires that the behaviour be reversible and reproducible from cycle to cycle. One possible way to achieve this was discovered by Busfield *et al.* (2004), whereby a modest swelling of the filler and rubber network with a suitable solvent resulted in the resistivity behaviour becoming more reversible. This work investigates if the reversible nature of the resistivity can be achieved by the judicious selection of an appropriate filler rather than by swelling. To do this a range of different carbon black fillers (MT N990, HAF Raven p-5, HAF N330, HAF CDX 7055 and Printex-XE2) each with different particles size and morphology were compounded into rubber at a volume fraction above the percolation threshold, using the formulations shown in Table 3.2, to investigate their behaviour under repeated straining.

## 6.2 Filled Elastomer

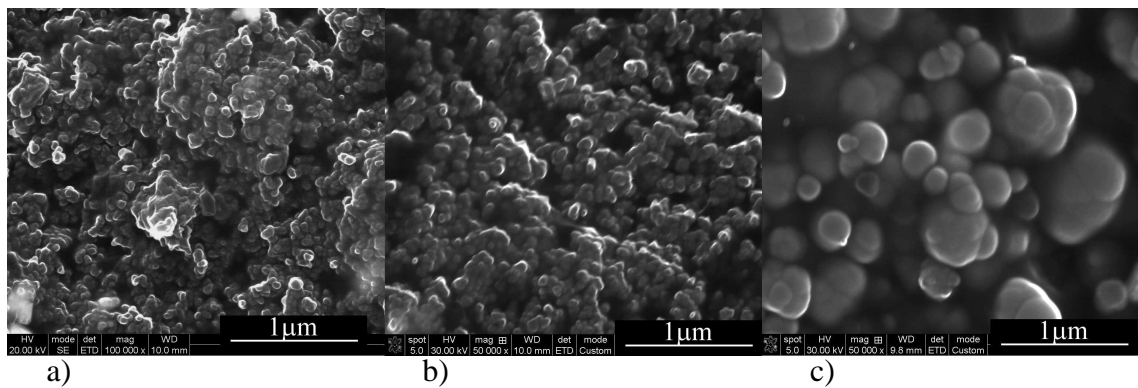
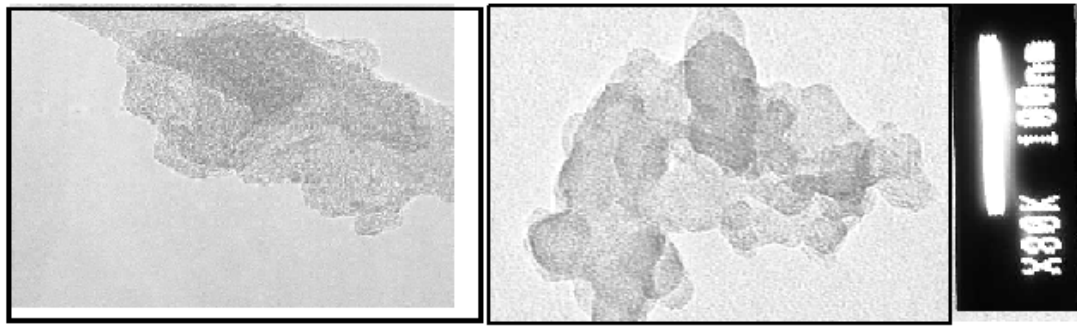


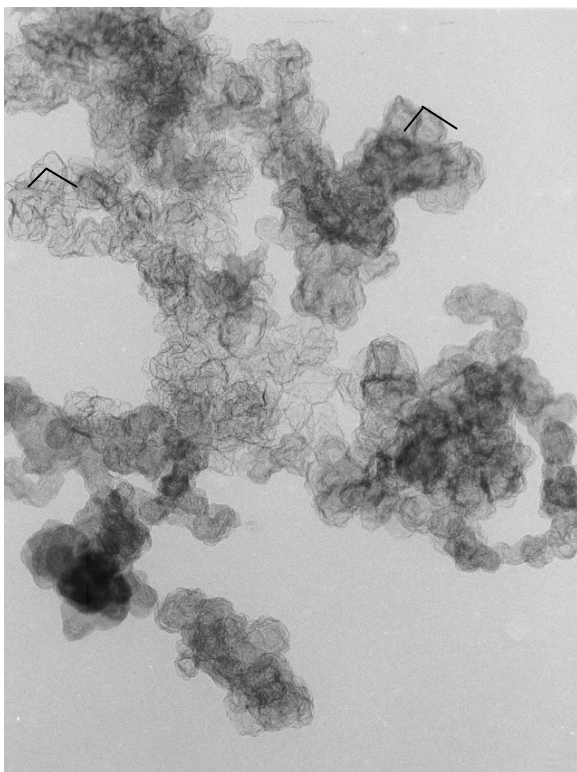
**Figure 6.1** SEM image of filled rubber showing varying aggregate size. a) SEM of Printex-XE2 (5.2%). b) SEM of HAF (N330) (21%). c) SEM of MT N990 (56%).





a) Printex-XE2

b) HAF N330



c).

**Figure 6.2** TEM Image of carbon black aggregate a) Printex-XE2 b) HAF N330, Printex-XE2 from Evonik Degussa GmbH.

SEM (Scanning electron microscope) image of the freeze fracture surface of NR filled with Printex-XE2, HAF N330 and MT N990 carbon black above percolation threshold is shown in Figure 6.1. A TEM (transmission electron microscopy) image of Printex-XE2 and HAF N330 carbon black aggregate is shown in Figure 6.2.

Printex-XE2 and HAF N330 appear to have a similar aggregate size as shown in Figure 6.1, Figure 6.2 and Table 3.1. Manufactures of Printex-XE2, Evonik Degussa GmbH, suggested that Printex-XE2 particles are hollow and hemispherical in shape. From Table 3.1 it is clear that Printex-XE2 has a much greater surface area and structure when compared to conventional HAF (N330, CDX 7055 and Raven p-5) and MT N990 carbon black. TEM images show Printex-XE2 has a higher surface area. MT N990 carbon black has the largest particles and the lowest tendency to form aggregate. (Donnet and Voet, 1976) explained that as the filler particle increased in size the reinforcement of filled rubber decreased. Figure 6.3 shows stress-strain curves of three different filled rubbers; Printex-XE2, HAF N330 and MT N990 carbon black at a similar filler volume fractions of 5.2%. There is increase in the stiffness as particle size decrease as shown in Figure 6.3 and Table 6.1

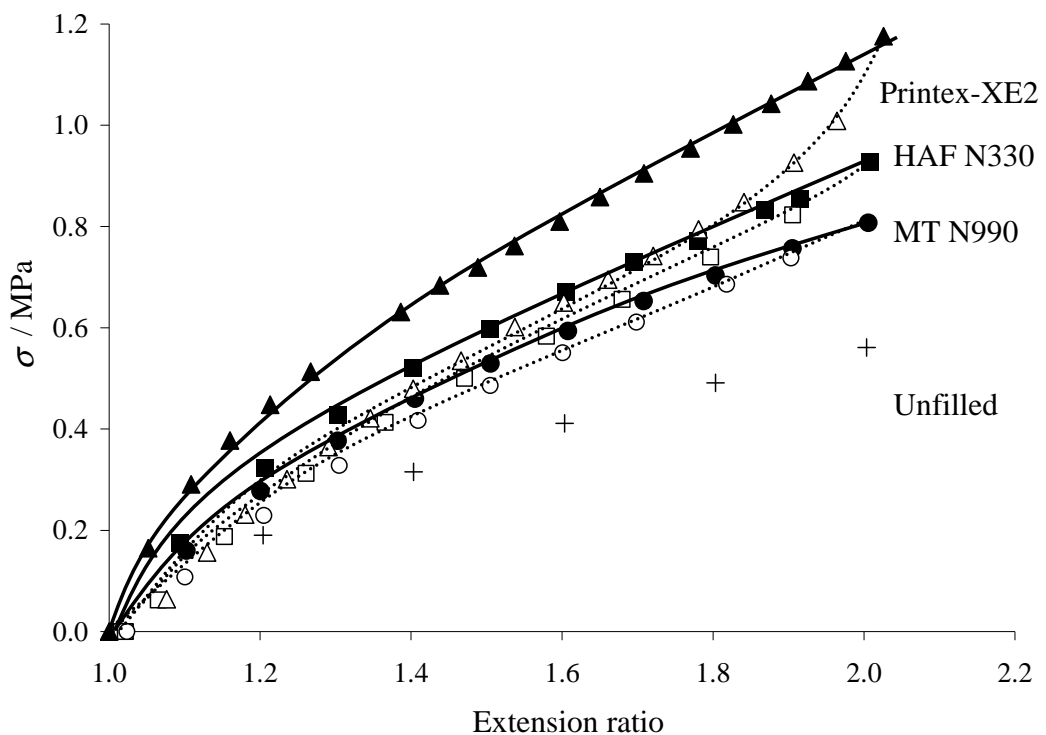


**Figure 6.3** Comparison of mechanical behaviours of different types of carbon black at a filler volume fraction of 5.2%.

Contrasting the loading and the unloading curves demonstrates the different amounts of hysteresis in the three kinds of rubber. Hysteresis losses of a filled rubber may be attributed to,

- (1) Molecular friction accompanying deformation of the rubber phase,
- (2) Polymer-filler detachment, and
- (3) Breakdown of filler structure and weak rubber chains (Kar and Bhowmick, 1997).

MT N990 carbon black filled rubber has the lowest amount of hysteresis as the filler particles are well dispersed and filler structure is low. This also suggest that the filler rubber interface is weakest in MT N990 carbon black filled sample and strongest in Printex-XE2 as confirmed as by the observations of Hess *et al.* (1967).

**Table 6.1** Chord moduli taken at 10% strain from stress-strain curve at filler volume fraction of 5.2% / 10phr from Figure 6.3.

	Printex-XE2	HAF (N330)	MT (N990)	Unfilled
Modulus / MPa	2.7	1.75	1.5	1.1
Mean primary particle (nm)	30	32	285	-
Surface area (CTAB) /m <sup>2</sup> gm <sup>-1</sup>	600	76	8	-
Oil absorption number (DBP)(cc/100gm)	380	102	43	-

Table 6.1 shows how the tensile chord modulus increases with increasing particle size and structure (DBP), calculated from Figure 6.3 where all three fillers have the same volume fraction. Printex-XE2 has the highest structure and the smallest particle size therefore has highest stiffening effect.

---

### 6.3 Effect of strain

Figure 6.4 shows how the electrical conductivity for Printex-XE2 changes under repeated straining up to 100% strain. At a volume fraction of 5.2% (which is equivalent to a 10 weight parts per hundred rubber) the filled elastomer conducts well in the unstrained state. Clearly for this filler the percolation threshold is at a volume fraction below 5.2%. This low percolation threshold is also anticipated by the earlier data by Probst (1984); which had shown that an increased geometric shape factor for the filler reduced the threshold (Figure 2.24). The initial electrical resistivity versus strain loading cycle is somewhat unique. However, beyond the first cycle, all subsequent loading cycles are indistinguishable. In addition, the difference between the first cycle and the subsequent ones is only modest. The resistance is seen to increase monotonically with strain and recover back somewhat to the original value after the strain is removed. During the first loading cycle the resistivity increases by 3 orders of magnitude to 100% strain. This is similar to the behaviour described by Zhang *et al.* (2007) for a polyurethane elastomer filled with carbon nanotubes and contrasts sharply to the data for other conducting fillers that have been reported previously by Yamaguchi *et al.* (2003) and Busfield *et al.* (2004, 2005b). Initial increases in resistivity with strain have previously been attributed to the breakdown of filler agglomerate structure. However, for Printex-XE2 the resistivity behaviour is virtually reversible with strain, suggesting that the filler network is not permanently altered.

The reversibility in resistivity probably results from the high structure and surface area of the carbon black and indicates that after the first cycle there is no further breakdown in filler aggregate structure under cyclic loading. This might arise because the surface area of the filler is so large and hollow hemispherical in shape that it is now much harder for the rubber to slide over the surface of the filler under strain. Therefore, the weak van der Waal forces that hold the filler network structure might be able to reform each time that the rubber is relaxed. Figure 6.5 shows that the stress strain behaviour for the Printex-XE2 filled elastomer is significantly stiffened. At a relatively modest volume fraction of just 5.2% Printex-XE2 has the dramatic

---

effect of doubling the stiffness when compared to an unfilled material with a broadly similar cross link density shown in Table 3.2 and Figure 6.5.

The reversibility in the electrical resistivity behaviour of Printex-XE2 is a significant discovery as it suggests that devices can be made that will be able to measure forces and strains from the changes to the electrical resistivity. This might allow a whole new generation of smart rubber devices to be developed.

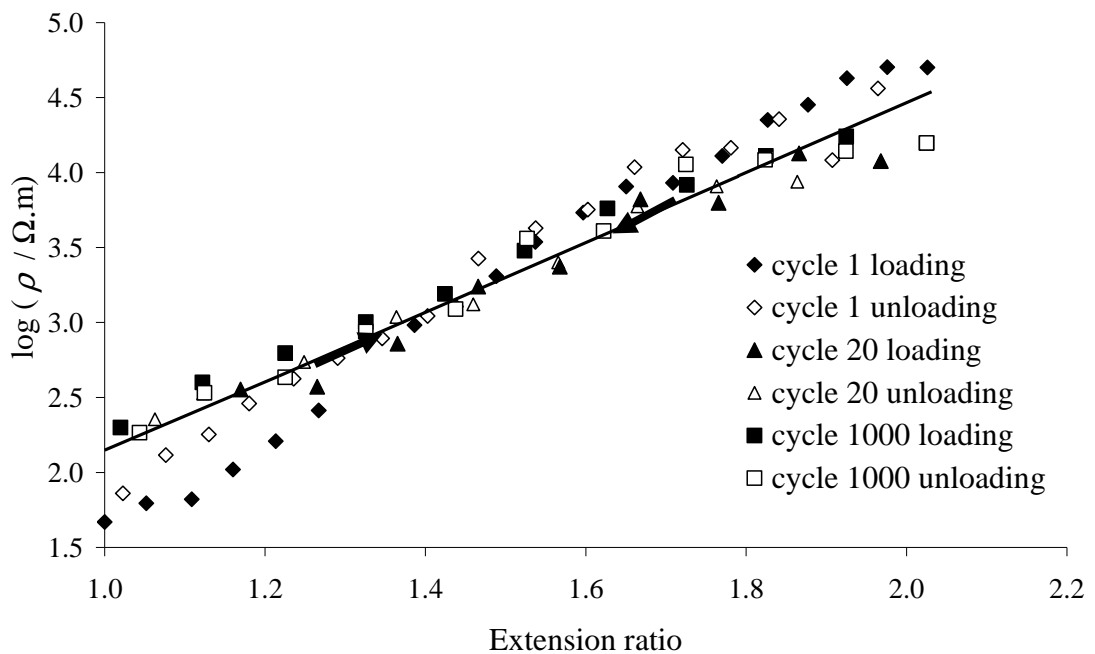


**Figure 6.4** Resistivity versus extension ratio for Printex-XE2 filled NR at a filler volume fraction of 5.2% under cyclic tensile strains.

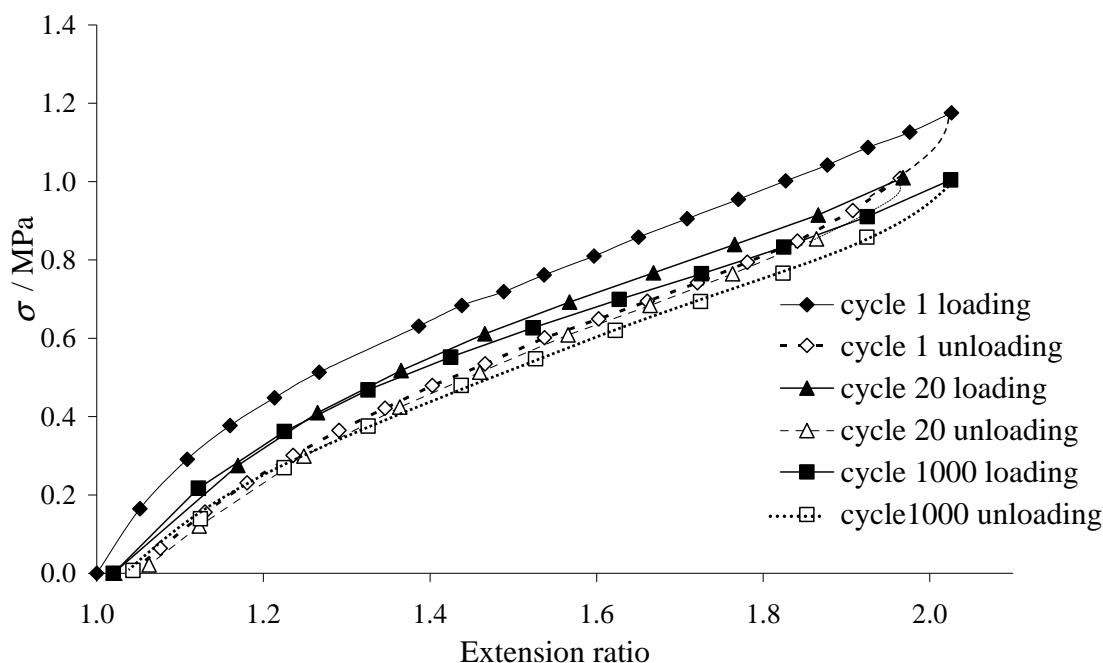


**Figure 6.5** Stress versus strain for Printex-XE2 filled NR at a filler volume fraction of 5.2% under cyclic tensile strains.

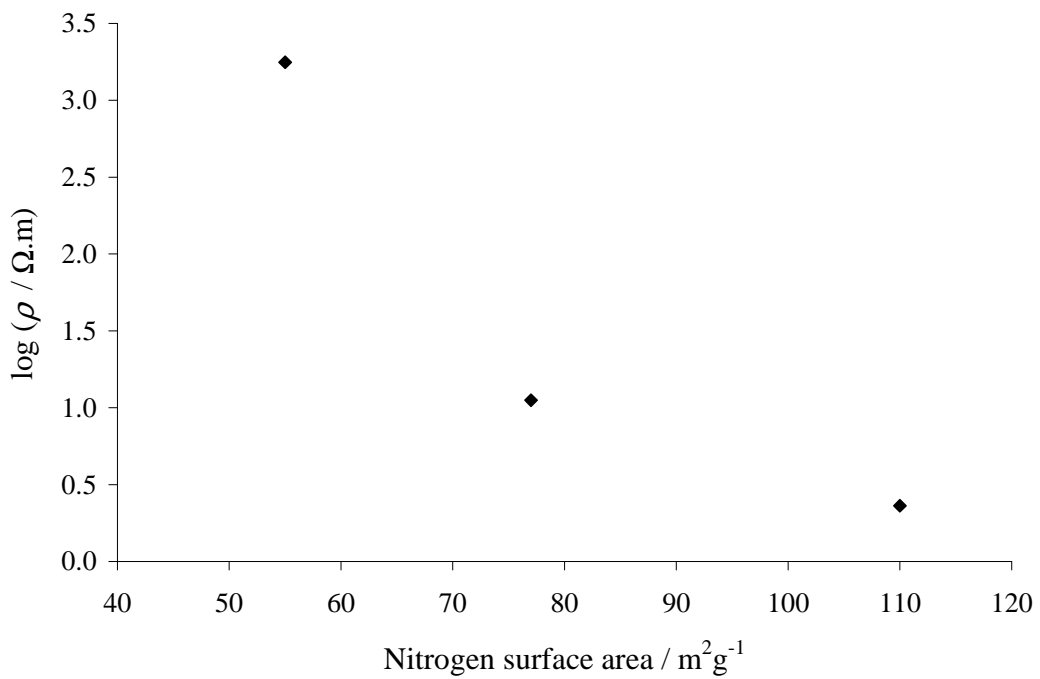
This unusual behaviour for Printex-XE2 contrasts with the observed behaviour for all the other materials examined in this work. Three HAF fillers were selected for this study were HAF Raven p-5; HAF Conductex 7055 (CDX 7055) and HAF N330. It is observed here in Figure 6.6 that as the filler surface area per unit volume increases, at equivalent filler volume fractions, there is a reduction in the initial unstrained resistivity. The electrical behaviour of a HAF N330 black filled elastomer under strain previously investigated by Yamaguchi *et al.* (2003) is remeasured here and is compared with the measured changes in electrical resistivity under strain for HAF Raven p-5 and HAF CDX 7055 fillers. Figure 6.7 shows that for the HAF N330 filler in its virgin first cycle that the resistivity increases up to 20% strain. This initial increase in resistivity has previously been attributed to the breakdown of the filler network structure in the rubber. When the applied tensile strain increases above this strain, the resistivity with strain graph reaches a plateau. This has been attributed to result from the orientation effects of filler under strain and also the effect of the reformation of some of the conduction paths. When the load is removed, the

---

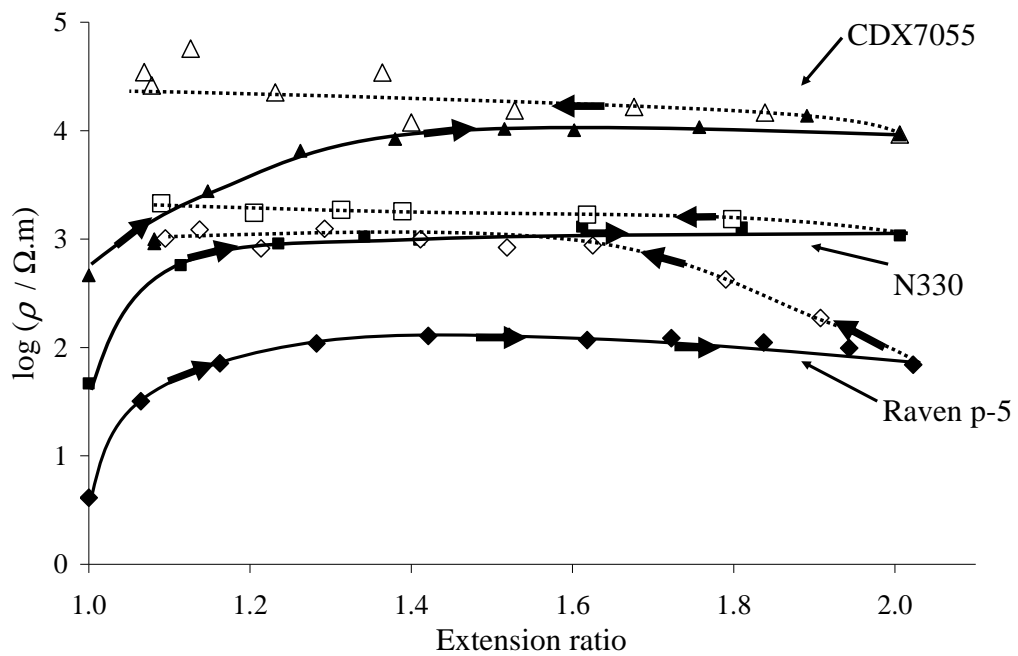
resistivity does not return to its original value but increases further. This indicates that some of the breakdown of the filler agglomerate structure is permanent.

Figure 6.7 shows that the first cycle electrical resistivity versus strain behaviour is similar for HAF Raven p-5, HAF N330 and HAF CDX 7055 filled elastomers each at a filler volume fraction of 21%. CDX 7055 has the largest change in resistivity between the strained and unstrained state. This can be explained using a theory of filler breakdown and “orientation” under strain. Figure 6.8 shows the stress versus extension ratio data for the three HAF filler types. The three materials each have similar stiffness and hysteresis behaviour.

Figure 6.9 shows the twentieth cycle electrical resistivity versus extension ratio data for each of the HAF fillers. Figure 6.10 shows the corresponding twentieth cycle stress versus extension ratio data. The twentieth cycle is chosen because a close examination of all the cycles shows that by the twentieth cycle the behaviour has reached steady state conditions. The twentieth cycle behaviour is now significantly different to the first loading cycle for each filler type. The resistivity behaviour has effectively become more reversible with strain. However, the resistivity reduces now as the strain is increased. The stiffness has also reduced from the first to the twentieth cycle as a result of cyclic stress softening and the hysteresis behaviour is also reduced. This suggests that the mechanical and the electrical measurements now reflect more reversible changes to the carbon black structure under strain in the twentieth cycle in stark contrast to the irreversible behaviour observed in the first cycle.



**Figure 6.6** Initial resistivity versus nitrogen surface area at a filler volume fraction of 21% for three HAF blacks shown in Table 3.1 and Figure 6.7.



**Figure 6.7** First cycle resistivity versus extension ratio at a filler volume fraction of 21% under cyclic tensile strains.



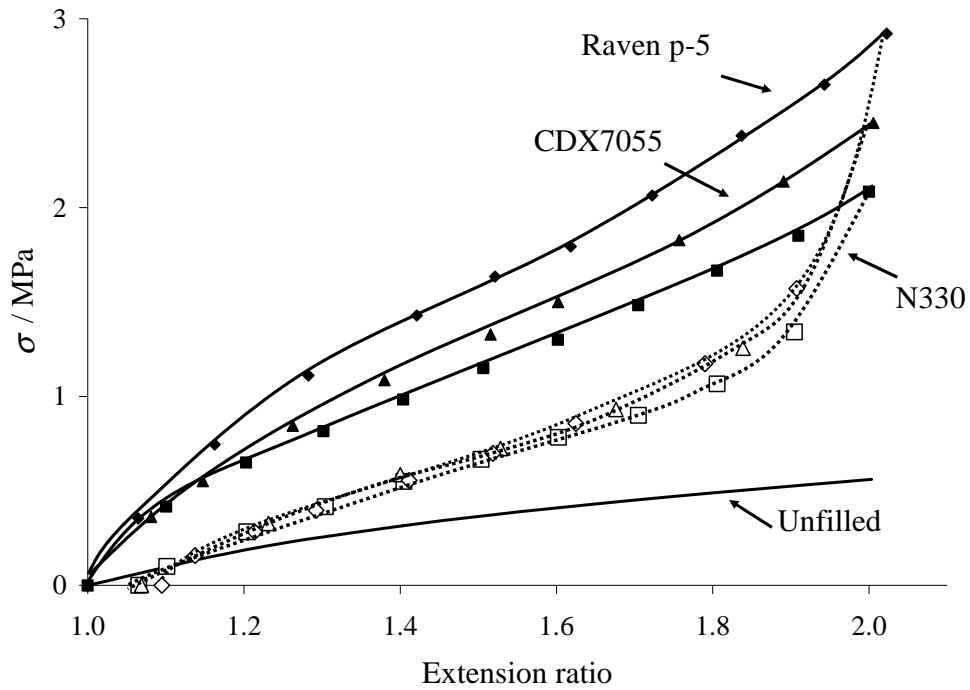


**Figure 6.8** First cycle stress versus strain for three different types of HAF black filled NR at a filler volume fraction of 21% under cyclic tensile strains.

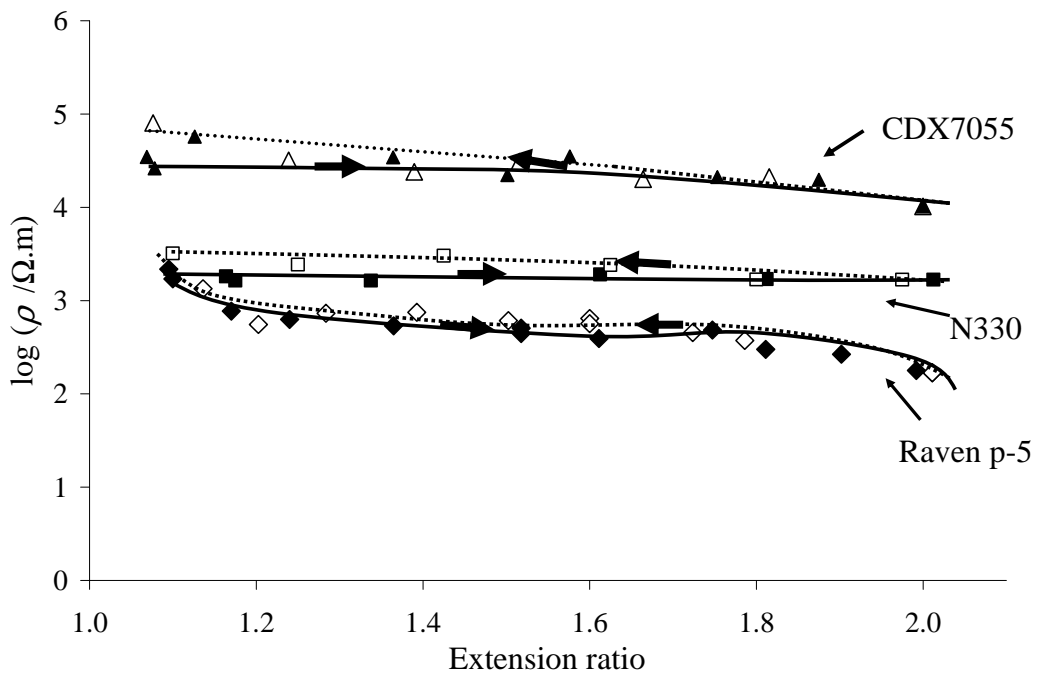


**Figure 6.9** Twentieth cycle resistivity versus extension ratio at a filler volume fraction of 21% under cyclic tensile strains.

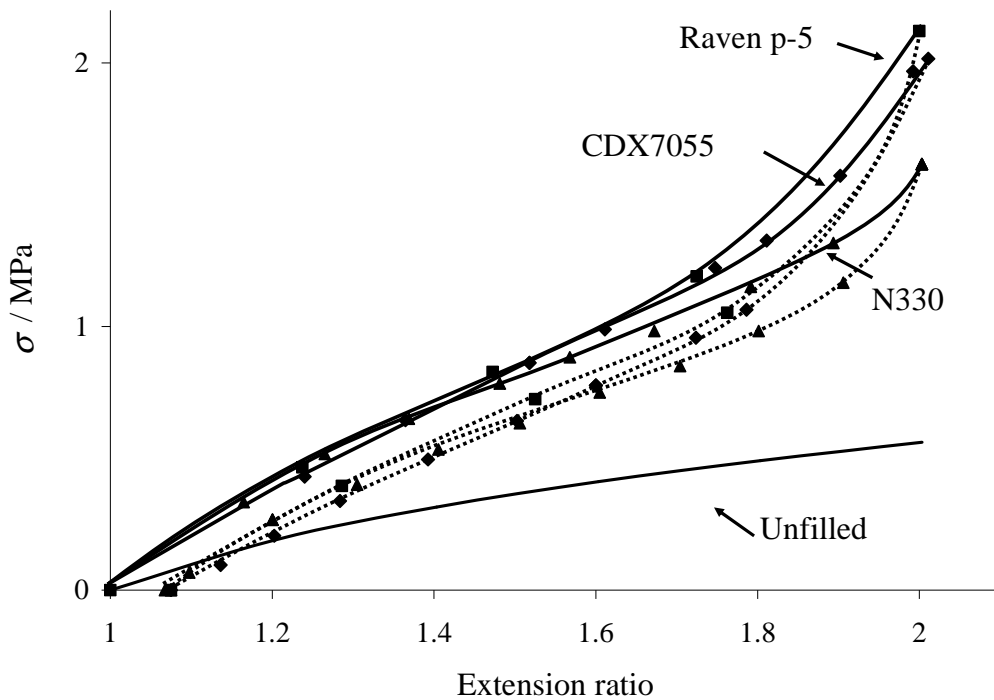


**Figure 6.10** Twentieth cycle stress versus strain for three different types of HAF black filled NR at a filler volume fraction of 21% under cyclic tensile strains (20<sup>th</sup> cycle).

A fifth filler, a medium thermal (MT) black, N990 with a dramatically different particle size and morphology to the other fillers was also examined (Table 6.1). MT N990 carbon black has a much lower surface area and a lower structure. This increases the percolation threshold as shown in Figure 2.24. In order to reach the percolation threshold for this material it was necessary to add carbon black with filler volume fraction above 45%. N990 has very low structure and is comprised principally of only the primary particles which are approximately spherical in shape. Figure 6.11 shows the changes in electrical resistivity under strain in the first cycle for a N990 filled rubber sample with a filler volume fraction of 56%. During the first loading cycle, the resistivity initially increases by an order of magnitude by the application of a 10% strain. It increases 100 fold up to 60% strain. This increase in resistivity can again be attributed to the breakdown of the filler network structure. Similar to the HAF blacks as the strain is increased further the changes in resistivity reach a plateau. During unloading further changes to the resistivity remains modest. This suggests that the bulk of the filler network has already been broken down

---

and that no orientation of the fillers take place. It is also clear for N990 that the breakdown of the filler network structure is irreversible. The stress versus extension ratio data for this highly filled elastomer is shown in Figure 6.12. At this high a volume fraction of filler, an MT carbon black sample exhibits extensive hysteresis particularly in the first cycle.

Figure 6.13 shows that during cyclic loading the resistivity changes in electrical behaviour for an N990 filled elastomer are significantly different to the first cycle. The resistivity of the N990 carbon black filled sample is reduced during cyclic loading in tension. The effect of ordering of carbon black under cyclic loading was reported by Fujimoto (1986). It appears that cyclic loading creates more conduction paths as the particles are reordered under strain. Beyond the first cycle, it appears that the resistivity initially decreases with strain and then increases as shown in Figure 6.13. Figure 6.14 shows the dramatic change to both the stiffness and the hysteresis behaviour with N990 filled NR under repeated straining. Explanation for this behaviour would be that the interaction at the filler surface is weak, allowing the rubber matrix to slide around the surface of the filler, resulting in changes to the morphology of the filler network under strain. Clearly the high percolation threshold and the irreversible behaviour make N990 unsuitable for use in strain measuring devices.

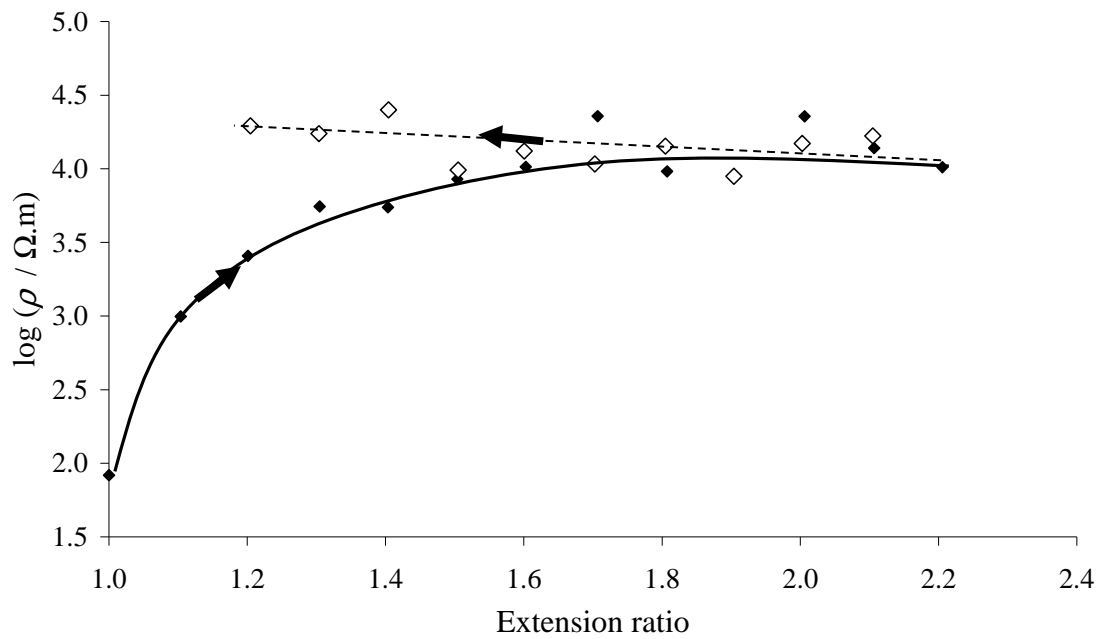


**Figure 6.11** First cycle resistivity versus extension ratio for MT N990 filled NR at a filler volume fraction of 56% under tension.

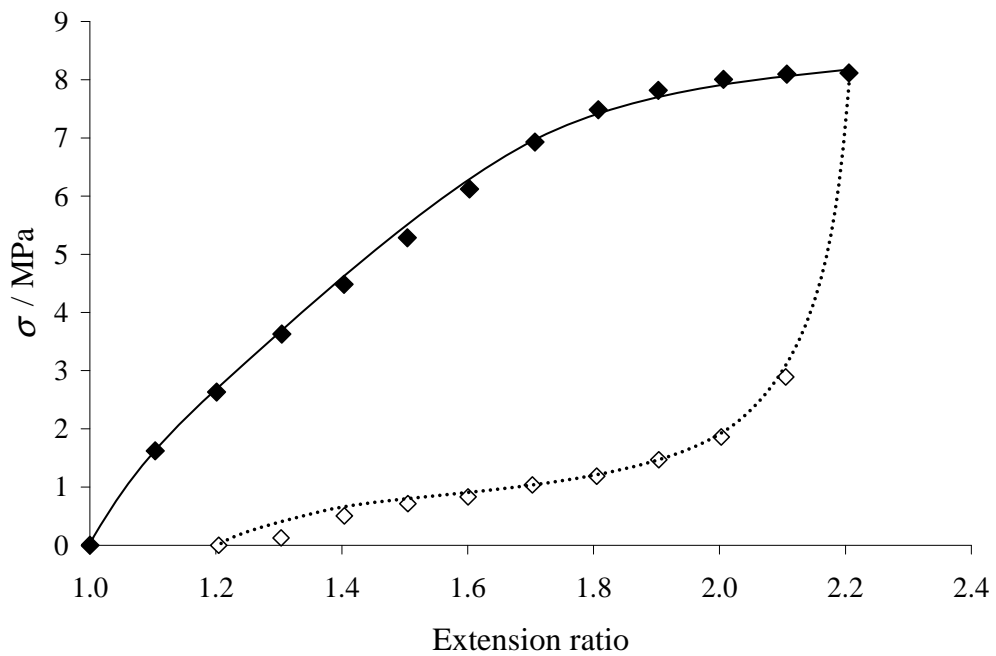


**Figure 6.12** First cycle stress versus strain MT N990 black filled NR at a filler volume fraction of 56% under tension.

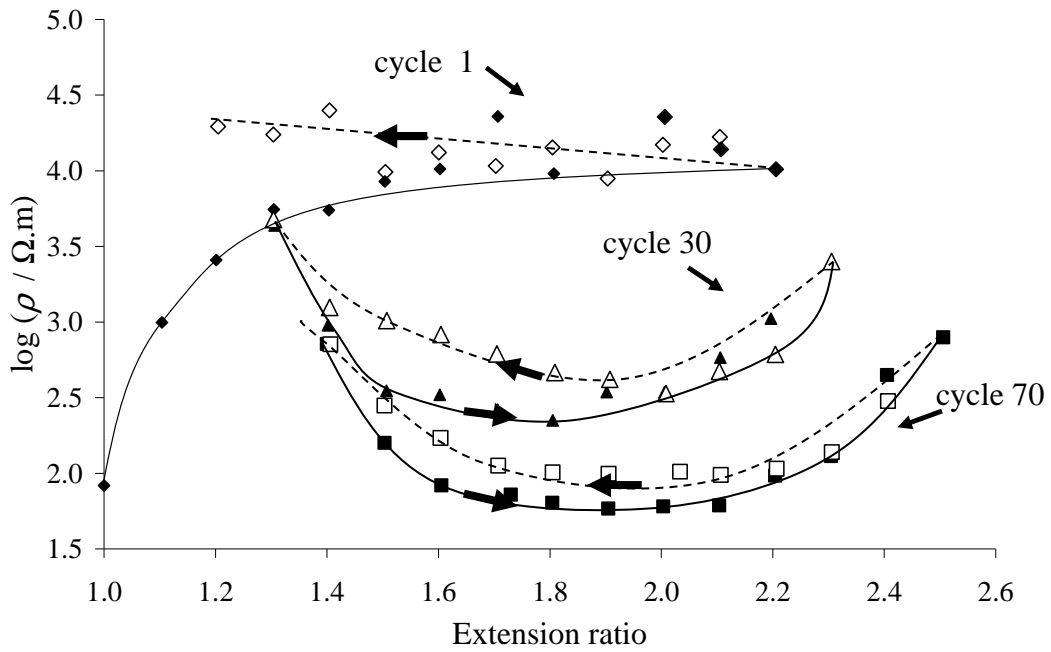


**Figure 6.13** Resistivity versus extension ratio for MT N990 filled NR at a filler volume fraction of 56% under cyclic tensile strains.

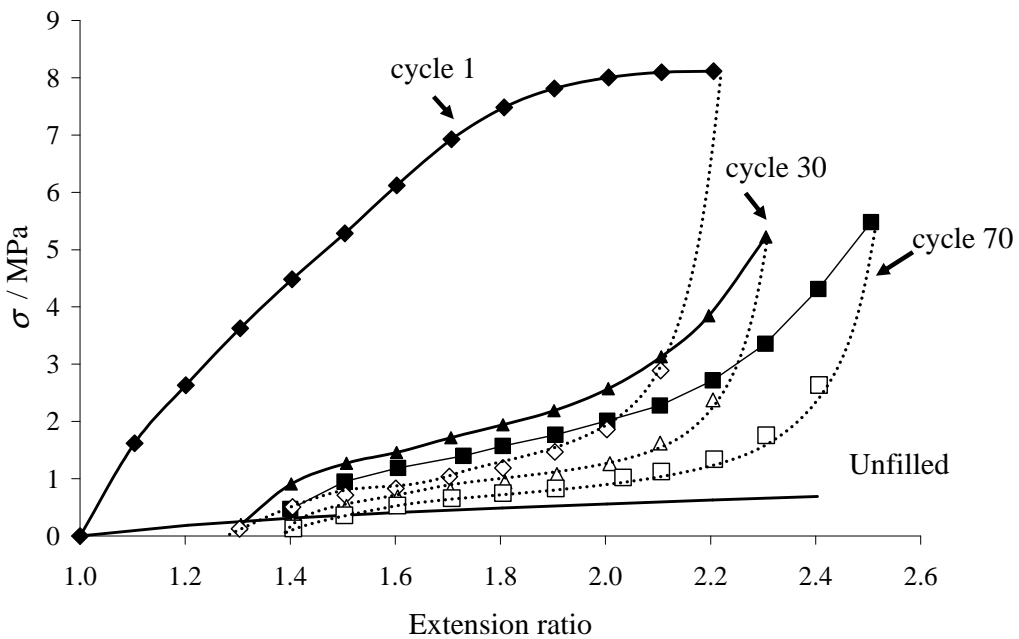


**Figure 6.14** Stress versus strain for MT N990 black filled NR at a filler volume fraction of 56% under cyclic tensile strains.

---

#### 6.4 Filled rubber conductivity: Printex -XE2

Printex-XE2 has very high surface area and structure whereas N990 has a very low structure and surface area as shown in Table 6.1 and Figure 6.1. Hence, Printex-XE2 has very low percolation threshold, 5.2%, shown in Figure 6.15. As the percolation threshold of Printex-XE2 is very low compared to other carbon blacks such as N990, Raven p-5 and Conductex 7055, the morphology of filler in filled elastomer was investigated using SEM. Sandler *et al.* (2003) and Loos *et al.* (2003) showed that conventional SEM can be used to provide 3 dimensional morphological image of single wall nano-tubes. Their technique relied upon the charge contrast imaging mode to provide the morphological information. This technique was used here to investigate the distribution of an elastomer filled with Printex-XE2 at a volume fraction of 5.2% shown in Figure 6.16, thus being above percolation threshold (charged at 30 kV). The secondary electrons make the conducting filler particle glow. Figure 6.18 shows that the Printex-XE2 particles are well dispersed in the elastomer matrix. It is likely that the primary conduction mechanism can be particle to particle contact. Another possibility due to the higher surface area and structure for Printex-XE2 is that being more graphitic means it may form more conductive paths in the elastomer.

Chapter 2 explains how, the flocculation theory or percolation theory relates to the resistivity of a filled elastomer to differences in the volume fraction loading of the filler. The exponent  $t$  in Equation 2.16 represents the dimensionality of the system. For a polymer filled with conducting nano-tubes, it has been shown by that a lower dimensionality value 1.4 suggest an agglomeration of carbon nanotube during sample preparation. Conversely a higher value of the exponent  $t$  indicates a better dispersion of the filler particles. Figure 6.17 shows how the exponents change with strain. This indicates that in the unstrained state, the particles are more agglomerated, and hence the conductivity is higher. As the strain increases, the exponent value increases, indicating the break down of the filler agglomerate structure.

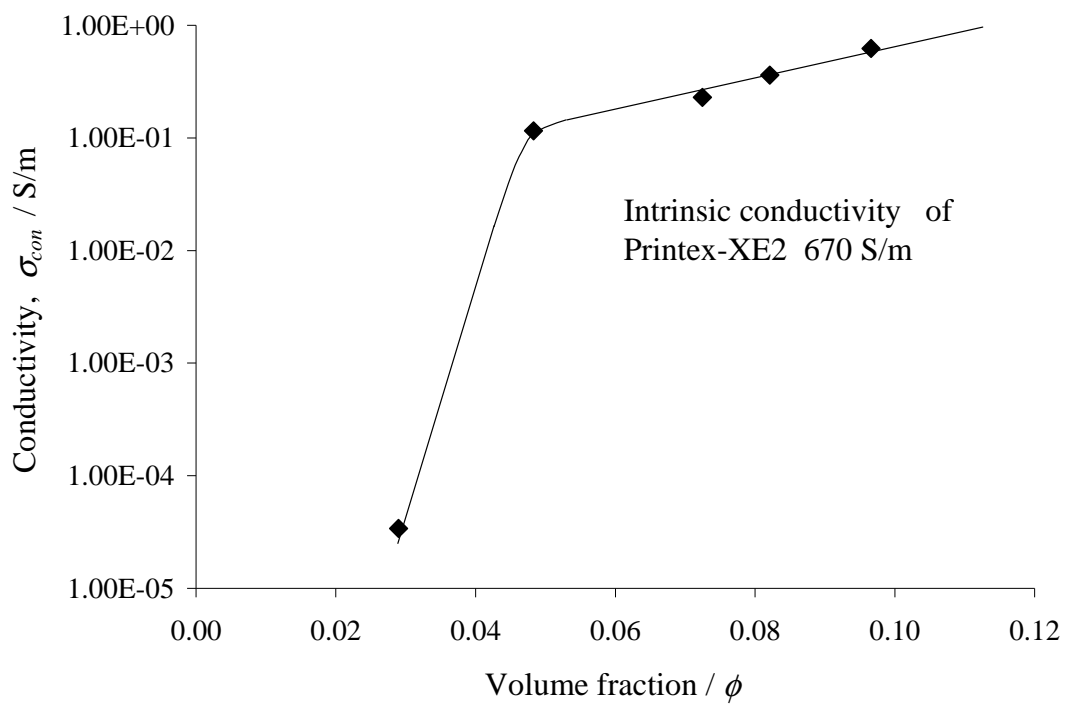


**Figure 6.15** Percolation behaviour of Printex-XE2 filled NR

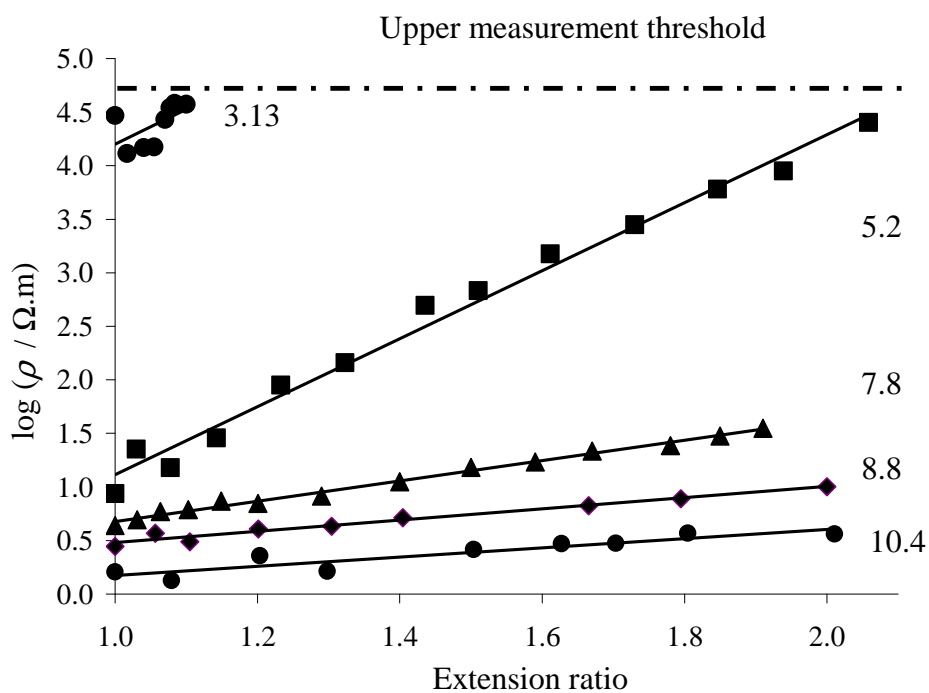


**Figure 6.16** Resistivity versus strain for different volume fractions of Printex-XE2.

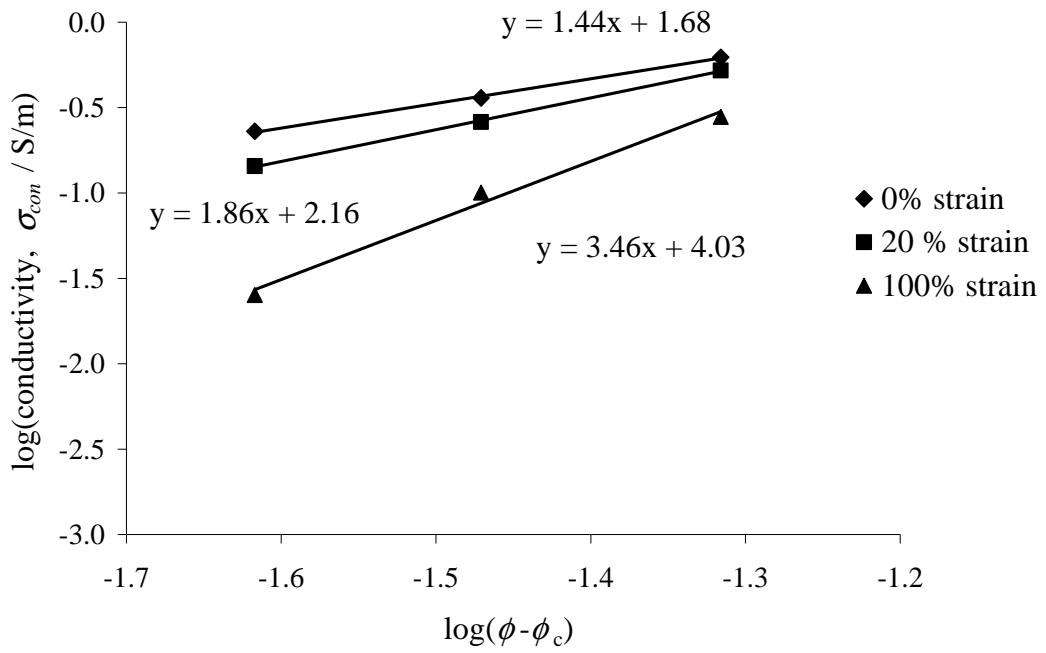


**Figure 6.17** The scaling law (Percolation theory) used to determine the critical exponent,  $t$  in Equation 2.16.

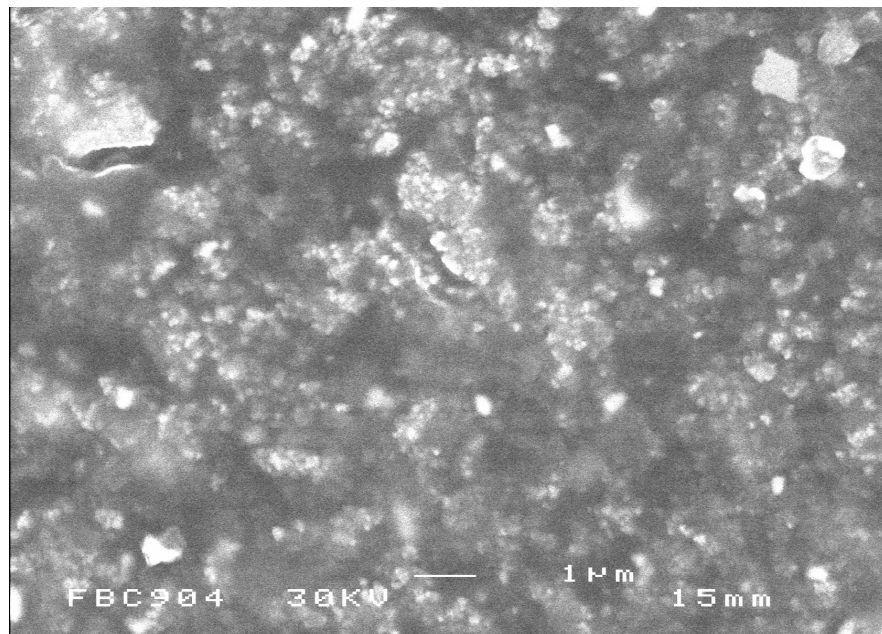


**Figure 6.18** SEM charge contrast image obtained for NR rubber filled with Printex-XE2 a volume fraction of 5.2%.



---

## 6.5 Effect of Temperature

The thermal expansion coefficient of rubber at 0.053%/°C is greater than that of the carbon black. Therefore, an increase in the temperature produces a volumetric expansion of the rubber matrix that should move further apart and hence, these conductive filler aggregate network should increased. However, Busfield *et al.* (2004) showed that, the changes in the resistivity under strain at a higher temperature for NR filled with HAF N330, the reverse is true. The effect of temperature produces more complicated effects and a simplistic approach cannot explain this phenomena. The effect of temperature can be understood by the following considerations,

(1) Temperature adds energy to the system; which in turn increases the effect of thermal assisted hopping increasing the conductivity (Sandler *et al.*, 2003).

(2) The particles/aggregates/polymers are randomly distributed in the matrix under pressure and at an elevated temperature during the curing process. This might result in a configuration and arrangement which is not the most energetically stable. Hence, when the temperature is increased they try to achieve the stability lost in the curing process by rearrangement. When the temperature increases carbon black particles tend to rearrange in order to decrease the energy state, and become more stable. This rearrangement might explain a decrease in the resistivity as more conductive networks are formed.

(3) Bound Rubber: It has been widely discussed that in a filled rubber; the filler has a surrounding layer extending a couple of nanometres which contains partially vulcanized or unvulcanized rubber (Fukahori, 2007). The unvulcanised rubber has a higher viscosity and a lower modulus than the rest of the rubber matrix. When there is an increase of temperature, its viscosity reduces and then a strain might allow it to flow out of the way and hence increase the contact between the filler particles and reduce the resistivity. As the surface area and structure of the filler particle increases the amount of bound rubber increases as shown in Figure 2.9 (Wolf *et al.*, 1991). Hence, Printex-XE2 has highest volume of bound rubber and MT N990 has least volume of bound rubber layer.

Figure 6.19 shows the effect of temperature on Printex-XE2. The Figure shows the changes in the resistivity with strain at 23°C and 80°C. A temperature change from 23°C to 80°C should produce a volumetric expansion of 3% in the natural rubber matrix. The volumetric expansion increases the inter-aggregate distance and should increase the resistance. However, competing phenomena as mentioned earlier dominate and decrease the resistivity. The rearrangement of the filler aggregate structure to a more energetically stable state results in the formation of more conduction paths. Also, the bound rubber consists of an unvulcanised layer with an increased mobility at a higher temperature contributing to the flow of rubber. This results in greater filler-filler interaction. Hence, as shown in Figure 6.19 Printex-XE2 filled NR becomes more conductive with strain as the temperature increases. The effect of temperature on conductivity in Printex-XE2 decreases the resistivity by one and half orders of magnitude (on a log scale) at 100% strain. In the unstrained state the conductivity increases only modestly in comparison. At a higher temperature of 80°C Printex-XE2 shows the same reversibility of the resistivity with strain as seen at room temperature.

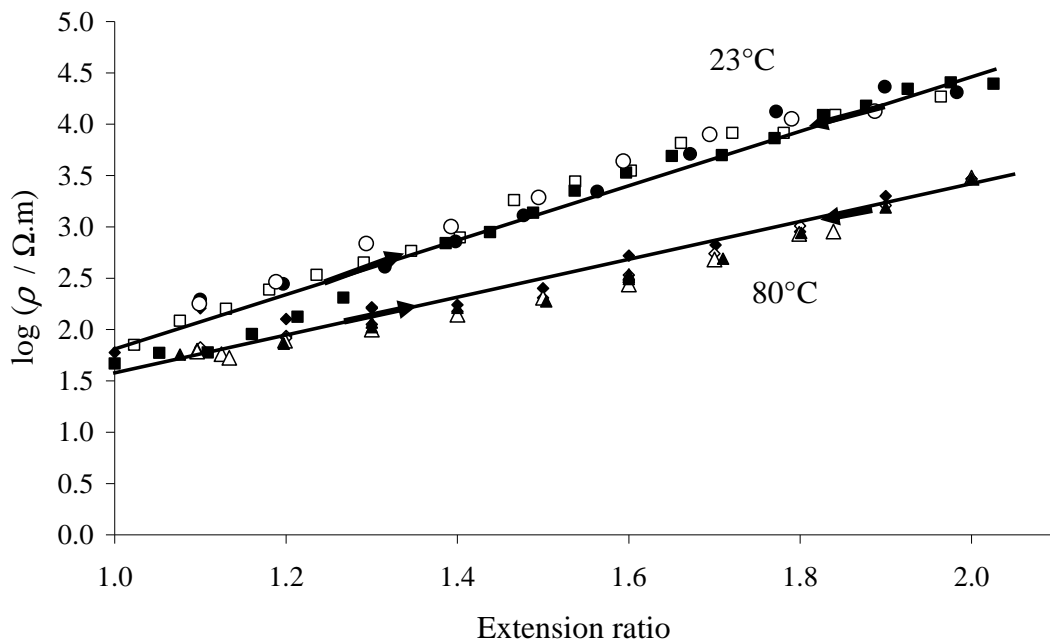


**Figure 6.19** Resistivity versus extension ratio for Printex-XE2 filled NR at a filler volume fraction of 5.2% under cyclic tensile strains at 23°C and 80°C.

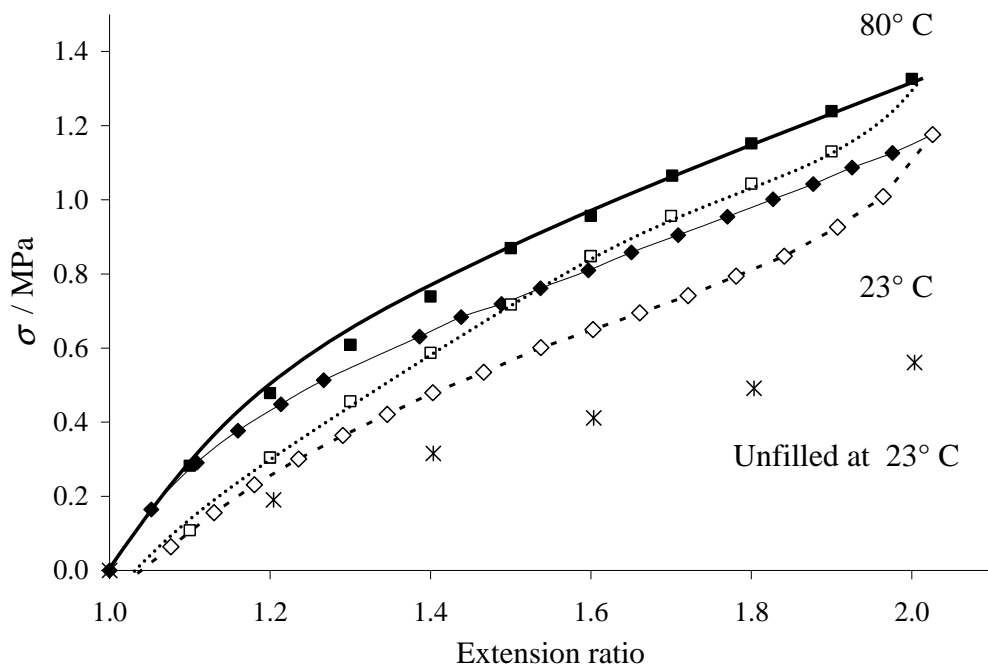


**Figure 6.20** Stress versus strain for Printex-XE2 filled NR at a filler volume fraction of 5.2% under cyclic tensile strains at 23°C and 80°C.

Figure 6.20 shows that at an elevated higher temperature of 80°C there is increase in the modulus by 20% for Printex-XE2 filled NR. In case of unfilled elastomers (NR) there is increase in the modulus with temperature shown in Equation 2.3. As explained by the entropy spring theory of rubber elasticity the modulus increases with absolute temperature. For the case of Printex-XE2 filled NR the stiffness increase can be attributed to the increase in the modulus of the matrix NR.

Printex-XE2 is a high structure and high surface area carbon black having a low percolation threshold below a volume of 5.2%. MT N990 carbon black is a low structure and low surface area black; having a percolation threshold above 45%. Figure 6.21 shows the effect of temperature on resistivity of MT N990 carbon filled rubber under strain. MT N990 carbon black filled natural rubbers at higher temperature of 80°C is also less resistant. The resistivity curve for the loading cycle is similar to the one at room temperature. The change in resistivity at an extension ratio of 1.8 is two orders of magnitude as temperature increases from 23°C to 80°C. At 80°C the unloading curve shows a modest increase in resistivity that rises

sharply once the material is almost fully unloaded. Clearly the elevated temperature produces a similar behaviour with strain but there is clearly additional mechanisms acting upon the system that lower the resistivity. One possible reason is, there exist a rubber layer at filler-rubber interface which is unvulcanised. This unvulcanised rubber layer at higher temperature flows out under stress and this forms more conduction paths which further reduces the resistivity. In MT N990 filled elastomer the re-ordering of the filler particles along the direction of strain could also reduce the resistivity (Fujimoto 1986). Figure 6.20 and 6.22 shows the stress-strain of Printex-XE2 filled NR and MT carbon black NR respectively. Figure 6.22 shows that for the MT carbon black filled elastomers the temperature rise produces a decrease in the modulus. This contrast with Printex-XE2 which shows an increase in modulus at a higher temperature of 80°C. This is most likely due to the very high filler content for the MT N990 black at a volume fraction of 56%. Hence, there is extensive weak filler-filler interaction in case MT carbon filled elastomers. Hess *et al.* (1967) suggested using an adhesion index that MT carbon black particles debonds easily under stress as shown in Figure 2.6. Hence, there is a greater slippage of rubber on the filler as modelled in chapter 5 and a greater filler-filler interaction at the higher temperature.

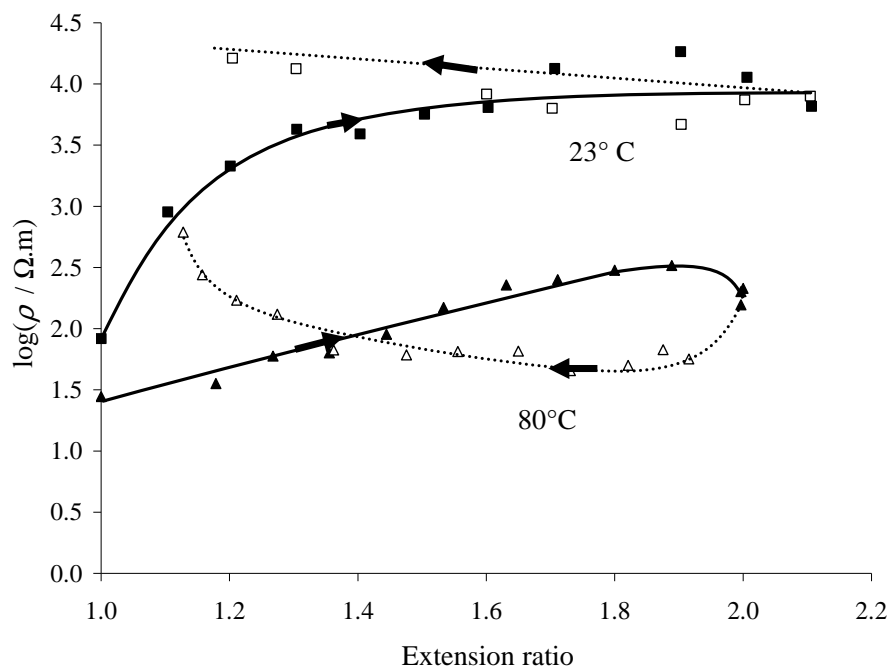


**Figure 6.21** Resistivity versus extension ratio for MT N990 filled NR at a filler volume fraction of 56% under cyclic tensile strains at 23°C and 80°C.

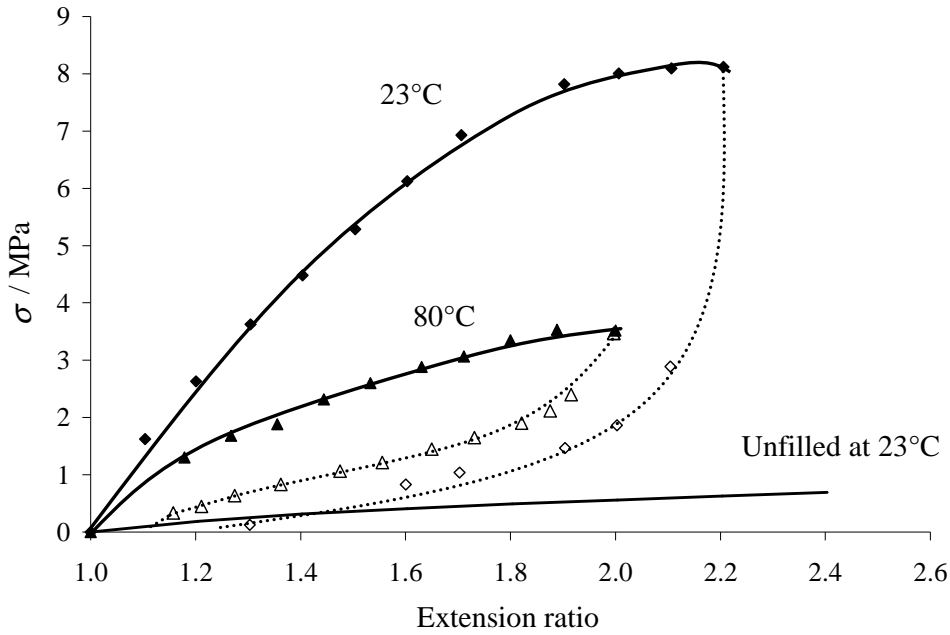


**Figure 6.22** Stress versus strain MT N990 black filled NR at a filler volume fraction of 56% under cyclic tensile strains at 23°C and 80°C.

The effect of temperature on the HAF (Raven p-5 & CDX 7055) filler is shown in Figure 6.23 and Figure 6.25 for CDX 7055 and Raven p-5 respectively. Figure 6.25 shows this reduction to not be obvious at low very low strains but once an extension ratio of about 1.2 is reached the effect of temperature on resistivity starts to increase giving values of half an order of magnitude lower than at room temperature. Figures 6.23 and 6.25 show for both CDX 7055 and Raven p-5 there is a decrease in resistivity over the entire range of strains with temperature as observed by Busfield *et al.* (2004) for N330. Once the sample reaches 100% strain the effect of temperature is slightly different in each of the rubber samples. CDX 7055 has only increased modestly in resistivity above the unstrained value whereas Raven p-5 changes by an order of magnitude. Figure 6.24 and Figure 6.26 shows that the stress versus strain behaviour at 80°C and 23°C are similar. Comparing these with Figure 6.20 and 6.22 it can be concluded that for HAF CDX7055 and HAF Raven p-5 both filler-filler and polymer-filler interaction are altered by strain. Also, HAF CDX 7055 and HAF Raven p-5 are reinforcing fillers having a higher adhesion index than MT carbon black as shown in Figure 2.6.

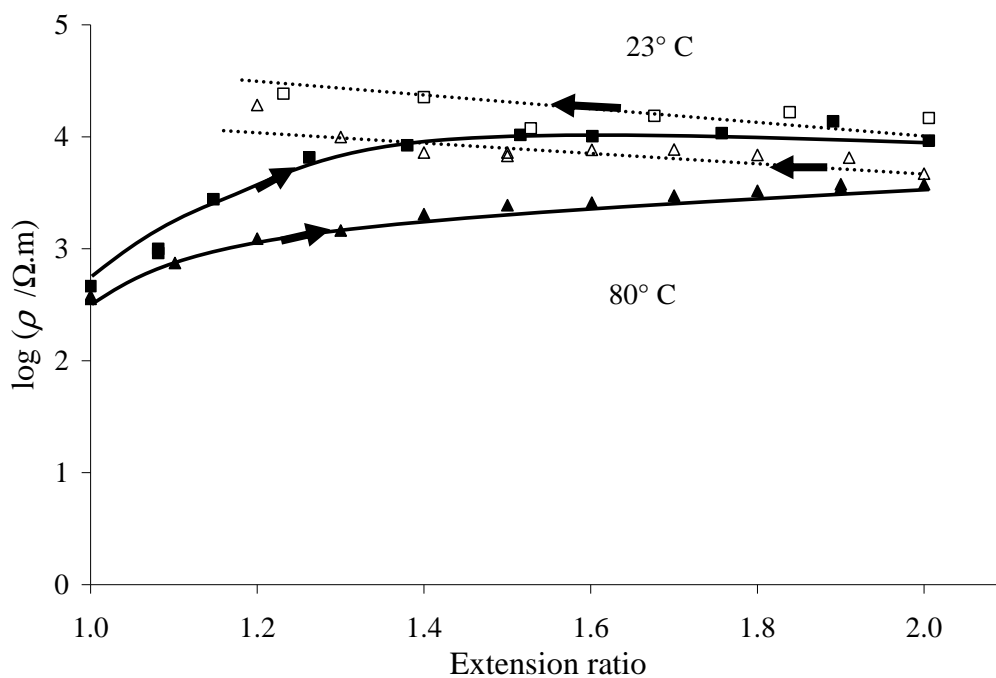


**Figure 6.23** Resistivity versus extension ratio for CDX 7055 filled NR at a filler volume fraction of 21% under cyclic tensile strain (1<sup>st</sup> cycle only) at 23°C and 80°C.

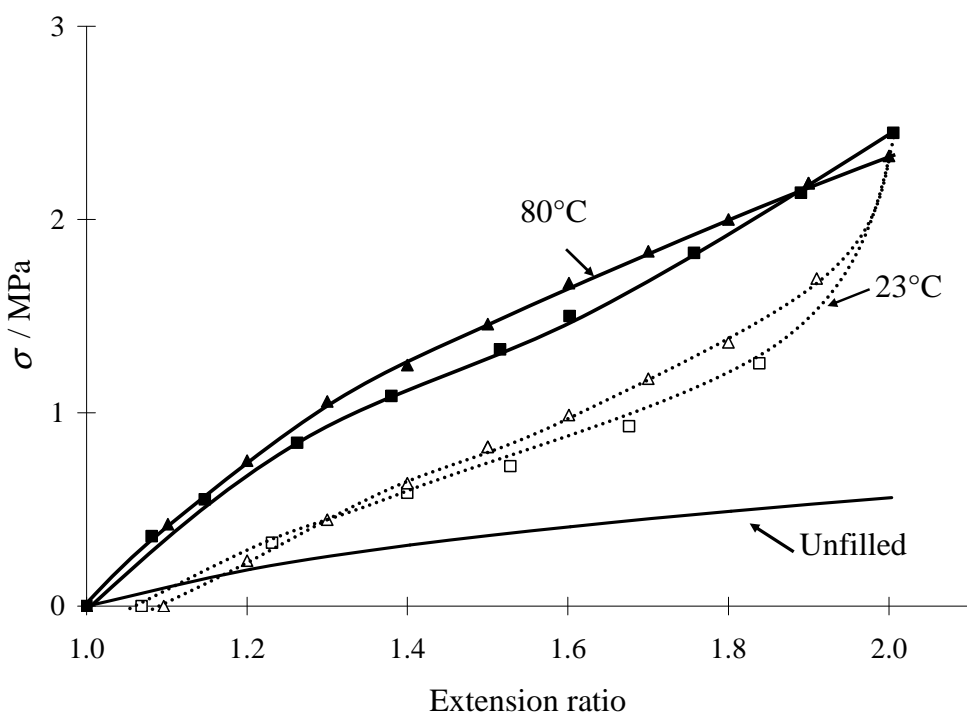


**Figure 6.24** Stress versus strain for CDX 7055 black filled NR at a filler volume fraction of 21% under cyclic tensile strains at 23°C and 80°C.

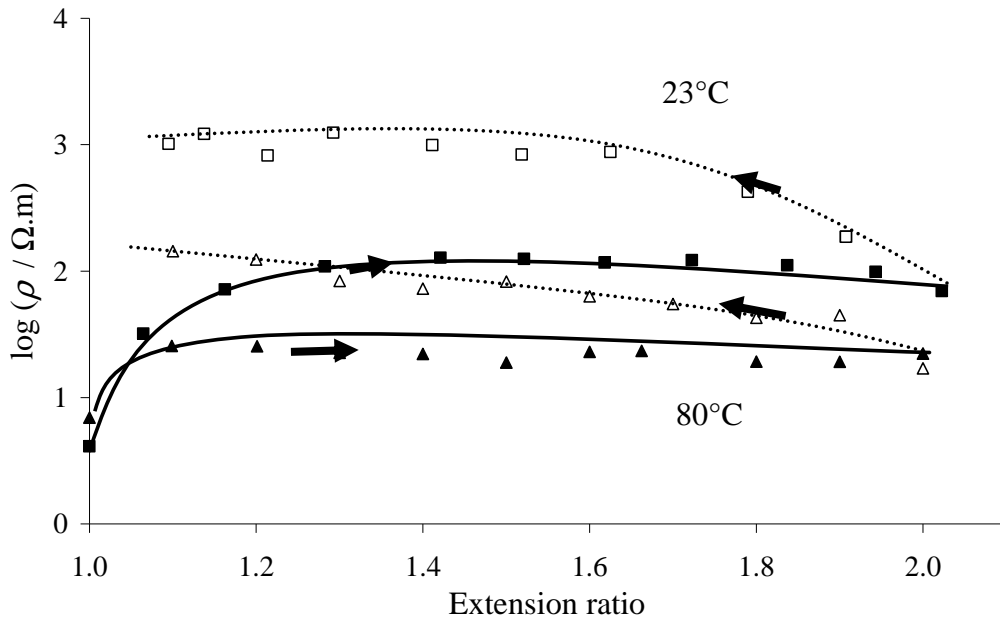


**Figure 6.25** Resistivity versus extension ratio for Raven p-5 filled NR at a filler volume fraction of 21% under cyclic tensile strain (1<sup>st</sup> cycle only) at 23°C and 80°C.

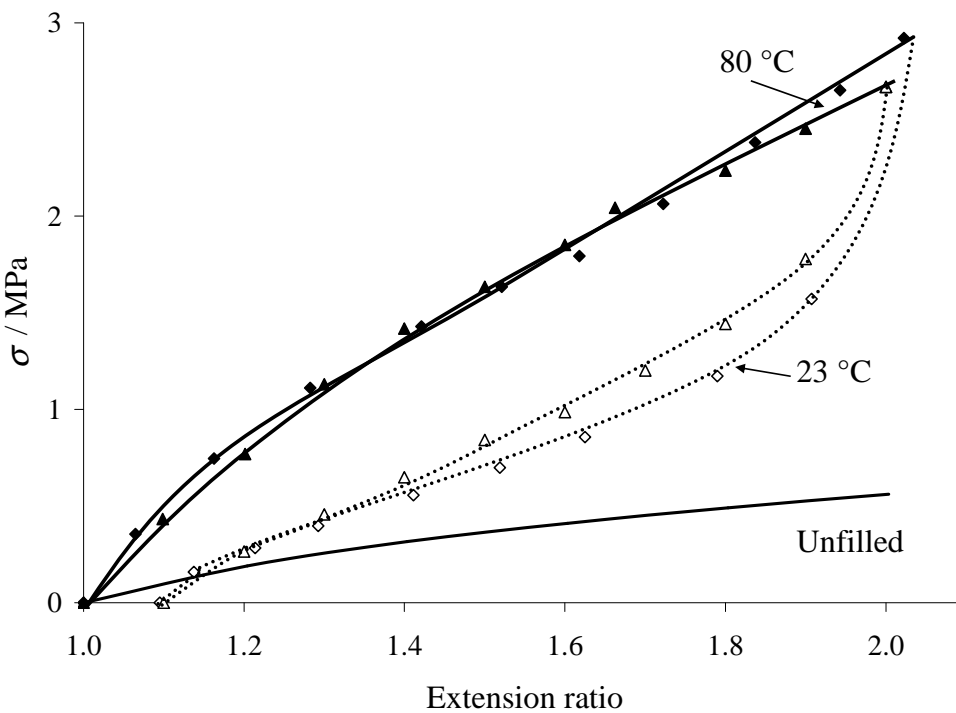


**Figure 6.26** Stress versus strain for Raven p-5 black filled NR at a filler volume fraction of 21% under cyclic tensile strains at 23°C and 80°C.

---

## 6.6 Effect of Swelling

When filled rubber is exposed to a suitable solvent it absorbs the solvent and swells to an extent that depends upon the polarity and the viscosity of solvent. This results in a volumetric expansion of the filled rubber that increases the inter-aggregate distance, resulting in a triaxial stress being applied in all directions. The properties of solvents xylene and DBA used in the present work are shown in Table 3.3. Busfield *et al.* (2004) have shown for HAF N330 filled NR swollen with solvent such as DBA and AC-12 that there is an increase in resistivity. They suggested that the solvent also shows a tendency to preferentially migrate to the filler rubber interface also resulting in a further increase in the resistivity. An observation later supported by (Carrillo *et al.* 2005).

The following Figures 6.27 and 6.29 show Printex-XE2 swollen in two different solvents, xylene and DBA. DBA is more viscous than xylene as explained in Chapter 3. This produces different effects on the rubber. Figure 6.27 shows changes in resistivity under strain for Printex-XE2 filled NR swollen in xylene. There is increase in resistivity of one order of magnitude from the non swollen Printex-XE2 with a  $V_r = 1$  to the ~20% swollen Printex-XE2, with a  $V_r = 0.82$ . At  $V_r$  of 0.92 Printex-XE2 gave half an order of magnitude change in resistivity. So, for Printex-XE2 filled NR swollen in xylene produced half an order of magnitude change for every ~10% of solvent in the rubber. Busfield *et al.* (2004) suggested the swelling causes the breakdown in the filler structure which is similar to the effect of a tensile strain as shown in Figure 6.4. Figure 6.28 shows the stress versus strain behaviour of Printex-XE2 filled NR swollen in xylene. Swelling causes a decrease in the filler-rubber and filler-filler aggregate interaction as a result the modulus decreases with increasing solvent content as shown in Figure 6.28 and 6.30. DBA is used as a plasticiser and has a greater viscosity than xylene. Figure 6.29 shows Printex-XE2 filled NR swollen in DBA to ~4% ( $V_r = 0.96$ ) there was an increase in resistivity of one and half orders of magnitude. The trend is for an increase in resistivity for a sample swollen with DBA shown in Figure 6.29 and is to similar sample swollen in xylene Figure 6.27. Unlike the experiments with xylene though, the slopes are not all parallel with strain,



---

with DBA having a less significant effect at higher strains. One possible explanation for this being that the DBA, first acted as an insulator, breaking the network of conductivity; but once the sample was strained the liquid at the filler polymer interface might be squeezed out allowing the conducting particles to move closer together.

Figures 6.31 and 6.33 show the changes in resistivity in MT N990 filled NR swollen in xylene and DBA respectively. Swelling MT N990 filled rubber in xylene and DBA increases the resistivity. This is due to an increase in the inter-aggregate distance resulting from the swelling. Swelling also causes a break down in filler aggregate structure and increases the resistivity. Figure 6.32 and Figure 6.34 show the stress strain curves for the MT carbon black sample filled swollen in xylene and DBA respectively. As DBA is oily and is used as a plasticizer there is a greater reduction in modulus than is in the case for xylene. This results in a greater increase in resistivity for the MT N990 carbon black filled NR swollen in DBA.

Figures 6.35 and 6.37 show rubber filled with HAF carbon black swollen to different degrees and then with the electrical and mechanical properties under strain. Figures 6.23, 6.25, 6.35 and 6.37 shows that the effect upon swelling in both solvents is much greater than the effect of increasing in temperature. In xylene CDX 7055 shows an initial change in resistivity of about 2.5 orders of magnitude when swollen by ~10%. In the case of Raven p-5 there is also a much bigger change in the electrical properties with strain in the sample swollen in xylene. Figure 6.36 and 6.38 show the reduction in modulus as the percent of swelling increases in the case of HAF filled rubbers.

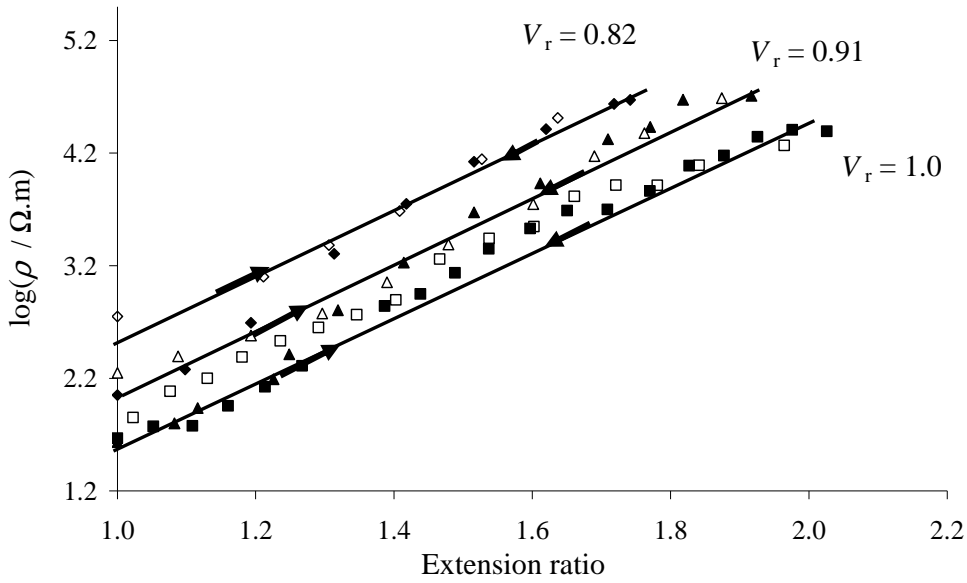


**Figure 6.27** Effect of swelling with xylene on resistivity versus extension ratio for Printex-XE2 filled NR at a filler volume fraction of 5.2% under cyclic tensile strains.

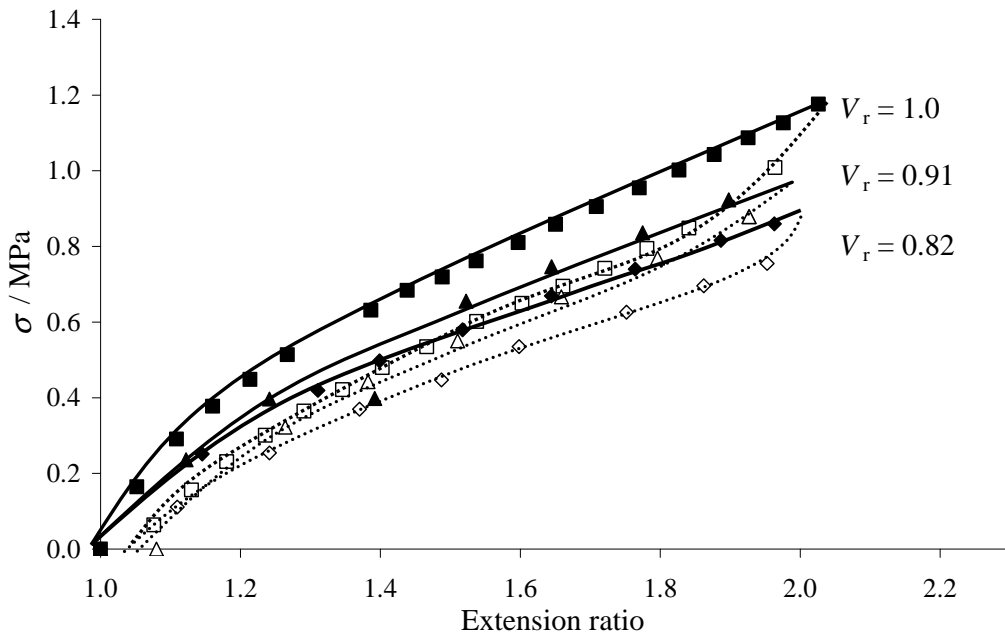


**Figure 6.28** Effect of swelling with xylene on stress versus strain for Printex-XE2 filled NR at a filler volume fraction of 5.2% under cyclic tensile strains

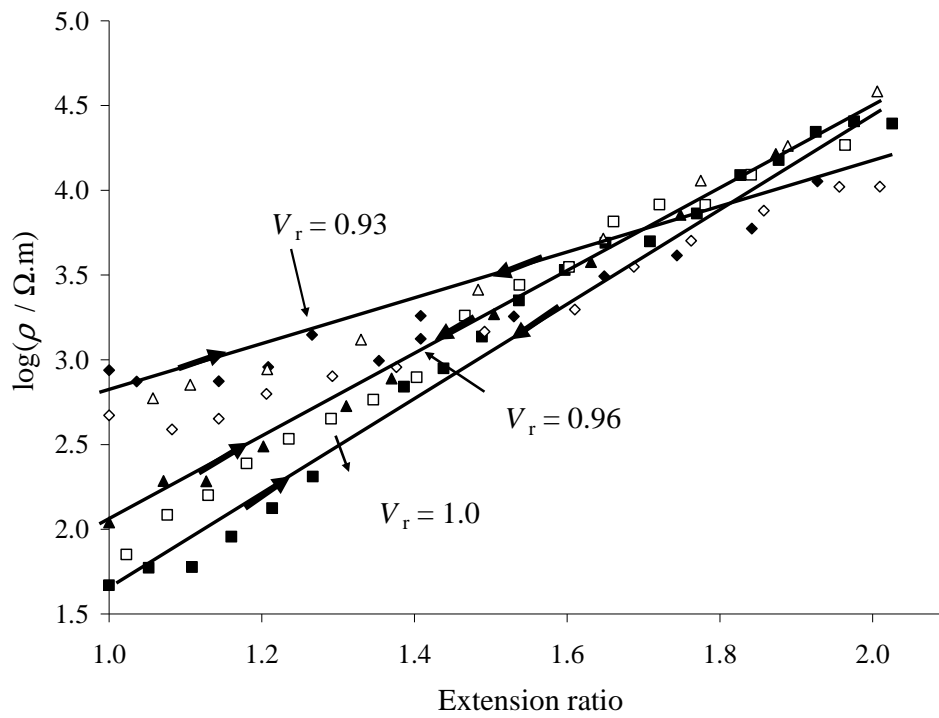


**Figure 6.29** Effect of swelling with DBA on resistivity versus extension ratio for Printex-XE2 filled NR at a filler volume fraction of 5.2% under cyclic tensile strains.

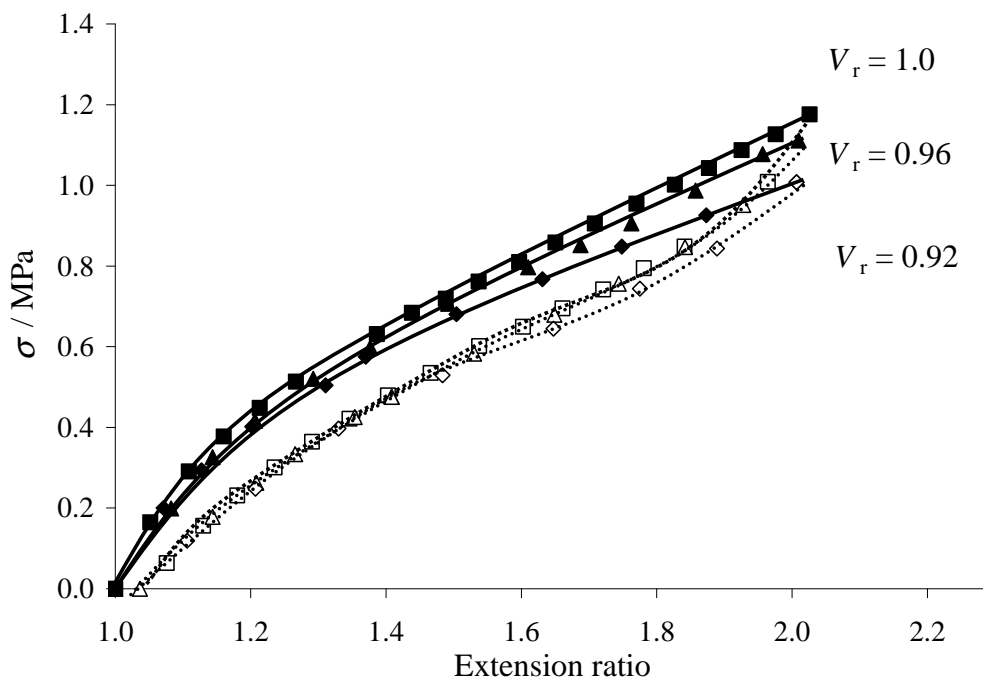


**Figure 6.30** Effect of swelling with DBA on stress versus strain for Printex-XE2 filled NR at a filler volume fraction of 5.2% under cyclic tensile strains

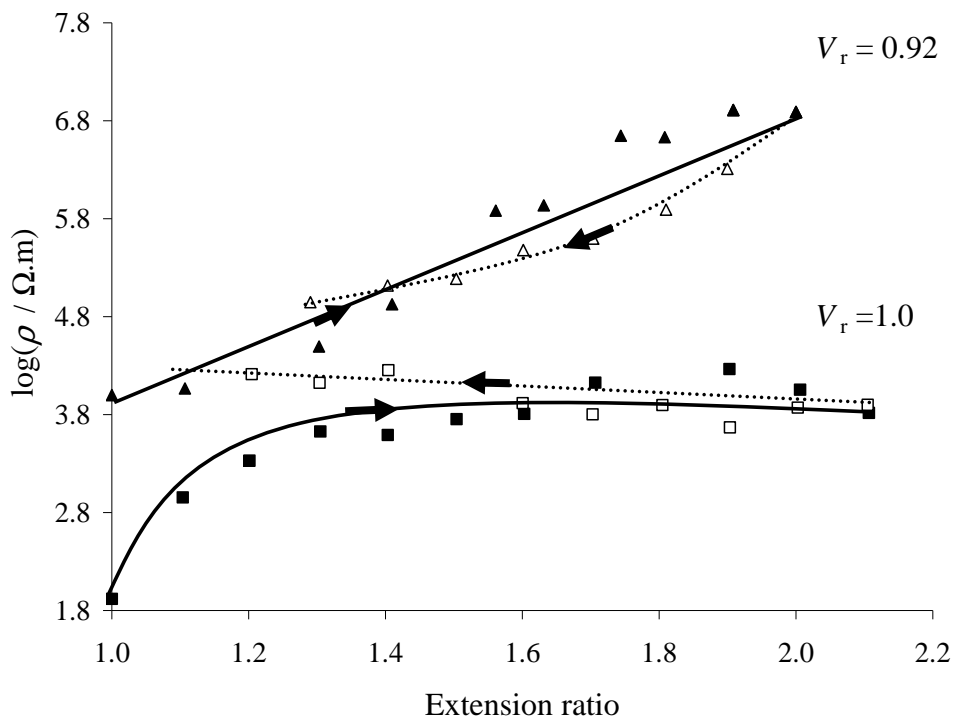


**Figure 6.31** Effect of swelling with xylene on resistivity versus extension ratio for MT N990 filled NR at a filler volume fraction of 56% under cyclic tensile strains.

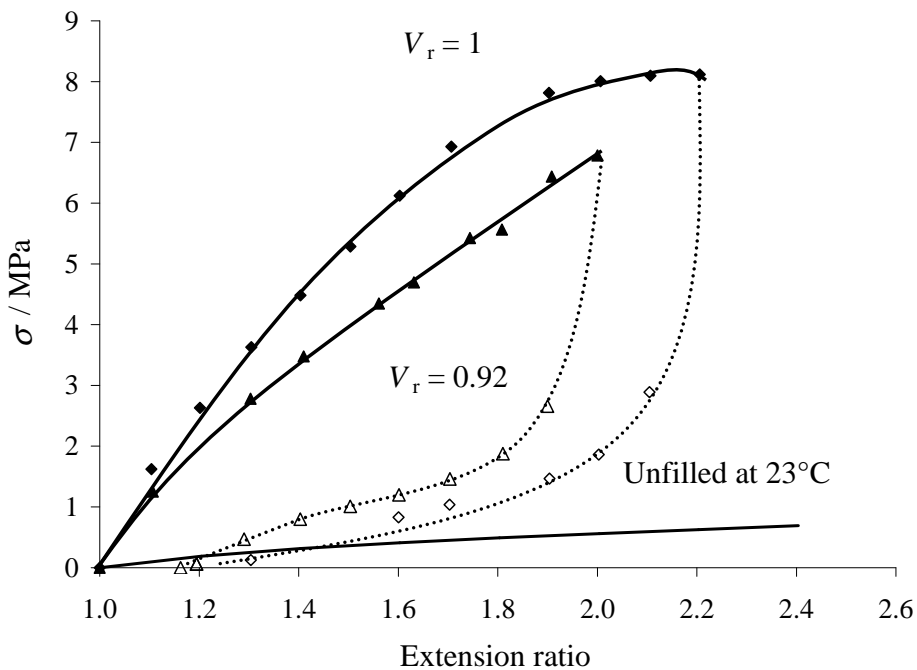


**Figure 6.32** Effect of swelling with xylene on stress versus strain for MT N990 black filled NR at a filler volume fraction of 56% under cyclic tensile strains.

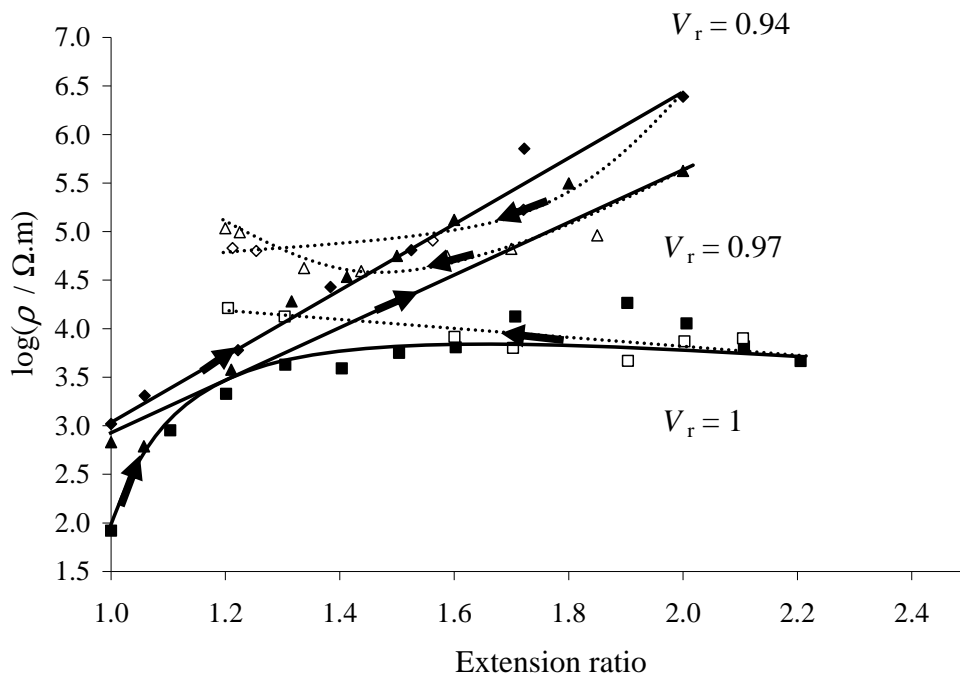


**Figure 6.33** Effect of swelling with DBA on resistivity versus extension ratio for MT N990 filled NR at a filler volume fraction of 56% under cyclic tensile strains.

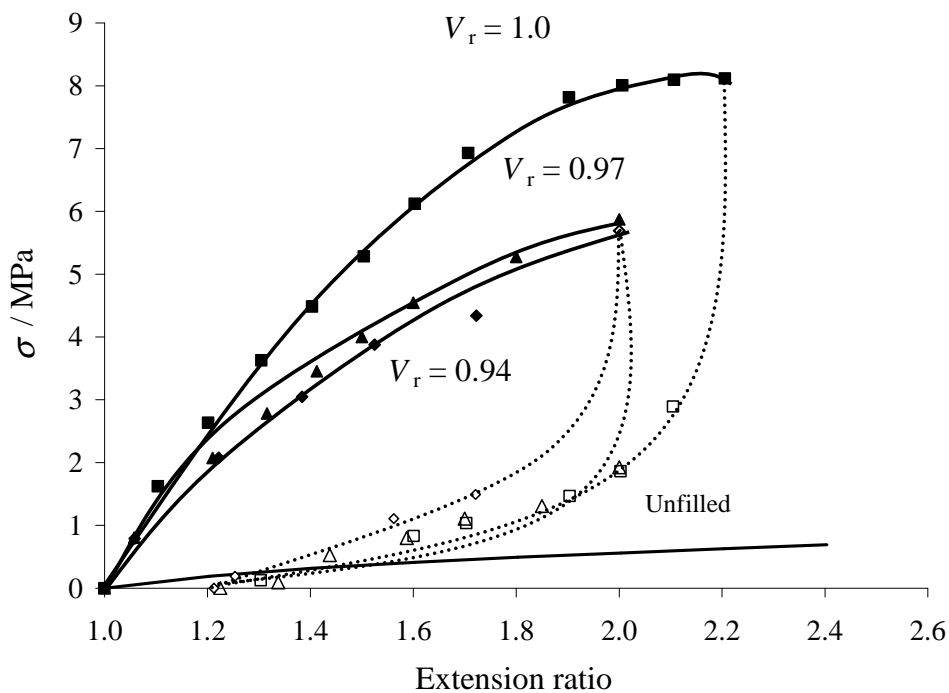


**Figure 6.34** Effect of swelling with DBA on stress versus strain for MT N990 black filled NR at a filler volume fraction of 56% under cyclic tensile strains.

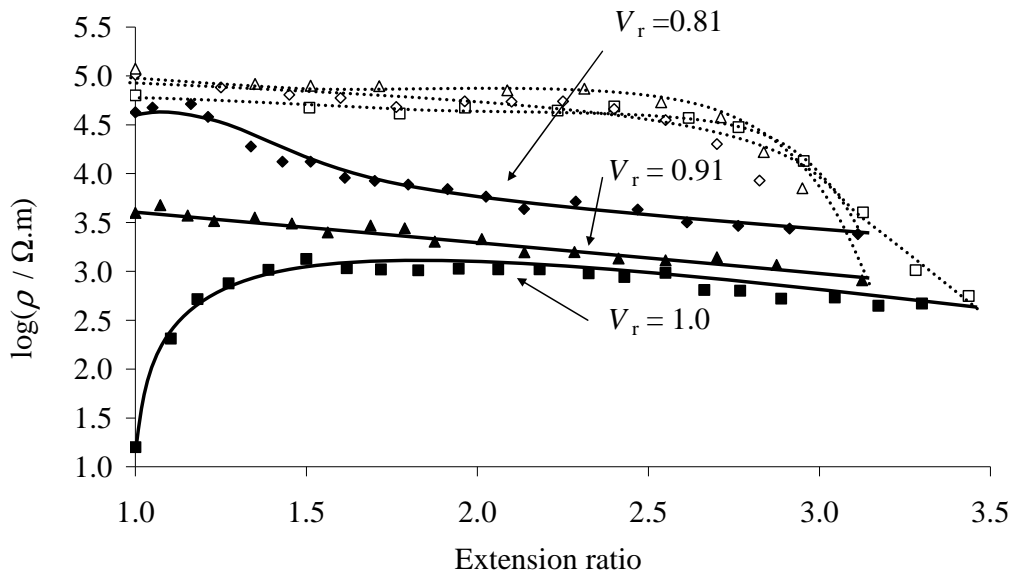


**Figure 6.35** Effect of swelling with xylene on resistivity versus extension ratio behaviour for CDX 7055 filled NR at a filler volume fraction of 21% under cyclic tensile strains. (1<sup>st</sup> cycle only).

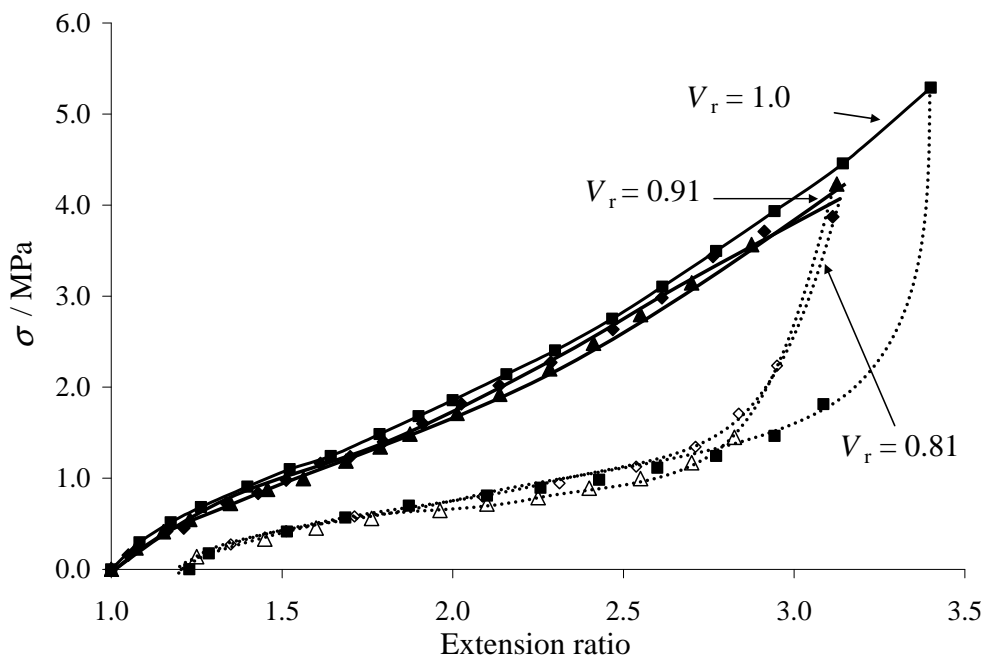


**Figure 6.36** Effect of swelling with xylene on stress versus strain for CDX 7055 carbon black filled NR at a filler volume fraction of 21% under cyclic tensile strains.

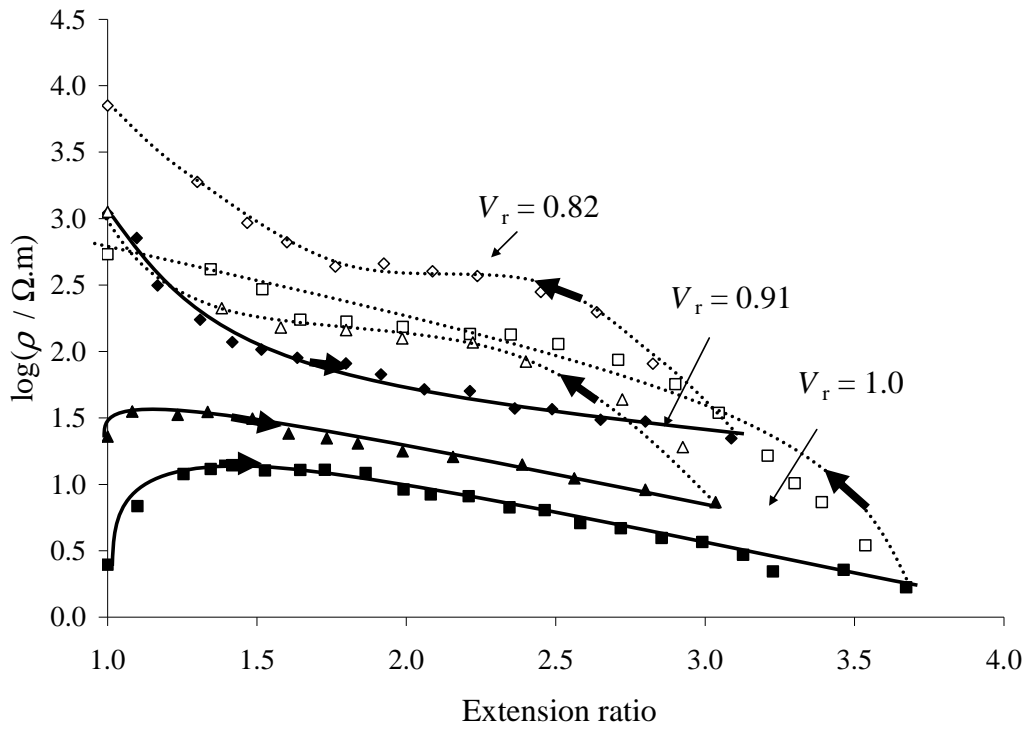


**Figure 6.37** Effect of swelling with xylene on resistivity versus extension ratio for Raven p-5 filled NR at a filler volume fraction of 21% under cyclic tensile strains. (1<sup>st</sup> cycle only).

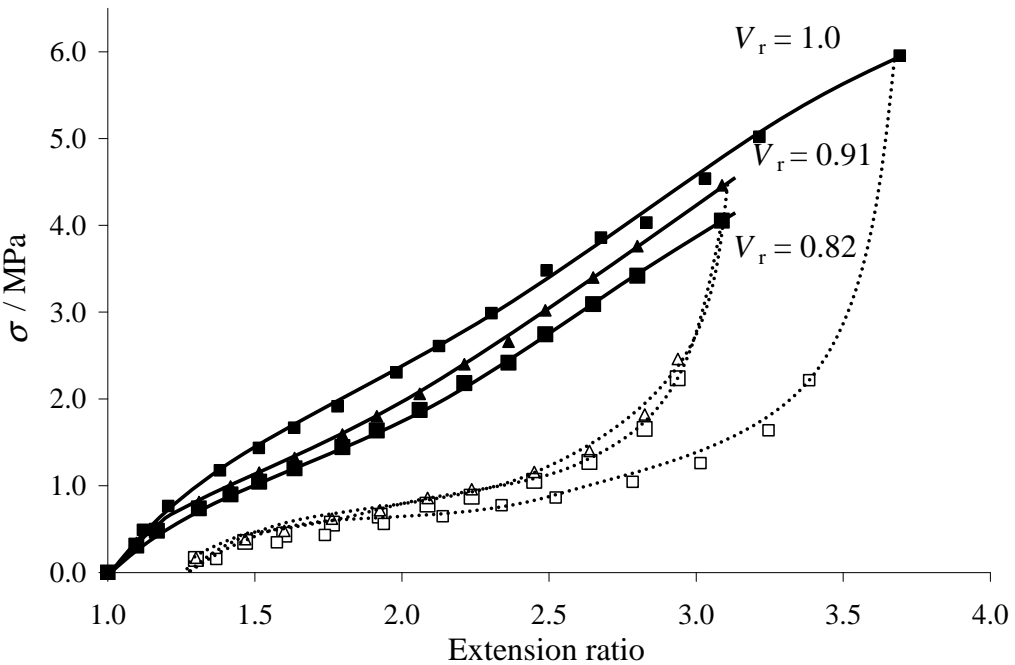


**Figure 6.38** Effect of swelling with xylene on the stress versus strain behaviour for Raven p-5 black filled NR at a filler volume fraction of 21% under cyclic tensile strains.

---

## 6.7 Proposed Model for filler aggregate structure

### 6.7.1 Introduction

In order to explain the effect of strain, temperature and swelling on the changes in resistivity under strain for the various filler types the following models are proposed for changes in the filler aggregates structure under strain. The proposed model involves five different types of filler aggregates structure. Their properties can be related to their size, structure and reinforcing strength shown in Table 3.1 and Figure 6.1. The proposed model based on the effect of filler particle size on the modulus (Donnet and Voet, 1976), the adhesion index of filler (Hess *et al.*, 1967), the model proposed by Busfield *et al.* (2004) for “orientation effects” of filler aggregates, the occluded rubber model, the slippage model (Dannenberg, 1966), the re-arrangement of particles under strain (Fujimoto, 1986) and the finite element analysis of MT carbon filled elastomer proposed by Jha *et al.* (2007). In order to discuss the various types of aggregates, they are labelled in accordance to their performance under strain. As shown in Figure 6.39:

Type 1: refers to the aggregates that do not break (shown in Figure 6.39-6.42 as ●);

Type 2: refers to the aggregates that break reversibly and which go back to reform conductive networks when the strain is removed (shown in Figure 6.39-6.42 as ○) (◀▶ sign indicate reversibility in Figure 6.39 and Figure 6.40);

Type 3: refers to aggregates that break irreversibly and do not reform the conductive networks once the strain is removed (shown in Figure 6.39-6.42 as ●);

Type 4: refers to the aggregates that do not form conductive networks in the first place (shown in Figure 6.39-6.42 as ○); and

Type 5: refers to a situation which are the aggregates are debonded or cavitate from the rubber, hence interrupting the rubber-filler interface. (shown in Figure 6.39-6.42



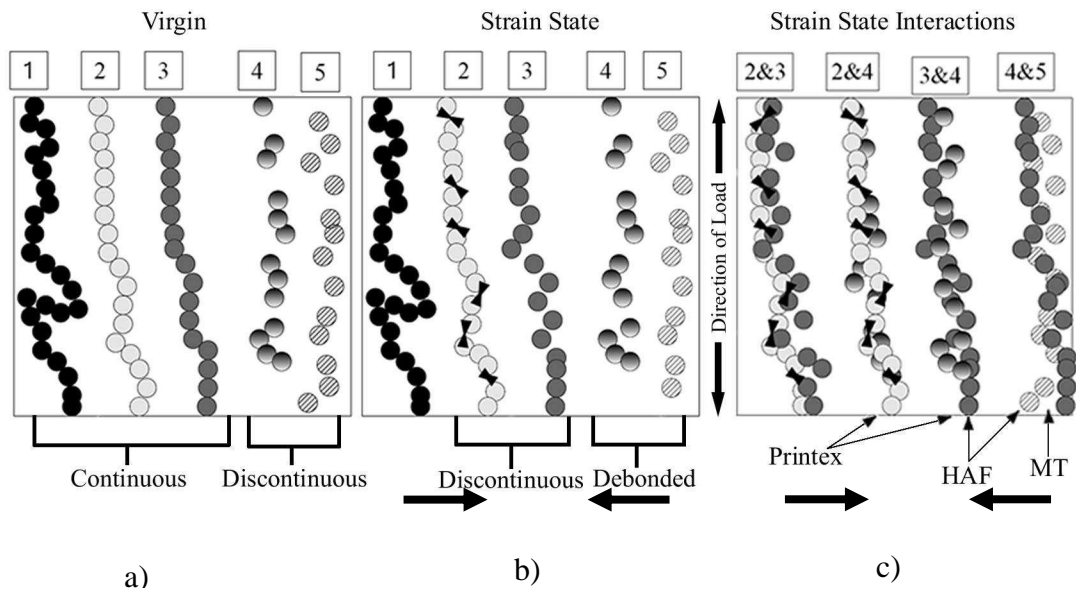
---

as  )

Figure 6.39 shows a schematic of each of these types of aggregate in three different states, (1) virgin state, when unstrained, (2) the strained state and (3) the strained state interactions, which occur due to the change in the cross-sectional area as different types of aggregates interact in the direction perpendicular to the direction of loading. Type 1 aggregates do not break hence they show no change in the conductivity as they are loaded while Type 2 aggregates show a change in the conductivity that is reversible, decreasing as it is loaded and increasing linearly as it is unloaded. Type 3 aggregates show irreversible changes in conductivity, decreasing rapidly as they are loaded but that do not go back as they are unloaded (Yamaguchi *et al.*, 2003). Type 4, are aggregates that do not form a conductive network as they are not in contact with other aggregates or sufficient aggregates to form the network. Type 5 aggregates are those that are debonded and have the potential to produce changes in conductivity (Hess *et al.*, 1967) not only increasing the resistivity but also as the polymer chains can move more easily around the aggregates (Dannenberg, 1966), it might possibly allow more conductive networks to be formed.

When strained the five different types of aggregate deformation mechanisms mentioned earlier either debond or slip and depending on the filler properties specified above could potentially interrupt or re-arranging the conducting network. Nevertheless, the strain also causes a reduction in cross sectional area which in turn causes the different aggregates to come into contact, producing interactions between the different types of fillers. These interactions increase the probability of the aggregates contacting and forming conductive networks, hence increasing the conductivity. In terms of the observed effect of strain on conductivity for the different filled rubbers and the basic understanding of the properties of the fillers, the following aggregate interactions were assumed to occur. The adhesion index proposed by Hess *et al.* (1967) gives a relationship between the stress required to see a specific percentage, of de-bonded/de-wetted particles that have arisen. A random measurement of de-wetted particles is taken shown in Figure 2.6 (Chapter 2). Once a

specific percentage is reached, the strain is recorded (Hess *et al.*, 1967). The adhesion index measures the effectiveness of the filler reinforcement.



1. ● ○ ● ● Filler aggregate are all bonded well to the rubber matrix;
2. ◐ Filler aggregate debonded from rubber matrix;  
(Representing Type1-5 aggregates as suggested in introduction to section 6.7.1).
3. ◀▶ Indicates that the aggregate breakdown is reversible under the application of a strain

**Figure 6.39** Proposed filler aggregate structure re-arrangement. ( ▶▶ Indicates when the aggregate breakdown is reversible under the application of a strain).

1. Figure 6.39a shows the five aggregate structures discussed in section 6.7.1. Virgin state means the filled rubber is unstrained. Type 1, 2 and 3 forms have a continuous network of filler aggregate structure that contribute to the conductivity of a filled rubber. Type 4 and 5 aggregate structures are discontinuous and do not contribute to the conductivity of an unstrained filled rubber.

2. Figure 6.39b shows the changes that might arise in aggregate structure under the application of strain. Type 1 aggregate can still form a continuous network structure and contribute to conductivity. However, aggregate Type 2 and 3 breakdown under application and this decreases the conductivity of the sample.

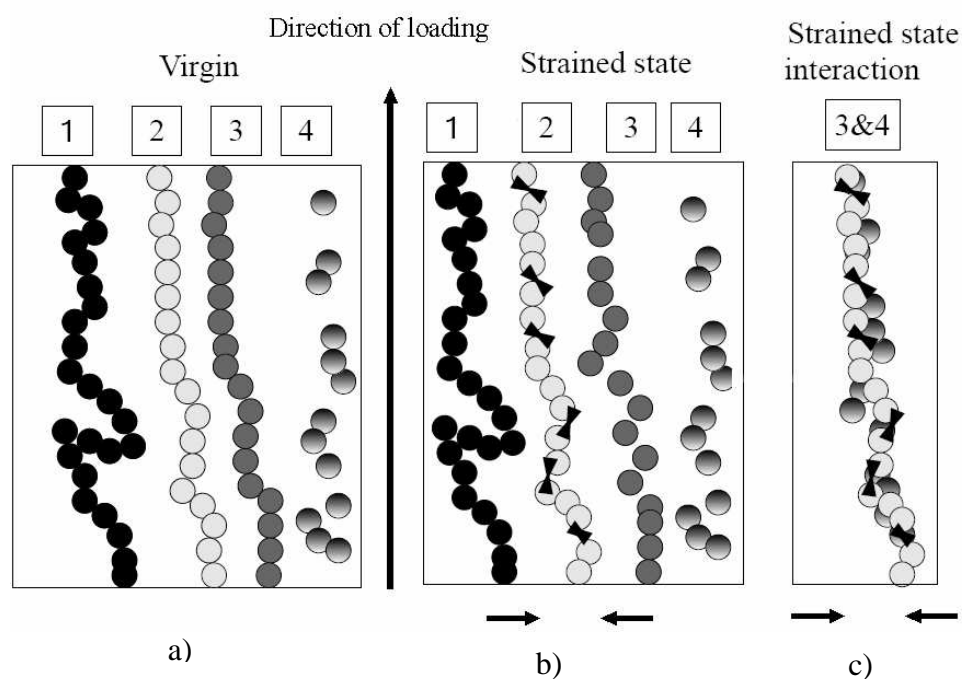
c) Figure 6.39c shows changes taking place in direction perpendicular to the direction of the application of the load referred to as strained state interaction. Here additional filler aggregate structure interactions might increase the conductivity.

---

Figure 2.6 (Chapter 2) shows experimental data for MT and HAF, where a stress is recorded when the de-wetting count is 20%. This behaviour can be explained with the proposed model. As can be seen in the graph, MT N990 debonds at low stresses, which correlates with the formation of a type 4 and 5 aggregates. For HAF, a higher stress is required to achieve this amount of dewetting. For Printex-XE2 there is no data but as particle structure and size is related to the adhesion index and the resulting stress strain curve, it can be estimated that the stress required to dewet 20% of the surface would be even higher.

In order to estimate the amount of dewetting at 100% strain for the filler volumes and types used in this work the maximum stresses were taken from the 1<sup>st</sup> cycle stress-strain curves and compared to assess how each type of filler behaves. The proposed model along with the adhesion index shows that the MT particles de-bond almost entirely at 100% strain, aggregates in HAF have little de-bonding and that the aggregates in Printex-XE2 do not de-bond. This evidence supports the mechanisms proposed to explain the conductivity behaviour observed experimentally.

## 6.7.2 Printex-XE2 Filler aggregate structure model



1. ● ○ ● ● Filler aggregates are all bonded well to the rubber matrix; (Representing Type1-4 aggregates as suggested in introduction to section 6.7.1).
3. ►► Indicates that the aggregates breakdown is reversible under the application of a strain

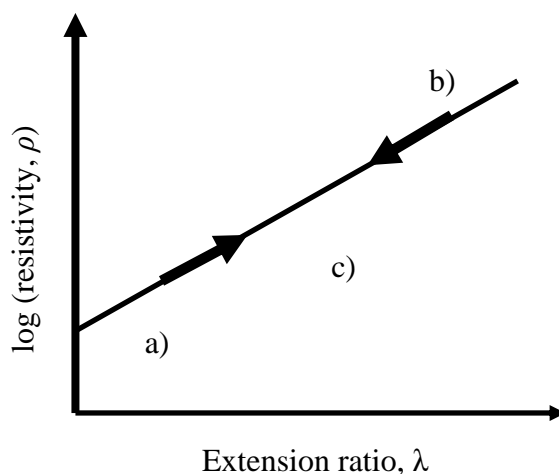


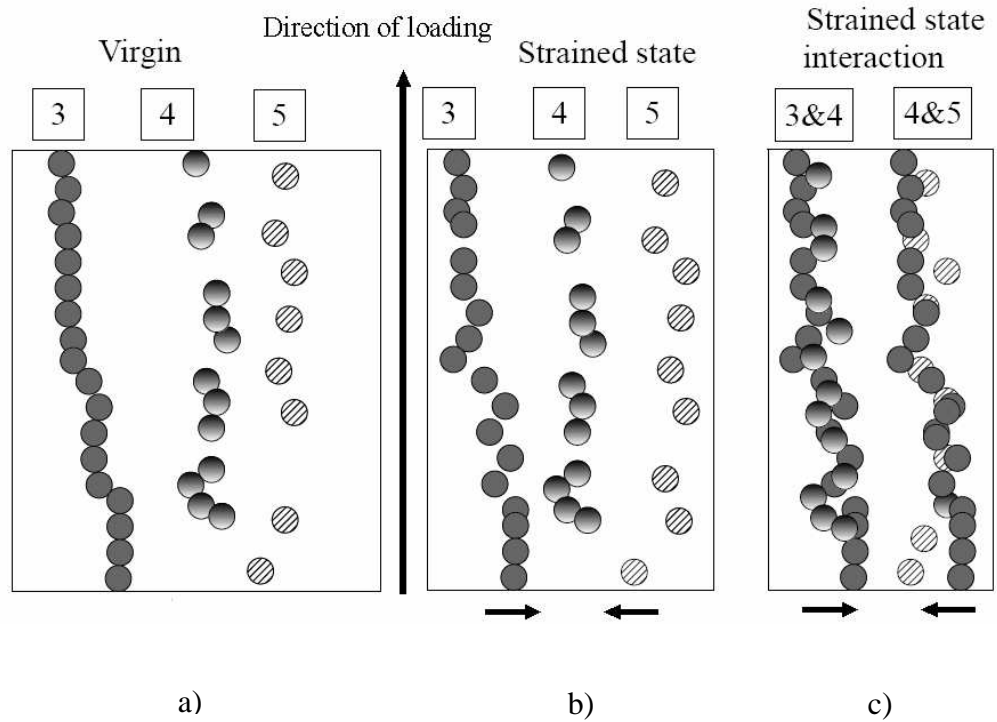
**Figure 6.40** Proposed filler aggregate structure re-arrangement for Printex-XE2 filled elastomer and the idealised behaviour of Printex-XE2 under cyclic strain. (►► Indicates the aggregates are broken in a reversible manner in Type 2)

Printex-XE2 shows reversible changes in resistivity under cyclic strain as shown in Figure 6.40. Printex-XE2 filled NR must have Type1-4 aggregates only present in

---

the unstrained state as shown Figure 6.40a. Figure 2.6 and Table 3.1 suggest Printex-XE2 might have a high adhesion index and hence would have a negligible amount of de-bonded Type 5 aggregates under strain. Printex-XE2 has the smallest particle size, highest surface area, highest structure with its proposed hollow hemispherical shape and greatest reinforcing effect indicating the formation of a greater proportion of Type 1 and Type 2 aggregates. Hence, Printex-XE2 filled elastomers have a low resistivity even at relatively low volume fractions. As a result in the strained state only small proportion of Type 2 and 3 aggregate structures breakdown as shown in Figures 6.40b. This explains the increase resistivity observed at higher strains. However, Type 2 aggregates recover their structure when the strain is removed which reduces the resistivity. In the strained state the filler aggregates may reform some conduction paths (especially in direction perpendicular to applied load). Possible interactions in the strained state contribute to the formation of new conduction paths as is also shown in Figure 6.40c. This model explains the reversible changes in resistivity for Printex-XE2 filled NR using filler aggregates interactions.

### 6.7.3 HAF Filler aggregate structure model



1. ● ○ ● ● Filler aggregate are all bonded well to the rubber matrix;
2. ◊ Filler aggregate debonded from rubber matrix;
3. ◀ ▶ Indicates that the aggregate breakdown is reversible under the application of a strain

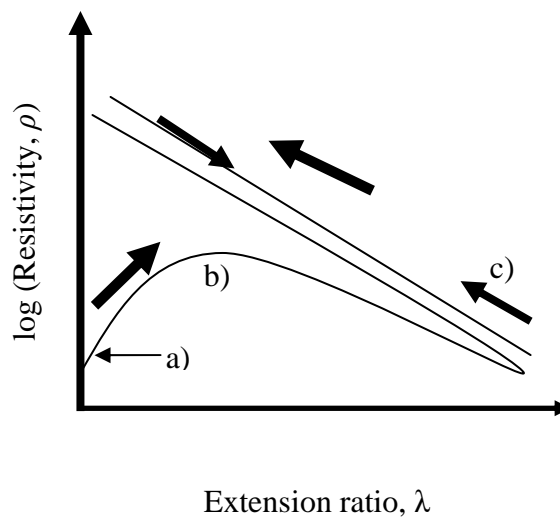


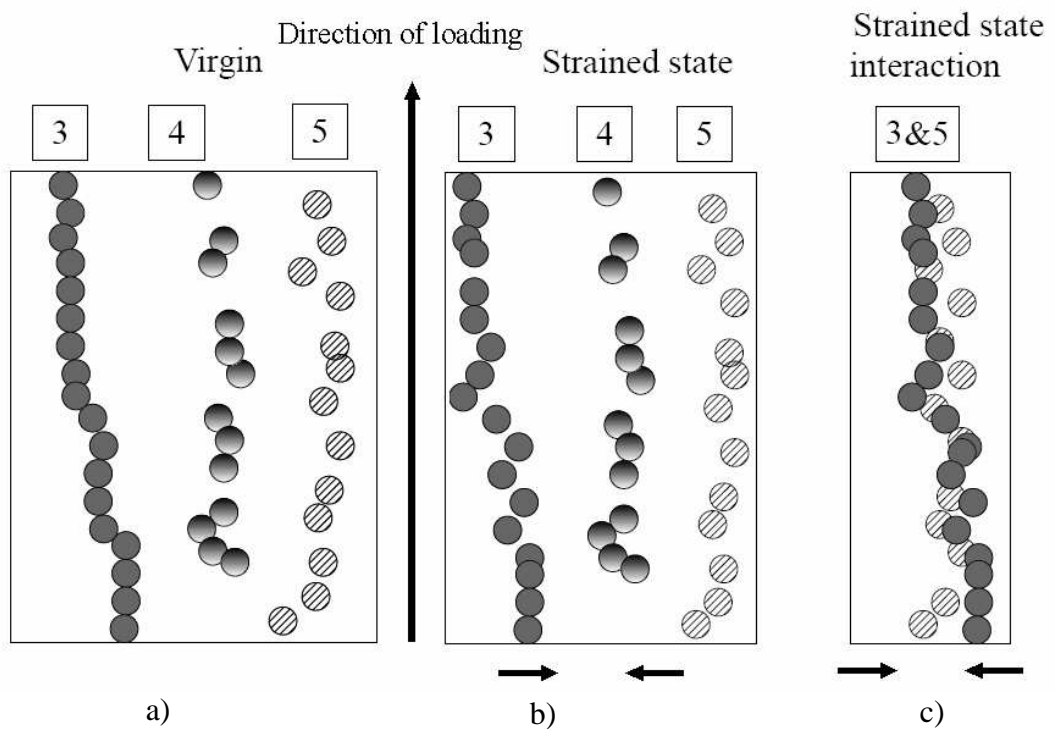
**Figure 6.41** Proposed filler aggregate structure re-arrangement for HAF Raven p-5 and CDX 7055 filled elastomer and idealised behaviour for the same blacks under cyclic strain.

---

Yamaguchi *et al.* (2003) measured the changes in the resistivity behaviour of HAF N330 filled NR. The data was remeasured here using Raven p-5 and CDX 7055 filled NR. Yamaguchi *et al.* (2003) assumed the filler aggregate structure was Type 3 and Type 4. Figures 6.41, 6.7 and 6.9 show how the resistivity changes under strain.

From Figures 2.6 and 6.1 and also from Table 3.1 (Chapter3) it can be assumed that HAF filled rubber possesses a greater proportion of de-bonded Type 5 aggregates than the Printex-XE2 filler as shown in Figure 6.41a. The idealised behaviour for the HAF filled elastomers is shown in Figure 6.41. Yamaguchi *et al.* (2003) attributed the initial increase in the resistivity to the breakdown of the agglomerate structure in the rubber (Type 3 aggregate), shown in figure 6.41b. When the applied tensile strain increases above this strain the change in resistivity with strain reaches a plateau. This has been attributed to result from the “orientation effects” in the perpendicular direction (strained state interaction in Figure 6.41) of the shaped fillers under strain. Reversible changes in resistivity are observed under cyclic loading and changes take place only due to “orientation effects” or in the present model the strained state interaction as shown Figure 6.41c.

### 6.7.4 MT Filler aggregate structure model



1. ● ○ ● ● Filler aggregate are all bonded well to the rubber matrix;
2. ◐ Filler aggregate from rubber matrix;  
(Representing Type1-5 aggregates as suggested in introduction to section 6.7.1).
3. ► Indicates that the aggregate breakdown is reversible under the application of a strain.

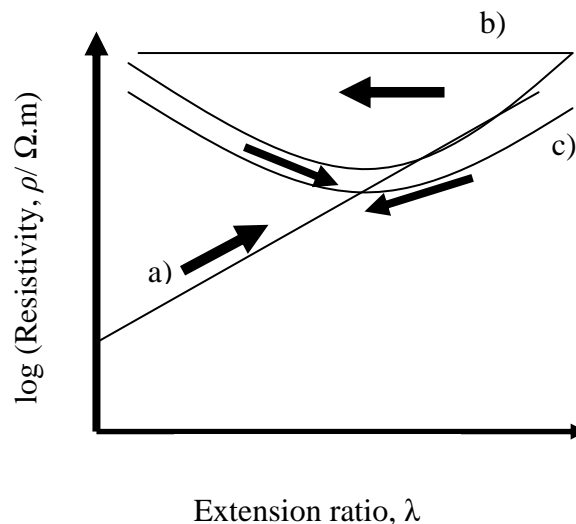


**Figure 6.42** Proposed filler aggregate structure re-arrangement for a MT N990 filled elastomer and the idealised behaviour for the same carbon black filler under cyclic strain.



---

Figures 6.42, 6.11 and 6.13 show the changes in resistivity under strain for a MT carbon black filled elastomer. MT N990 carbon filled elastomers have Type 3-5 aggregates as shown Figure 6.42 based on Figures 2.6 and 6.1 and Table 3.1. MT N990 carbon filler structure debonds easily during loading shown 6.42b.. Hence, the resistivity increases initially. Figure 2.6 shows that MT carbon black has low value for the adhesion index and it can assumed that most of the fillers after the first cycle have debonded and become Type 5. The resistivity values do not recover after unloading and the change in the filler aggregate structure is irreversible as shown in Figure 6.42b. For MT N990 carbon blacks there are greater filler-filler interaction as the volume fraction is very high. Fujimoto (1986) observed the rearrangement of particles along the direction of strain under cyclic loading. In chapter 5 it has been proposed that rubber can slip around the filler. Due to these effects and the strained state interaction shown in Figure 6.42c under cyclic loading the filler aggregate structure can align along the direction of strain and this can explain the change in resistivity of MT carbon filled rubber under cyclic loading.

## **6.8. Evaluation conductive bonding agent**

### **6.8.1 Introduction**

In smart devices or systems, the electrical resistance is seen to change under strain. Measurement of the current flow at an appropriate voltage will reveal the extent of strain in the component. The aim is to develop a bonding agent with a low resistance and high reliability so that a conductive connector can be bonded into the rubber. This would enable measurement of the electrical properties to monitor the mechanical performance. One of the most effective techniques is to add conductive fillers to the polymer matrix. The most common conductive particles used in the industry are gold, palladium, silver, nickel, copper, graphite and carbon black. The peel energy as described in section 3.2.8 can used evaluate the impact of filler loading on the bond strength of conductive adhesive.

---

### 6.8.2 Adhesion test results

The present work studies the effect of increased silver filler volume fraction on the resistivity and the bond peel energy. The percolation threshold of nanosized silver particles is approximately 29% by volume (Novak *et al.*, 2004). Hence, in the present case adhesion test have been done for silver filler incorporated in bonding agent at a volume fraction of 7.5% and 31%. The experimental step up for 90° peel test is shown in Figures 3.4 and 3.5. The sample preparation is discussed in Chapter 3 section 3.2.8. The adhesion test results are shown in Table 6.2 and Figures 6.43 and 6.44. A 90° peel test is used to obtain force versus extension ratio (mm) behaviour as shown in Figure 6.43. From this plot, the average force ( $F$ ) required for bond fracture was measured which was converted to average stress as shown in Table 6.2. A tensile test of same filled rubber was carried out in order to obtain the stress-extension ratio. Average force ( $F$ ) needed for bond fracture calculated earlier, was used to calculate the average extension ratio using this stress versus extension ratio relationship. Stress-extension ratio was converted to a plot of strain energy density ( $W$ ) versus extension ratio ( $\lambda$ ) as shown in Figure 6.44. Using the average extension ratio values, we can get the corresponding strain energy density ( $W$ ) in rubber during bond fracture. Using these value and Equation 3.8, allows the peel energy to be calculated as is shown in Table 6.2.

Two types of failure are indicated in the last column in Table 4.2. There, R indicates that the failure was in the rubber, RC indicates that the failure was at the rubber-adhesive interface. At a silver filler volume fraction of 0% and 7.5% the failure is in the rubber, which indicates that the bond is stronger than the rubber. However, at silver filler volume fraction of 31% the failure is at the rubber-cover cement interface. The bond strength is degraded as the silver filler volume fraction increases. The adhesion test results revealed that, the bond strength is degraded by the increasing filler loading. However, there is a good potential for silver filled bonding agent in developing a good conductiverubber to metal bond.

**Table 6.2** Adhesion test Results at 25°C

Volume fraction of silver in adhesive / %	Peel Energy/KJ/m <sup>2</sup>	Average Peel stress/MPa	Type of Break	Resistivity/Ω.m
0	25.3	3.53	R	-
7.5	22.44	3.20	R	1.9*10 <sup>8</sup>
31	16.79	2.88	RC	5.5*10 <sup>2</sup>

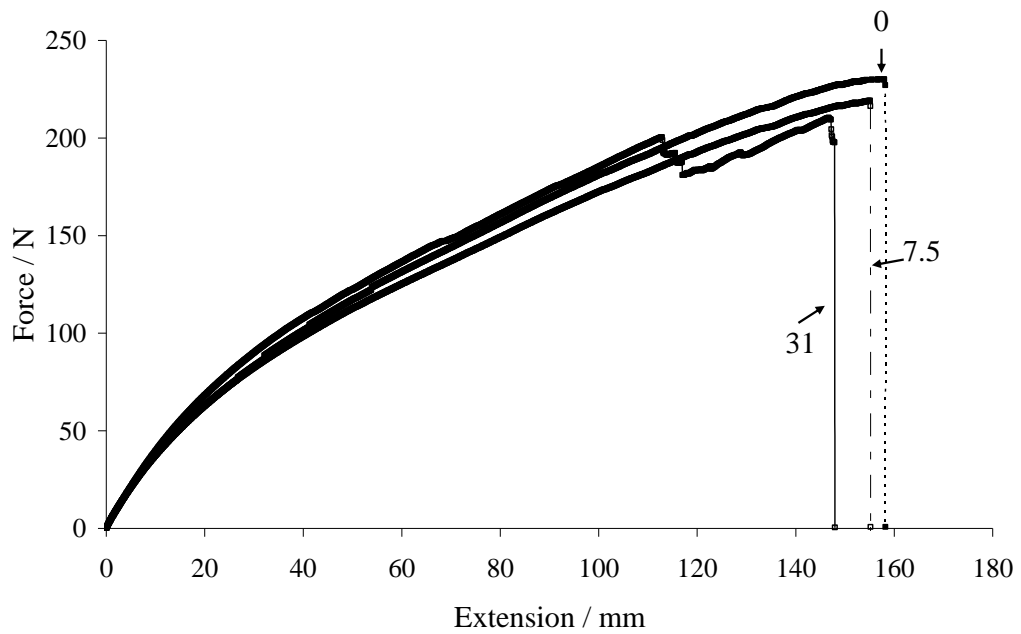


**Figure 6.43** 90° peel test measurement of force versus extension required to fracture the rubber bonded to steel plate using silver filled adhesive.

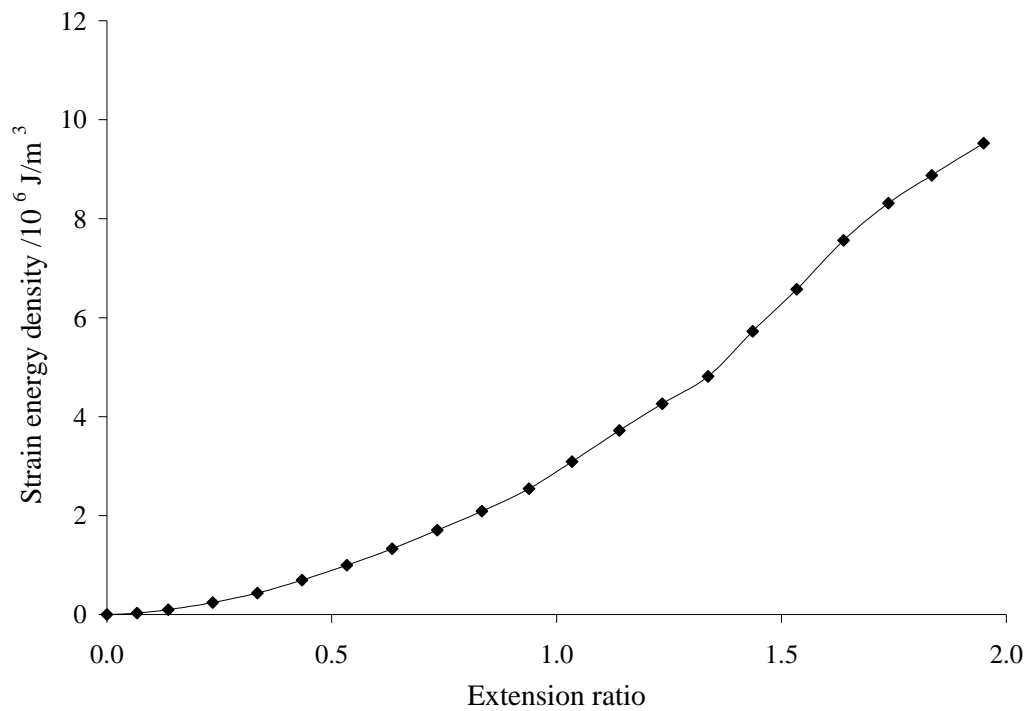


**Figure 6.44** Strain energy density for a rubber sample.

## 6.9 Conclusions:

### 6.9.1 Effect of strain

The behaviour of N990, Printex-XE2 and three HAF blacks Raven p-5, CDX 7055 and N330 all indicate that the filler properties such as surface area and structure have significant effect on the conductivity behaviour under a tensile strain, both in the first loading cycle and then under subsequent cyclic loading.

Printex-XE2 has a very high surface area and structure. This results in a percolation threshold at a filler volume fraction of below 5.2%. It is thought that the significant increase in the area of the filler rubber interface results in a more reversible behaviour in the electrical and mechanical behaviour under strain. This reversible behaviour of Printex-XE2 under strain has potential application in a wide range of smart rubber strain measuring devices. The reversible nature also suggests that only limited slippage occurs at the rubber filler interface.

---

The three HAF carbon black all have similar mechanical and electrical properties, and their behaviour is consistent with that described by Yamaguchi *et al.* (2003) for N330. In stark contrast is the behaviour of N990 carbon black, which has a very low surface area per unit mass and a low structure and hence has a very high percolation threshold. Both the electrical and mechanical behaviour under strain indicate that the filler does not adhere well to the rubber matrix and it is suggested that extensive slippage at filler rubber interface takes place under strain. The changes in the electrical conductivity behaviour under strain also supports the theory that under repeated cyclic deformation, the particles rearrange themselves.

### **6.9.2 Effect of Temperature**

Broadly speaking two conflicting mechanism could be present as the temperature of the test piece is changed.

1. Thermal expansion which results in an increases in the resistance
2. An increase in polymer mobility with increasing temperature, which results in deceases in the resistance.

To understand the effect of temperature on the resistivity behaviour under strain requires a consideration of the activation energy, the thermal assisted hopping mechanism and the bound rubber layer. An increase in temperature contributes to some mechanisms and creates an increase in the number of conduction paths. For all filled elastomers there is a decrease in the resistivity as the temperature is increased.

The modulus for an unfilled elastomer varies directly with temperature as is deduced for the thermodynamic theory for rubber elasticity. Also, as the temperature increases, the filler interaction with the polymer might reduce. Hence, for Printex-XE2 filled elastomers having a volume fraction of 5.2% at a higher temperature, the modulus increases suggesting the importance of the polymer chain to the overall modulus. The other extreme is MT carbon black which at volume fraction 56% shows greater extent of filler-filler interaction and hence a modulus decrease. HAF filled elastomers

---

containing Raven p-5, CDX 7055 and N330 all show an intermediate trend and clearly have both significant filler-filler and polymer-polymer interaction effecting the behaviour.

### **6.9.3 Effect of swelling**

Swelling the filled rubber sample in both xylene and DBA increases the resistivity of a filled rubber sample under strain. This is because swelling increases the inter-aggregate distance. Also, the preferential migration of the solvent to the interface results in breakdown of conduction paths and the resistivity of the polymer (Busfield 2004) increases. DBA swollen samples showed the greatest increase in resistivity. For DBA, which is used as a plasticiser, the oil could act as a lubricant and this might allow the particles to move closer together.

---

## Conclusions and Future Work

This work has studied the reinforcement of elastomer by carbon black fillers using finite element microstructural models. It has also investigated the resulting mechanical and electrical behaviour of these filled elastomers under strain. A range of microstructural finite element models were evaluated. To model the finite extensibility effects at strains above 100% then an appropriate stored energy function such as that suggested by Gent (1996) was required. The different boundary conditions used evaluated, namely plane surface and free surface boundary conditions. Models using a plane surface boundary showed an unrealistic increase in modulus due to the geometric limitation of the models. Models using a free surface boundary conditions were found to be suitable for prediction of stiffness of elastomer at higher strains. It has been noted that as the number of fillers present in the unit cell increased that there was an increase in the predicted stiffening effect at a constant filler volume fraction, with a final stiffness being reached at a large number of fillers in the unit cell.

Two different microstructural modelling approaches were examined under strain with up to 36 filler particles present in each. The first approach has a smooth spherical surface for each of the fillers and the second having a more irregular surface which has been constructed on a cubic lattice. The first type of model, containing spherical fillers, became progressively stiffer as the number of fillers was increased. This resulted from an increase in the volume of rubber in the unit cell being constrained between the fillers as the filler number increased even if the volume fraction of fillers remained the same between the different models. Comparisons at up to 50% strain in shear and tension showed that an eight filler particle model of this type was essentially isotropic. However, there were considerable meshing and modelling

---

difficulties associated with creating models with a totally random arrangement of smooth surface spherical fillers resulting from the requirement that the rubber be modelled using a finite element mesh of six sided brick elements. The second modelling approach adopted reduced this complication by using a perfect cubic lattice where only some of the elements, in regions to give the approximate shape of the filler and of the appropriate number to give an accurate representation of the filler volume fraction, were defined as having the properties of the filler. Using this approach a model containing just nine discrete fillers was significantly stiffer than the experimentally observed behaviour. This was because the effective filler volume fraction modelled was greater than expected. As a result of the stepped filler surface there were a significant number of rubber elements adjacent to the filler with a reduced mobility. This is potentially similar to occluded rubber where some of the rubber chains within the confines of the filler are constrained. This increases the effective filler volume fraction. In the present case, the amount of the occluded rubber was calculated from the volume which was restricted to move due to filler surface. At small strains (2%) the effective filler volume fraction and the initial stiffness calculated by the Guth and Gold (1938) relation were in good agreement. Checks again showed that this model exhibited isotropic behaviour.

This cubic lattice approach shows considerable promise as a technique to more easily create representative volumes that can investigate filler reinforcement whereby the filler distribution and geometry have been experimentally observed by using say TEM tomography techniques. In the case of models with cubic lattice (rough surface model) and model having greater number of filler particle it was found the FEA models generally over-predict the experimental observed behaviour. This might be because of phenomenon such as cavitation and dilation observed in filled elastomer has not been considered. The dilation of rubber under strain has been reported previously to be related to the amount the filler particles present in the rubber matrix. The effect of cavitation on the mechanical behaviour has also to be studied. The prediction can then be verified by carrying out the accurate density measurement under strain which can be compared to FEA prediction of dewetting at the rubber-filler interface. The finite element analysis behaviour must also be mapped on the



---

experimental observed behaviour to check validity of filler orientation model which has a significant effect on the prediction of the behaviour of a filled elastomer. A series of models exploring the effect of filler orientation in polymer matrix can be made to study the effect of filler orientations. In this thesis only MT carbon filled rubbers were modelled. This is due to simplicity in the approximation of MT carbon black filler shape to a perfect sphere. Therefore, to model fillers shape such as HAF or Printex-XE2 additional effects such as cavitation might be important. Further, work is needed in order to identify the number of fillers, shape and boundary conditions required for filler having more complicated shape than MT carbon black. One of the possible solutions would be to use multiscale modelling approach.

One underlying assumption up to this point had been that the filler rubber interface was considered to be perfectly bonded. An alternative approach used was to introduce an appropriate amount of slippage at the interface. In present case the slippage of the rubber over the filler surface was modelled using a shear stress friction law. The rubber slipped over the filler when the shear stress reaches a critical value. Both 2D and 3D models were used to understand the behaviour. These slippage models showed that as filler volume increased the slippage models experienced a marked reduction in the predicted modulus. These models could be adapted to model viscoelastic behaviour such as hysteresis, cyclic stress softening and dynamic properties of filled rubber. Hence, a realistic filled rubber model should have a filler rubber interface where rubber is allowed to slip under realistic conditions over the filler surface. It was realised during the finite element simulation of the microstructural models that observed behaviour could be better explained if the interfacial properties were clearly understood (Fukahori, 2007). In further work, the mechanical properties of the interface could be studied using a modified AFM probe. This would enable a detailed understanding of how the interfacial mechanical properties might contribute to the filler reinforcement of elastomers.

Finite elements analysis has shown that filler properties such as surface area, shape and structure all alter the filler reinforcement and filler rubber properties. Hence, to investigate the effect filler properties such as surface area and structure the

---

electrical changes of filled elastomers were measured under strain upto 100- 300%, at higher temperature and after swelling in a solvent. A range of filled natural rubber compounds incorporating blacks ranging from non the non reinforcing MT carbon blacks, through to the more typical reinforcing HAF carbon blacks up to and including very high surface area blacks such as Printex-XE2 filled natural rubber were all investigated.

MT carbon has a low surface area, structure and it is a non- reinforcing carbon black. MT carbon black has highly irreversible behaviour; measured either from its mechanical properties as well as from measurements of its change in resistivity with strain. HAF has an intermediate surface area, structure and is considered to be a reinforcing carbon black. HAF carbon black filled elastomers show an irreversible electrical behaviour under strain for the first cycle. However, under cyclic loading a more reversible electrical behaviour is developed. Printex-XE2 carbon black has the highest surface area of the materials studied. It is proposed by the manufacturers that its structure is that of hollow hemispherical particles that are highly aggregated together. It is a very interesting observation that Printex-XE2 filled NR shows essentially reversible electrical behaviour under strain. Hence, there has a good potential to develop this into a sensor material. Also, Printex-XE2 filled elastomer behaved like an ideal sensor material by showing only limited changes in properties with time. Printex-XE2 filled elastomer shows reversible behaviour at higher temperatures and after swelling with a solvent. Hence, this could be used for sensor devices used for gas and chemical leak detection. With help of silver filler, a conductive adhesive used for rubber to metal bonded sensor system was developed. These systems could be versatile in use, with applications as pressure sensor and remote sensing.

All the work done here was above 5% strain (between 100%- 300%), Dynamic mechanical analysis can be used to measure changes in storage modulus and  $\tan \delta$  of the filled elastomers at much smaller strains. These can be used to understand and verify the changes in the filler network structure. As shown in the present work in order to understand the resistivity behaviour of rubbers filled with carbon black

---

grades such as N990, N330, N220 and Printex-XE2 under strain, changes in the filler aggregate structure need to be understood. As suggested earlier, this can be achieved by observing the changes in filler aggregate structure using a micro-tomography technique as shown by (Kohjiya *et. al.* 2006). A very thin sample of rubber is observed under strain using advanced microscopy technique such as micro-tomography in combination with transmission electron microscopy. This can throw more light on phenomena such as de-wetting, dilatation and vacuole formation in the case of filled rubbers. Scanning tunnelling microscopy can also be used to understand the carbon black structure in detail as shown in Figure 7.1. These should enables to understand effect of the surface energy and the origin of nano-scale flaws and thier effect on the behaviour of filled rubbers. In the present work carbon black fillers with surface areas ranging from  $8\text{m}^2/\text{gm}$  to  $600\text{ m}^2/\text{gm}$  were studied as shown in Table 3.1 (chapter 3). However, fillers with surface area in the middle range between 200-550  $\text{m}^2/\text{gm}$  were not investigated. Hence, further work with fillers having surface between 200-550  $\text{m}^2/\text{gm}$  must be studied in order get a better understanding of the effect of filler properties such as surface area on reinforcement and reversible resistivity behaviour under application of strain.

Increasing the temperature decreased the resistivity of all the filled elastomers under strain irrespective of the type of filled elastomer used. This indicates that the increase in temperature favours the mechanism which decreases the resistivity. One possible explanation is that in bound rubber consists of inner an unvulcanised rubber layer at the filler rubber interface, where the rubber flows out more readily at a high temperature under strain. This result in the filler aggregates moving and forming more conduction paths as polymer layer moves and this reduced the resistivity. Further work needs to be carried out to understand the filler rubber interface compositions, mechanical properties and effects of different environmental on interface properties. The effect of temperature on the resistivity is still difficult to explain using the models suggested in present work. As a result, technique such as thermal imaging or FEA should be used to understand the phenomenon in more detail.

---

Swelling of filled rubbers with solvents results in application of triaxial stress in filled rubber. Swelling of a range filled elastomer also resulted in a preferential migration solvent on to the filler-rubber interface. This results in the breakdown of the filler aggregate structure increasing the resistivity of sample.

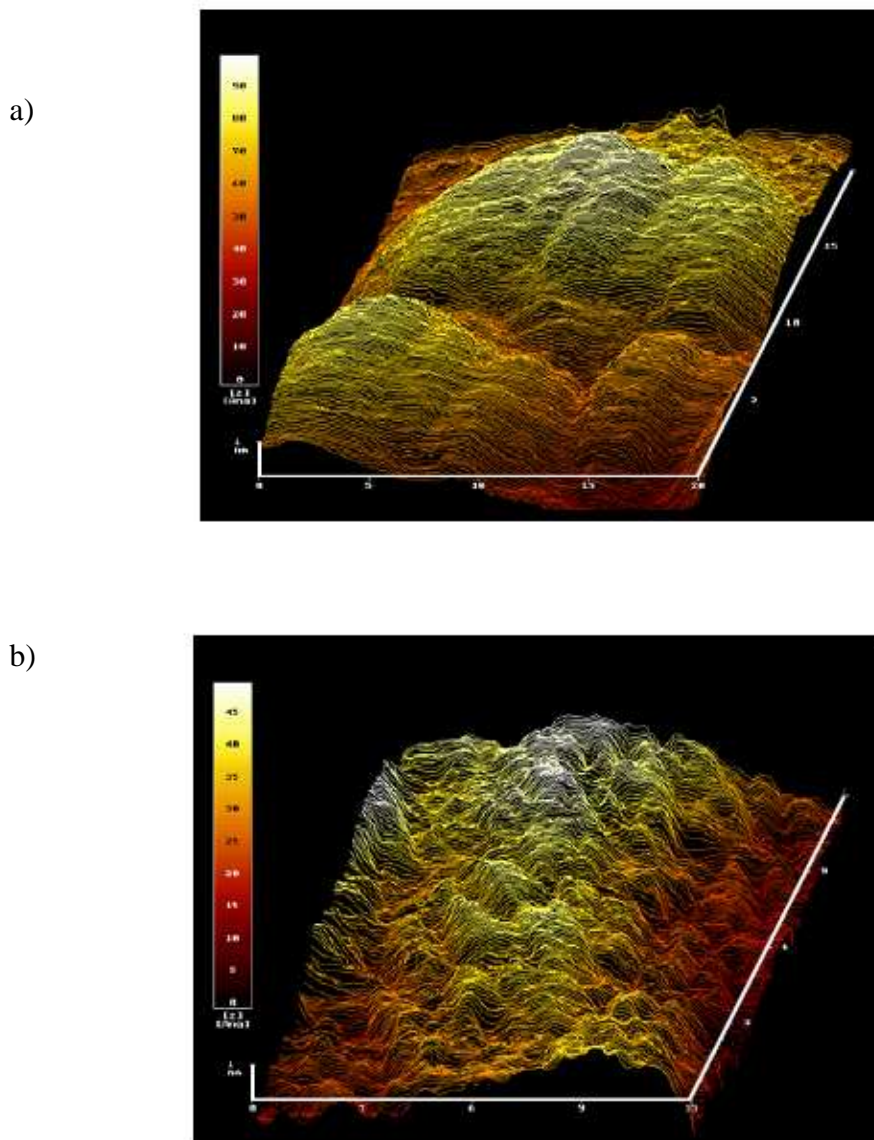


**Figure 7.1** STM (Scanning Tunnelling microscopy) analysis of carbon black  
a) N 234 b) Nanostructure blacks.

---

Abaqus Technical Note 2: Coulomb Friction in User Subroutine FRIC Using the Penalty Method Hibbitt, Version 6.4., Karlsson & Sorensen, Inc, Pawtucket, USA, Abaqus, (2001).

Abaqus Standard User's Manual, Version 6.4., Hibbitt, Karlsson & Sorensen, Inc, Pawtucket, USA, Abaqus, (2004).

Abdel-Ghani, S. A.; Madkour, T. M.; Osman, H. M.; Mohamed, A. R., Study of the Electrical Properties and Swelling Mechanism in Compressed Butyl Rubber Loaded with Carbon Black. *Egypt. J. Sol.* **23**, 307, (2000).

Abraham, J. K.; Philip, B.; Witchurch, A.; Varadan, V. K.; Reddy, C. C., A novel nanocomposite from multiwalled carbon nanotubes functionalized with a conducting polymer. *Smart Mater. Struct.* **13**, 1045, (2004).

Aminabhavi, T. M.; Cassidy, P. E., Electrical resistivity of carbon-black-loaded rubbers. *Rubber Chem. Technol.* **63**, 451, (1990).

Aneli, J. N.; Zaikov, G. E.; Khananashvili, L. M., Effects of mechanical deformations on the structurization and electric conductivity of electric conducting polymer composites. *J. Appl. Polym. Sci.* **74**, 601, (1999).

ASTM Standard D 2414-88 Test Method for Carbon Black-Dibutyl Phthalate Absorption Number, Annual Book of ASTM Standards publisher, **09** (01),435, (1989).

ASTM Standard D 3037-88 Test Method for Carbon Black-Surface Area by Nitrogen Adsorption, Annual Book of ASTM Standards publisher, **09** (01), 466, (1989).

Balberg, I., Tunneling and nonuniversal conductivity in composite materials. *Phys Rev Lett.* **59**, 1305, (1987).

Balberg, I.; Azulay, D.; Toker, D.; Millo O., Percolation and tunneling in composite mater materials. *Int J. Modern Phys. B*, **18**, 2091, (2004).

Beek, L. K. H.; Van Pul, B.I.C.F., Internal field emission in carbon black-loaded natural rubber vulcanizates. *J. Appl. Polym. Sci.* **6** (24), 651, (1962).

Bergström, J. S.; Boyce, M. C., Mechanical behaviour of particle filled elastomers. *Rubber Chem. Technol.* **72**, 633, (1999).

Bicerano, J.; Grant, N. K.; Seitz, J. T.; Pant, K., Microstructural model for prediction of stress-strain curves of amorphous and semicrystalline elastomers. *J. Polym. Sci.: Part B: Polym. Phys.* **35**, 2715, (1997).

---

Blanchard, A. F.; Parkinson, D. Structures in rubber reinforced by carbon black *Second Rubber Technol. Conference*, London, Great Britain, (1948).

Blanchard, A. F.; Parkinson, D., Breakage of Carbon-Rubber Networks by Applied Stress. *Ind. Eng. Chem.* **44**, 799, (1952).

Blaszkiecwicz, M.; McLachlan, D.; Newnham R.E., The volume fraction and temperature dependence of the resistivity in carbon black and graphite polymer composites: an effective media: percolation approach. *Polym. Eng. Sci.* **32**, 421, (1992).

Bloor, D.; Donnelly, K.; Hands, P. J.; Laughlin, P.; Lussey, D., A metal-polymer composite with unusual properties. *J. Phys. D: Appl. Phys.* **38**, 2851, (2005).

Boonstra, B. B.; Dannenberg, E. M., Performance of Carbon Blacks - Influence of Surface Roughness and Porosity. *Ind. Eng. Chem.* **47**, 339, (1955).

Boonstra, B. B., Mixing of carbon black and polymer: Interaction and reinforcement. *J. Appl Polym Sci.* **11**, 389, (1967).

Brien, J.O.; Cashell, E.; Wardell, G. E.; McBrierty, V. J., An NMR Investigation of the Interaction between Carbon Black and cis-Polybutadiene. *Macromolecules* **9**, 653, (1976).

Brunauer, S.; Emmett, P. H.; Teller, E., Adsorption of gases in multimolecular layers. *J. American Chem. Soc.* **60**, 309, (1938).

Bueche, F., Molecular Basis for the Mullins effect. *J. Appl. Polym. Sci.* **4**, 107, (1960).

Bueche, F., Mullins effect and rubber-filler interaction. *J. Appl. Polym. Sci.* **5**, 271, (1961).

Bueche, F., “*Reinforcement of elastomer*” Edited by Kraus G, New York: Wiley inter-science, (1965).

Burton, L.C.; Hwang, K.; Zhang, T., Dynamic electrical and electromechanical properties of carbon-black-loaded rubber. *Rubber Chem. Technol.* **62**, 838, (1989).

Busfield, J. J. C.; Thomas, A. G.; Yamaguchi, K., Electrical and mechanical behaviour of filled elastomers 2: The effect of swelling and temperature. *J. Polym. Sci.: Part B: Polym. Phys.* **42**, 2161, (2004).

Busfield, J. J. C.; Jha, V.; Hon, A. A.; Thomas A.G., Micro-structural finite element modelling of the stiffness of filled elastomers: The effect of filler number, shape

---

and position in the rubber matrix. *Proceeding of the ECCMR conference Constitutive Models for Rubber IV* Lisse: Balkema, 459, (2005a).

Busfield, J.J.C.; Thomas, A.G.; Yamaguchi, K., Electrical and mechanical behavior of filled rubber. III. Dynamic loading and the rate of recovery. *J. Polym. Sci. Part B: Polym. Phys.* **43**, 1649, (2005b).

Busfield, J. J. C.; Jha, V.; Liang, H.; Papadopoulos, I. C.; Thomas, A. G., Prediction of fatigue crack growth using finite element analysis techniques applied to three-dimensional elastomeric components. *Plastic, Rubber and Composites* **34**, 349, (2005c).

Bush A. W. *Contact Mechanics, in Rough Surfaces* Edited by T.R. Thomas *et al.*, London: Longman, (1982).

Carmona, F.; Canet, R.; Delhaes, P., Piezoresistivity of heterogeneous solids. *J. Appl. Phys.* **61**, 2550, (1986).

Carrillo, A.; Martin-dominguez, I. R.; Glossman, D.; Marquez, A., Study of the effect of solvent induced swelling on the resistivity of butadiene based elastomers filled with carbon particles: Part I. Elucidating second order effects. *Sensors and actuators A: Physical.* **119**, 157, (2005).

Coveney, V. A.; Johnson D. E.; Turner D.M., A Triboelastic Model for the Cyclic Mechanical Behavior of Filled Vulcanizates. *Rubber Chem. Technol.* **68**, 660, (1995).

Coveney, V. A.; Johnson D. E., Modeling of carbon black filled natural rubber vulcanizates by the standard triboelastic solid. *Rubber Chem. Technol.* **72** (4), 779, (1999).

Coveney, V. A.; Johnson D. E., Rate-dependent modeling of a highly filled vulcanizate. *Rubber Chem. Technol.* **73**, 779, (2000).

Dannenberg, E. M., [Bound rubber and carbon black reinforcement](#). *Ind. Eng. Sci.* **21**, 809, (1981).

Dannenberg, E. M., The effects of surface chemical interactions on the properties of filler-reinforced rubbers. *Rubber Chem. Technol.* **48**, 410, (1975).

Dannenberg, E. M., Bound rubber and carbon black reinforcement. *Rubber Chem. Technol.* **59**, 512, (1986).

Dannenberg, E. M., Molecular slippage mechanism of reinforcement. *Trans. Inst. Rubber. Ind.* **42**, 26, (1966).

- 
- Deeprasertkul, C., "Dynamic Properties of Carbon Black Filled Elastomers Containing Liquids", PhD. Thesis, Queen Mary, University of London, (1999).
- Dessewffy, O., Dependence of bound rubber on concentration of filler and on temperature. i. *Rubber Chem. Technol.* **35**, 599, (1962).
- Derham, C. J.; Thomas, A. G., Creep of rubber under repeated stressing. *Rubber Chem. Technol.* **50**, 397, (1977).
- Donnet, J. B.; Voet, A., "Carbon Black, Phys., Chem., and Elastomer Reinforcement" New York: Marcel Dekker, (1976).
- Einstein, A., Eine neue Bestimmung der Moleküldimensionen. *Ann. d. Physik* **19**, 289, (1906).
- Einstein, A., Berechtigung zu meiner Arbeit: Eine neue Bestimmung der Moleküldimensionen. *Ann. d. Physik* **34**, 591, (1911).
- Flandin, L.; Chang, A.; Nazarenko, S.; Hiltner, A.; Baer, E., Effect of strain on the properties of an ethylene-octene elastomer with conductive carbon fillers. *J. Appl. Polym. Sci.* **76**, 894, (1999).
- Flandin, L.; Hiltner, A.; Baer, E., Interrelationships between electrical and mechanical properties of a carbon black-filled ethylene-octene elastomer. *Polym.* **42**, 827, (2001).
- Fletcher, W. P.; Gent, A. N., Measurement of the Dynamic Properties of Rubber. *Trans. Inst. Rubber. Ind.* **26**, 45, (1950).
- Frenkel, On the Electrical Resistance of Contacts between Solid Conductors. *Phys. Rev.* **36**, 1604, (1930).
- Fujimoto, K.; Kofuji, H.; Ueki, T.; Mifune, N., Study of three-dimensional stress fatigue in particle-reinforcement of rubber vulcanisates. Part 1. Structural changes due to fatigue caused three-dimensional stresses. *Nippon Gomu Kyokaish* **10**, 574, (1986).
- Fukahori, Y.; Seki, W., Stress-analysis of elastomeric materials at large extensions using the finite-element method. 2. stress and strain distribution around rigid spherical-particles. *J. Mat. Sci.* **28**, 4471, (1993).
- Fukahori, Y., Generalized concept of the reinforcement of elastomers. Part 1: Carbon black reinforcement of rubbers. *Rubber Chem. Technol.* **80**, 701, (2007).



- 
- Gent, A. N., A new constitutive relation for rubber. *Rubber Chem. Technol.* **69**, 59, (1996).
- Gent, A. N.; Campion, R. P., “*Engineering With Rubber: How to Design Rubber Components*” American Chemical Society. Division of Rubber, Munich: Hanser Publishers, (1992).
- Gent, A. N.; Hwang, Y.C., Internal failures in model elastomeric composites. *J. Mat. Sci.* **25**, 4981, (1990).
- Geuskens, G.; Gielens, J.; Desheef, L.; Deltour, D. R., The electrical conductivity of polymer blends filled with carbon black. *Eur. Polym.* **23**, 12, (1987).
- Guth, E., Theory of Filler Reinforcement. *J. Appl. Phys.* **16**, 20, (1945).
- Guth, E.; Gold, O., On the hydrodynamical theory of the viscosity of suspensions. *Phys. Rev.* **53**, 322, (1938).
- Harwood, J. A. C.; Mullins, L.; Payne, A. R., Stress-softening in rubbers—A review. *J. of IRI* **1**, 17, (1967).
- Harwood, J. A. C.; Payne, A. R.; Smith, A new approach to rubber reinforcement. *J. Rubber Chem. Technol* **43**, 687, (1970).
- Hashem, A. A.; Ghani, A. A.; Eatah, A. I., Effect of preextension on electrical conductivity and physicomechanical properties of butyl rubber (iir) loaded with different types of carbon black. *J. Appl. Polym. Sci.* **42**, 1081, (1991).
- He, X. J.; Du, J. H.; Ying, Z.; Cheng, H. M., Positive temperature coefficient effect in multiwalled carbon nanotube/high-density polyethylene composites. *Apply. Phys. Lett.* **86**, 062112, (2005).
- Heinrich, G.; Kluppel, M., Recent Advances in the Theory of Filler Networking in Elastomers. *Advances in Polymer Science* **160**, 1, (2002).
- Heinrich, G.; Vilgis, T. A., Physical adsorption of polymers on disordered filler surfaces. *Rub. Chem. Technol.* **6**, 26, (1995).
- Hepburn, C. M., Filler Reinforcement of Rubber. *Plastics and Rubber International* **9** (2), 11, (1984).
- Herd, C. R.; Mc Donald, G. C.; Hess, W. M., Morphology of carbon-black aggregates: fractal versus euclidean geometry. *Rubber chem. Technol.* **65**, 1, (1991).
- Hess, W. M.; Lyon, F.; Burgess, K. A. A., EinfluB der adhesion zwischen ruB und

---

kautschuk auf die eigenschaften der vulkanisate. *Kautsch Gummi Kunstst* **20** (3), 135, (1967).

Holm, R., "Electric Contact Theory and Application" Springer, **9**, (1967).

Hon, A. A., "Modelling Filler Reinforcement in Elastomers," PhD Thesis, Queen Mary, University of London, (2005).

Hon, A. A.; Busfield, J. J. C.; Thomas, A. G., Stiffness prediction of MT carbon-black-filled elastomer systems using FEM. *Tire Technology International* 100, (2004).

Hon, A. A.; Busfield, J. J. C.; Thomas, A. G., Filler reinforcement in rubber carbon-black systems. *Constitutive models of rubber 3* Lisse: Balkema, 300, (2003).

Janzen, J., On the critical conductive filler loading in antistatic composites. *J. Appl. Phys.* **46**, 966, (1975).

Jesse, S.; Guillorn, M. A.; Ivanov, I. N.; Poretzky, A. A.; Howe, J. Y.; Britt, P. F.; Geohegan, D. B., In situ electric-field-induced contrast imaging of electronic transport pathways in nanotube-polymer composites. *Appl. Phys. Lett.* **89**, 013114, (2006).

Jha, V.; Hon, A. A.; Thomas, A. G.; Busfield, J. J. C., Modeling of the effect of rigid fillers on the stiffness of rubbers. *J. Appl. Polym. Sci.* **107**, 2572, (2007).

Jiang, M. J.; Dang, Z. M.; Xu, H. P., Significant temperature and pressure sensitivities of electrical properties in chemically modified multiwall carbon nanotube/methylvinyl silicone rubber nanocomposites. *Appl. Phys. Lett.* **89**, 182902, (2006).

Kang, I.; M. Schulz, J.; Kim, J. H.; Shanov, V.; Shi, D., A carbon nanotube strain sensor for structural health monitoring. *Smart Mater. Struct.* **15**, 737, (2006).

Kar, K.; Bhowmick, K., High-strain hysteresis of rubber vulcanizates over a range of compositions, rates, and temperatures. *J. Appl. Polym. Sci.* **65**, 1429, (1997).

Kashani, M. R.; Padovan, J., Modelling reinforcement of rubber with carbon black filler. *Plastics Rubbers and Composite* **6**, 47, (2007).

Kaufman, S.; Slichter, W. P.; Davis, D. D., Nuclear magnetic resonance study of rubber-carbon black interactions. *J. Polym. Sci. Part A-2 Polym. Phys.* **9**, 829, (1971).

Kloczkowski, A.; Sharaf, M. A.; Mark, J. E., Computer-Simulations on Filled Elastomeric Materials. *Chem. Eng. Sci.* **49**, (17), 2889, (1994).

- 
- Kluppel, M. & Meier, J., Modeling of soft matter viscoelasticity for FE-applications. *Proceedings of the First European Conference on Constitutive Models for Rubber* Sept., Hannover, 11, (2001).
- Kluppel, M.; Schramm, J., An advanced micro-mechanical model of hyperelasticity and stress softening of reinforced rubbers. *Proceedings of Constitutive Models for Rubber* Balkema, Rotterdam, (1999).
- Kohjiya, S.; Katohb, A.; Sudab, T.; Shimanukib, J.; Ikeda, Y., Visualisation of carbon black networks in rubbery matrix by skeletonisation of 3D-TEM image. *Polym. Communication* **47** (10), 3298, (2006).
- Kost, J.; Foux, A.; Narkis, M., Quantitative model relating electrical resistance, strain, and time for carbon black loaded silicone rubber. *Polym. Eng. Sci.* **34**, 1628, 59, (1994).
- Kraus, G., Reinforcement of elastomers by carbon black. *Adv. Polymer Sci.* **8**, 155, (1971).
- Kraus, G., Reinforcement of elastomers by carbon black. *Angewandte Makromolekulare Chemie* **60** (1), 215, (1976).
- Kraus, G., Reinforcement of elastomers by carbon black. *Rubber Chem. Technol.*, **51**, 297, (1978).
- Kraus, G.; Svetlik, J. F., Electrical Conductivity of Carbon Black-Reinforced Elastomers. *J. of Electrochemical Society* **103**, 337, (1956).
- Leblanc, J. L., Rubber–filler interactions and rheological properties in filled compounds. *Progress in Polym. Sci.* **27** (4), 627, (2002).
- Loos, J.; Alexeev, A.; Grossiord, N.; Koning, C. E.; Regev, O., Visualization of single-wall carbon nanotube (SWNT) networks in conductive polystyrene nanocomposites by charge contrast imaging. *Ultramicroscopy* **104**, 160, (2005).
- Lundberg, B.; Sundqvist, B., Resistivity of a composite conducting polymer as a function of temperature, pressure, and environment: Applications as a pressure and gas concentration transducer. *J. Appl. Phys.* **60**, 1074, (1986).
- Material data sheet, Degussa, <http://www.degussa-fp.com/fp/en/gesch/gummiru/default.htmlProduct=5142> & Product 5010.
- McLachlan, D. S., An equation for the conductivity of binary mixtures with anisotropic grain structures. *J. Phys. C: Solid State Phys.* **20**, 865, (1987).

- 
- McLachlan, D. S., Measurement and analysis of a model dual-conductivity medium using a generalised effective-medium theory. *J. Phys.* **C21**, 1521, (1988).
- McLachlan, D. S.; Blaszkiewicz, M.; Newnham, R. E., Electrical Resistivity of Composites. *J. Am. Ceram. Soc.* **73**, 2187, (1990).
- Medalia, A. I., Morphology of aggregates VI. Effective volume of aggregates of carbon black from electron microscopy. *J. Colloid Interf. Sci.* **32**, 115, (1970).
- Medalia, A. I., Effective degree of immobilization of rubber occluded within carbon black aggregates. *Rubber Chem. Technol.* **45**, 1171, (1972).
- Medalia, A. I., Electrical conduction in carbon black composites. *Rubber Chem. Technol.* **59**, 432, (1986).
- Miyasaka, K.; Watanabe, K.; Jojima, E.; Aida, H.; Sumita, M.; Ishikawa, K., Electrical conductivity of carbon-polymer composites as a function of carbon content. *J. Material sci.* **21**, 809, (1982).
- Mooney, M. A., Theory of Large Elastic Deformation. *J. Appl. Phys.* **11**, 582, (1940).
- Moshev, V. V.; Kozhenikova, L. L., Structural cell of particulate elastomeric composites under extension and compression. *International J. of Solids and Structures* **39**, 449, (2002).
- Mullins, L.; Tobin, N. R., Stress softening in rubber vulcanizates. Part I. Use of a strain amplification factor to describe the elastic behavior of filler-reinforced vulcanized rubber. *J. Appl. Polymer Sci.* **9**, 2993, (1965).
- Nakajima, N.; Scobbo, J., Strain amplification of elastomers filled with carbon black in tensile deformation. *J. Rubber Chem. Tech.* **61**, 137, (1988).
- Norman, R. H., “*Conductive Rubbers and Plastics*” Elsevier: New York, (1970).
- Novak, I.; Krupa, I.; Chodak, I., Electroconductive adhesives based on epoxy and polyurethane resins filled with silver-coated inorganic fillers. *Syntehtic metals* **144**, 13, (2004).
- Paipetis, S. A., Interfacial phenomena and reinforcing mechanisms in rubber/carbon black composites. *Fibre Sci. Tech.* **21**, 107, (1984).
- Payne, A. R., The dynamic properties of carbon black-loaded natural rubber vulcanizates. I. *J. Appl. Polym. Sci.* **6**, 57, (1962).
- Payne, A. R. Whittaker, R. E., Low strain dynamic properties of filled rubbers. *Rubber Chem. Technol.* **44**, 440, (1971).

- 
- Probst, N., Conductive compounds on the move. *European rubber journal* **166**, 27, (1984).
- Rubin, Z., Sunshine, S. A., Heaney, M. B., Bloom, I. Balberg I., Critical behavior of the electrical transport properties in a tunneling-percolation system. *Phys. Rev. B.* **59**, 19, (1999).
- Rivlin, R. S., *Rheology* Edited by F.R. Eirich, New York: Academic Press, (1956).
- Robert, A. D., A guide to estimating the friction of rubber. *Rubber Chem. Technol.* **65**, 673, (1992).
- Rogers, S. A.; Kaiser, A. B., Thermopower and resistivity of carbon nanotube networks and organic conducting polymers. *Appl. Phys.* **4**, 407, (2004).
- Sandler, J. K. W.; Kirk, J. E.; Kinloch, I. A.; Shaffer, M. S. P.; Windle, A. H., Ultra-low electrical percolation threshold in carbon-nanotube-epoxy composites. *Polym.* **44**, 5893, (2003).
- Sau, K. P.; Chaki, T. K.; Khastgir, D., The change in conductivity of a rubber-carbon black composite subjected to different modes of pre-strain. *Composites, Part A.* **29A**, 363, (1998).
- Sen, T. Z.; Sharaf, M. A.; Mark, J. E.; Kloczkowski, A., Modeling the elastomeric properties of stereoregular polypropylenes in nanocomposites with spherical fillers. *Polym.* **46** (18), 7301, (2005).
- Sluis, Van der, O.; Schreurs, P. J. G.; Meijer, H. E. H., Homogenisation of structured elastoviscoplastic solids at finite strains. *Mechanics of Solids* **33**, 499, (2001).
- Sharaf, M.A.; Kloczkowski, A.; Mark, J. E., Monte Carlo simulations on reinforcement of an elastomer by oriented prolate particles. *Computational and Theoretical Polym. Sci.* **11** (4), 251, (2001).
- Sichel, E. K., “*Carbon Black–Poly. Composites*” Marcel Dekker: New York, **51**, (1982).
- Simões, R.; Cunha, A. M.; Brostow, W., Computer simulations of true stress development and viscoelastic behavior in amorphous polymeric materials. *Computational Mat. Sci.* **36** (3), 319, (2006).
- Sircar, A. K.; Lamond, T. G., Effect of carbon-black particle-size distribution on electrical-conductivity. *Rubber Chem. Technol.* **51**, 126, (1978).

- 
- Sircar, A. K.; Cook, F. R.; Voet, A., Relaxation of stress and electrical resistivity in carbon-filled vulcanizates at minute shear strains. *Rubber Chem. Technol.* **44**, 185, (1971).
- Smallwood, H. M., Limiting law of the reinforcement of rubber. *J. Appl. Phys.* **15**, 758, (1944).
- Smit, R. J. M.; Brekelmans, W. A. M.; Meijer, H. E. H., Predictive modelling of the properties and toughness of polymeric materials Part II Effect of microstructural properties on the macroscopic response of rubber-modified polymers. *J. Mat. Sci.* **35**, 2869, (2000).
- Stauffer, D.; Aharony, A., “*Introduction to Percolation Theory*” Taylor and Francis, London, 4th ed., (1985).
- Strumpler, R.; Glatz-Reichenbach, J., Conducting Polymer Composites. *J. Electroceram.* **3**, 329, (1999).
- Toker, D.; Azulay, D.; Shimoni, N.; Balberg, I.; Millo O., Tunneling and percolation in metal-insulator composite materials, *Phys. Rev. B.* **68**, 041403, (2003).
- Taylor, G. I., The viscosity of a fluid containing small drops of another fluid. *Proceedings of the Royal Society of London A* **138**, 41, (1932).
- Treloar, L. R. G., The statistical length of paraffin molecules. *Trans. Faraday Soc.*, **39**, 36, (1943).
- Tsunoda, K.; Busfield, J. J. C.; Davies, C. K. L.; Thomas, A. G., Effect of materials variables on the tear behaviour of a non-crystallising elastomer. *J. Mater. Sci.* **35**, 5187, (2000).
- Verhelst, W. F.; Wolthuis, K.; Voet, A.; Ehrburger, P.; Donnet, J., The role of morphology and structure of carbon blacks in the electrical conductance of vulcanizates. *Rubber Chem. Technol.* **50**, 735, (1977).
- Voet, A.; Cook, F. R., Investigation of carbon chains in rubber vulcanizates by means of dynamic electrical conductivity. *Rubber Chem. Technol.* **41**, 1207, (1968).
- Voet, A.; Cook, F. R.; Sircar, A. K., Relaxation of stress and electrical resistivity in carbon-filled vulcanizates at minute shear strains. *Rubber Chem. Technol.* **44**, 175, (1971).
- Voet, A.; Sircar, A. K.; Mullens, T. J., Electrical properties of stretched carbon black loaded vulcanizates. *Rubber Chem. Technol.* **42**, 874, (1969).

- 
- Wack, P. E.; Anthony, R. L.; Guth, E., Electrical Conductivity of GR-S and Natural Rubber Stocks Loaded with Shawinigan and R-40 Blacks. *J. Appl. Phys.* **18** (5), 456, (1947).
- Wang, L.; Ding, T.; Wang, P., Effects of compression cycles and precompression pressure on the repeatability of piezoresistivity for carbon black-filled silicone rubber composite. *J. Polym. Sci. Part B. Polym. Phys.* **46**, 1050, (2008).
- Wei, C.; Dai, L.; Roy, A.; Tolle, T. B., Multifunctional chemical vapor sensors of aligned carbon nanotube and polymer composites. *J. Am. Chem. Soc.* 412, (2006).
- Wolff, S. M.; Wang, J.; Tan, E. H., *Meeting of the Rubber Division ACS*. (1991), Detroit.
- Wolff, S., Chemical aspects of rubber reinforcement by fillers. *Rubber Chem. Technol.* **69**, 325, (1996).
- Wu, J.; McLachlan, D. S., Percolation exponents and thresholds obtained from the nearly ideal continuum percolation system graphite-boron nitride. *Physical review B* **56**, 3, (1997).
- Xu, H.; Dang, Z.; Shi, D.; Bai, Remarkable selective localization of modified nanoscaled carbon black and positive temperature coefficient effect in binary-polymer matrix composites. *J. J. Mat. Chem.* **18**, 2685, (2008).
- Yamaguchi, K., "The Mechanical and Electrical Behaviours of Carbon Black filled Elastomer under Strain," PhD Thesis, Queen Mary, University of London, (2002).
- Yamaguchi, K.; Busfield, J. J. C.; Thomas, A. G., Electrical and mechanical behaviour of filled elastomers. I. The effect of strain. *J. Polym. Sci.: Part B: Polym. Phys.* **41**, 2079, (2003).
- Zhang, B.; Fu, R. W.; Zhang, M. Q.; Dong, X. M.; Lan, P. L.; Qiu, J. S., Preparation and characterization of gas-sensitive composites from multi-walled carbon nanotubes/polystyrene. *Sens. Actuators B* **109**, 323, (2005).
- Zhang, R.; Baxendale, M.; Peijs, T., Universal resistivity–strain dependence of carbon nanotube/polymer composites. *Physical Review B* **76**, 195433, (2007).
- Zhang, Y.; Ge, S.; Tang, B.; Koga, T.; Rafailovich, M. H.; Sokolov, J. C.; Peiffer, D. G.; Li, Z.; Dias, A. J.; McElrath, K. O.; Lin, M. Y.; Satija, S. K.; Urquhart, S. G.; Ade, H.; Nguyen, D., Effect of Carbon Black and Silica Fillers in Elastomer Blends. *Macromolecules* **34** (20), 7056, (2001).

---

Zhu, A.; Sternstein, S. S., Nonlinear viscoelasticity of nanofilled polymers: interfaces, chain statistics and properties recovery kinetics. *Composites Science and Technology* **63**, 1113, (2003).

Zienkiewicz, O. C.; Taylor, R. L., “*The finite element analysis method*” **1**, (2000).

.



---

## *Appendix*

*Refereed journal papers and conference papers submitted by the author as part of this research*

### *Investigation of interfacial slippage on filler reinforcement in carbon-black filled elastomers.*

V. Jha, A.A. Hon, J.J.C. Busfield & A.G. Thomas

Materials Department, Queen Mary, University of London, London, UK

*Proceeding of the ECCMR conference, Constitutive Models for Rubber IV. 459-464, 2005.*

ABSTRACT: Reinforcing fillers are added to elastomeric materials to enhance mechanical properties such as the modulus, strength and wear resistance. Einstein's (1906, 1911) viscosity law predicted the viscosity of liquid containing rigid spherical particles. This theory has been modified by Guth and Gold (1938) to predict how the Young's modulus of an elastomer can be related to the volume fraction and shape factor of the filler present in the elastomer. Despite this advance the actual reinforcement mechanism due to carbon fillers is still not fully resolved and continues to be a subject of great interest. Here, finite element analysis techniques have been used to investigate the reinforcement mechanisms further. The results of these models were then compared to experimental results. In the present work, filler particles were modelled to simulate the filler reinforcement behaviour. This was carried out at different volume fractions of fillers. The types of models that are required to accurately predict the correct experimental behaviour can also help identify the nature of the reinforcing mechanisms. For example, the slippage mechanisms at the filler elastomer interface can be examined using this approach. The results of finite element analysis were compared to new and well established theories in this area.

---

***Micro-structural Finite Element Modelling of the Stiffness of Filled Elastomers: The effect of filler number, shape and position in the rubber matrix.***

V. Jha, A.G. Thomas, Y. Fukahori and J.J.C. Busfield

Department of Materials, Queen Mary, University of London, Mile End Road,  
London, E1 4NS, UK

*Proceeding of the ECCMR conference, Constitutive Models for Rubber V, 165-172, 2007.*

**ABSTRACT**

Previous work (Jha et al., 2007, Busfield et al., 2005, Hon et al., 2003) has shown that the stiffness of filled elastomers over a wide range of strains using micro structural finite element models can be achieved at low filler volume fractions with a reasonable accuracy. To do this an appropriate stored energy function such as that by Gent (1996) is required to show realistic stiffening at higher strains for unfilled rubbers. It has been noted that as the number of fillers present in the unit cell is increased from 1 to 4 that there was an increase in the predicted stiffening effect at a constant filler volume fraction. The question remains, however, as to how many filler particles would be required in the unit cell to ensure that the behaviour of the filler is accurately represented. In the present work two different types of micro-structural model are examined under strain with a range of up to 36 filler particles present. The first type having smooth spherical surfaces and the second having a more irregular surface constructed out of cubes. In this study the effect of the position of the filler particles is investigated by repositioning them into more random confirmations than that suggested by the single filler models. It appears that a large number of fillers have to be incorporated to predict the behaviour, especially at higher filler volume fractions when filler-filler interactions become significant. Also, the model made with basic cubic elements is stiffer than the real materials, as within the model there is a considerable amount of additional ‘occluded’ rubber that increases the effective filler volume fraction.

---

## ***Modelling of the effect of fillers on the stiffness of rubbers***

Vineet Jha, Amir A. Hon, Alan G. Thomas and James J.C. Busfield

*Department of Materials, Queen Mary, University of London, UK*

*Journal of Applied Polymer Science, Vol 107, pp 2572-2577, 2007.*

### ABSTRACT

Elastomer components fail at cyclic strain amplitudes much lower than their catastrophic tear strength as a result of cumulative cyclic fatigue crack growth. Cracks typically develop in regions of high stress concentrations. In general, the rate of growth is determined by the shape of the component, and the nature and magnitude of the deformation imposed. Extensive earlier work has been done on the prediction of fatigue life of components. However, the reproducibility of the results was poor and, in addition, there was a low degree of accuracy. A fracture mechanics approach, which uses finite element analysis techniques to calculate strain energy release rates for cracks located in three-dimensional components, was used in combination with experimental measurements of cyclic crack growth rates of specific strain energy release rate to predict the cyclic crack growth propagation rate and the eventual fatigue failure of an elastomeric engineering component in three modes of deformation, namely: tension, simple shear and combined shear and tensile (45° angle) deformations. The fatigue crack growth for the gearbox mount under investigation was predicted within a factor of 2 at different displacements for all three modes of deformation.

---

## ***Electrical resistivity under strain***

V. Jha, A.G. Thomas, M. Bennett & J.J.C. Busfield.

*Proceedings of Institute of Materials, Minerals and Mining, Elastomers for Engineering, IOM3, London, UK, 2006.*

### **ABSTRACT**

Unfilled elastomers are highly resistive polymer. Filler added to elastomers to make it useful for industrial application. Filler reinforces the elastomers improving its mechanical properties. It also reduces the resistivity of elastomers. The choice of fillers depends on many factors such as stiffness required, fatigue life and loading conditions. These fillers have different size, surface area, structure, porosity and surface activity. In the present case effect of surface area and structure of fillers on resistivity under strain has been studied. These provide an insight filler-rubber interaction under strain. It helps us understand filler reinforcement and conduction mechanism in filled elastomer.

---

## ***Reversible electrical behaviour with strain for a carbon black filled natural rubber***

V. Jha, A.G. Thomas, M. Bennett & J.J.C. Busfield

*Journal of applied polymer science (Submitted, 2008)*

### ABSTRACT

Most unfilled elastomers exhibit a high electrical resistance. Fillers are usually added to elastomers to enhance their mechanical properties. Frequently the filler type used is an electrically conductive carbon black and the inclusion of such fillers reduces the resistivity of the elastomer compound. Previous work has shown that for elastomers containing N330 (or N300 series) carbon black fillers at a volume fraction above the percolation threshold the resistivity changes with strain, the precise resistivity versus strain behaviour being non linear and irreversible for HAF fillers. A strain measuring device, deriving strain directly from a measure of the resistivity, requires that the behaviour be reversible and reproducible from cycle to cycle. This work presents the electrical resistivity behaviour of a natural rubber (NR) compound filled with Printex XE2 carbon black. This type of filler has a significantly different morphology to the HAF blacks examined previously. The Printex was incorporated into the rubber at a volume fraction above its percolation threshold and its behaviour is contrasted to that observed with HAF carbon black filled natural rubber. Here and for the first time reversible electrical resistivity dependence with strain is reported for an elastomer filled with Printex XE2. This reversible behaviour under strain opens up the possibility of applications such as a flexible load sensor, pressure sensor or switch.